

ARCHER, CATHRO & ASSOCIATES (1981) LIMITED
1016 - 510 West Hastings Street
Vancouver, B.C. V6B 1L8

Telephone: 604-688-2568

Fax: 604-688-2578

ASSESSMENT REPORT

describing

**SOIL SAMPLING AND DETAILED INTERPRETATION
OF 2007 VTEM GEOPHYSICAL SURVEY**

at the

CABIN LAKE PROPERTY

CL Claims 1-93

NTS 105B/04

Latitude 60°06'N; Longitude 131°47'W

in the

Watson Lake Mining District,
Yukon Territory

prepared by

Archer, Cathro & Associates (1981) Limited

for

TARSIS CAPITAL CORP.

by

W.A.Wengzynowski, P.Eng.

April 2009

TABLE OF CONTENTS

	<u>Page</u>
INTRODUCTION	1
PROPERTY LOCATION, CLAIM DATA AND ACCESS	1
HISTORY	2
GEOMORPHOLOGY	2
GEOLOGY	2
MINERALIZATION AND GEOCHEMISTRY	4
PRE 2007 GEOPHYSICS SURVEYS	5
2007 GEOPHYSICAL SURVEYS	6
DISCUSSION AND CONCLUSIONS	7
REFERENCES	9

APPENDICES

- I STATEMENT OF QUALIFICATIONS
- II CERTIFICATES OF ANALYSIS
- III GEOPHYSICAL REPORT BY GEOTECH LTD.
- IV GEOPHYSICAL REPORT BY CONDOR CONSULTING INC.

FIGURES

<u>No.</u>	<u>Description</u>	<u>Follows Page</u>
1	Property Location	1
2	Claim Location	1
3	Tectonic Setting	2
4	Regional Geology	3
5	Stratigraphic Column	3
6	Property Geology	3
7	Copper Soil Geochemistry	4
8	Silver Soil Geochemistry	4
9	Lead Soil Geochemistry	4
10	Zinc Soil Geochemistry	4
11	2008 Copper Soil Geochemistry	5
12	2008 Zinc Soil Geochemistry	5

TABLES

	<u>Page</u>
I Main Lithological Units	3

INTRODUCTION

The Cabin Lake property covers a potential volcanogenic hosted massive sulphide (VHMS) prospect located in southern Yukon. It is owned 100% by Tarsis Capital Corp.

This report describes the results of a soil survey conducted between June 26 to July 1, 2008 and a detail interpretation of a Versatile Time Domain Electromagnetic (VTEM) survey completed in 2007. The grid geochemical survey was conducted by Archer, Cathro and supervised by the author. The author's Statement of Qualifications appear in Appendix I.

PROPERTY LOCATION, CLAIM DATA AND ACCESS

The Cabin Lake property consists of 93 contiguous mineral claims located in southern Yukon on NTS map sheets 105B/04 at latitude 60°06'N and longitude 131°47'W (Figure 1). The claims are registered with the Watson Lake Mining Recorder in the name of Tarsis Capital. The locations of individual claims are shown on Figure 2 while claim registration data are listed below.

<u>Claim Name</u>	<u>Grant Number</u>	<u>Expiry Date *</u>
CL 1-16	YC72589-YC72604	April 14, 2012
CL 17-22	YB89158-YB89163	April 14, 2013
CL 23-32	YC72605-YC72614	April 14, 2012
CL 33-38	YB89173-YB89178	April 14, 2013
CL 39-48	YC72615-YC72624	April 14, 2012
CL 49-50	YB89216-YB89217	April 14, 2013
CL 51-60	YC72625-YC72634	April 14, 2012
CL 61-62	YB89228-YB89229	April 14, 2013
CL 63-72	YC72635-YC72644	April 14, 2012
CL 73	YB89240	April 14, 2013
CL 74-87	YC72645-YC72658	April 14, 2012
CL 88	YB89255	April 14, 2013
CL 89	YC72659	April 14, 2012
CL 90	YB89257	April 14, 2013
CL 91-93	YC72660-YC72662	April 14, 2012

* Expiry dates include 2008 work which has been filed for assessment credit but not yet accepted.

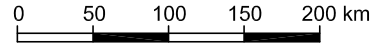
The Cabin Lake property is located 53 km east of Teslin, a village that lies alongside the Alaska Highway, approximately 183 km by road southeast of Whitehorse. In 2008, the crew was based at a field camp servicing the Mor property. Daily transport to the Cabin Lake property was provided by a Hughes 500D helicopter operated by Fireweed Helicopter Ltd. of Whitehorse, YT.

TARSIS CAPITAL CORP.

ARCHER, CATHRO & ASSOCIATES (1981) LIMITED

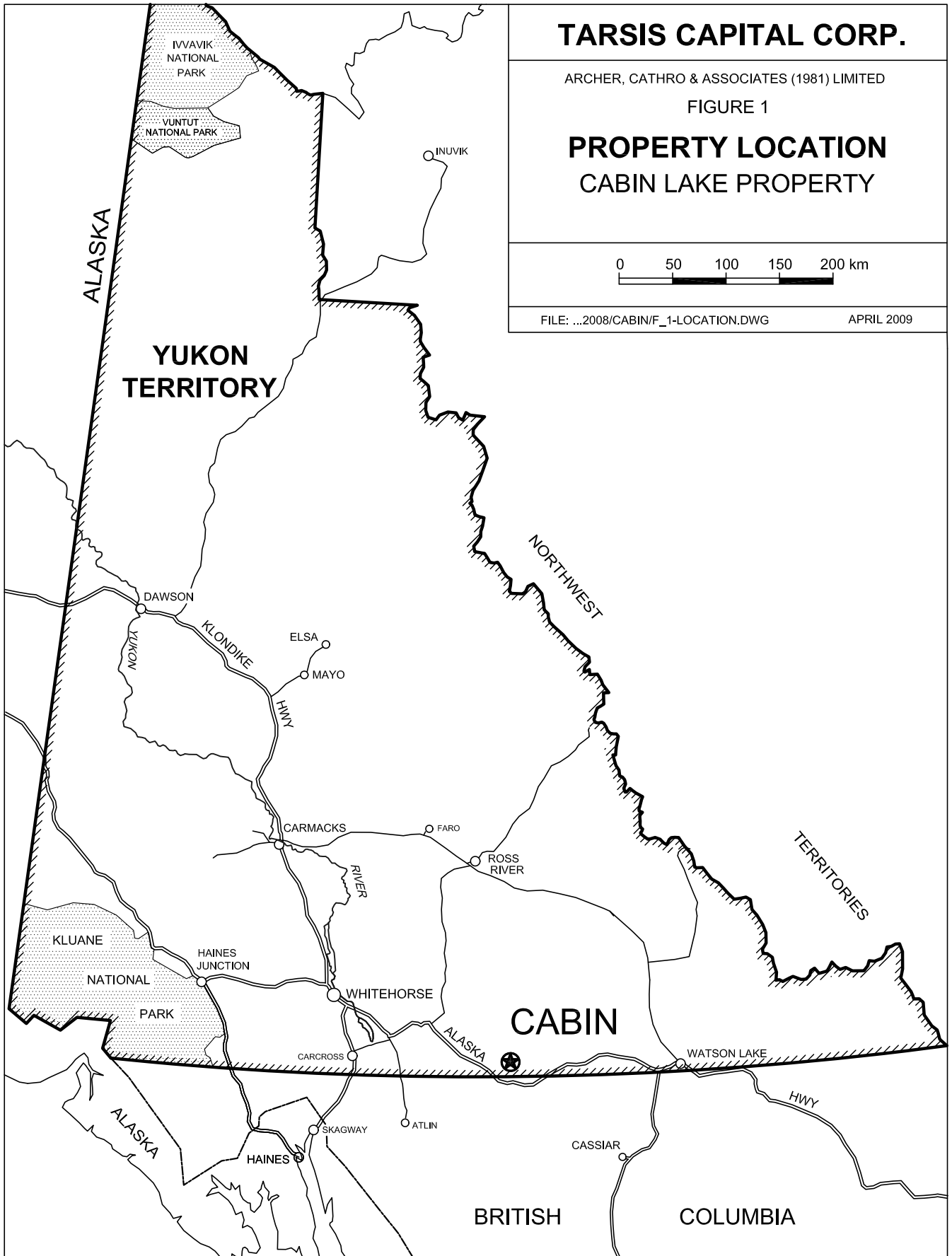
FIGURE 1

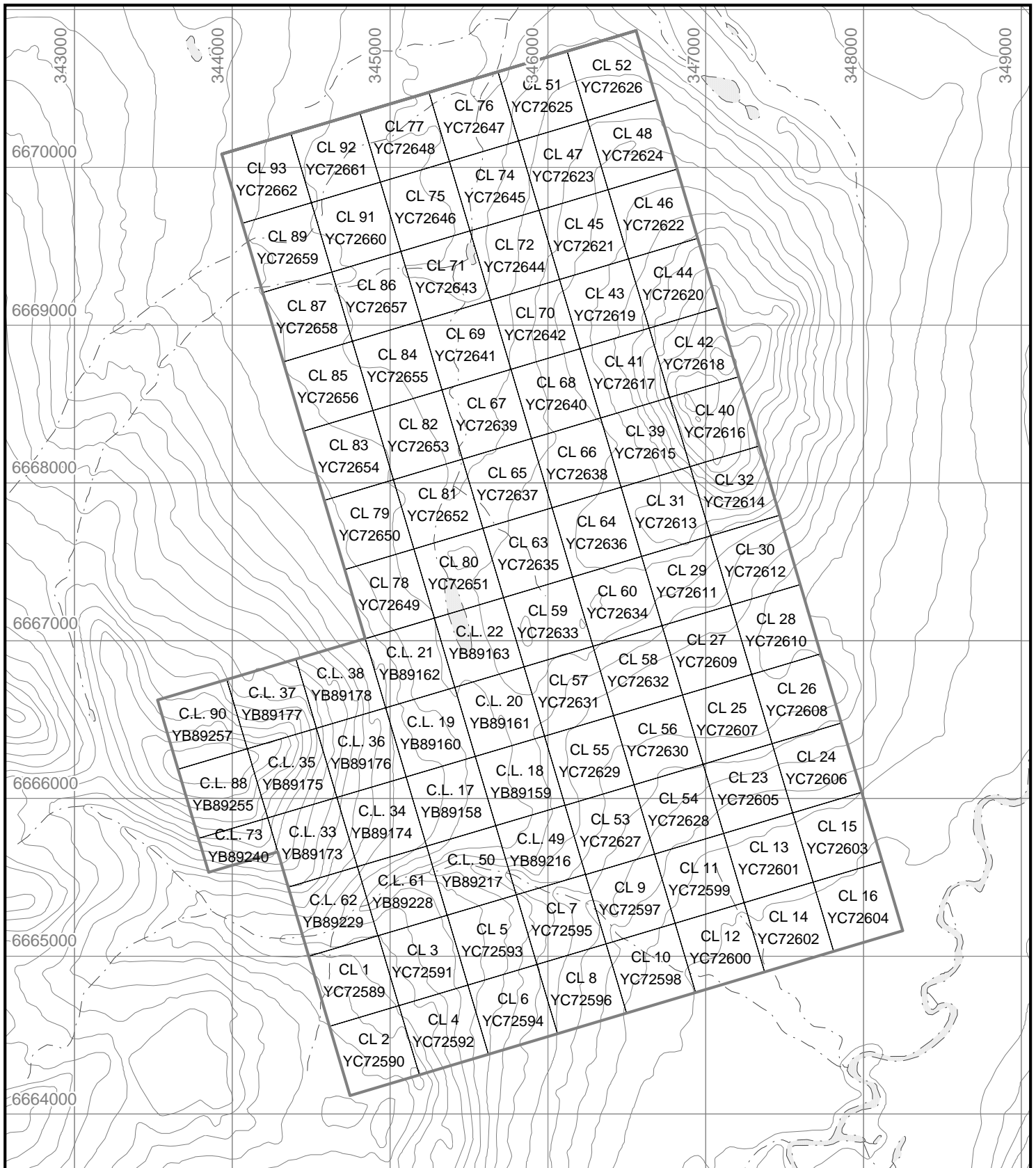
PROPERTY LOCATION CABIN LAKE PROPERTY



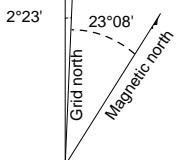
FILE: ...2008/CABIN/F_1-LOCATION.DWG

APRIL 2009





T.N.



Annual change decreasing 23'

TARSIS CAPITAL CORP.

FIGURE 2
 ARCHER, CATHRO & ASSOCIATES (1981) LIMITED
CLAIM LOCATION
CABIN LAKE PROPERTY



UTM ZONE 9W, NAD 83, 105 B/4

HISTORY

In 1980 the Cabin Lake area was prospected by Cordilleran Engineering for Regional Resources Ltd. but no claims were staked. In 1996 Fairfield Minerals Ltd. carried out reconnaissance stream sediment sampling and follow-up prospecting programs in the area, the results of which led the company to stake the CL 1-100 claims. After an initial program of prospecting, geological mapping, geochemical sampling and airborne geophysics, the company staked CL 101-122 in July 1997. In 1998, Fairfield carried out Induced Polarization (IP) surveys, soil geochemical sampling, prospecting and excavator trenching.

In 2002 Fairfield was amalgamated with Almaden Resources Corporation to form Almaden Minerals Ltd. and the title of the claims for the Cabin Lake property was subsequently transferred and later purchased by Tarsis in April 2007.

GEOMORPHOLOGY

The property lies along the northwestern flank of the Cassiar Mountains and covers 1945 hectares north and east of Hazel Ridge down to the Smart River at the southeastern edge of the property. Local topography is generally moderate to steep, with elevations ranging from 1000 to 1700 meters. A local drainage in the west central part of the property, referred to as Copper Creek, drains much of the central and southern portion of the property, and flows easterly through a steep-walled valley. The northern and eastern CL claims drain to the north, via Antennae Lake and its outflow, Meadow Creek. These creeks ultimately flow into the Pacific Ocean via the Teslin and Yukon Rivers.

Bedrock exposure is generally sporadic at higher elevation and notably poor in topographically lower areas where alluvium and glacial till are prevalent. The CL claims are underlain by intermittent permafrost, particularly in areas of thick moss and dense forest cover.

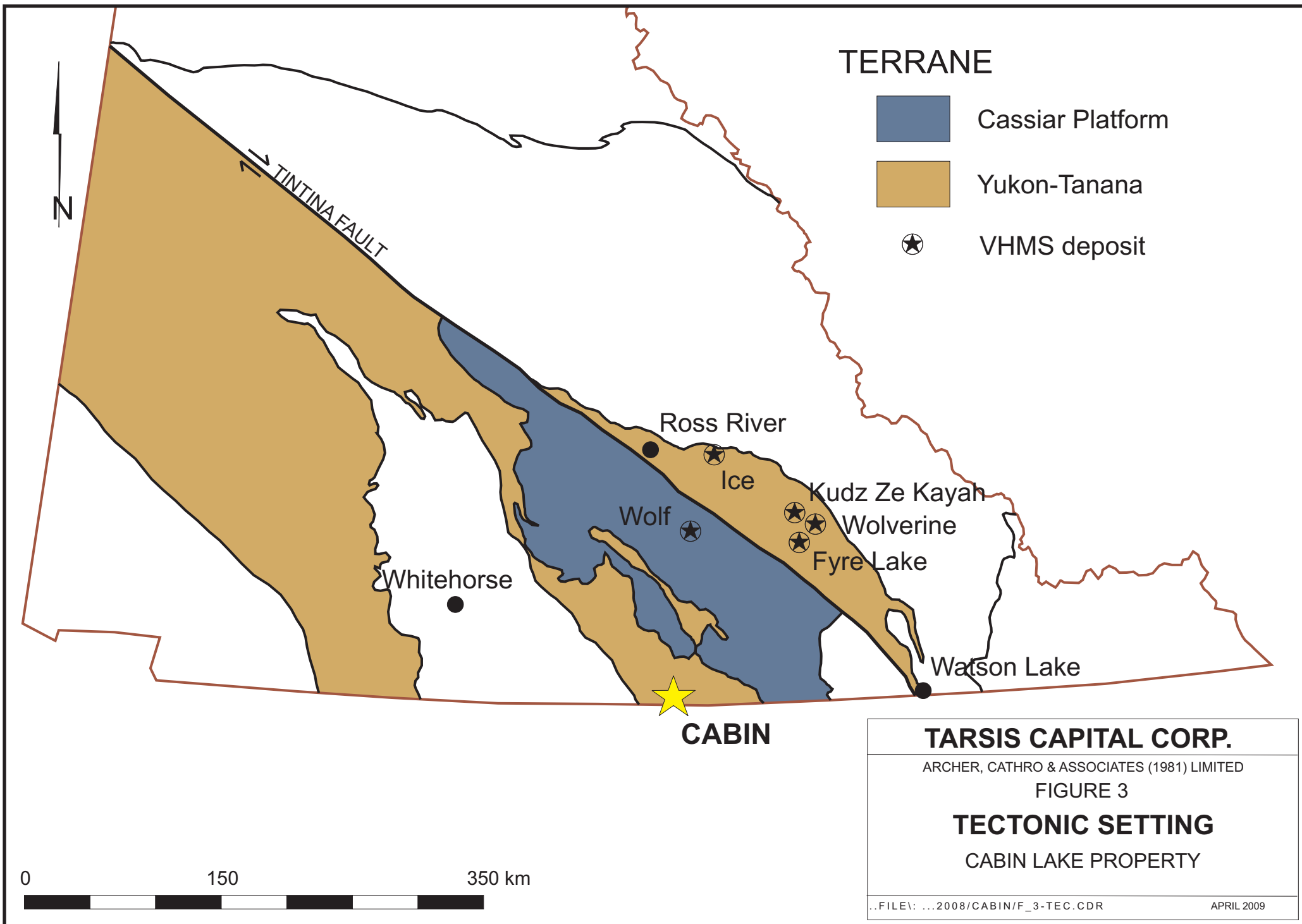
Vegetation consists of thick stands of spruce, and fir on lower slopes, that become interspersed with grassy subalpine meadows at higher elevations. Swamps with willow, dwarf birch, alder and stunted conifers are interspersed throughout the property. Treeline in the vicinity of the Cabin Lake property occurs at 1450 m.

GEOLOGY

Regional Geology

The property lies within a belt of Yukon-Tanana Terrane rocks on the southwest side of the Tintina Fault Zone (Figure 3). Yukon-Tanana Terrane rocks underlie much of west-central Yukon, including a displaced block immediately northeast of the Tintina Fault Zone referred to as the Finlayson Lake District, which hosts a number of VHMS deposits and prospects.

The most recent classification of the Yukon-Tanana Terrane southwest of the Tintina Fault Zone near the B.C.-Yukon border was addressed in a special paper published by the Geological Association of Canada, 2006. This portion of the cordillera is segregated into three belts referred



TERRANE

- Cassiar Platform
- Yukon-Tanana
- VHMS deposit

CABIN

TARSIS CAPITAL CORP.

ARCHER, CATHRO & ASSOCIATES (1981) LIMITED

FIGURE 3

TECTONIC SETTING

CABIN LAKE PROPERTY

to as the eastern, central and western belts (Roots et al., 2006) and all three belts comprise stratigraphy associated with Permian and older sedimentation, arc related volcanism and coeval intrusions. Stratigraphy within all belts has been intruded by Eocene to early Jurassic intrusions.

The western belt hosts the Cabin Lake property and is bound by the strike-slip Teslin Fault to the west and an unnamed fault to the northeast (Figure 4). Stratigraphic units belong mostly to the Big Salmon Complex and comprise bimodal arc-volcanic rocks, phyllite, siliceous metasedimentary rocks and minor carbonate units. Coeval orthogneiss is common throughout the sequence and ranges in age from late Devonian to Jurassic. The upper portion of the volcanic sequence of the Big Salmon Complex is marked by a rose coloured manganiferous metachert believed to represent an exhalative volcanic pulse (Mihalynuk et al, 2006). The metavolcanic rocks of the Big Salmon Complex are considered age equivalent to the Finlayson Assemblage northeast of the Tintina Fault Zone (Colpron et al, 2006). The magnetic cycles associated with these rocks span upper Devonian through mid Mississippian and are age equivalent to the Finlayson and Wolverine Magmatic Cycles (Figure 5).

Klinkit Group unconformably overlies stratigraphy of the Big Salmon Complex. It consists of pale coloured marble and intermediate to mafic tuffs plus volcanic-derived metasedimentary rocks, with lesser volcanic flows, quartz sandstone and interlayered dark siltstone. Volcanic rocks are more abundant near the base of the succession. These sequences were deposited between Middle Mississippian and Permian.

The main lithologies in the vicinity of the Cabin Lake property are summarized on the Table I.

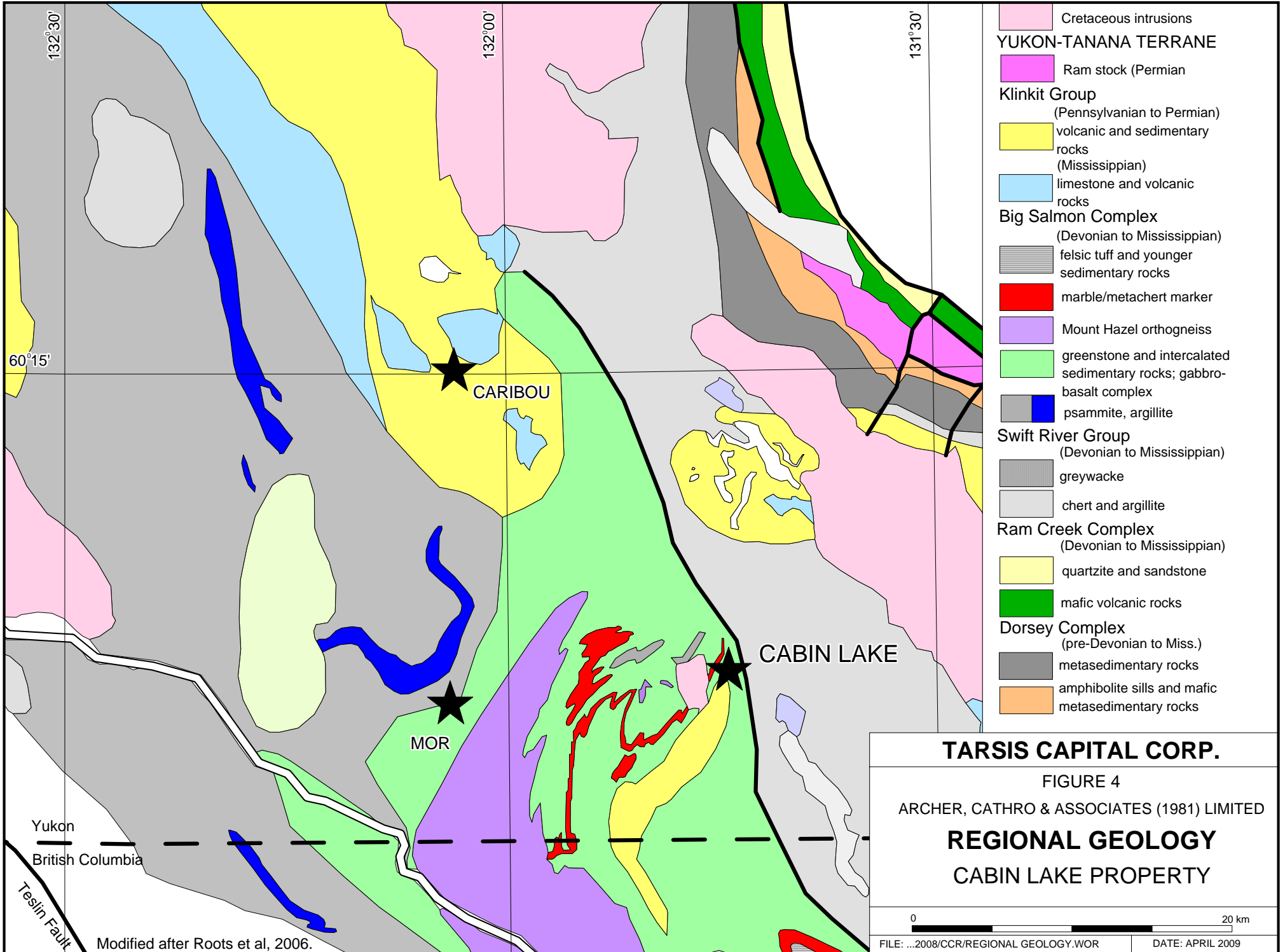
Table I: Main Lithological Units

<u>Quaternary</u> Overburden	Glacial till, lateral and terminal moraines and glaciofluvial outwash
<u>Mid-Cretaceous or Early Tertiary</u> Cassiar Suite	Granodiorite and biotite-quartz monzonite porphyry
<u>Pennsylvanian to Permian</u> Klinkit Group	Volcaniclastic and sedimentary rocks
<u>Mississippian</u> Klinkit Group	Limestone and volcanic rocks
<u>Devonian to Mississippian</u> Big Salmon Complex	Mount Hazel orthogneiss Greenstone and intercalated sedimentary rocks

(Roots et al, 2006)

Property Geology

The Cabin Lake property is underlain by siliceous metasedimentary and metavolcaniclastic rocks believed to be part of the Devono-Mississippian Big Salmon Complex and metavolcaniclastic schist of the Klinkit Group. These rocks have been locally intruded by two Early Jurassic (Figure 6) intrusions in the southern part of the property and a cretaceous intrusion in the northern part of the claim block. Previous authors (Ritcey and Balon, 1998) segregated these



TARSIS CAPITAL CORP.

FIGURE 4

ARCHER, CATHRO & ASSOCIATES (1981) LIMITED

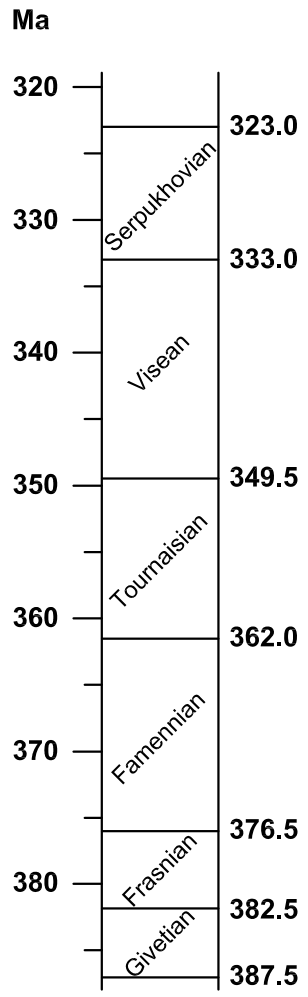
REGIONAL GEOLOGY

CABIN LAKE PROPERTY

Modified after Roots et al, 2006.

MISSISSIPPIAN

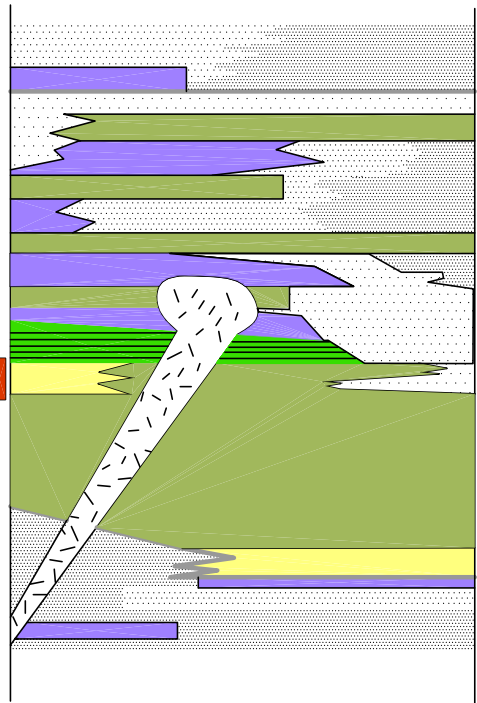
DEVONIAN



**WOLVERINE
MAGMATIC
CYCLE**

**FINLAYSON
MAGMATIC
CYCLE**

CABIN?



**KLINKIT
ASSEMBLAGE**

MAP UNIT

CPK

**FINLAYSON
ASSEMBLAGE
(clastic dominated)**

DMFs

**FINLAYSON
ASSEMBLAGE
(volcanic dominated)**

DMFvi, DMFvf

**SNOWCAP
ASSEMBLAGE**

Ds

- lower to mid Mississippian granite
- exhalite (manganiferous "crinkle" chert)
- felsic volcanic sequence
- mafic to intermediate volcanic sequence
- marble
- conglomerate
- quartzite
- psammite

after Mihalynuk et al (2000)

TARSIS CAPITAL CORP.

ARCHER, CATHRO & ASSOCIATES (1981) LIMITED

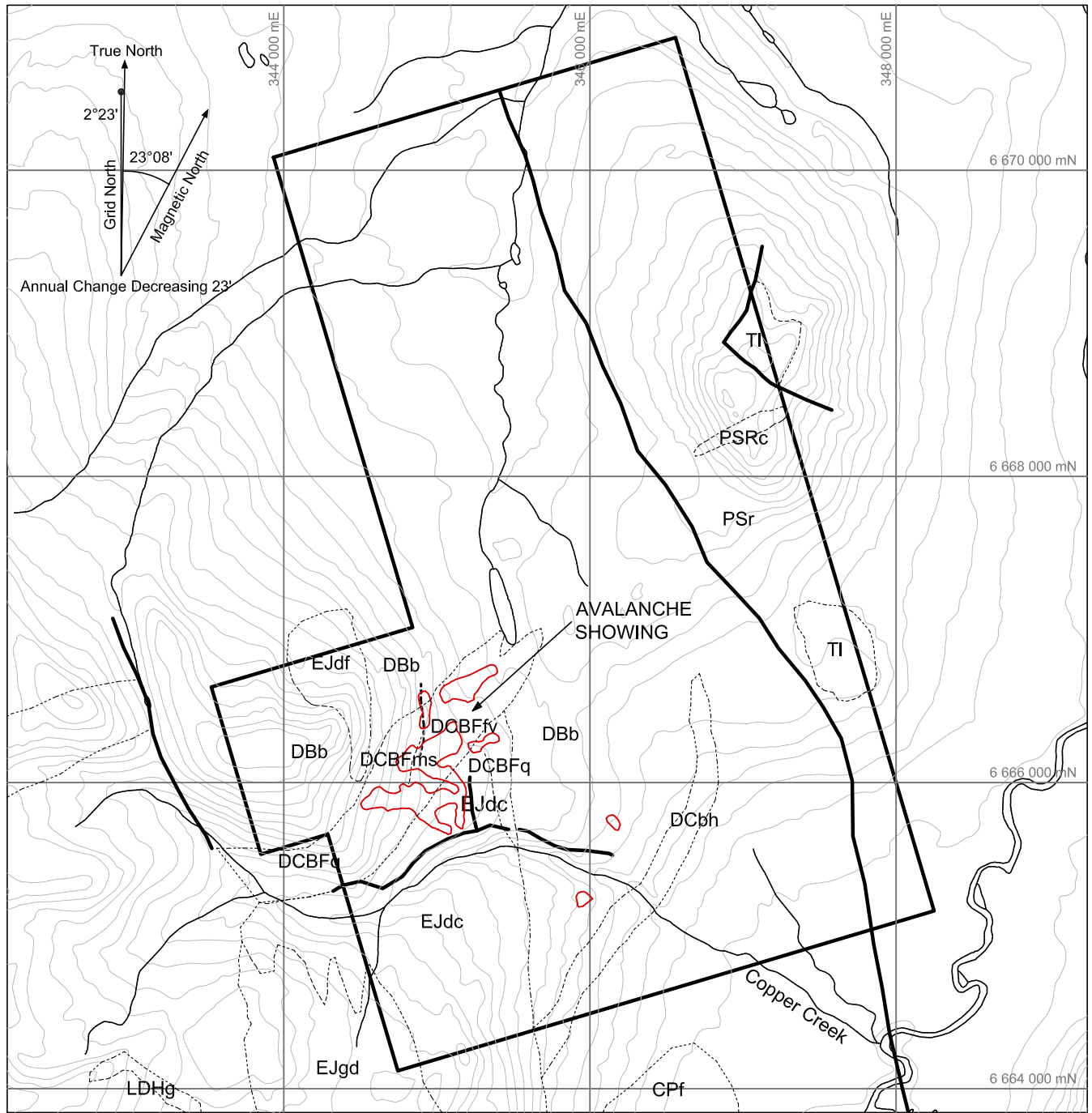
FIGURE 5

STRATIGRAPHIC COLUMN

YUKON TANANA TERRANE

TESLIN AREA

YUKON AND NORTHERN BRITISH COLUMBIA



- EJgd Granodiorite: medium-grained with lesser quartz monzonite
- EJdf Diorite: fine-grained undeformed
- EJdc Diorite: coarse-grained sheared and chloritized
- TL Black slate and phyllonite, Ilmey metasandstone and pebble conglomerate; minor dark grey limestone
- Cpf Upper clastic member: brown weathering indurated meta-siltstone and sandstone
- BIG SALMON COMPLEX**
- DCBFfv Quartz-sericite schist felsic metavolcanics
- DCBFms Siliceous schist, sulphide-bearing probably metasediment
- DCBFq Quartz-muscovite schist 'quartzite' and psammite
- LDHg Meta-diorite
- DCbh Mount Hazel Metachert: Laminated quartzite (crinkle chert)
- DBb Greenstone: metavolcanics and metasediments
- Klinkit Group**
- PSr Dark coloured quartz plagioclase grit, meta-sandstone
- PSRc Light grey to beige limestone and marble lenses
- >200 ppm Cu in soils after Roots et. al., 2004 and Ritcey and Balon 1997

PROPERTY GEOLOGY

ARCHER, CATHRO & ASSOCIATES (1981) LIMITED

FIGURE 6

PROPERTY GEOLOGY

CABIN LAKE PROPERTY

NAD 83, UTM ZONE 9
105B/04

FILE: ...2008/CABIN/F_5-GEO.DWG	DATE: APRIL 2009
---------------------------------	------------------

regional units into several distinct map units as described below. The individual units have been correlated to the respective “Complex” or “Group”.

The stratigraphic units exposed in the central part of the Cabin Lake property north of Copper Creek are part of the Big Salmon Complex. The oldest unit is composed of variably deformed and metamorphosed andesitic to dacitic tuffs and flows (DBb). This is overlain by gently eastward dipping schistose metaquartzite/psammite with micaceous partings (DCBFq). Pyritic purple/grey quartz-rich schist (DCBFms) is documented near the break in slope on the central and western claims. These rocks are overlain by variably pyritic, pale grey quartz-sericite schist (DCBFfv) that has undergone intense clay alteration.

The classification of the intrusive rocks in the southern part of the property is ambiguous. Regional mapping by Roots et al suggest these rocks are part of the Devonian-Mississippian Mount Hazel orthogneiss but descriptions by Ritcey and Balon are of undeformed porphyritic bodies composed of either fine- to medium-grained grey diorite/granodiorite (EJdf) or medium- to coarse-grained grey magnetite bearing biotite granodiorite with lesser pink-grey quartz monzonite (EJgd). EJdf has been mapped locally cutting the strata in the west central part of the claim block. Sheared and chloritized medium to coarse-grained metadiorite (EJdc) is exposed at several localities north of Copper Creek.

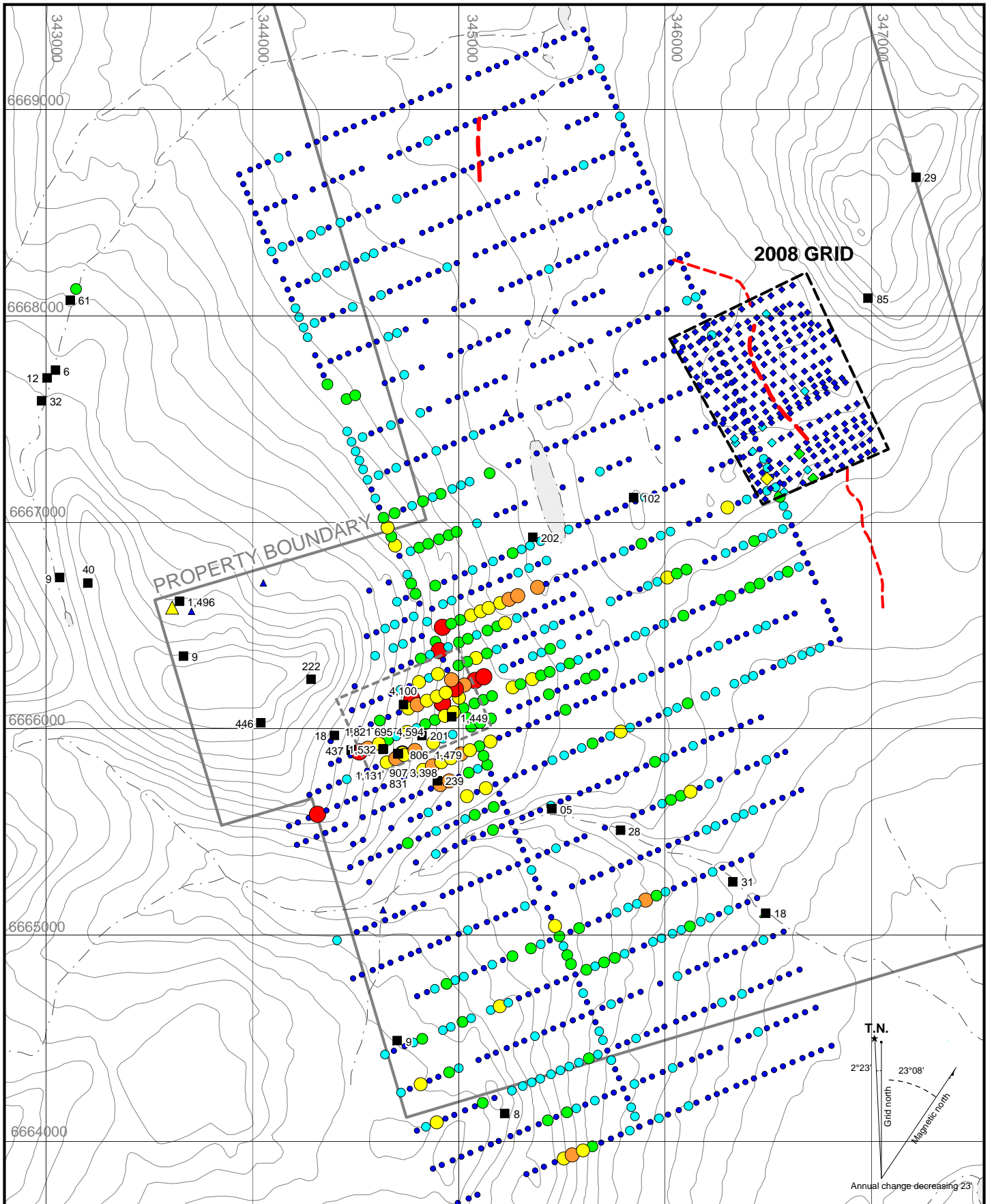
Quartz veining is locally common on the claim block and is most prevalent near brittle fault zones in the central and northwestern part of the property. Structural trends are interpreted from air photos to be oriented roughly east and north-northwest.

MINERALIZATION AND GEOCHEMISTRY

Initial prospecting by Fairfield outlined several “kill zones” in the southwestern part of the claim block where disseminated and semi-massive bands of pyrite and lesser chalcopyrite were identified within the felsic metavolcanic stratigraphy. Sulphide mineralization is interpreted to be stratabound. Chip samples from excavator trenches returned up to 0.35% Cu across 18.4 m. The true thickness of the exposure, however, is unknown.

Grid soil sampling over a 1200 by 1200 m area outlined a strong 900 m by 500 m copper-in-soil geochemical anomaly with values greater than 150 ppm to a peak of 6324 ppm. Accompanying lead and zinc values in this area are generally low yielding peak values up to 220 ppm and 263 ppm, respectively. Historical survey results for copper, silver, lead and zinc are illustrated on Figures 7 to 10. All other pathfinder elements were subdued.

Most of the prospecting conducted on the property was localized in the vicinity of the main soil geochemical anomaly where pyrite and chalcopyrite were identified in talus and several bedrock exposures. The highest concentration of sulphide was obtained from a purple weathering blocky schist outcrop suggested to contain up to 5% chalcopyrite. A sample of this material reportedly returned 1.21% copper, 4.0 g/t silver and low values for all other pathfinder elements. All other talus and outcrop samples yielded less than 1% copper.



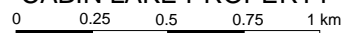
Copper (ppm)

1997 silt	2008 soil	1997 soil	Copper (ppm)
▲	◆	●	≥1,000
▲	◆	●	≥500 < 1,000
▲	◆	●	≥200 < 500
▲	◆	●	≥100 < 200
▲	◆	●	≥50 < 100
▲	◆	●	0 < 50

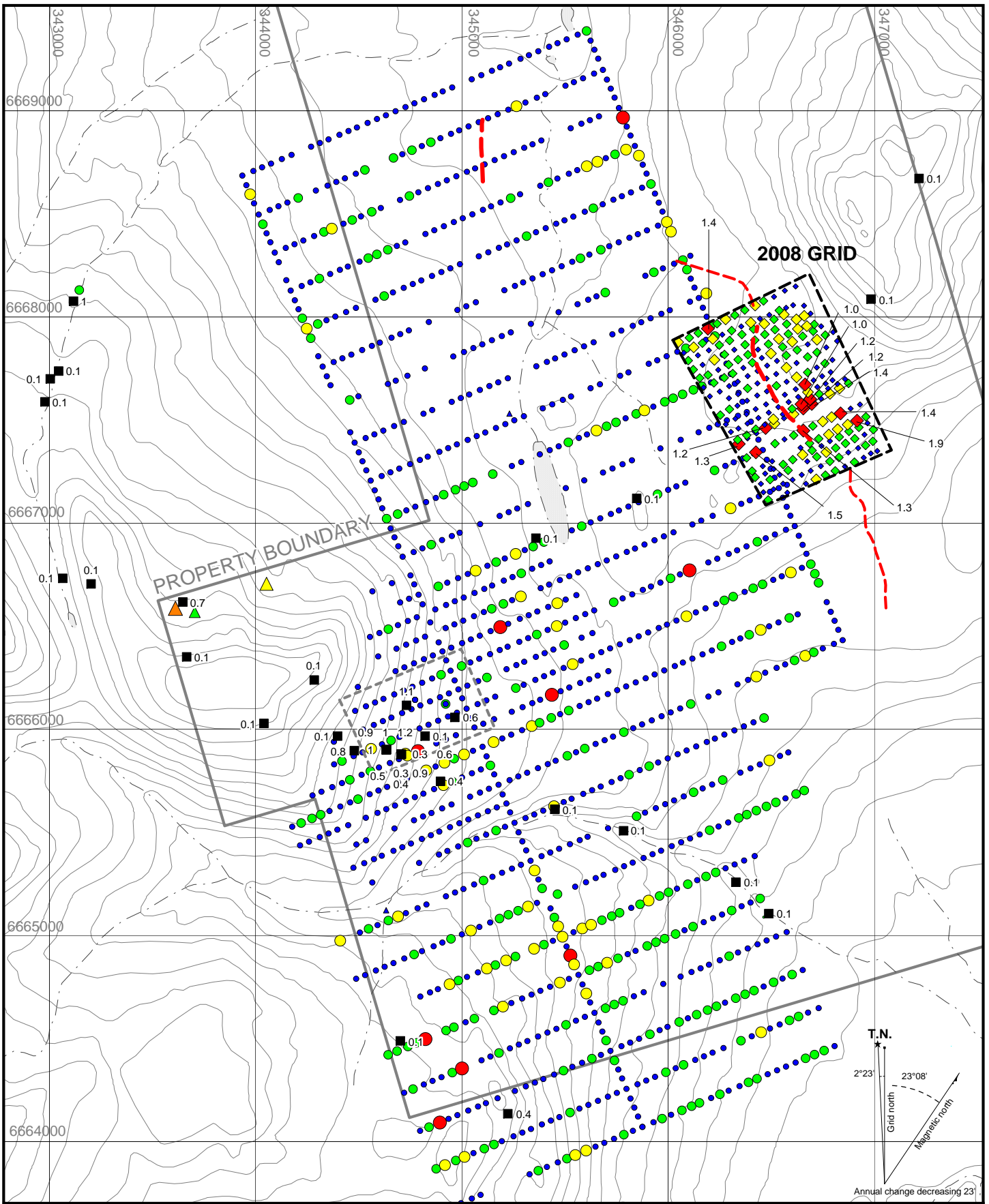
- 8 1997 rock sample (ppm Cu)
- Area of historic trenching
- - - V-TEM anomaly (primary, secondary)

TARSIS CAPITAL CORP.

FIGURE 7
 ARCHER, CATHRO & ASSOCIATES (1981) LIMITED
COPPER SOIL GEOCHEMISTRY
 CABIN LAKE PROPERTY



UTM ZONE 8W, NAD 83, 105 B/4



Silver (ppm)

1997 silt 2008 soil 1997 soil

- | | | | |
|---|---|---|------------|
| ▲ | ◆ | ● | ≥1 |
| ▲ | ◆ | ● | ≥0.5 < 1 |
| ▲ | ◆ | ● | ≥0.3 < 0.5 |
| ▲ | ◆ | ● | 0 < 0.3 |

■ 8

1997 rock sample (ppm Ag)



Area of historic trenching



V-TEM anomaly (primary, secondary)

TARSIS CAPITAL CORP.

FIGURE 8
ARCHER, CATHRO & ASSOCIATES (1981) LIMITED
SILVER SOIL GEOCHEMISTRY
CABIN LAKE PROPERTY

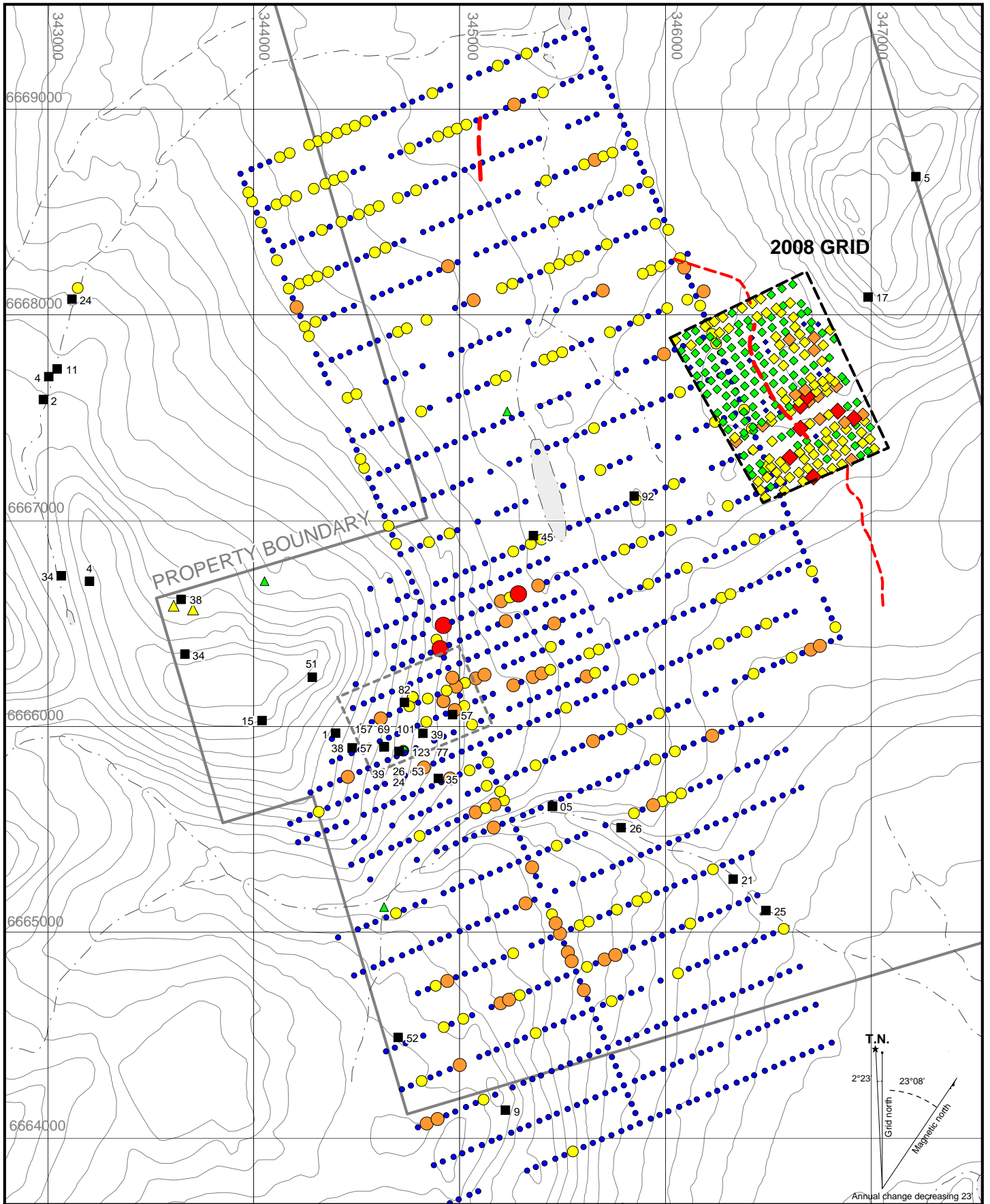
0 0.25 0.5 0.75 1 km

UTM ZONE 8W, NAD 83, 105 B/4

...2008/CABIN/FIGURES/CABIN_AG.WOR

DATE: APRIL 2009

T.N.
 2°23' Grid north
 23°08' Magnetic north
 Annual change decreasing 23'



Zinc (ppm)

1997 silt	2008 soil	1997 soil	
▲	◆	●	≥ 200
▲	◆	●	≥ 100 < 200
▲	◆	●	≥ 50 < 100
▲	◆	●	≥ 20 < 50
▲	◆	●	0 < 20

■ 8	1997 rock sample (ppm Zn)
⋯	Area of historic trenching
---	V-TEM anomaly (primary, secondary)

TARSIS CAPITAL CORP.

FIGURE 10
 ARCHER, CATHRO & ASSOCIATES (1981) LIMITED
ZINC SOIL GEOCHEMISTRY
 CABIN LAKE PROPERTY

0 0.25 0.5 0.75 1 km

UTM ZONE 8W, NAD 83, 105 B/4

T.N.
 2°23' 23°08'
 Grid north
 Magnetic north
 Annual change decreasing 23

Trenching undertaken by a track mounted Kubota KH41 excavator across targets in the main copper-in-soil geochemical anomaly exposed predominantly quartz rich schist cut by diorite to andesite dykes. The best results were obtained from trench CLT9-3 where a series of continuous samples across 18.4 m returned 0.35% copper. None of the samples collected from the trenches were significantly elevated for lead, silver and zinc.

In 2008, two hundred thirty-nine soil samples were collected on a 900 x 700 m grid on the eastern side of the property over a prominent VTEM conductor identified by the 2007 survey (Figures 7 to 10). Samples were taken at 50 m intervals on lines spaced 50 m apart and were located by means of compass and hip-chain surveys with frequent checks using handheld GPS units. Sample sites are marked by aluminum tags inscribed with the sample numbers and affixed to 0.5m wooden lath that were driven into the ground. Soil samples were collected from 10 to 30 cm deep holes dug by mattock. They were placed into individually pre-numbered Kraft paper bags.

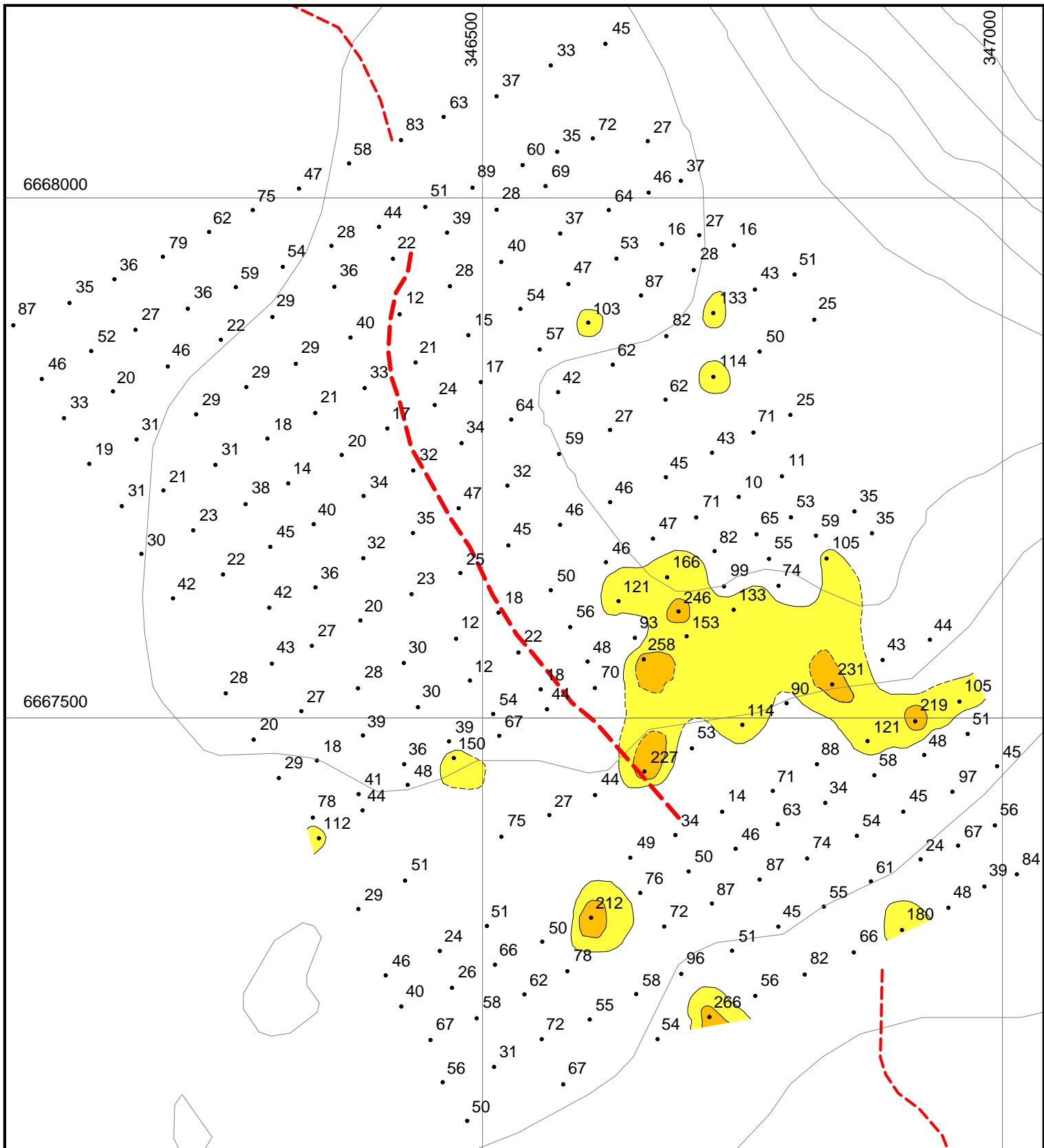
Soil samples were flown from the Cabin Lake property to the Mor exploration camp by helicopter and transported from there to Whitehorse by truck, escorted by an Archer Cathro representative. The samples were then shipped by commercial carrier to ALS Chemex in North Vancouver, B.C. where they were dried, screened to -180 microns, dissolved in aqua regia solution and then analyzed for 35 elements using the inductively coupled plasma with atomic emission spectroscopy technique (ME-ICP41). Analytical certificates are contained in Appendix II.

Soil sampling efforts were often frustrated by thick glacial till mantling most of the grid and as a result values are generally subdued. Copper and zinc are the most anomalous of the VHMS indicator elements and outline several semi-coincident spot anomalies on either side of a prominent VTEM conductor as illustrated on Figures 11 and 12.

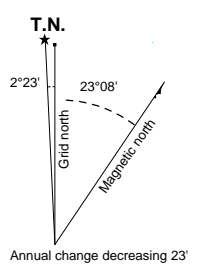
PRE 2007 GEOPHYSICAL SURVEYS

Aerodat Inc carried out an airborne geophysical survey employing a five frequency electromagnetic system and a high sensitivity cesium vapor magnetometer over the entire property, in June 1997 (Young, 2003).

The largest aeromagnetic feature on the Cabin Lake property is the relatively high field area underlain by granodiorite in the southwestern quadrant, which is in sharp contrast to an elongate zone of low total magnetic field that extends from the southern boundary of the claim group, along the eastern flank of the pluton, and northward into the soil geochemical grid. Dioritic rocks to the northwest of the grid may be indicated, at least in part, by a relatively weak magnetic high. The northern part of the large low-magnetic swath may reflect the presence of metamorphosed felsic volcanic rocks (quartz-sericite schist) in the grid area (and extending to the east), whereas the more intense low extending south of Copper Creek likely represents either the continuation of felsic units or a zone of hydrothermal alteration along the intrusive contact. In the core of this magnetic low, a single high amplitude EM conductor approximately 300 meters long. The only other high amplitude conductors are a series of discontinuous linear zones that appear to



- Main VTEM anomaly
- Secondary VTEM anomaly
- 56 • Soil sample location, ppm Zinc
- >200 ≤ 400 ppm Zn
- >100 ≤ 200 ppm Zn



TARSIS CAPITAL CORP.

FIGURE 12

ARCHER, CATHRO & ASSOCIATES (1981) LIMITED
2008 ZINC SOIL GEOCHEMISTRY
CABIN PROPERTY



correspond with the interpreted contact between Big Salmon Complex and the Swift River Group near the eastern property boundary.

An induced polarization geophysical survey employing a 3 kw transmitter and 6 channel receiver was carried out in two phases, over 7050 meters of cut line, by Amerok Geosciences Ltd. in September 1997. This survey was undertaken primarily to determine the subsurface extent of mineralization discovered in the vicinity of the Avalanche Showing. Survey lines were cut and surveyed at 100 meter spacings across the main mineralized zone and were established at 200 meter spacings to the north, east and south of the main mineralized zone.

Technical problems were encountered with field equipment along portions of survey lines 4900N, 5000N, 5200N and 5300N. Calculated values of apparent resistivity, and to a lesser degree chargeability, may have been in error for some of the areas. Significant chargeability anomalies were recorded on all survey lines in the grid area and in general, the higher chargeability zones correspond to elevated values of apparent resistivity, although the anomalies rarely coincide directly. Irregular zones of chargeability are also present at depth. A number of higher amplitude anomalies were identified within the broad anomalous areas. The strongest near-surface IP responses on lines correspond roughly with the location of the historical airborne magnetic-EM anomaly.

Additional IP surveys were conducted in 1998 to investigate copper mineralization associated with the felsic volcanoclastic strata. A total of 5.5 line km of surveys were conducted and confirmed the existence of highly chargeable zones in the vicinity of the 1997 anomalies (Smith, 1998).

2007 GEOPHYSICAL SURVEY

Geotech Ltd. of Aurora, Ontario, performed a 167.4 line-km VTEM and magnetometer survey between September 18 and 29, 2007. The survey was conducted using an Astar B3 helicopter operated by TRK Helicopters and attempted to maintain a mean terrain clearance of 85 m. The block was flown at 100 m line spacings with a tie line spacing of approximately 1000 m. VTEM conductor axes are illustrated on Figures 7 to 12. Survey equipment and techniques used are described in a report contained in Appendix III.

Rendered magnetic inversion data highlight a large positive magnetic anomaly in the southwestern part of the claim block that is associated with the previously mapped undeformed granitic stock. Most of the remaining magnetic clusters are aligned along a northwesterly trend parallel to and subparallel to the local stratigraphic trend.

The most striking EM conductors are located near the eastern edge of the survey and appear to be somewhat coincident with the regional contact mapped between the Big Salmon Complex and Swift River Group. The strongest of the anomalies is a 600 m long section within a much broader anomaly in the east-central part of the survey block that has been modelled by Geotech as a shallowly dipping thick plate that may represent an accumulation of massive sulphide.

Additional modelling and assessment of the VTEM data was carried out by Condor Consulting Inc. of Colorado during 2008. A copy of this report is contained in Appendix IV. This work

suggests relatively continuous EM response along the east-central part of the survey is likely associated with a formational conductor at or near the contact of the Big Salmon Complex and the Swift River Group. The most interesting anomaly from the detail interpretation occurs in the northwestern part of the survey where an isolated 600 m long conductor is situated on the western edge of the extensive formational anomaly. The conductor has a weak coincident magnetic signature and is estimated to be roughly 500 m below surface.

The only EM response of consequence in the vicinity of the historical Copper Creek grid soil geochemical anomalies and excavator trenches is a broad weak response likely associated with a porphyry style target. Depth to the top of the anomaly is estimated to be 500 m or greater.

DISCUSSION AND CONCLUSIONS

The Cabin Lake property covers a potential Kuroko style VHMS target in southern Yukon believed to be associated with favourable volcanoclastic stratigraphy of the Yukon-Tarana Terrane. Exploration programs conducted by previous operators identified pyrite and chalcopyrite bearing felsic volcanoclastic strata in the vicinity of a well defined copper-in-soil geochemical anomaly adjacent to an Early Jurassic stock. Soil and rock geochemical results from grid sampling, prospecting traverses and excavator trench sampling yielded elevated copper values but subdued response for other typical Kuroko VHMS pathfinder elements.

The origin of the copper mineralization is somewhat enigmatic at this time and may be associated with a hydrothermal alteration halo in proximity to the nearby intrusion, which reportedly contains chalcopyrite-molybenite-pyrite bearing quartz veinlets. The proximity of the intrusion may also partially account for the sericite and chlorite alteration plus local silification documented in the trenches.

Property-wide VTEM surveys did not identify significant EM conductors associated with the geochemically anomalous volcanoclastic strata in the west central part of the claim block. The strongest VTEM anomaly occurs along the eastern edge of the survey block approximately coincident with the contact between the Big Salmon Complex and Swift River Group. The anomaly most likely to represent a VHMS target is situated in the northeastern part of the claim block but is blind to surface and without additional supportive evidence for this type of target. No further work is recommended at this time.

Respectfully Submitted

Archer, Cathro & Associates (1981) Limited

W.A. Wengzynowski, P.Eng.

REFERENCES

- Colpron M., Nelson, J. L., Murphy, D.C.
 2006 A tectonostratigraphic framework for the pericratonic terranes of the northern Cordillera, in Colpron, M. and Nelson, J.L., eds. *Paleozoic Evolution and Metallogeny of Pericratonic Terranes at the Ancient Pacific Margins of North America, Canadian and Alaskan Cordillera: Geological Association of Canada, Special Paper 45*, p. 1-23.
- Mihalynuk M.G., Nelson J. and Friedman R.M.
 1998 Regional geology and mineralization of the Big Salmon Complex (104 N NE and 104 O NW). *In: Geological Fieldwork 1997, British Columbia Survey Branch, Paper 1998-1*, p. 6-1 to 6-20.
- Mihalynuk, M.G., Friedman, R.M., Devine, F. and Heaman, L.M.,
 2006 Protolith age and deformation history of the Big Salmon Complex, relicts of a Paleozoic continental arc in northern British Columbia, in Colpron, M. and Nelson, J.L., eds., *Paleozoic Evolution and Metallogeny of Pericratonic Terranes at the Ancient Pacific Margins of North America, Canadian and Alaskan Cordillera: Geological Association of Canada, Special Paper 45*, p. 179-200.
- Ritcey, D.H. and Balon, E.A
 1998 1997 Geological, Geochemical, Geophysical and Trenching Report on the Cabin Lake Property (CL 1-2 Claims) May, 1998 (1997 Assessment Report).
- Roots, C.F., Nelson, J.L., Simard, R.-L. and Harms, T.A.,
 2006 Continental fragments, mid Paleozoic arcs and overlapping later Paleozoic arc and Triassic sedimentary strata in the Yukon-Tanana terrane of northern British Columbia and southern Yukon, in Colpron, M and Nelson, J.L., eds., *Paleozoic Evolution and Metallogeny of Pericratonic Terranes at the Ancient Pacific Margin of North America, Canadian and Alaskan Cordillera: Geological Association of Canada, Special Paper 45*, p.154-177.
- Smith G.J
 1998 Induced Polarization survey at the Cabin Lake Property, Smart River Area, Yukon Territory, by Amerok Geosciences Ltd.
- Young, J.R
 2003 Summary Report on the Morley River Gold - VMS Project for Kobex Resources Ltd.

APPENDIX I
STATEMENT OF QUALIFICATIONS

STATEMENT OF QUALIFICATIONS

I, William A. Wengzynowski, geological engineer, with business addresses in Vancouver, British Columbia and Whitehorse, Yukon Territory and residential address at 301 Fairway Drive, North Vancouver, British Columbia, V7G 1L4 do hereby certify that:

1. I am President of Archer, Cathro & Associates (1981) Limited.
2. I graduated from the University of British Columbia in 1993 with a B.A.Sc. in Geological Engineering, Option 1, mineral and fuel exploration.
3. I registered as a Professional Engineer in the Province of British Columbia on December 12, 1998 (Licence Number 24119).
4. From 1983 to present, I have been actively engaged in mineral exploration in the Yukon Territory, Northwest Territories, northern British Columbia and Mexico.
5. I have personally participated in and supervised the fieldwork reported herein.

William A. Wengzynowski, B.A.Sc., P. Eng.

APPENDIX II
CERTIFICATES OF ANALYSIS



ALS Chemex

EXCELLENCE IN ANALYTICAL CHEMISTRY

ALS Canada Ltd.

212 Brooksbank Avenue
North Vancouver BC V7J 2C1

Phone: 604 984 0221 Fax: 604 984 0218 www.alschemex.com

To: ARCHER, CATHRO AND ASSOCIATES (1981)
LIMITED
1016-510 W HASTINGS ST
VANCOUVER BC V6B 1L8

Page: 1
Finalized Date: 15-OCT-2008
Account: F

CERTIFICATE VA08143882

Project: CABIN

P.O. No.:

This report is for 6 Soil samples submitted to our lab in Vancouver, BC, Canada on 8-OCT-2008.

The following have access to data associated with this certificate:

AL ARCHER
VANCOUVER OFFICE

DOUG EATON
BILL WENGZYNOWSKI

JOAN MARIACHER

SAMPLE PREPARATION

ALS CODE	DESCRIPTION
FND-02	Find Sample for Addn Analysis

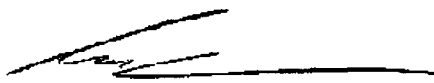
ANALYTICAL PROCEDURES

ALS CODE	DESCRIPTION	INSTRUMENT
Au-AA23	Au 30g FA-AA finish	AAS

To: ARCHER, CATHRO AND ASSOCIATES (1981) LIMITED
1016-510 W HASTINGS ST
VANCOUVER BC V6B 1L8

This is the Final Report and supersedes any preliminary report with this certificate number. Results apply to samples as submitted. All pages of this report have been checked and approved for release.

Signature:


Colin Ramshaw, Vancouver Laboratory Manager



ALS Chemex

EXCELLENCE IN ANALYTICAL CHEMISTRY

ALS Canada Ltd.

212 Brooksbank Avenue

North Vancouver BC V7J 2C1

Phone: 604 984 0221 Fax: 604 984 0218 www.alschemex.com

To: ARCHER, CATHRO AND ASSOCIATES (1981)

LIMITED

1016-510 W HASTINGS ST

VANCOUVER BC V6B 1L8

Page: 2 - A

Total # Pages: 2 (A)

Finalized Date: 15-OCT-2008

Account: F

Project: CABIN

CERTIFICATE OF ANALYSIS VA08143882

Sample Description	Method Analyte Units LOR	Au-AA23 Au ppm 0.005
CC45023		<0.005
CC45069		<0.005
CC45100		<0.005
CC49066		<0.005
CC49128		<0.005
CC49129		<0.005



ALS Chemex

EXCELLENCE IN ANALYTICAL CHEMISTRY

ALS Canada Ltd.

212 Brooksbank Avenue

North Vancouver BC V7J 2C1

Phone: 604 984 0221 Fax: 604 984 0218 www.alschemex.com

To: ARCHER, CATHRO AND ASSOCIATES (1981)
LIMITED
1016-510 W HASTINGS ST
VANCOUVER BC V6B 1L8

Page: 1
Finalized Date: 6-AUG-2008
Account: F

CERTIFICATE VA08096080

Project: CABIN

P.O. No.:

This report is for 239 Soil samples submitted to our lab in Vancouver, BC, Canada on 14-JUL-2008.

The following have access to data associated with this certificate:

AL ARCHER
VANCOUVER OFFICE

DOUG EATON
BILL WENGZYNOWSKI

JOAN MARIACHER

SAMPLE PREPARATION

ALS CODE	DESCRIPTION
WEI-21	Received Sample Weight
LOG-22	Sample login - Rcd w/o BarCode
SCR-41	Screen to -180um and save both

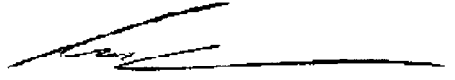
ANALYTICAL PROCEDURES

ALS CODE	DESCRIPTION	INSTRUMENT
ME-ICP41	35 Element Aqua Regia ICP-AES	ICP-AES

To: ARCHER, CATHRO AND ASSOCIATES (1981) LIMITED
1016-510 W HASTINGS ST
VANCOUVER BC V6B 1L8

This is the Final Report and supersedes any preliminary report with this certificate number. Results apply to samples as submitted. All pages of this report have been checked and approved for release.

Signature:


Colin Ramshaw, Vancouver Laboratory Manager



ALS Chemex

EXCELLENCE IN ANALYTICAL CHEMISTRY

ALS Canada Ltd.

212 Brooksbank Avenue

North Vancouver BC V7J 2C1

Phone: 604 984 0221 Fax: 604 984 0218 www.alschemex.com

To: ARCHER, CATHRO AND ASSOCIATES (1981)

LIMITED

1016-510 W HASTINGS ST

VANCOUVER BC V6B 1L8

Page: 2 - A

Total # Pages: 7 (A - C)

Finalized Date: 6-AUG-2008

Account: F

Project: CABIN

CERTIFICATE OF ANALYSIS VA08096080

Sample Description	Method Analyte Units LOR	WEI-21	ME-ICP41	ME-ICP41	ME-ICP41	ME-ICP41	ME-ICP41	ME-ICP41	ME-ICP41	ME-ICP41	ME-ICP41	ME-ICP41	ME-ICP41	ME-ICP41	ME-ICP41	ME-ICP41
		Recvd Wt. kg	Ag ppm	Al %	As ppm	B ppm	Ba ppm	Be ppm	Bi ppm	Ca %	Cd ppm	Co ppm	Cr ppm	Cu ppm	Fe %	Ga ppm
CC45001		0.22	0.4	2.43	9	<10	200	<0.5	<2	0.17	<0.5	9	40	61	3.24	10
CC45002		0.24	0.4	1.49	7	<10	130	<0.5	<2	0.13	<0.5	4	25	22	2.38	10
CC45003		0.26	0.3	1.32	7	<10	80	<0.5	<2	0.13	<0.5	4	27	13	2.40	10
CC45004		0.30	0.2	1.22	9	<10	80	<0.5	<2	0.14	<0.5	4	21	10	2.18	10
CC45005		0.28	0.5	1.58	12	<10	110	<0.5	<2	0.13	<0.5	6	28	15	2.55	10
CC45006		0.32	<0.2	0.63	<2	<10	40	<0.5	<2	0.11	<0.5	2	13	3	0.89	10
CC45007		0.30	0.3	1.12	8	<10	70	<0.5	<2	0.14	<0.5	4	29	8	2.04	10
CC45008		0.28	1.0	1.09	7	<10	160	<0.5	<2	0.19	1.3	4	29	19	1.97	10
CC45009		0.20	1.2	1.24	14	<10	300	<0.5	<2	0.46	3.7	6	40	35	2.55	<10
CC45010		0.26	0.4	2.45	10	<10	160	0.5	<2	0.48	0.5	9	55	30	3.16	10
CC45011		0.24	<0.2	1.16	7	<10	80	<0.5	<2	0.21	<0.5	5	34	13	2.48	10
CC45012		0.22	<0.2	1.25	5	<10	150	<0.5	<2	0.14	<0.5	5	31	16	2.45	10
CC45013		0.18	0.2	0.86	4	<10	90	<0.5	<2	0.12	<0.5	3	26	10	1.52	10
CC45014		0.24	0.3	0.73	2	<10	70	<0.5	<2	0.14	<0.5	2	21	7	1.19	10
CC45015		0.22	0.6	1.70	5	<10	160	<0.5	<2	0.28	1.0	12	38	26	2.59	10
CC45016		0.20	0.6	1.30	7	<10	180	0.7	<2	0.38	0.7	12	29	18	2.49	<10
CC45017		0.22	0.2	2.59	4	<10	130	<0.5	<2	0.53	1.3	9	37	32	3.08	10
CC45018		0.24	1.4	1.38	9	<10	220	<0.5	<2	0.39	3.0	7	37	27	2.76	10
CC45019		0.30	1.2	1.36	7	<10	170	<0.5	<2	0.29	2.3	7	37	20	2.39	10
CC45020		0.22	0.7	1.41	11	<10	130	<0.5	<2	0.14	0.7	5	32	17	2.09	10
CC45021		0.24	0.2	1.14	5	<10	90	<0.5	<2	0.13	<0.5	4	23	11	1.71	10
CC45022		0.26	0.5	1.90	13	<10	100	<0.5	<2	0.16	<0.5	6	40	16	2.67	10
CC45023		0.22	1.2	3.97	41	<10	270	0.7	<2	0.14	<0.5	14	67	78	6.32	20
CC45024		0.24	<0.2	1.59	10	<10	80	<0.5	<2	0.17	<0.5	7	28	20	3.31	10
CC45025		0.24	0.2	1.32	9	<10	80	<0.5	<2	0.15	<0.5	6	25	20	2.67	10
CC45026		0.12	1.3	3.32	14	<10	600	0.9	<2	1.01	<0.5	12	58	72	3.68	10
CC45051		0.22	<0.2	2.59	9	<10	100	0.5	<2	0.14	<0.5	10	41	37	3.97	10
CC45052		0.22	<0.2	3.21	5	<10	80	<0.5	<2	0.31	<0.5	15	122	38	4.04	10
CC45053		0.20	<0.2	1.48	9	<10	140	<0.5	<2	0.15	<0.5	7	34	26	2.74	10
CC45054		0.26	0.2	1.68	7	<10	230	<0.5	<2	0.51	<0.5	12	36	51	2.99	10
CC45055		0.16	<0.2	1.24	5	<10	160	<0.5	<2	0.17	0.6	6	35	17	1.89	10
CC45056		0.22	0.3	0.94	2	<10	90	<0.5	<2	0.19	0.7	4	26	8	1.39	10
CC45057		0.18	0.3	1.50	7	<10	120	0.5	<2	0.34	0.5	6	29	13	1.84	<10
CC45058		0.28	0.2	1.39	3	<10	140	<0.5	<2	0.33	0.5	5	32	12	2.02	10
CC45059		0.20	<0.2	0.66	<2	<10	60	<0.5	<2	0.13	0.5	2	16	4	0.84	<10
CC45060		0.22	0.3	1.66	5	<10	100	<0.5	<2	0.21	0.8	5	35	10	2.77	10
CC45061		0.26	0.4	1.38	4	<10	100	<0.5	<2	0.18	<0.5	5	26	11	1.84	<10
CC45062		0.22	<0.2	1.54	2	<10	150	<0.5	<2	0.18	0.8	7	32	12	2.32	10
CC45063		0.22	0.2	0.88	2	<10	70	<0.5	<2	0.17	0.5	3	22	5	1.64	10
CC45064		0.22	<0.2	1.00	<2	<10	80	<0.5	<2	0.16	<0.5	3	27	8	1.56	10



ALS Chemex

EXCELLENCE IN ANALYTICAL CHEMISTRY

ALS Canada Ltd.

212 Brooksbank Avenue

North Vancouver BC V7J 2C1

Phone: 604 984 0221 Fax: 604 984 0218 www.alschemex.com

To: ARCHER, CATHRO AND ASSOCIATES (1981)

LIMITED

1016-510 W HASTINGS ST

VANCOUVER BC V6B 1L8

Page: 2 - B

Total # Pages: 7 (A - C)

Finalized Date: 6-AUG-2008

Account: F

Project: CABIN

CERTIFICATE OF ANALYSIS VA08096080

Sample Description	Method Analyte Units LOR	ME-ICP41	ME-ICP41	ME-ICP41	ME-ICP41	ME-ICP41	ME-ICP41	ME-ICP41	ME-ICP41	ME-ICP41	ME-ICP41	ME-ICP41	ME-ICP41	ME-ICP41	ME-ICP41	ME-ICP41
		Hg ppm	K %	La ppm	Mg %	Mn ppm	Mo ppm	Na %	Ni ppm	P ppm	Pb ppm	S %	Sb ppm	Sc ppm	Sr ppm	Th ppm
CC45001		<1	0.16	10	0.69	343	1	0.01	23	450	10	0.02	<2	3	14	<20
CC45002		<1	0.11	10	0.35	207	<1	0.01	9	1000	13	0.01	2	2	11	<20
CC45003		<1	0.08	10	0.32	160	<1	0.01	10	520	10	<0.01	<2	3	10	<20
CC45004		<1	0.08	10	0.33	219	<1	0.01	8	600	10	<0.01	<2	2	10	<20
CC45005		1	0.13	10	0.36	233	<1	0.01	12	680	13	0.01	2	3	11	<20
CC45006		<1	0.04	10	0.11	71	<1	0.01	4	280	11	<0.01	<2	1	9	<20
CC45007		<1	0.05	10	0.34	146	2	0.01	13	460	7	0.01	<2	2	10	<20
CC45008		<1	0.05	10	0.27	207	2	0.01	14	500	9	0.02	<2	1	28	<20
CC45009		<1	0.06	10	0.35	337	5	0.01	33	1080	11	0.03	3	1	75	<20
CC45010		1	0.07	10	0.89	358	1	0.03	24	920	11	0.02	<2	3	102	<20
CC45011		<1	0.06	10	0.38	161	1	0.01	15	350	8	0.01	<2	2	27	<20
CC45012		<1	0.05	10	0.43	176	1	0.01	14	410	8	0.02	<2	1	33	<20
CC45013		<1	0.04	10	0.23	93	1	0.01	10	350	8	0.01	<2	1	21	<20
CC45014		<1	0.05	10	0.17	83	<1	0.01	8	240	10	0.01	<2	1	14	<20
CC45015		<1	0.08	10	0.57	541	2	0.01	24	650	10	0.02	<2	2	35	<20
CC45016		<1	0.07	10	0.34	756	1	0.01	12	1230	11	0.04	<2	1	48	<20
CC45017		<1	0.08	10	1.39	456	<1	0.03	17	690	6	0.03	<2	5	101	<20
CC45018		<1	0.06	10	0.45	484	2	0.01	20	630	8	0.02	<2	2	70	<20
CC45019		<1	0.06	10	0.45	364	4	0.01	23	610	8	0.02	<2	2	40	<20
CC45020		<1	0.10	10	0.33	205	2	0.01	17	810	9	0.03	<2	1	15	<20
CC45021		<1	0.08	10	0.25	148	<1	0.01	10	540	11	0.01	<2	2	11	<20
CC45022		<1	0.11	10	0.54	317	<1	0.01	17	720	16	0.01	<2	3	11	<20
CC45023		1	0.36	10	1.06	549	1	0.01	41	1510	15	0.01	<2	7	15	<20
CC45024		<1	0.09	<10	0.56	277	<1	0.01	13	950	8	0.01	<2	4	14	<20
CC45025		<1	0.08	<10	0.55	261	<1	0.01	13	590	6	0.01	<2	3	12	<20
CC45026		<1	0.22	10	0.69	676	3	0.02	38	1800	8	0.13	<2	2	45	<20
CC45051		<1	0.07	10	0.81	384	1	0.01	21	360	8	0.01	<2	4	13	<20
CC45052		1	0.06	<10	2.31	403	<1	0.01	38	230	6	0.01	<2	6	41	<20
CC45053		<1	0.05	10	0.66	268	4	0.01	17	220	8	0.01	<2	3	12	<20
CC45054		<1	0.08	10	0.59	608	6	0.01	15	360	14	0.02	<2	3	28	<20
CC45055		1	0.05	10	0.41	173	2	0.01	16	240	8	0.01	<2	3	18	<20
CC45056		<1	0.05	10	0.35	131	1	0.01	10	420	8	0.01	<2	1	18	<20
CC45057		<1	0.06	10	0.47	217	<1	0.02	22	540	7	0.01	<2	2	34	<20
CC45058		<1	0.05	10	0.42	193	<1	0.01	14	410	8	0.02	<2	2	40	<20
CC45059		<1	0.04	10	0.16	77	<1	0.01	6	210	10	0.01	<2	1	11	<20
CC45060		<1	0.06	10	0.46	196	1	0.01	15	590	9	0.02	<2	3	15	<20
CC45061		<1	0.05	10	0.29	155	<1	0.01	14	380	9	0.02	<2	2	14	<20
CC45062		<1	0.06	10	0.41	242	2	0.01	15	390	11	0.01	<2	3	22	<20
CC45063		<1	0.05	10	0.23	126	<1	0.01	8	300	12	0.01	<2	2	14	<20
CC45064		<1	0.06	10	0.27	148	1	0.01	9	540	13	0.01	<2	2	24	<20



ALS Chemex

EXCELLENCE IN ANALYTICAL CHEMISTRY

ALS Canada Ltd.

212 Brooksbank Avenue

North Vancouver BC V7J 2C1

Phone: 604 984 0221 Fax: 604 984 0218 www.alschemex.com

To: ARCHER, CATHRO AND ASSOCIATES (1981)

LIMITED

1016-510 W HASTINGS ST

VANCOUVER BC V6B 1L8

Page: 2 - C

Total # Pages: 7 (A - C)

Finalized Date: 6-AUG-2008

Account: F

Project: CABIN

CERTIFICATE OF ANALYSIS VA08096080

Sample Description	Method Analyte Units LOR	ME-ICP41	ME-ICP41	ME-ICP41	ME-ICP41	ME-ICP41	ME-ICP41
		Ti %	Ti ppm	U ppm	V ppm	W ppm	Zn ppm
		0.01	10	10	1	10	2
CC45001		0.09	<10	<10	74	<10	78
CC45002		0.12	<10	<10	71	<10	41
CC45003		0.15	<10	<10	76	<10	36
CC45004		0.14	<10	<10	62	<10	39
CC45005		0.15	<10	<10	74	<10	54
CC45006		0.15	<10	<10	33	<10	18
CC45007		0.10	<10	<10	61	<10	48
CC45008		0.06	<10	<10	60	<10	93
CC45009		0.05	<10	<10	82	<10	246
CC45010		0.12	<10	<10	112	<10	99
CC45011		0.11	<10	<10	81	<10	55
CC45012		0.08	<10	<10	78	<10	59
CC45013		0.08	<10	<10	60	<10	35
CC45014		0.08	<10	<10	40	<10	35
CC45015		0.08	<10	<10	74	<10	105
CC45016		0.03	<10	<10	74	<10	74
CC45017		0.15	<10	<10	112	<10	133
CC45018		0.07	<10	<10	81	<10	153
CC45019		0.07	<10	<10	63	<10	258
CC45020		0.04	<10	<10	51	<10	70
CC45021		0.10	<10	<10	47	<10	44
CC45022		0.16	<10	<10	76	<10	67
CC45023		0.14	<10	<10	126	<10	150
CC45024		0.11	<10	<10	78	<10	48
CC45025		0.14	<10	<10	66	<10	44
CC45026		0.03	<10	<10	73	<10	112
CC45051		0.22	<10	<10	90	<10	72
CC45052		0.22	<10	<10	105	<10	55
CC45053		0.16	<10	<10	101	<10	58
CC45054		0.13	<10	<10	91	<10	96
CC45055		0.09	<10	<10	57	<10	51
CC45056		0.09	<10	<10	46	<10	45
CC45057		0.09	<10	<10	40	<10	55
CC45058		0.10	<10	<10	55	<10	61
CC45059		0.10	<10	<10	30	<10	24
CC45060		0.12	<10	<10	71	<10	67
CC45061		0.09	<10	<10	43	<10	56
CC45062		0.14	<10	<10	72	<10	84
CC45063		0.15	<10	<10	57	<10	39
CC45064		0.17	<10	<10	58	<10	48



ALS Chemex

EXCELLENCE IN ANALYTICAL CHEMISTRY

ALS Canada Ltd.

212 Brooksbank Avenue

North Vancouver BC V7J 2C1

Phone: 604 984 0221 Fax: 604 984 0218 www.alschemex.com

To: ARCHER, CATHRO AND ASSOCIATES (1981)

LIMITED

1016-510 W HASTINGS ST

VANCOUVER BC V6B 1L8

Page: 3 - A

Total # Pages: 7 (A - C)

Finalized Date: 6-AUG-2008

Account: F

Project: CABIN

CERTIFICATE OF ANALYSIS VA08096080

Sample Description	Method Analyte Units LOR	WEI-21	ME-ICP41	ME-ICP41	ME-ICP41	ME-ICP41	ME-ICP41	ME-ICP41	ME-ICP41	ME-ICP41	ME-ICP41	ME-ICP41	ME-ICP41	ME-ICP41	ME-ICP41	
		Recvd Wt. kg	Ag ppm	Al %	As ppm	B ppm	Ba ppm	Be ppm	Bi ppm	Ca %	Cd ppm	Co ppm	Cr ppm	Cu ppm	Fe %	Ga ppm
		0.02	0.2	0.01	2	10	10	0.5	2	0.01	0.5	1	1	1	0.01	10
CC45065		0.26	0.3	2.06	6	<10	160	0.5	<2	0.47	0.7	10	43	19	2.89	10
CC45066		0.20	0.2	2.00	5	<10	290	0.6	<2	0.56	0.7	9	42	26	2.41	10
CC45067		0.24	0.3	1.39	15	<10	120	<0.5	<2	0.30	1.3	9	52	21	2.59	10
CC45068		0.14	0.3	1.32	4	<10	100	<0.5	<2	0.26	0.8	5	37	13	1.77	10
CC45069		0.26	0.5	2.35	57	<10	430	0.6	<2	1.09	1.0	17	55	133	3.62	10
CC45070		0.24	<0.2	1.72	5	<10	100	<0.5	<2	0.14	<0.5	8	26	30	2.85	10
CC45071		0.20	<0.2	2.50	<2	<10	120	<0.5	<2	0.31	<0.5	8	23	51	2.89	10
CC45072		0.20	0.3	1.43	9	<10	70	<0.5	<2	0.14	<0.5	7	25	28	3.59	10
CC45073		0.24	0.2	1.83	12	<10	150	<0.5	<2	0.15	<0.5	6	38	26	2.54	10
CC45074		0.18	0.4	1.58	10	<10	70	<0.5	<2	0.18	<0.5	5	36	17	2.38	10
CC45075		0.18	<0.2	0.77	21	<10	40	<0.5	<2	0.07	<0.5	2	17	4	1.47	10
CC45076		0.22	0.5	1.57	8	<10	80	<0.5	<2	0.16	<0.5	5	36	15	2.01	10
CC45077		0.26	0.2	1.52	10	<10	70	<0.5	<2	0.16	<0.5	5	37	15	2.36	10
CC45078		0.30	<0.2	2.93	26	<10	190	0.8	<2	0.15	<0.5	10	57	53	3.62	10
CC45079		0.26	0.3	1.52	5	<10	130	<0.5	<2	0.46	<0.5	9	37	28	2.25	10
CC45080		0.34	0.2	1.05	6	<10	80	<0.5	<2	0.41	<0.5	4	25	11	1.71	10
CC45081		0.32	<0.2	1.52	10	<10	160	<0.5	<2	0.33	<0.5	7	33	23	2.47	10
CC45088		0.26	<0.2	1.09	4	<10	70	<0.5	<2	0.21	<0.5	5	34	13	1.61	<10
CC45089		0.24	0.2	1.05	3	<10	50	<0.5	<2	0.14	<0.5	3	24	8	1.39	10
CC45090		0.22	0.2	1.08	7	<10	90	<0.5	<2	0.13	<0.5	4	23	14	1.76	10
CC45091		0.38	0.4	1.62	9	<10	150	<0.5	<2	0.32	<0.5	8	42	25	2.40	10
CC45092		0.20	0.5	1.73	14	<10	160	<0.5	<2	0.25	<0.5	7	43	32	2.61	10
CC45093		0.28	0.4	2.12	11	<10	100	<0.5	<2	0.26	<0.5	9	38	29	2.94	10
CC45094		0.28	0.3	1.48	9	<10	80	<0.5	<2	0.13	<0.5	4	31	11	2.28	10
CC45095		0.18	0.5	2.73	<2	<10	150	0.5	<2	0.51	<0.5	6	49	14	2.41	10
CC45096		0.24	0.4	1.44	10	<10	90	<0.5	<2	0.15	<0.5	6	36	21	2.35	10
CC45097		0.24	1.4	2.13	14	<10	160	<0.5	<2	0.12	<0.5	5	42	35	2.86	10
CC45098		0.32	0.4	1.11	7	<10	60	<0.5	<2	0.13	<0.5	3	25	8	1.61	10
CC45099		0.24	0.3	0.93	4	<10	60	<0.5	<2	0.12	<0.5	4	37	6	1.44	10
CC45100		0.20	0.5	2.00	44	<10	390	0.6	<2	1.11	<0.5	9	84	29	2.45	10
CC45101		0.18	0.4	0.91	6	<10	60	<0.5	<2	0.11	<0.5	3	24	8	1.54	10
CC45102		0.18	0.2	1.21	8	<10	80	<0.5	<2	0.17	<0.5	5	42	10	2.14	10
CC45103		0.20	0.8	1.33	13	<10	80	<0.5	<2	0.12	<0.5	5	37	14	2.38	10
CC45104		0.20	0.4	0.91	4	<10	70	<0.5	<2	0.10	<0.5	3	19	8	1.30	10
CC45105		0.22	0.7	1.01	11	<10	90	<0.5	<2	0.09	<0.5	3	22	11	1.69	10
CC49006		0.34	0.2	1.23	11	<10	70	<0.5	<2	0.15	<0.5	5	24	9	2.04	10
CC49007		0.32	<0.2	0.82	8	<10	60	<0.5	<2	0.14	<0.5	2	18	4	1.18	10
CC49008		0.38	0.2	1.61	14	<10	90	<0.5	<2	0.14	<0.5	4	31	11	2.11	10
CC49009		0.40	<0.2	1.15	11	<10	80	<0.5	<2	0.15	<0.5	4	31	7	1.87	10
CC49010		0.40	0.2	1.05	13	<10	80	<0.5	<2	0.13	<0.5	4	25	7	2.13	10



ALS Chemex

EXCELLENCE IN ANALYTICAL CHEMISTRY

ALS Canada Ltd.

212 Brooksbank Avenue

North Vancouver BC V7J 2C1

Phone: 604 984 0221 Fax: 604 984 0218 www.alschemex.com

To: ARCHER, CATHRO AND ASSOCIATES (1981)

LIMITED

1016-510 W HASTINGS ST

VANCOUVER BC V6B 1L8

Page: 3 - B

Total # Pages: 7 (A - C)

Finalized Date: 6-AUG-2008

Account: F

Project: CABIN

CERTIFICATE OF ANALYSIS VA08096080

Sample Description	Method Analyte Units LOR	ME-ICP41	ME-ICP41	ME-ICP41	ME-ICP41	ME-ICP41	ME-ICP41	ME-ICP41	ME-ICP41	ME-ICP41	ME-ICP41	ME-ICP41	ME-ICP41	ME-ICP41	ME-ICP41	ME-ICP41
		Hg	K	La	Mg	Mn	Mo	Na	Ni	P	Pb	S	Sb	Sc	Sr	Th
		ppm	%	ppm	%	ppm	ppm	%	ppm	ppm	ppm	%	ppm	ppm	ppm	ppm
		1	0.01	10	0.01	5	1	0.01	1	10	2	0.01	2	1	1	20
CC45065		<1	0.06	10	0.71	351	1	0.02	21	580	9	0.02	<2	3	61	<20
CC45066		<1	0.09	10	0.63	328	1	0.02	30	770	10	0.03	<2	4	69	<20
CC45067		<1	0.07	10	0.58	449	3	0.01	23	570	10	0.02	<2	3	38	<20
CC45068		<1	0.07	10	0.48	164	2	0.01	19	710	6	0.03	<2	2	23	<20
CC45069		<1	0.11	10	0.81	1175	5	0.02	30	580	11	0.04	<2	5	50	<20
CC45070		<1	0.05	10	0.80	292	1	0.01	11	230	10	0.01	<2	3	13	<20
CC45071		<1	0.04	<10	0.98	540	1	0.01	21	110	3	0.01	<2	2	16	<20
CC45072		<1	0.06	10	0.44	409	2	0.01	12	510	9	0.02	<2	3	11	<20
CC45073		<1	0.11	10	0.48	217	1	0.01	20	770	10	0.01	<2	4	18	<20
CC45074		<1	0.10	10	0.50	205	1	0.01	18	520	8	0.01	<2	3	16	<20
CC45075		<1	0.07	10	0.17	105	<1	0.01	5	420	20	0.01	<2	2	7	<20
CC45076		<1	0.06	10	0.45	167	<1	0.01	15	650	10	0.02	<2	3	20	<20
CC45077		<1	0.06	10	0.51	178	1	0.01	18	560	9	0.01	<2	3	18	<20
CC45078		1	0.17	10	0.66	420	1	0.02	32	730	12	0.02	2	4	19	<20
CC45079		<1	0.08	10	0.60	344	1	0.02	28	650	8	0.02	<2	3	24	<20
CC45080		<1	0.06	10	0.29	149	1	0.01	10	240	10	0.02	<2	2	19	<20
CC45081		<1	0.08	10	0.50	207	<1	0.02	17	450	8	0.03	<2	2	35	<20
CC45088		<1	0.07	10	0.41	150	2	0.02	15	290	7	0.02	<2	2	14	<20
CC45089		<1	0.05	10	0.29	109	1	0.01	11	390	8	0.02	<2	2	10	<20
CC45090		<1	0.06	10	0.29	124	<1	0.01	10	350	7	0.02	2	2	12	<20
CC45091		<1	0.09	10	0.62	238	1	0.02	24	760	8	0.02	2	3	23	<20
CC45092		<1	0.16	10	0.48	326	2	0.02	21	800	10	0.05	<2	1	23	<20
CC45093		<1	0.10	10	0.76	211	1	0.01	28	850	7	0.02	<2	3	17	<20
CC45094		<1	0.09	10	0.34	174	<1	0.01	11	540	7	0.01	<2	3	14	<20
CC45095		<1	0.06	10	1.00	315	1	0.10	15	870	9	0.02	<2	4	144	<20
CC45096		<1	0.10	10	0.48	213	1	0.01	21	470	9	0.02	<2	3	17	<20
CC45097		1	0.16	10	0.37	232	2	0.01	19	1100	16	0.02	<2	3	16	<20
CC45098		<1	0.06	10	0.27	123	1	0.01	10	290	11	0.01	<2	2	9	<20
CC45099		<1	0.10	10	0.30	147	<1	0.01	9	310	19	0.01	<2	2	10	<20
CC45100		1	0.13	10	0.68	462	1	0.03	29	1000	9	0.06	<2	3	70	<20
CC45101		<1	0.05	10	0.24	153	<1	0.01	9	440	17	0.02	<2	1	9	<20
CC45102		<1	0.08	10	0.40	212	1	0.02	18	410	17	0.02	<2	2	14	<20
CC45103		<1	0.08	10	0.37	258	2	0.01	14	540	16	0.02	2	3	9	<20
CC45104		<1	0.11	10	0.23	98	2	0.01	8	340	9	0.02	<2	1	11	<20
CC45105		<1	0.08	10	0.19	138	2	0.01	10	550	11	0.01	<2	2	10	<20
CC49006		1	0.06	10	0.38	241	1	0.01	8	550	12	0.01	<2	3	13	<20
CC49007		<1	0.05	10	0.23	97	1	0.01	6	340	12	0.01	<2	2	11	<20
CC49008		<1	0.07	10	0.37	179	2	0.01	12	400	15	0.02	<2	3	11	<20
CC49009		<1	0.06	10	0.32	149	2	0.01	13	510	13	0.01	3	3	12	<20
CC49010		<1	0.06	10	0.29	141	2	0.01	10	490	9	0.01	<2	2	13	<20



ALS Chemex

EXCELLENCE IN ANALYTICAL CHEMISTRY

ALS Canada Ltd.

212 Brooksbank Avenue

North Vancouver BC V7J 2C1

Phone: 604 984 0221 Fax: 604 984 0218 www.alschemex.com

To: ARCHER, CATHRO AND ASSOCIATES (1981)

LIMITED

1016-510 W HASTINGS ST

VANCOUVER BC V6B 1L8

Page: 3 - C

Total # Pages: 7 (A - C)

Finalized Date: 6-AUG-2008

Account: F

Project: CABIN

CERTIFICATE OF ANALYSIS VA08096080

Sample Description	Method Analyte Units LOR	ME-ICP41	ME-ICP41	ME-ICP41	ME-ICP41	ME-ICP41	ME-ICP41
		Ti %	Tl ppm	U ppm	V ppm	W ppm	Zn ppm
		0.01	10	10	1	10	2
CC45065		0.13	<10	<10	78	<10	180
CC45066		0.10	<10	<10	55	<10	66
CC45067		0.09	<10	<10	87	<10	82
CC45068		0.07	<10	<10	58	<10	56
CC45069		0.10	<10	<10	92	<10	266
CC45070		0.30	<10	<10	108	<10	54
CC45071		0.19	<10	<10	59	<10	67
CC45072		0.22	<10	<10	99	<10	50
CC45073		0.11	<10	<10	65	<10	59
CC45074		0.12	<10	<10	61	<10	54
CC45075		0.13	<10	<10	46	<10	28
CC45076		0.11	<10	<10	62	<10	44
CC45077		0.12	<10	<10	72	<10	51
CC45078		0.10	<10	<10	87	<10	89
CC45079		0.10	<10	<10	49	<10	60
CC45080		0.12	<10	<10	55	<10	35
CC45081		0.07	<10	<10	61	<10	72
CC45088		0.11	<10	<10	43	<10	45
CC45089		0.11	<10	<10	41	<10	33
CC45090		0.09	<10	<10	50	<10	37
CC45091		0.10	<10	<10	57	<10	63
CC45092		0.04	<10	<10	71	<10	83
CC45093		0.13	<10	<10	81	<10	58
CC45094		0.09	<10	<10	59	<10	47
CC45095		0.12	<10	<10	75	<10	75
CC45096		0.10	<10	<10	58	<10	62
CC45097		0.09	<10	<10	70	<10	79
CC45098		0.13	<10	<10	47	<10	36
CC45099		0.24	<10	<10	58	<10	35
CC45100		0.08	<10	10	59	<10	87
CC45101		0.19	<10	<10	58	<10	33
CC45102		0.25	<10	<10	63	<10	46
CC45103		0.18	<10	<10	74	<10	52
CC45104		0.08	<10	<10	38	<10	27
CC45105		0.13	<10	<10	55	<10	36
CC49006		0.16	<10	<10	66	<10	42
CC49007		0.15	<10	<10	43	<10	22
CC49008		0.14	<10	<10	65	<10	45
CC49009		0.17	<10	<10	62	<10	40
CC49010		0.13	<10	<10	71	<10	34



ALS Chemex

EXCELLENCE IN ANALYTICAL CHEMISTRY

ALS Canada Ltd.

212 Brooksbank Avenue

North Vancouver BC V7J 2C1

Phone: 604 984 0221 Fax: 604 984 0218 www.alschemex.com

To: ARCHER, CATHRO AND ASSOCIATES (1981)

LIMITED

1016-510 W HASTINGS ST

VANCOUVER BC V6B 1L8

Page: 4 - A

Total # Pages: 7 (A - C)

Finalized Date: 6-AUG-2008

Account: F

Project: CABIN

CERTIFICATE OF ANALYSIS VA08096080

Sample Description	Method Analyte Units LOR	WEI-21	ME-ICP41	ME-ICP41	ME-ICP41	ME-ICP41	ME-ICP41	ME-ICP41	ME-ICP41	ME-ICP41	ME-ICP41	ME-ICP41	ME-ICP41	ME-ICP41	ME-ICP41	ME-ICP41
		Recvd Wt. kg	Ag ppm	Al %	As ppm	B ppm	Ba ppm	Be ppm	Bi ppm	Ca %	Cd ppm	Co ppm	Cr ppm	Cu ppm	Fe %	Ga ppm
		0.02	0.2	0.01	2	10										
CC49011		0.38	<0.2	1.20	10	<10	70	<0.5	<2	0.15	<0.5	4	29	11	1.89	10
CC49012		0.34	<0.2	0.88	11	<10	70	<0.5	<2	0.11	<0.5	3	19	7	1.93	10
CC49013		0.30	<0.2	2.14	8	<10	60	<0.5	<2	0.16	<0.5	5	41	7	3.67	20
CC49014		0.30	0.3	0.90	7	<10	100	<0.5	<2	0.16	1.1	3	24	11	1.37	10
CC49015		0.34	0.3	2.05	8	<10	110	0.5	<2	0.30	<0.5	8	43	23	2.81	10
CC49016		0.30	<0.2	1.90	10	<10	130	<0.5	<2	0.40	<0.5	9	40	27	2.53	10
CC49017		0.28	0.9	2.19	9	<10	240	0.7	<2	0.81	0.8	10	46	30	2.78	10
CC49018		0.28	0.4	1.14	9	<10	100	<0.5	<2	0.12	<0.5	4	27	14	1.60	<10
CC49019		0.38	<0.2	1.29	7	<10	100	<0.5	<2	0.18	<0.5	6	34	13	2.05	10
CC49020		0.42	<0.2	1.05	4	<10	60	<0.5	<2	0.10	<0.5	3	21	8	1.44	10
CC49021		0.30	0.2	1.41	13	<10	80	<0.5	<2	0.11	<0.5	5	30	16	2.51	10
CC49022		0.42	0.4	1.95	15	<10	240	0.6	<2	0.34	<0.5	8	44	28	2.61	10
CC49023		0.34	0.3	2.23	7	<10	120	0.5	<2	0.28	<0.5	8	39	35	2.62	10
CC49024		0.20	0.2	0.67	3	<10	110	<0.5	<2	0.17	0.8	2	17	12	1.06	10
CC49025		0.24	0.7	1.13	17	<10	70	<0.5	<2	0.11	0.6	4	29	18	2.20	10
CC49026		0.28	<0.2	1.18	8	<10	60	<0.5	<2	0.13	<0.5	3	26	8	1.70	10
CC49027		0.28	<0.2	0.98	11	<10	70	<0.5	<2	0.14	<0.5	4	25	10	2.27	10
CC49028		0.36	0.2	1.31	9	<10	70	<0.5	<2	0.14	<0.5	4	27	10	1.93	10
CC49029		0.40	0.3	1.22	9	<10	80	<0.5	<2	0.13	<0.5	3	24	7	1.82	10
CC49030		0.38	0.2	1.36	13	<10	80	<0.5	<2	0.15	<0.5	4	28	9	2.04	10
CC49031		0.52	0.2	1.84	12	<10	100	<0.5	<2	0.18	<0.5	5	37	10	2.24	10
CC49032		0.32	0.3	1.79	12	<10	80	<0.5	<2	0.17	<0.5	6	31	13	2.87	10
CC49033		0.28	0.3	1.00	9	<10	50	<0.5	<2	0.13	<0.5	3	18	9	1.80	10
CC49034		0.26	0.3	1.66	12	<10	90	<0.5	<2	0.16	<0.5	6	30	14	2.79	10
CC49035		0.30	0.2	1.06	7	<10	70	<0.5	<2	0.13	<0.5	2	18	6	1.46	10
CC49036		0.28	<0.2	0.85	7	<10	60	<0.5	<2	0.13	<0.5	2	17	4	1.22	10
CC49037		0.30	0.2	0.85	8	<10	80	<0.5	<2	0.14	<0.5	3	21	5	1.48	10
CC49038		0.26	<0.2	0.84	7	<10	70	<0.5	<2	0.12	<0.5	3	21	6	1.64	10
CC49039		0.32	0.3	1.28	7	<10	70	<0.5	<2	0.14	<0.5	4	29	12	2.23	10
CC49040		0.34	<0.2	1.14	13	<10	60	<0.5	<2	0.15	<0.5	4	28	10	2.19	10
CC49041		0.28	0.6	1.19	6	<10	80	<0.5	<2	0.15	<0.5	4	28	13	1.80	10
CC49042		0.32	0.3	0.94	6	<10	110	<0.5	<2	0.12	<0.5	3	24	10	1.67	10
CC49043		0.28	<0.2	1.01	12	<10	60	<0.5	<2	0.11	<0.5	3	27	11	2.17	10
CC49044		0.34	0.3	1.98	15	<10	100	<0.5	<2	0.25	<0.5	6	48	20	2.94	10
CC49045		0.28	0.2	0.88	8	<10	80	<0.5	<2	0.11	<0.5	2	20	7	1.12	10
CC49051		0.24	<0.2	0.81	3	<10	50	<0.5	<2	0.13	<0.5	2	15	5	1.12	10
CC49052		0.30	0.2	1.34	7	<10	70	<0.5	<2	0.15	<0.5	4	25	8	1.94	10
CC49053		0.22	<0.2	0.96	7	<10	80	<0.5	<2	0.14	<0.5	3	20	6	1.78	10
CC49054		0.24	0.2	1.19	7	<10	90	<0.5	<2	0.16	<0.5	5	24	11	1.91	10
CC49055		0.18	0.2	0.68	4	<10	50	<0.5	<2	0.09	<0.5	1	13	3	0.75	<10



ALS Chemex

EXCELLENCE IN ANALYTICAL CHEMISTRY
ALS Canada Ltd.

212 Brooksbank Avenue
North Vancouver BC V7J 2C1
Phone: 604 984 0221 Fax: 604 984 0218 www.alschemex.com

To: ARCHER, CATHRO AND ASSOCIATES (1981)
LIMITED
1016-510 W HASTINGS ST
VANCOUVER BC V6B 1L8

Page: 4 - B
Total # Pages: 7 (A - C)
Finalized Date: 6-AUG-2008
Account: F

Project: CABIN

CERTIFICATE OF ANALYSIS VA08096080

Sample Description	Method Analyte Units LOR	ME-ICP41	ME-ICP41	ME-ICP41	ME-ICP41	ME-ICP41	ME-ICP41	ME-ICP41	ME-ICP41	ME-ICP41	ME-ICP41	ME-ICP41	ME-ICP41	ME-ICP41	ME-ICP41	ME-ICP41
		Hg ppm	K %	La ppm	Mg %	Mn ppm	Mo ppm	Na %	Ni ppm	P ppm	Pb ppm	S %	Sb ppm	Sc ppm	Sr ppm	Th ppm
CC49011		<1	0.06	10	0.36	155	1	0.01	12	430	8	0.02	2	2	14	<20
CC49012		<1	0.06	10	0.22	156	2	0.01	7	630	8	0.01	2	2	14	<20
CC49013		<1	0.05	<10	1.48	367	1	0.01	6	470	7	0.02	<2	10	23	<20
CC49014		<1	0.04	10	0.16	121	4	0.01	7	450	14	0.03	<2	1	23	<20
CC49015		<1	0.06	10	0.74	233	2	0.02	27	820	6	0.03	2	3	36	<20
CC49016		<1	0.05	10	0.79	320	1	0.02	23	1070	7	0.02	2	3	50	<20
CC49017		<1	0.09	10	0.52	861	2	0.02	22	1880	8	0.09	3	1	66	<20
CC49018		<1	0.07	10	0.30	167	2	0.01	10	490	12	0.01	2	2	17	<20
CC49019		<1	0.06	10	0.44	178	1	0.01	19	470	9	0.01	3	3	13	<20
CC49020		<1	0.04	10	0.20	141	2	0.01	7	580	11	0.01	3	2	16	<20
CC49021		<1	0.05	10	0.34	177	2	0.01	12	540	9	0.02	<2	2	18	<20
CC49022		<1	0.10	10	0.59	363	2	0.02	19	1100	13	0.04	<2	1	37	<20
CC49023		1	0.10	10	0.72	259	1	0.02	31	1030	6	0.03	<2	3	27	<20
CC49024		<1	0.05	10	0.10	72	1	0.01	6	460	10	0.03	2	1	33	<20
CC49025		<1	0.05	10	0.53	141	4	0.01	14	500	9	0.02	<2	2	20	<20
CC49026		1	0.06	10	0.32	138	2	0.01	8	330	10	0.01	<2	2	17	<20
CC49027		1	0.07	10	0.29	204	1	0.01	10	700	9	0.02	<2	2	15	<20
CC49028		<1	0.06	10	0.34	157	2	0.01	12	510	8	0.02	2	2	13	<20
CC49029		<1	0.06	10	0.27	156	2	0.01	9	380	11	0.01	<2	2	12	<20
CC49030		<1	0.07	10	0.36	186	2	0.01	12	400	9	0.02	<2	2	12	<20
CC49031		<1	0.08	10	0.50	217	2	0.01	14	390	15	0.02	<2	3	13	<20
CC49032		<1	0.06	10	0.56	230	1	0.01	10	810	8	0.02	2	3	14	<20
CC49033		<1	0.04	10	0.28	152	1	0.01	6	430	6	0.02	<2	2	11	<20
CC49034		<1	0.10	10	0.48	248	1	0.01	11	660	10	0.01	<2	3	14	<20
CC49035		<1	0.05	10	0.25	121	1	0.01	6	330	12	0.02	<2	2	11	<20
CC49036		<1	0.05	10	0.18	100	1	0.01	5	360	10	0.01	<2	2	10	<20
CC49037		1	0.05	10	0.22	103	1	0.01	7	400	10	0.01	<2	2	12	<20
CC49038		<1	0.05	10	0.22	115	2	0.01	7	510	9	0.01	<2	2	13	<20
CC49039		1	0.06	10	0.38	178	2	0.01	12	610	9	0.02	<2	2	16	<20
CC49040		<1	0.07	10	0.36	163	2	0.01	11	600	12	0.02	2	2	15	<20
CC49041		<1	0.05	10	0.31	132	2	0.01	12	690	9	0.02	<2	2	23	<20
CC49042		<1	0.05	10	0.19	184	1	0.01	9	420	11	0.02	<2	1	19	<20
CC49043		1	0.06	10	0.24	144	2	0.01	9	540	10	0.02	<2	2	14	<20
CC49044		<1	0.07	10	0.67	211	2	0.01	24	850	9	0.03	<2	3	27	<20
CC49045		<1	0.05	10	0.15	79	1	0.01	6	510	10	0.01	<2	1	17	<20
CC49051		1	0.04	10	0.18	94	1	0.01	5	300	8	0.01	<2	1	11	<20
CC49052		<1	0.05	10	0.37	160	1	0.01	7	330	9	0.01	<2	3	15	<20
CC49053		<1	0.06	10	0.28	129	1	0.01	6	540	12	0.01	<2	2	12	<20
CC49054		<1	0.09	10	0.32	143	1	0.01	10	350	8	0.02	2	2	13	<20
CC49055		<1	0.03	10	0.08	58	1	0.01	3	320	10	0.01	<2	1	10	<20



ALS Chemex

EXCELLENCE IN ANALYTICAL CHEMISTRY

ALS Canada Ltd.

212 Brooksbank Avenue

North Vancouver BC V7J 2C1

Phone: 604 984 0221 Fax: 604 984 0218 www.alschemex.com

To: ARCHER, CATHRO AND ASSOCIATES (1981)

LIMITED

1016-510 W HASTINGS ST

VANCOUVER BC V6B 1L8

Page: 4 - C

Total # Pages: 7 (A - C)

Finalized Date: 6-AUG-2008

Account: F

Project: CABIN

CERTIFICATE OF ANALYSIS VA08096080

Sample Description	Method Analyte Units LOR	ME-ICP41	ME-ICP41	ME-ICP41	ME-ICP41	ME-ICP41	ME-ICP41
		Ti %	Ti ppm	U ppm	V ppm	W ppm	Zn ppm
		0.01	10	10	1	10	2
CC49011		0.11	<10	<10	55	<10	32
CC49012		0.15	<10	<10	71	<10	34
CC49013		0.25	<10	<10	173	<10	64
CC49014		0.07	<10	<10	50	<10	42
CC49015		0.10	<10	<10	78	<10	62
CC49016		0.08	<10	<10	79	<10	82
CC49017		0.03	<10	<10	73	<10	133
CC49018		0.12	<10	<10	51	<10	43
CC49019		0.12	<10	<10	53	<10	51
CC49020		0.15	<10	<10	57	<10	25
CC49021		0.11	<10	<10	84	<10	50
CC49022		0.05	<10	<10	76	<10	114
CC49023		0.09	<10	<10	73	<10	62
CC49024		0.06	<10	<10	37	<10	27
CC49025		0.10	<10	<10	76	<10	59
CC49026		0.14	<10	<10	63	<10	32
CC49027		0.15	<10	<10	69	<10	47
CC49028		0.11	<10	<10	53	<10	35
CC49029		0.14	<10	<10	59	<10	32
CC49030		0.14	<10	<10	58	<10	36
CC49031		0.18	<10	<10	67	<10	42
CC49032		0.12	<10	<10	73	<10	49
CC49033		0.13	<10	<10	56	<10	28
CC49034		0.14	<10	<10	74	<10	43
CC49035		0.14	<10	<10	47	<10	27
CC49036		0.14	<10	<10	42	<10	20
CC49037		0.16	<10	<10	51	<10	23
CC49038		0.14	<10	<10	55	<10	25
CC49039		0.12	<10	<10	65	<10	45
CC49040		0.17	<10	<10	82	<10	46
CC49041		0.10	<10	<10	54	<10	46
CC49042		0.09	<10	<10	64	<10	45
CC49043		0.12	<10	<10	76	<10	43
CC49044		0.10	<10	<10	86	<10	71
CC49045		0.10	<10	<10	52	<10	25
CC49051		0.12	<10	<10	37	<10	20
CC49052		0.13	<10	<10	58	<10	27
CC49053		0.14	<10	<10	55	<10	28
CC49054		0.13	<10	<10	49	<10	30
CC49055		0.11	<10	<10	32	<10	12



ALS Chemex
EXCELLENCE IN ANALYTICAL CHEMISTRY
 ALS Canada Ltd.

212 Brooksbank Avenue
 North Vancouver BC V7J 2C1
 Phone: 604 984 0221 Fax: 604 984 0218 www.alschemex.com

To: ARCHER, CATHRO AND ASSOCIATES (1981)
 LIMITED
 1016-510 W HASTINGS ST
 VANCOUVER BC V6B 1L8

Page: 5 - A
 Total # Pages: 7 (A - C)
 Finalized Date: 6-AUG-2008
 Account: F

Project: CABIN

CERTIFICATE OF ANALYSIS VA08096080

Sample Description	Method Analyte Units LOR	WEI-21	ME-ICP41	ME-ICP41	ME-ICP41	ME-ICP41	ME-ICP41	ME-ICP41	ME-ICP41	ME-ICP41	ME-ICP41	ME-ICP41	ME-ICP41	ME-ICP41	ME-ICP41	ME-ICP41
		Recvd Wt. kg	Ag ppm	Al %	As ppm	B ppm	Ba ppm	Be ppm	Bi ppm	Ca %	Cd ppm	Co ppm	Cr ppm	Cu ppm	Fe %	Ga ppm
CC49056		0.18	0.2	0.58	6	<10	50	<0.5	<2	0.09	<0.5	2	14	3	0.79	10
CC49057		0.18	0.2	1.36	13	<10	70	<0.5	<2	0.17	<0.5	6	33	16	2.28	<10
CC49058		0.16	0.2	1.08	8	<10	70	<0.5	<2	0.13	<0.5	3	26	10	1.73	10
CC49059		0.24	1.0	1.03	8	<10	90	<0.5	<2	0.19	1.1	3	28	13	1.79	10
CC49060		0.18	0.2	1.59	8	<10	110	<0.5	<2	0.19	<0.5	6	43	15	2.89	10
CC49061		0.14	<0.2	0.44	<2	<10	70	<0.5	<2	0.06	<0.5	1	11	3	0.34	<10
CC49062		0.12	0.2	0.45	2	<10	50	<0.5	<2	0.04	<0.5	1	11	5	0.52	<10
CC49063		0.22	0.2	0.78	6	<10	110	<0.5	<2	0.10	0.6	3	23	9	1.51	10
CC49064		0.24	0.2	1.01	13	<10	100	<0.5	<2	0.14	0.7	4	27	12	1.93	10
CC49065		0.24	<0.2	3.37	5	<10	240	0.5	<2	0.49	<0.5	18	49	45	4.76	10
CC49066		0.16	0.5	2.10	124	<10	160	0.7	<2	1.05	3.4	16	57	72	3.67	10
CC49067		0.18	<0.2	1.53	8	<10	140	<0.5	<2	0.23	1.3	9	38	14	2.46	10
CC49068		0.18	0.2	1.63	10	<10	80	<0.5	<2	0.17	<0.5	5	33	15	2.24	10
CC49069		0.18	<0.2	0.65	4	<10	50	<0.5	<2	0.09	<0.5	2	15	4	0.97	10
CC49070		0.18	<0.2	0.57	3	<10	40	<0.5	<2	0.11	<0.5	1	13	2	0.60	10
CC49071		0.20	<0.2	0.95	7	<10	70	<0.5	<2	0.13	<0.5	2	18	6	1.80	10
CC49072		0.16	<0.2	1.32	12	<10	90	<0.5	<2	0.15	<0.5	5	28	13	2.39	10
CC49073		0.16	0.2	0.74	5	<10	80	<0.5	<2	0.11	<0.5	2	15	7	1.01	10
CC49074		0.22	<0.2	1.27	10	<10	100	<0.5	<2	0.16	<0.5	3	24	12	1.63	10
CC49075		0.12	<0.2	0.97	4	<10	70	<0.5	<2	0.16	<0.5	5	22	7	1.61	10
CC49076		0.16	0.3	0.70	<2	<10	100	<0.5	<2	0.09	<0.5	2	34	8	0.88	10
CC49077		0.22	0.4	1.47	9	<10	80	<0.5	<2	0.16	<0.5	4	32	7	1.76	10
CC49078		0.18	0.3	0.73	2	<10	120	<0.5	<2	0.12	<0.5	1	15	7	0.71	10
CC49079		0.24	0.2	0.75	4	<10	50	<0.5	<2	0.12	<0.5	2	17	4	0.97	10
CC49080		0.20	0.3	0.70	3	<10	60	<0.5	<2	0.10	<0.5	1	17	3	0.82	<10
CC49081		0.18	0.2	0.67	6	<10	60	<0.5	<2	0.11	<0.5	3	17	5	1.06	10
CC49082		0.16	0.7	0.72	4	<10	90	<0.5	<2	0.10	<0.5	2	17	10	0.76	10
CC49083		0.20	0.3	1.48	20	<10	80	<0.5	<2	0.13	<0.5	3	37	19	2.25	10
CC49084		0.20	0.9	1.80	7	<10	230	0.5	<2	0.78	1.1	8	36	30	2.22	10
CC49085		0.20	0.4	1.65	9	<10	120	<0.5	<2	0.43	0.5	9	45	34	2.73	10
CC49086		0.18	0.4	1.02	3	<10	70	<0.5	<2	0.14	<0.5	3	25	18	1.31	<10
CC49087		0.18	0.2	0.26	3	<10	30	<0.5	<2	0.05	<0.5	4	14	4	0.35	<10
CC49088		0.20	0.3	0.76	<2	<10	50	<0.5	<2	0.13	<0.5	3	20	8	1.04	10
CC49089		0.08	0.5	0.74	3	<10	80	<0.5	<2	0.09	<0.5	2	16	11	0.84	<10
CC49090		0.14	0.5	1.08	7	<10	70	<0.5	<2	0.16	0.6	4	31	20	1.65	10
CC49091		0.16	0.3	1.06	4	<10	70	<0.5	<2	0.17	<0.5	3	30	8	1.44	10
CC49092		0.16	0.5	1.30	16	<10	70	<0.5	<2	0.13	<0.5	4	31	12	2.24	10
CC49093		0.26	0.4	0.69	5	<10	50	<0.5	<2	0.09	<0.5	2	16	4	0.74	10
CC49094		0.26	0.2	0.68	3	<10	50	<0.5	<2	0.09	<0.5	2	17	6	0.90	10
CC49095		0.36	0.4	1.31	6	<10	80	<0.5	<2	0.12	<0.5	3	26	10	1.59	10



ALS Chemex

EXCELLENCE IN ANALYTICAL CHEMISTRY

ALS Canada Ltd.

212 Brooksbank Avenue

North Vancouver BC V7J 2C1

Phone: 604 984 0221 Fax: 604 984 0218 www.alschemex.com

To: ARCHER, CATHRO AND ASSOCIATES (1981)

LIMITED

1016-510 W HASTINGS ST

VANCOUVER BC V6B 1L8

Page: 5 - B

Total # Pages: 7 (A - C)

Finalized Date: 6-AUG-2008

Account: F

Project: CABIN

CERTIFICATE OF ANALYSIS VA08096080

Sample Description	Method Analyte Units LOR	ME-ICP41	ME-ICP41	ME-ICP41	ME-ICP41	ME-ICP41	ME-ICP41	ME-ICP41	ME-ICP41	ME-ICP41	ME-ICP41	ME-ICP41	ME-ICP41	ME-ICP41	ME-ICP41	ME-ICP41
		Hg ppm	K %	La ppm	Mg %	Mn ppm	Mo ppm	Na %	Ni ppm	P ppm	Pb ppm	S %	Sb ppm	Sc ppm	Sr ppm	Th ppm
CC49056		<1	0.04	10	0.10	66	1	0.01	4	280	10	0.01	3	1	10	<20
CC49057		<1	0.07	10	0.44	191	2	0.01	16	860	8	0.01	3	3	14	<20
CC49058		<1	0.06	10	0.32	138	2	0.01	11	330	9	0.01	2	2	18	<20
CC49059		<1	0.05	10	0.29	123	2	0.01	12	530	8	0.03	3	1	26	<20
CC49060		<1	0.07	10	0.58	255	2	0.01	19	560	8	0.02	<2	3	29	<20
CC49061		<1	0.02	10	0.03	22	1	0.01	2	170	9	0.01	2	<1	14	<20
CC49062		1	0.03	10	0.03	31	1	0.01	3	240	12	0.02	<2	<1	10	<20
CC49063		<1	0.05	10	0.16	97	2	0.01	10	380	10	0.01	<2	1	15	<20
CC49064		1	0.07	10	0.32	150	1	0.01	12	420	8	0.01	2	2	25	<20
CC49065		<1	0.26	10	1.63	894	1	0.03	24	1120	3	0.02	<2	7	60	<20
CC49066		<1	0.07	20	1.16	865	3	0.03	40	1890	8	0.06	2	5	113	<20
CC49067		<1	0.06	10	0.46	596	3	0.02	16	480	8	0.02	<2	2	26	<20
CC49068		<1	0.07	10	0.42	253	2	0.01	19	800	7	0.02	3	2	13	<20
CC49069		<1	0.04	10	0.13	72	1	0.01	5	350	7	0.01	<2	1	9	<20
CC49070		<1	0.03	10	0.09	56	1	0.01	4	240	11	0.01	3	1	10	<20
CC49071		<1	0.06	10	0.21	236	1	0.01	5	610	8	0.01	<2	2	12	<20
CC49072		<1	0.08	10	0.40	192	1	0.01	12	820	10	0.01	<2	3	13	<20
CC49073		<1	0.04	10	0.15	86	1	0.01	5	460	9	0.01	<2	1	11	<20
CC49074		<1	0.09	10	0.29	156	1	0.01	8	380	9	0.02	2	2	14	<20
CC49075		<1	0.06	10	0.37	145	1	0.01	7	330	13	0.02	2	2	14	<20
CC49076		<1	0.05	10	0.13	88	1	0.02	13	350	16	0.02	<2	1	12	<20
CC49077		1	0.07	10	0.34	141	2	0.01	13	430	12	0.02	3	3	15	<20
CC49078		<1	0.05	10	0.08	49	1	0.01	5	370	12	0.02	2	<1	16	<20
CC49079		<1	0.04	10	0.17	96	1	0.01	5	250	9	0.01	3	2	13	<20
CC49080		<1	0.03	10	0.13	62	2	0.01	6	280	8	<0.01	<2	1	13	<20
CC49081		<1	0.05	10	0.17	78	1	<0.01	6	260	6	<0.01	<2	1	11	<20
CC49082		<1	0.04	10	0.08	70	2	0.01	4	340	11	0.01	<2	<1	15	<20
CC49083		<1	0.07	10	0.45	149	3	0.01	17	600	11	0.01	<2	2	13	<20
CC49084		<1	0.08	10	0.44	245	4	0.02	22	950	8	0.04	<2	1	82	<20
CC49085		<1	0.07	10	0.76	301	2	0.02	23	1090	7	0.03	<2	3	42	<20
CC49086		<1	0.06	10	0.25	102	1	0.01	10	580	6	0.02	<2	1	17	<20
CC49087		<1	0.04	10	0.06	22	1	<0.01	4	100	5	<0.01	<2	1	6	<20
CC49088		<1	0.05	10	0.19	101	2	0.01	7	230	11	0.01	2	1	9	<20
CC49089		<1	0.04	10	0.08	54	1	0.01	5	820	6	0.03	<2	<1	12	<20
CC49090		<1	0.07	10	0.29	138	1	0.01	11	390	10	0.02	<2	1	21	<20
CC49091		<1	0.06	10	0.43	109	2	0.01	10	580	8	0.01	<2	2	18	<20
CC49092		<1	0.08	10	0.42	166	2	0.01	12	620	11	0.01	2	3	18	<20
CC49093		<1	0.04	10	0.13	59	1	0.01	5	270	11	0.01	<2	1	12	<20
CC49094		<1	0.04	10	0.12	67	1	0.01	5	300	10	<0.01	<2	1	11	<20
CC49095		<1	0.07	10	0.27	147	2	0.01	9	600	13	0.01	<2	2	15	<20



ALS Chemex

EXCELLENCE IN ANALYTICAL CHEMISTRY

ALS Canada Ltd.

212 Brooksbank Avenue

North Vancouver BC V7J 2C1

Phone: 604 984 0221 Fax: 604 984 0218 www.alschemex.com

To: ARCHER, CATHRO AND ASSOCIATES (1981)

LIMITED

1016-510 W HASTINGS ST

VANCOUVER BC V6B 1L8

Page: 5 - C

Total # Pages: 7 (A - C)

Finalized Date: 6-AUG-2008

Account: F

Project: CABIN

CERTIFICATE OF ANALYSIS VA08096080

Sample Description	Method Analyte Units LOR	ME-ICP41	ME-ICP41	ME-ICP41	ME-ICP41	ME-ICP41	ME-ICP41
		Ti	Ti	U	V	W	Zn
		%	ppm	ppm	ppm	ppm	ppm
		0.01	10	10	1	10	2
CC49056		0.14	<10	<10	39	<10	18
CC49057		0.11	<10	<10	57	<10	50
CC49058		0.12	<10	<10	71	<10	46
CC49059		0.07	<10	<10	57	<10	47
CC49060		0.15	<10	<10	101	<10	71
CC49061		0.04	<10	<10	20	<10	10
CC49062		0.05	<10	<10	30	<10	11
CC49063		0.09	<10	<10	61	<10	53
CC49064		0.10	<10	<10	67	<10	65
CC49065		0.19	<10	<10	131	<10	82
CC49066		0.03	<10	<10	101	<10	166
CC49067		0.10	<10	<10	71	<10	121
CC49068		0.10	<10	<10	56	<10	56
CC49069		0.10	<10	<10	34	<10	22
CC49070		0.14	<10	<10	28	<10	12
CC49071		0.14	<10	<10	54	<10	30
CC49072		0.16	<10	<10	73	<10	39
CC49073		0.13	<10	<10	42	<10	18
CC49074		0.12	<10	<10	56	<10	29
CC49075		0.16	<10	<10	55	<10	30
CC49076		0.09	<10	<10	32	<10	23
CC49077		0.13	<10	<10	52	<10	38
CC49078		0.03	<10	<10	27	<10	14
CC49079		0.14	<10	<10	40	<10	20
CC49080		0.11	<10	<10	33	<10	17
CC49081		0.12	<10	<10	43	<10	24
CC49082		0.07	<10	<10	29	<10	17
CC49083		0.11	<10	<10	86	<10	57
CC49084		0.05	<10	10	62	<10	103
CC49085		0.09	<10	<10	80	<10	87
CC49086		0.05	<10	<10	36	<10	28
CC49087		0.17	<10	<10	33	<10	16
CC49088		0.11	<10	<10	33	<10	27
CC49089		0.01	<10	<10	21	<10	16
CC49090		0.08	<10	<10	56	<10	53
CC49091		0.11	<10	<10	69	<10	47
CC49092		0.13	<10	<10	79	<10	54
CC49093		0.12	<10	<10	34	<10	15
CC49094		0.12	<10	<10	33	<10	21
CC49095		0.13	<10	<10	51	<10	33



ALS Chemex

EXCELLENCE IN ANALYTICAL CHEMISTRY

ALS Canada Ltd.

212 Brooksbank Avenue

North Vancouver BC V7J 2C1

Phone: 604 984 0221 Fax: 604 984 0218 www.alschemex.com

To: ARCHER, CATHRO AND ASSOCIATES (1981)

LIMITED

1016-510 W HASTINGS ST

VANCOUVER BC V6B 1L8

Page: 6 - A

Total # Pages: 7 (A - C)

Finalized Date: 6-AUG-2008

Account: F

Project: CABIN

CERTIFICATE OF ANALYSIS VA08096080

Sample Description	Method Analyte Units LOR	WEI-21	ME-ICP41	ME-ICP41	ME-ICP41	ME-ICP41	ME-ICP41	ME-ICP41	ME-ICP41	ME-ICP41	ME-ICP41	ME-ICP41	ME-ICP41	ME-ICP41	ME-ICP41	ME-ICP41
		Recvd Wt. kg	Ag ppm	Al %	As ppm	B ppm	Ba ppm	Be ppm	Bi ppm	Ca %	Cd ppm	Co ppm	Cr ppm	Cu ppm	Fe %	Ga ppm
		0.02	0.2	0.01	2	10	10	0.5	2	0.01	0.5	1	1	1	0.01	10
CC49096		0.30	0.3	0.98	6	<10	70	<0.5	<2	0.14	<0.5	2	21	7	1.24	10
CC49097		0.20	0.3	0.78	4	<10	50	<0.5	<2	0.12	<0.5	2	18	4	0.91	10
CC49098		0.22	<0.2	0.94	4	<10	70	<0.5	<2	0.15	<0.5	3	23	5	1.32	10
CC49099		0.16	0.3	0.68	<2	<10	60	<0.5	<2	0.12	<0.5	2	17	5	0.93	10
CC49100		0.22	0.3	0.94	6	<10	60	<0.5	<2	0.15	<0.5	3	25	8	1.49	10
CC49101		0.20	0.3	1.50	3	<10	100	<0.5	<2	0.16	<0.5	3	22	11	2.05	10
CC49102		0.14	1.5	3.02	5	<10	200	0.6	<2	0.17	<0.5	8	46	90	2.87	10
CC49103		0.16	0.3	2.19	26	<10	330	0.6	<2	0.54	<0.5	12	52	60	3.08	10
CC49104		0.14	0.2	0.91	4	<10	80	<0.5	<2	0.16	<0.5	2	22	10	1.18	10
CC49105		0.16	0.3	1.14	14	<10	90	<0.5	<2	0.14	<0.5	4	25	23	2.04	10
CC49106		0.16	1.3	2.29	6	<10	450	0.7	<2	0.94	3.4	14	45	35	2.90	10
CC49107		0.30	0.4	1.12	6	<10	150	<0.5	<2	0.43	1.3	6	28	11	1.68	<10
CC49108		0.30	0.6	1.30	5	<10	150	<0.5	<2	0.48	3.1	7	35	18	2.08	<10
CC49109		0.18	0.5	1.71	5	<10	110	<0.5	<2	0.41	0.8	7	44	20	2.83	10
CC49110		0.18	1.4	1.87	12	<10	160	0.5	<2	0.66	1.4	10	70	44	2.90	10
CC49111		0.16	<0.2	1.06	4	<10	110	<0.5	<2	0.15	<0.5	5	29	14	2.45	10
CC49112		0.12	0.2	0.93	2	<10	120	<0.5	<2	0.22	<0.5	5	25	10	1.71	10
CC49113		0.16	0.3	2.37	21	<10	280	0.5	<2	0.40	<0.5	8	37	34	4.03	10
CC49114		0.16	1.9	2.27	9	<10	230	0.8	<2	0.28	4.8	12	41	38	3.34	10
CC49115		0.14	0.8	1.46	5	<10	140	<0.5	<2	0.51	2.5	6	39	26	2.16	<10
CC49116		0.24	0.7	1.33	11	<10	120	<0.5	<2	0.41	0.8	8	33	28	1.96	<10
CC49117		0.18	0.7	1.08	<2	<10	140	<0.5	<2	0.34	1.5	5	29	8	1.62	10
CC49118		0.14	0.3	0.45	<2	<10	50	<0.5	<2	0.10	<0.5	1	12	3	0.62	<10
CC49119		0.16	0.3	0.79	4	<10	90	<0.5	<2	0.20	0.5	3	23	7	1.33	10
CC49120		0.22	0.2	1.15	6	<10	120	<0.5	<2	0.26	<0.5	5	28	14	1.71	10
CC49121		0.18	0.2	1.83	12	<10	70	<0.5	<2	0.11	<0.5	6	31	33	3.18	10
CC49122		0.16	0.2	1.05	3	<10	60	<0.5	<2	0.08	<0.5	3	20	10	2.10	10
CC49123		0.18	0.3	1.50	3	<10	70	<0.5	<2	0.12	<0.5	7	30	19	2.56	10
CC49124		0.18	0.3	1.66	3	<10	110	<0.5	<2	0.16	<0.5	5	26	47	2.36	10
CC49125		0.18	0.2	1.02	4	<10	50	<0.5	<2	0.09	<0.5	3	18	13	2.30	10
CC49126		0.20	0.2	2.33	13	<10	80	<0.5	<2	0.12	<0.5	8	37	48	3.95	10
CC49127		0.34	0.3	1.78	8	<10	180	<0.5	<2	0.41	<0.5	7	34	44	2.65	10
CC49128		0.12	0.4	2.30	68	<10	350	0.5	<2	0.91	0.7	15	74	46	3.93	10
CC49129		0.20	0.6	1.81	123	<10	320	0.7	<2	0.82	<0.5	14	101	149	2.66	<10
CC49130		0.22	0.3	1.31	7	<10	80	<0.5	<2	0.20	<0.5	5	32	12	1.89	10
CC49131		0.16	0.2	0.98	5	<10	90	<0.5	<2	0.18	0.6	3	25	9	1.49	10
CC49132		0.22	0.2	1.35	3	<10	140	<0.5	<2	0.39	0.5	7	33	12	1.96	<10
CC49133		0.20	0.4	0.74	2	<10	140	<0.5	<2	0.49	<0.5	3	20	7	1.00	<10
CC49134		0.20	0.4	1.43	8	<10	130	0.5	<2	0.40	0.7	8	32	16	2.00	<10
CC49135		0.18	0.3	1.00	4	<10	100	<0.5	<2	0.30	0.7	5	26	11	1.73	10



ALS Chemex

EXCELLENCE IN ANALYTICAL CHEMISTRY

ALS Canada Ltd

212 Brooksbank Avenue

North Vancouver BC V7J 2C1

Phone: 604 984 0221 Fax: 604 984 0218 www.alschemex.com

To: ARCHER, CATHRO AND ASSOCIATES (1981)

LIMITED

1016-510 W HASTINGS ST

VANCOUVER BC V6B 1L8

Page: 6 - B

Total # Pages: 7 (A - C)

Finalized Date: 6-AUG-2008

Account: F

Project: CABIN

CERTIFICATE OF ANALYSIS VA08096080

Sample Description	Method Analyte Units LOR	ME-ICP41	ME-ICP41	ME-ICP41	ME-ICP41	ME-ICP41	ME-ICP41	ME-ICP41	ME-ICP41	ME-ICP41	ME-ICP41	ME-ICP41	ME-ICP41	ME-ICP41	ME-ICP41	ME-ICP41
		Hg ppm	K %	La ppm	Mg %	Mn ppm	Mo ppm	Na %	Ni ppm	P ppm	Pb ppm	S %	Sb ppm	Sc ppm	Sr ppm	Th ppm
CC49096		<1	0.05	10	0.22	101	1	0.01	6	350	10	0.01	<2	2	14	<20
CC49097		<1	0.04	10	0.17	77	1	0.01	6	330	9	0.01	<2	2	9	<20
CC49098		<1	0.06	10	0.26	115	1	0.01	9	380	11	<0.01	<2	2	10	<20
CC49099		<1	0.05	10	0.12	122	1	0.01	4	290	11	0.01	<2	1	11	<20
CC49100		<1	0.06	10	0.31	177	1	0.01	8	370	14	0.01	<2	2	12	<20
CC49101		<1	0.04	10	0.32	159	1	0.01	8	430	5	0.01	2	2	13	<20
CC49102		<1	0.12	10	0.62	210	2	0.02	29	530	9	0.03	<2	3	16	<20
CC49103		<1	0.13	10	0.72	620	2	0.02	30	850	7	0.03	2	3	31	<20
CC49104		<1	0.06	10	0.19	101	1	0.01	8	380	9	0.02	<2	1	15	<20
CC49105		<1	0.05	10	0.27	142	3	0.01	10	230	11	0.01	<2	2	12	<20
CC49106		<1	0.12	10	0.58	1020	5	0.02	35	640	9	0.04	2	4	90	<20
CC49107		<1	0.06	10	0.36	220	2	0.01	15	520	8	0.01	<2	2	43	<20
CC49108		<1	0.08	10	0.53	351	2	0.02	23	650	6	0.01	<2	3	47	<20
CC49109		<1	0.08	10	0.85	301	2	0.02	18	740	6	0.02	<2	4	42	<20
CC49110		<1	0.07	10	1.05	459	5	0.02	35	1020	8	0.02	2	4	59	<20
CC49111		<1	0.05	10	0.28	190	2	0.01	11	410	6	0.02	<2	1	27	<20
CC49112		<1	0.06	10	0.32	175	2	0.01	10	320	8	0.01	2	2	29	<20
CC49113		<1	0.06	10	0.66	391	3	0.02	21	1110	6	0.03	<2	3	144	<20
CC49114		<1	0.06	10	0.66	973	5	0.02	25	770	7	0.02	<2	3	43	<20
CC49115		<1	0.06	10	0.60	366	4	0.02	21	630	7	0.02	<2	2	52	<20
CC49116		<1	0.06	10	0.52	271	1	0.01	31	620	13	0.03	<2	2	32	<20
CC49117		<1	0.05	10	0.38	206	2	0.01	11	310	7	0.01	<2	2	38	<20
CC49118		<1	0.03	10	0.07	51	1	0.01	3	240	10	0.01	<2	1	10	<20
CC49119		<1	0.05	10	0.23	134	2	0.01	8	240	9	0.02	<2	1	19	<20
CC49120		<1	0.05	10	0.46	176	2	0.01	13	270	5	0.01	<2	2	18	<20
CC49121		<1	0.04	10	0.54	247	2	0.01	13	340	4	0.02	<2	3	8	<20
CC49122		<1	0.03	10	0.32	143	1	<0.01	5	320	6	0.01	<2	2	9	<20
CC49123		<1	0.05	<10	0.69	295	2	0.01	13	220	5	0.01	<2	3	10	<20
CC49124		<1	0.05	10	0.45	251	3	0.01	10	330	8	0.02	<2	2	13	<20
CC49125		<1	0.04	<10	0.26	203	2	0.01	6	340	7	0.01	<2	2	8	<20
CC49126		<1	0.05	10	0.75	342	2	0.01	18	600	4	0.02	<2	3	10	<20
CC49127		<1	0.04	10	0.75	268	4	0.01	15	330	4	0.02	<2	3	20	<20
CC49128		<1	0.09	10	0.90	1445	7	0.02	30	1180	5	0.06	<2	4	42	<20
CC49129		<1	0.12	20	0.76	489	4	0.03	27	1130	6	0.05	<2	5	44	<20
CC49130		<1	0.08	10	0.50	194	1	0.01	14	370	9	0.01	<2	3	14	<20
CC49131		<1	0.05	10	0.27	126	1	0.01	10	390	8	0.01	<2	1	19	<20
CC49132		<1	0.06	10	0.53	276	2	0.01	19	500	6	0.01	<2	2	42	<20
CC49133		<1	0.04	10	0.21	113	1	0.01	7	220	7	0.02	<2	1	46	<20
CC49134		<1	0.07	10	0.46	230	1	0.02	26	630	5	0.02	2	2	31	<20
CC49135		<1	0.05	10	0.33	153	2	0.01	11	270	6	0.02	<2	2	30	<20



ALS Chemex

EXCELLENCE IN ANALYTICAL CHEMISTRY

ALS Canada Ltd.

212 Brooksbank Avenue

North Vancouver BC V7J 2C1

Phone: 604 984 0221 Fax: 604 984 0218 www.alschemex.com

To: ARCHER, CATHRO AND ASSOCIATES (1981)

LIMITED

1016-510 W HASTINGS ST

VANCOUVER BC V6B 1L8

Page: 6 - C

Total # Pages: 7 (A - C)

Finalized Date: 6-AUG-2008

Account: F

Project: CABIN

CERTIFICATE OF ANALYSIS VA08096080

Sample Description	Method Analyte Units LOR	ME-ICP41	ME-ICP41	ME-ICP41	ME-ICP41	ME-ICP41	ME-ICP41
		Ti %	Ti ppm	U ppm	V ppm	W ppm	Zn ppm
		0.01	10	10	1	10	2
CC49096		0.13	<10	<10	44	<10	21
CC49097		0.11	<10	<10	34	<10	18
CC49098		0.15	<10	<10	45	<10	31
CC49099		0.15	<10	<10	39	<10	21
CC49100		0.19	<10	<10	54	<10	31
CC49101		0.16	<10	<10	53	<10	29
CC49102		0.11	<10	<10	66	<10	51
CC49103		0.07	<10	<10	67	<10	75
CC49104		0.06	<10	<10	35	<10	27
CC49105		0.17	<10	<10	83	<10	44
CC49106		0.10	<10	10	67	<10	227
CC49107		0.10	<10	<10	42	<10	53
CC49108		0.10	<10	<10	50	<10	114
CC49109		0.12	<10	<10	87	<10	90
CC49110		0.08	<10	<10	90	<10	231
CC49111		0.09	<10	<10	80	<10	43
CC49112		0.12	<10	<10	62	<10	44
CC49113		0.04	<10	<10	112	<10	105
CC49114		0.06	<10	<10	87	<10	219
CC49115		0.07	<10	<10	71	<10	121
CC49116		0.07	<10	<10	43	<10	88
CC49117		0.11	<10	<10	46	<10	71
CC49118		0.14	<10	<10	29	<10	14
CC49119		0.13	<10	<10	50	<10	34
CC49120		0.09	<10	<10	47	<10	49
CC49121		0.15	<10	<10	72	<10	51
CC49122		0.22	<10	<10	75	<10	24
CC49123		0.23	<10	<10	80	<10	46
CC49124		0.19	<10	<10	73	<10	40
CC49125		0.27	<10	<10	92	<10	26
CC49126		0.18	<10	<10	92	<10	66
CC49127		0.10	<10	<10	68	<10	50
CC49128		0.07	<10	10	81	<10	212
CC49129		0.08	<10	<10	87	<10	76
CC49130		0.13	<10	<10	53	<10	50
CC49131		0.08	<10	<10	43	<10	46
CC49132		0.09	<10	<10	48	<10	63
CC49133		0.09	<10	<10	30	<10	34
CC49134		0.08	<10	<10	43	<10	58
CC49135		0.10	<10	<10	52	<10	48



ALS Chemex

EXCELLENCE IN ANALYTICAL CHEMISTRY

ALS Canada Ltd.

212 Brooksbank Avenue

North Vancouver BC V7J 2C1

Phone: 604 984 0221 Fax: 604 984 0218 www.alschemex.com

To: ARCHER, CATHRO AND ASSOCIATES (1981)

LIMITED

1016-510 W HASTINGS ST

VANCOUVER BC V6B 1L8

Page: 7 - A

Total # Pages: 7 (A - C)

Finalized Date: 6-AUG-2008

Account: F

Project: CABIN

CERTIFICATE OF ANALYSIS VA08096080

Sample Description	Method Analyte Units LOR	WEI-21	ME-ICP41	ME-ICP41	ME-ICP41	ME-ICP41	ME-ICP41	ME-ICP41	ME-ICP41	ME-ICP41	ME-ICP41	ME-ICP41	ME-ICP41	ME-ICP41	ME-ICP41	ME-ICP41
		Recvd Wt. kg	Ag ppm	Al %	As ppm	B ppm	Ba ppm	Be ppm	Bi ppm	Ca %	Cd ppm	Co ppm	Cr ppm	Cu ppm	Fe %	Ga ppm
		0.02	0.2	0.01	2	10	10	0.5	2	0.01	0.5	1	1	0.01	0.5	10
CC49136		0.14	0.2	1.50	3	<10	80	<0.5	<2	0.20	<0.5	5	28	21	2.41	10
CC49137		0.16	0.3	1.31	3	<10	110	<0.5	<2	0.30	<0.5	7	32	25	2.63	10
CC49138		0.20	0.2	1.52	3	<10	180	<0.5	<2	0.27	1.0	6	38	12	2.02	10
CC49139		0.28	0.3	0.73	3	<10	70	<0.5	<2	0.19	<0.5	4	25	7	1.42	10
CC49140		0.24	0.3	1.33	3	<10	150	<0.5	<2	0.29	0.7	5	30	12	1.82	10
CC49141		0.22	0.3	1.45	8	<10	100	<0.5	<2	0.23	0.7	6	40	13	3.08	10
CC49142		0.20	0.6	1.60	8	<10	110	0.6	<2	0.36	0.9	7	35	15	2.31	10
CC49143		0.22	0.3	2.06	13	<10	170	0.7	<2	0.19	1.1	7	48	22	3.12	10
CC49144		0.20	0.2	2.84	8	<10	110	<0.5	<2	0.42	<0.5	14	120	49	3.78	10
CC49145		0.18	0.3	3.28	9	<10	80	0.6	<2	0.14	<0.5	12	41	62	4.28	10
CC49146		0.20	<0.2	2.25	13	<10	80	<0.5	<2	0.12	<0.5	9	40	37	4.82	10
CC49147		0.38	0.4	1.82	6	<10	210	0.5	<2	0.73	<0.5	13	32	299	3.00	<10
CC49148		0.20	0.2	1.78	5	<10	100	<0.5	<2	0.30	<0.5	9	27	43	3.22	10
CC49149		0.14	0.2	1.44	<2	<10	80	<0.5	<2	0.14	<0.5	7	23	32	3.41	10
CC49150		0.12	<0.2	1.05	3	<10	110	<0.5	<2	0.13	<0.5	5	26	12	2.58	10
CC49377		0.20	0.3	0.65	4	<10	80	<0.5	<2	0.12	<0.5	2	19	5	0.94	10
CC49378		0.24	<0.2	1.06	6	<10	90	<0.5	<2	0.16	<0.5	4	24	7	1.66	10
CC49379		0.28	0.7	1.19	7	<10	70	<0.5	<2	0.13	<0.5	3	27	7	1.31	10
CC49380		0.18	0.3	1.27	7	<10	70	<0.5	<2	0.12	<0.5	3	26	8	1.66	10
CC49381		0.16	0.2	0.92	7	<10	70	<0.5	<2	0.11	<0.5	2	25	7	1.25	10
CC49382		0.22	0.3	1.18	11	<10	80	<0.5	<2	0.13	<0.5	4	28	14	1.91	10
CC49383		0.20	0.3	0.56	<2	<10	50	<0.5	<2	0.10	<0.5	1	18	5	0.64	10
CC49384		0.26	0.3	1.09	6	<10	80	<0.5	<2	0.10	<0.5	3	36	8	1.33	10
CC49385		0.18	0.3	0.78	2	<10	50	<0.5	<2	0.10	<0.5	1	24	7	0.93	10
CC49386		0.24	0.3	1.42	11	<10	90	<0.5	<2	0.17	<0.5	5	34	19	1.82	<10
CC49387		0.22	0.6	1.54	15	<10	130	<0.5	<2	0.19	<0.5	6	41	22	2.14	10
CC49388		0.22	0.3	1.76	10	<10	150	<0.5	<2	0.71	<0.5	8	40	36	2.28	10
CC49389		0.26	0.6	1.48	5	<10	110	0.5	<2	0.75	<0.5	7	38	44	1.97	10
CC49390		0.22	0.2	1.27	6	<10	130	<0.5	<2	0.60	<0.5	5	30	14	1.80	10
CC49391		0.08	0.2	0.74	5	<10	110	<0.5	<2	0.17	0.5	2	25	12	0.93	10
CC49392		0.18	0.7	2.11	22	<10	110	<0.5	<2	0.21	<0.5	8	47	29	3.03	10
CC49393		0.20	0.3	1.01	9	<10	60	<0.5	<2	0.11	<0.5	2	27	7	1.45	10
CC49394		0.34	0.5	1.23	12	<10	70	<0.5	<2	0.18	<0.5	3	30	10	1.60	10
CC49395		0.26	0.4	0.78	5	<10	50	<0.5	<2	0.11	<0.5	2	22	6	1.02	10
CC49396		0.24	0.3	1.18	10	<10	70	<0.5	<2	0.18	<0.5	4	32	10	1.73	10
CC49397		0.18	0.3	0.91	8	<10	80	<0.5	<2	0.12	<0.5	3	27	9	1.55	10
CC49398		0.22	0.3	0.74	5	<10	70	<0.5	<2	0.12	<0.5	2	21	5	1.08	10
CC49399		0.28	<0.2	1.32	12	<10	70	<0.5	2	0.19	<0.5	4	34	9	1.93	10
CC49400		0.18	0.2	1.32	6	<10	80	<0.5	<2	0.16	<0.5	2	79	6	1.15	10



ALS Chemex

EXCELLENCE IN ANALYTICAL CHEMISTRY

ALS Canada Ltd.

212 Brooksbank Avenue

North Vancouver BC V7J 2C1

Phone: 604 984 0221 Fax: 604 984 0218 www.alschemex.com

To: ARCHER, CATHRO AND ASSOCIATES (1981)

LIMITED

1016-510 W HASTINGS ST

VANCOUVER BC V6B 1L8

Page: 7 - B

Total # Pages: 7 (A - C)

Finalized Date: 6-AUG-2008

Account: F

Project: CABIN

CERTIFICATE OF ANALYSIS VA08096080

Sample Description	Method	ME-ICP41	ME-ICP41	ME-ICP41	ME-ICP41	ME-ICP41	ME-ICP41	ME-ICP41	ME-ICP41	ME-ICP41	ME-ICP41	ME-ICP41	ME-ICP41	ME-ICP41	ME-ICP41	ME-ICP41	ME-ICP41
	Analyte	Hg	K	La	Mg	Mn	Mo	Na	Ni	P	Pb	S	Sb	Sc	Sr	Th	Units
LOR	ppm	%	ppm	%	ppm	ppm	ppm	%	ppm	ppm	ppm	%	ppm	ppm	ppm	ppm	
CC49136		<1	0.04	10	0.41	177	2	0.01	14	640	6	0.04	<2	2	33	<20	
CC49137		<1	0.06	10	0.55	268	3	0.01	15	420	5	0.02	2	4	38	<20	
CC49138		<1	0.06	10	0.51	277	3	0.01	20	280	7	0.01	<2	3	23	<20	
CC49139		<1	0.07	10	0.24	123	2	0.01	10	240	6	0.01	<2	2	18	<20	
CC49140		<1	0.05	10	0.33	190	2	0.01	14	430	9	0.02	<2	1	37	<20	
CC49141		<1	0.08	10	0.53	244	2	0.01	17	640	7	0.02	<2	3	24	<20	
CC49142		1	0.07	10	0.47	268	2	0.01	19	590	8	0.03	<2	1	39	<20	
CC49143		<1	0.07	10	0.70	271	3	0.02	24	710	7	0.02	<2	4	22	<20	
CC49144		<1	0.05	<10	2.05	470	3	0.01	37	300	4	0.02	<2	4	36	<20	
CC49145		<1	0.05	10	0.86	445	2	0.01	18	440	4	0.02	<2	4	11	<20	
CC49146		<1	0.06	10	0.83	345	2	0.01	17	410	5	0.02	<2	4	11	<20	
CC49147		<1	0.13	10	0.89	629	2	0.02	24	710	3	0.03	2	5	33	<20	
CC49148		<1	0.07	10	0.71	354	6	0.01	16	210	5	0.02	<2	3	16	<20	
CC49149		<1	0.06	<10	0.61	333	3	0.01	10	360	5	0.01	<2	3	10	<20	
CC49150		<1	0.04	10	0.33	184	3	0.01	12	180	5	0.01	<2	2	10	<20	
CC49377		<1	0.05	10	0.18	105	1	0.01	10	280	11	0.02	<2	1	12	<20	
CC49378		<1	0.06	10	0.31	131	<1	0.01	11	360	12	0.01	<2	2	13	<20	
CC49379		<1	0.06	10	0.27	119	1	0.01	10	380	11	0.01	<2	2	10	<20	
CC49380		<1	0.05	10	0.25	106	1	0.01	11	410	8	0.01	<2	2	11	<20	
CC49381		<1	0.07	10	0.22	120	<1	0.01	11	320	8	0.01	<2	1	13	<20	
CC49382		<1	0.08	10	0.31	228	1	0.02	11	610	12	0.01	<2	2	14	<20	
CC49383		<1	0.03	10	0.07	41	<1	0.01	6	330	7	0.01	<2	<1	10	<20	
CC49384		<1	0.06	10	0.35	105	<1	0.01	10	440	10	0.01	<2	1	16	<20	
CC49385		<1	0.04	10	0.25	66	1	0.01	8	280	9	0.01	<2	1	13	<20	
CC49386		<1	0.08	10	0.51	147	1	0.02	19	470	8	0.01	<2	2	22	<20	
CC49387		<1	0.11	10	0.52	194	<1	0.02	20	450	10	0.02	<2	2	22	<20	
CC49388		<1	0.07	10	0.62	291	2	0.02	22	910	6	0.04	3	3	31	<20	
CC49389		<1	0.06	10	0.55	388	3	0.02	19	810	6	0.04	<2	2	29	<20	
CC49390		<1	0.05	10	0.44	159	3	0.02	12	300	8	0.02	<2	3	27	<20	
CC49391		<1	0.05	10	0.11	85	1	0.02	10	470	8	0.03	<2	<1	23	<20	
CC49392		1	0.12	10	0.65	278	1	0.01	26	890	8	0.02	<2	3	20	<20	
CC49393		<1	0.05	10	0.29	120	<1	0.01	10	330	10	0.01	<2	2	13	<20	
CC49394		<1	0.08	10	0.42	128	1	0.01	14	550	14	0.01	<2	3	19	<20	
CC49395		<1	0.05	10	0.20	86	<1	0.01	8	230	11	0.01	<2	2	13	<20	
CC49396		<1	0.08	10	0.40	148	<1	0.01	14	400	8	0.01	2	3	15	<20	
CC49397		<1	0.07	10	0.24	143	1	0.02	12	480	8	0.02	<2	2	14	<20	
CC49398		1	0.04	10	0.17	88	<1	0.01	7	340	9	0.01	<2	1	11	<20	
CC49399		<1	0.07	10	0.44	185	1	0.01	15	430	11	0.01	2	3	13	<20	
CC49400		<1	0.06	10	0.40	84	<1	0.01	10	380	17	0.01	<2	1	24	<20	



ALS Chemex

EXCELLENCE IN ANALYTICAL CHEMISTRY

ALS Canada Ltd.

212 Brooksbank Avenue

North Vancouver BC V7J 2C1

Phone: 604 984 0221 Fax: 604 984 0218 www.alschemex.com

To: ARCHER, CATHRO AND ASSOCIATES (1981)

LIMITED

1016-510 W HASTINGS ST

VANCOUVER BC V6B 1L8

Page: 7 - C

Total # Pages: 7 (A - C)

Finalized Date: 6-AUG-2008

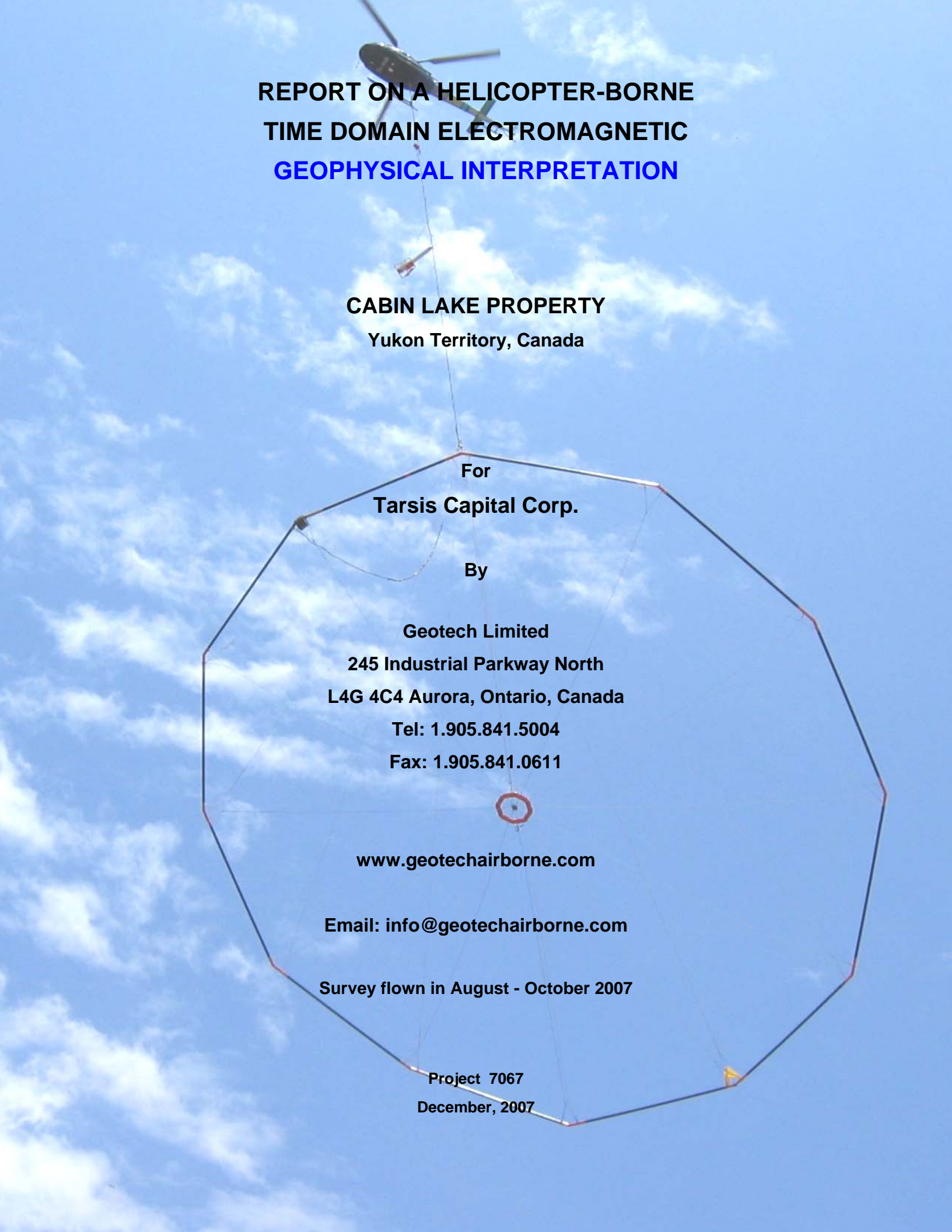
Account: F

Project: CABIN

CERTIFICATE OF ANALYSIS VA08096080

Sample Description	Method Analyte Units LOR	ME-ICP41	ME-ICP41	ME-ICP41	ME-ICP41	ME-ICP41	ME-ICP41
		Ti	Ti	U	V	W	Zn
		%	ppm	ppm	ppm	ppm	ppm
		0.01	10	10	1	10	2
CC49136		0.14	<10	<10	86	<10	51
CC49137		0.10	<10	<10	78	<10	45
CC49138		0.10	<10	<10	53	<10	97
CC49139		0.16	<10	<10	47	<10	45
CC49140		0.09	<10	<10	48	<10	54
CC49141		0.17	<10	<10	92	<10	74
CC49142		0.08	<10	<10	51	<10	87
CC49143		0.13	<10	<10	83	<10	87
CC49144		0.18	<10	<10	101	<10	72
CC49145		0.19	<10	<10	85	<10	78
CC49146		0.28	<10	<10	110	<10	62
CC49147		0.13	<10	<10	62	<10	58
CC49148		0.19	<10	<10	70	<10	67
CC49149		0.28	<10	<10	94	<10	56
CC49150		0.20	<10	<10	86	<10	31
CC49377		0.11	<10	<10	28	<10	19
CC49378		0.17	<10	<10	52	<10	31
CC49379		0.11	<10	<10	39	<10	29
CC49380		0.09	<10	<10	40	<10	29
CC49381		0.09	<10	<10	46	<10	29
CC49382		0.13	<10	<10	62	<10	40
CC49383		0.03	<10	<10	20	<10	12
CC49384		0.09	<10	<10	50	<10	28
CC49385		0.13	<10	<10	63	<10	40
CC49386		0.11	<10	<10	51	<10	37
CC49387		0.09	<10	<10	62	<10	64
CC49388		0.09	<10	<10	54	<10	46
CC49389		0.07	<10	<10	50	<10	46
CC49390		0.11	<10	<10	59	<10	37
CC49391		0.04	<10	<10	31	<10	27
CC49392		0.10	<10	<10	76	<10	69
CC49393		0.11	<10	<10	50	<10	28
CC49394		0.12	<10	<10	49	<10	39
CC49395		0.15	<10	<10	40	<10	22
CC49396		0.12	<10	<10	50	<10	36
CC49397		0.11	<10	<10	51	<10	29
CC49398		0.11	<10	<10	38	<10	22
CC49399		0.14	<10	<10	52	<10	46
CC49400		0.17	<10	<10	48	<10	20

APPENDIX III
GEOPHYSICAL REPORT BY GEOTECH LTD.



**REPORT ON A HELICOPTER-BORNE
TIME DOMAIN ELECTROMAGNETIC
GEOPHYSICAL INTERPRETATION**

CABIN LAKE PROPERTY
Yukon Territory, Canada

For
Tarsis Capital Corp.

By

Geotech Limited
245 Industrial Parkway North
L4G 4C4 Aurora, Ontario, Canada
Tel: 1.905.841.5004
Fax: 1.905.841.0611

www.geotechairborne.com

Email: info@geotechairborne.com

Survey flown in August - October 2007

Project 7067
December, 2007

TABLE OF CONTENTS

1. INTRODUCTION	3
2. SURVEY DESCRIPTION	5
3. GEOLOGICAL CONSIDERATIONS	6
3.1 Topography	6
3.2 Regional geological context.....	7
3.3 Geological context of the CABIN LAKE Property.....	8
3.4 Mineralization	9
4. INTERPRETATION OF THE MAGNETIC DATA	10
4.1 Introduction.....	10
4.2 Analysis of the Magnetic data.....	10
4.3 Inversion of the magnetic data.....	15
5. INTERPRETATION of VTEM DATA	17
5.1 Introduction.....	17
5.2 VTEM anomalies shape.....	17
5.3 Analysis of the EM results.....	18
5.4 Selected Anomalies.....	24
5.5 Conductivity Depth Sections	24
6. CONCLUSIONS AND RECOMMENDATIONS	29
7. REFERENCES	30
 Appendix A: VTEM Anomaly Modelling.....	 31

REPORT ON A HELICOPTER-BORNE TIME DOMAIN ELECTROMAGNETIC INTERPRETATION

CABIN LAKE Property, Yukon Territory, Canada

1. INTRODUCTION

In September, 2007 a helicopter-borne electromagnetic survey was carried out by Geotech Ltd. for Tarsis Capital Corp. over the CABIN LAKE Property located in Yukon Territory, Canada.

This report includes the results of the geophysical interpretation, over this Property. The Property is located at approximately 190 km south-east from Whitehorse, in the Yukon Territory. The geographic coordinates of the block extents are: longitudes, 131° 49' 48" W and 131° 44' 44" W, and latitudes, 60° 05' 15" N and 60° 08' 08" N. The surveyed area is 16 km², and the total line kilometers flown are 160 km (Fig. 1).

The survey was conducted using the Geotech Ltd VTEM system. Principal geophysical sensors included a versatile time domain electromagnetic system and a high resolution cesium magnetometer. Ancillary equipment included a GPS navigation system and a radar altimeter.

Data processing and map compilation, including generation of final digital data products were achieved at the office of Geotech Ltd in Aurora, Ontario.

The present report describes the results of the geophysical interpretation of this Property.



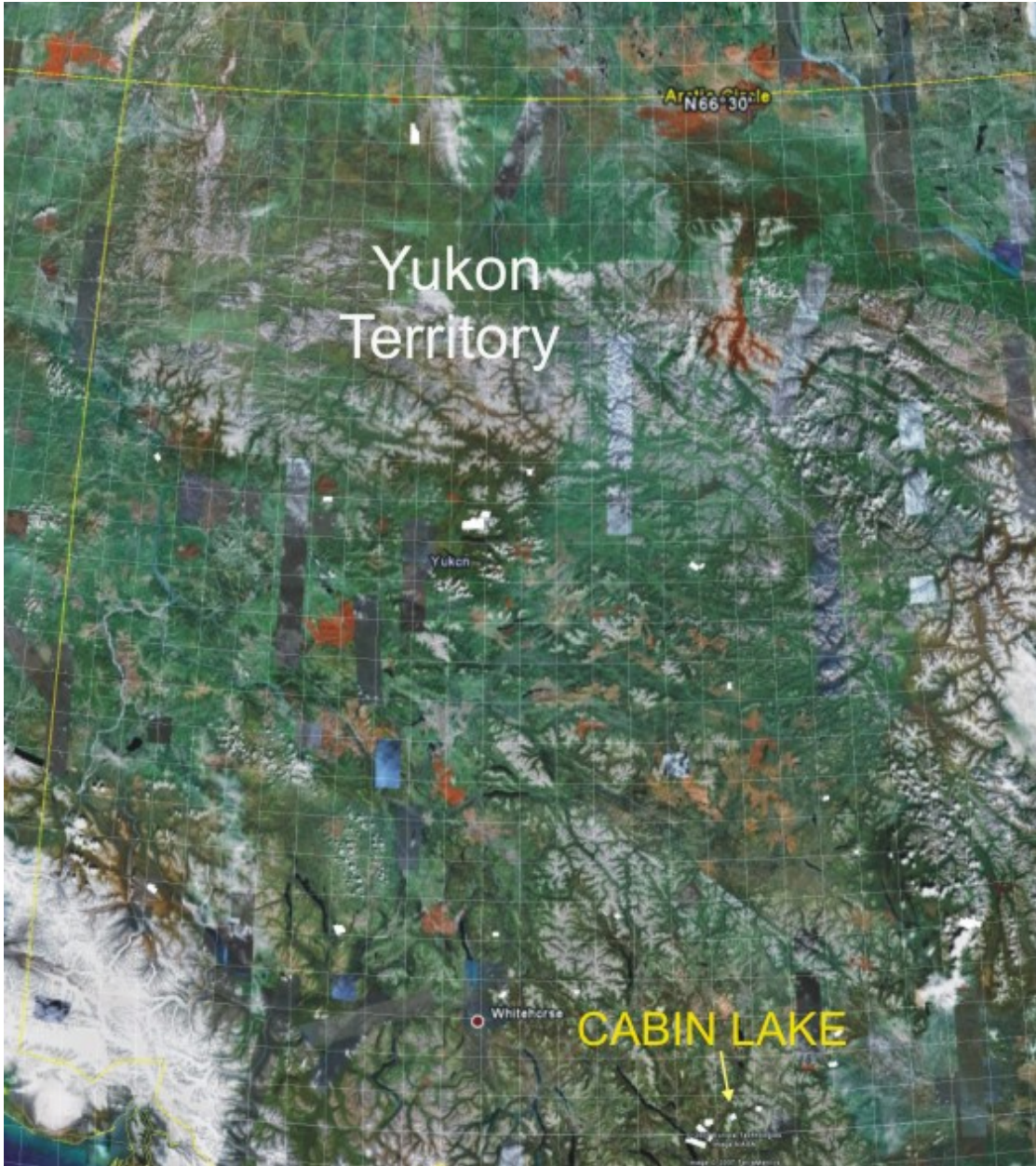


Fig. 1 Location of the CABIN LAKE Property on the satellite image.

2. SURVEY DESCRIPTION

In September 2007, Geotech Ltd. carried out a helicopter-borne geophysical survey over the CABIN LAKE property located in Yukon. Geotech Ltd. utilized a Versatile Time Domain Electromagnetic System to measure the electromagnetic induction field (B-field) and the vertical component of its time derivative (dB/dt). The electromagnetic measurements were made at the off-time mode. The concentric in-loop system was towed at a distance of 42 m from the helicopter. The VTEM Transmitter uses a trapezoid waveform shape with 7.2 ms duration operating at a base frequency of 30Hz. The dipole moment was approximately 425 000 NIA. The half-waveform period was 16.7 ms. A towed cesium and high resolution magnetometer was used to measure the Earth's magnetic field intensity. Data positioning and navigation were assured by a Novatel WAA GPS with accuracy less than 3m.

A Terra TRA radar altimeter was used to measure the terrain clearance. The helicopter was flying at a constant speed of 80 km/h and was keeping a constant ground clearance of 90 m when the terrain allowed it. The traverse lines direction was N74°E and the tie lines direction was N16°W. The distance between the traverse lines and the tie lines was 100m and 1000m, respectively. A more detailed description of the survey parameters is provided in the logistics/processing report.

3. GEOLOGICAL CONSIDERATIONS

3.1 Topography

The terrain is very rugged with a high mountain belt trending roughly in the NS direction. The absolute altitudes range from 950 m to 1250 m approximately. Due to the terrain roughness, it was difficult to keep a constant ground clearance while surveying this area.



Fig.2 Topography of the CABIN LAKE Property with the flight path.

3.2 Regional geological context

The Yukon Territory is situated in the northern part of the large geologic (and physiographic) belt known as the Cordillera. It is composed of relatively young mountain belts that range from Alaska to Mexico. The Yukon Territory is composed of a diverse type of rocks recording more than a billion years of geological history. Most of them have been affected by folding, faulting, metamorphism and uplift during various tectono-metamorphic events over at least the last 190 million years. This deformation has resulted in a complex arrangement of rock units and the mountainous terrain that has shaped today's geology. Geologically, Yukon is divided into two main components which are largely separated by the Tintina Trench. Formations northeast of the Tintina Fault consist of a thick, older sequence of sedimentary rocks which was deposited upon a stable geological basement. Rocks southwest of the Tintina Trench are composed of a younger, complex mosaic of igneous and metamorphic, representing numerous accreted terranes (Fig. 3).

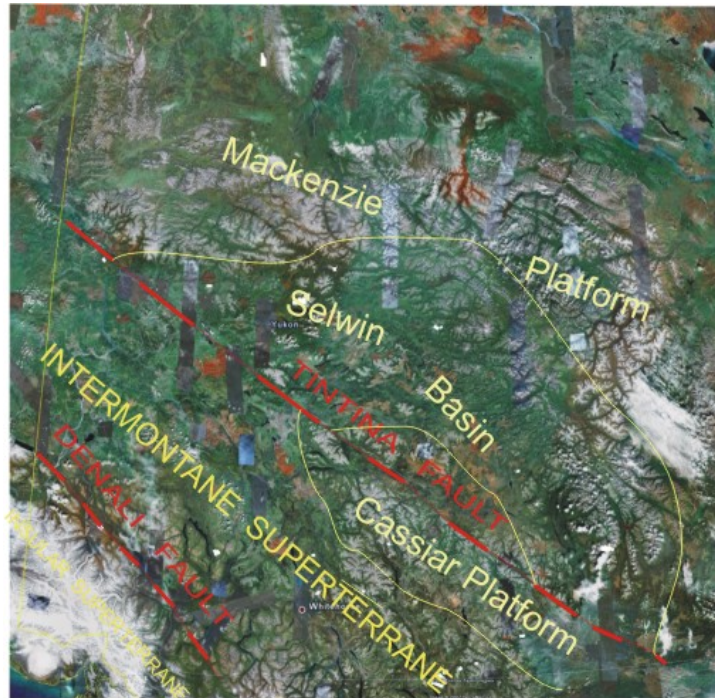


Fig.3. The major tectonic elements of Yukon superimposed on the satellite image. The figure indicates that the territory is composed of two dominant rock packages separated by the Tintina Fault: thick packages of sediments (northeast) and accreted Terranes (Southwest).

3.3 Geological context of the CABIN LAKE Property

The Cabin Lake property is underlain by bi-modal volcanic sequences hosting disseminated sulphides. These rocks are prospective for Volcanogenic Massive Sulphide mineralization. The volcanic rocks are trending in the north-northeast direction and are shallowly dipping eastwardly. These volcanic rocks are intruded by three different types of intrusions, comprising undeformed granodiorite and diorite. Major and minor structures appear to be dominated by a north steeply dipping northwest trend. Subordinate structures are oriented roughly east-west.

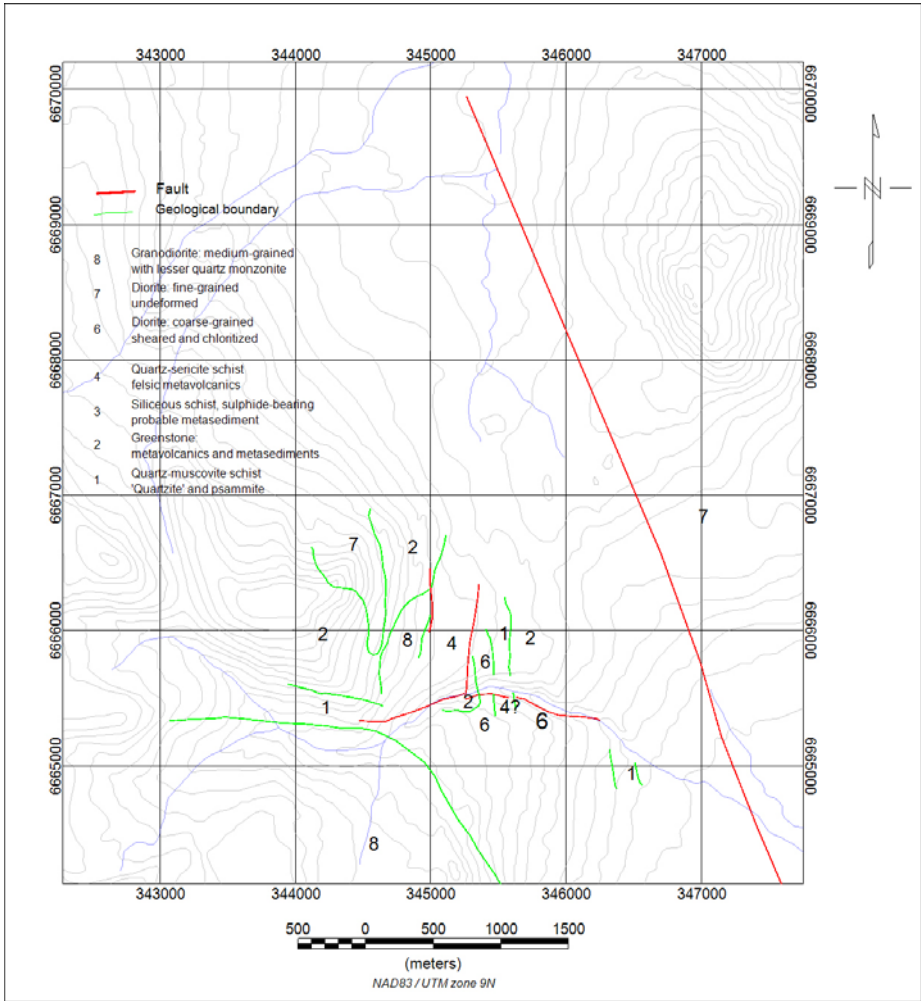


Fig. 4 Geological scheme of the CABIN LAKE Property.

3.4 Mineralization

The main mineralization known in the CABIN LAKE Property consists of disseminated sulfides associated with volcanic rocks. Massive sulfide mineralization has not been identified in this block.

4. INTERPRETATION OF THE MAGNETIC DATA

4.1 Introduction

Aeromagnetic surveys are routinely used as a powerful tool at different stages in mining exploration and in geological mapping. Because geological formations have different concentrations of magnetic minerals, they exhibit different magnetic signatures in the magnetic field, depending on the susceptibility contrast of rocks and the characteristics of the magnetic field. Thus, observed magnetic field over an area, can provide useful information that can assist the lithological and the structural mapping. It can be used to detect iron-rich mineral deposits, and/or mineral deposits associated with highly magnetic rocks (mafic and ultramafic formations).

4.2 Analysis of the Magnetic data

The observed magnetic field over the CABIN LAKE Property is shown in Fig.5. The magnetic field values are ranging from 57500 nT to 64600 nT, yielding a difference in the magnetic field intensity of more than 7000 nT. This large difference is due to the strong circular anomaly observed in the extreme SW corner of the map. The nature of this anomaly could be a mafic or ultramafic structure not indicated in the geological map. Magnetic lineaments trending in the NW direction are observed in the eastern part of the area. They could be related to mafic dykes and / or faults containing magnetic material (magnetite, pyrrhotite, etc..) . In the central area, the magnetic field expresses a more or less quiet character with low intensities. Several short wavelength lineaments trending in the NW direction are indicated in the northwestern portion of the map. An anomalous zone that coincides with the outcrop of dioritic rocks is clearly indicated in the central area.

Since the contents of the observed magnetic maps include the response of shallow and deep magnetic sources, it is difficult to analyze the maps containing different wavelength anomalies. Distinguishing shallow features from deeper ones can be performed via several methods of field separation and filtering.

Figure 6 shows the reduced to the pole magnetic field map, and upward continued to 100m. The short wavelength anomalies related to shallow sources have been suppressed. The map highlights the NS trending lineament (eastern part) and the outlines of the magnetic structure (Southwestern corner).

Figure 7 illustrates the vertical gradient of the TMI. The vertical gradient map shows the enhancement effect of magnetic signals caused by shallow sources and related to faults and contacts. The tilt derivative map illustrated in Fig. 8 yields another example of amplifying short wavelength signals generated by shallow sources. The tilt derivative known as being the local phase is computed from the vertical and horizontal gradients. As illustrated in the Tilt derivative map several shallow magnetic lineaments trending mostly in the NW direction can be identified in this area. Most of them are probably associated with faults or hidden mafic dykes. Both maps provide a better focalization of the strong anomaly observed in the southwestern corner of the map.

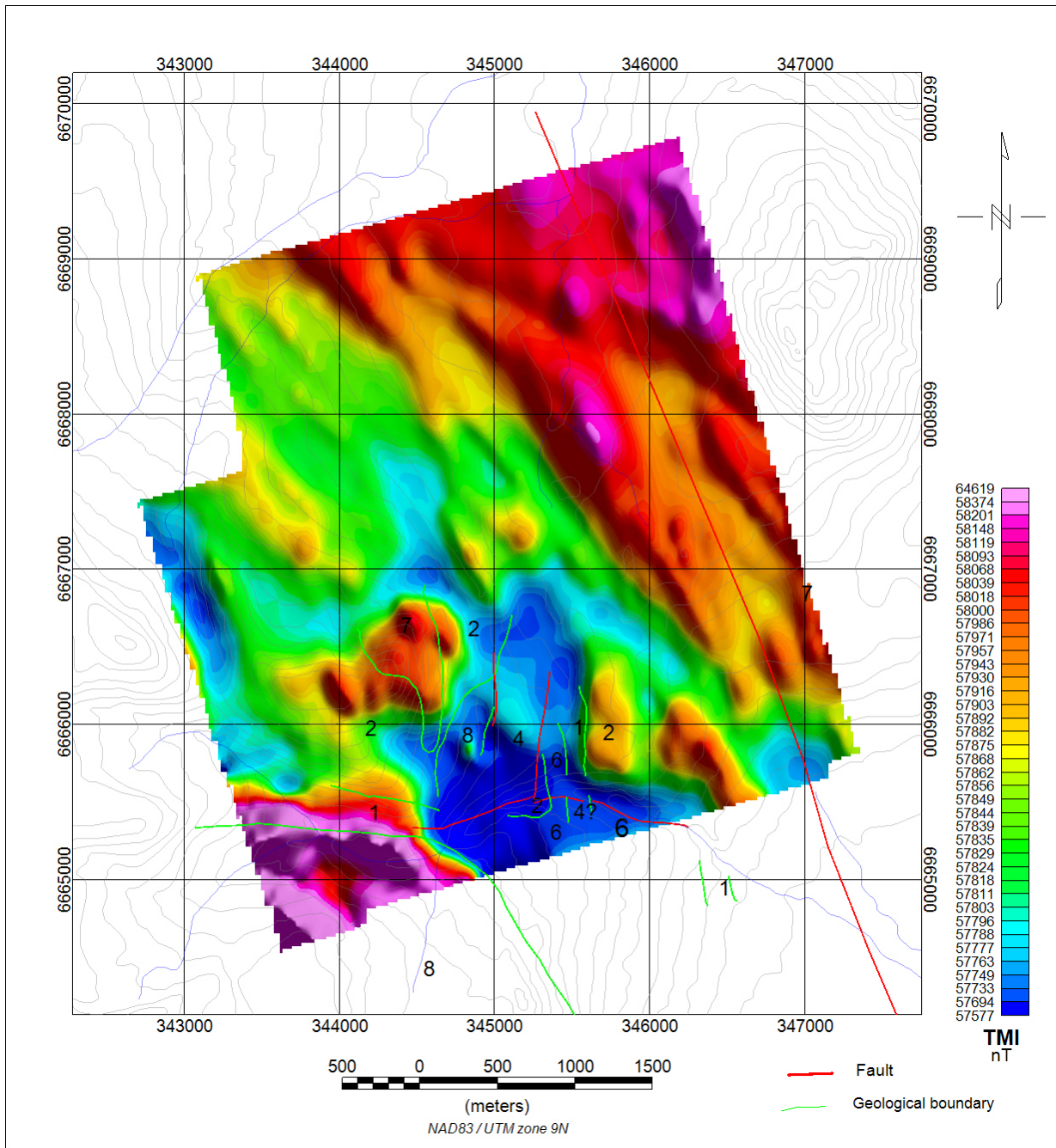


Fig. 5 TMI image of the CABIN LAKE Property.

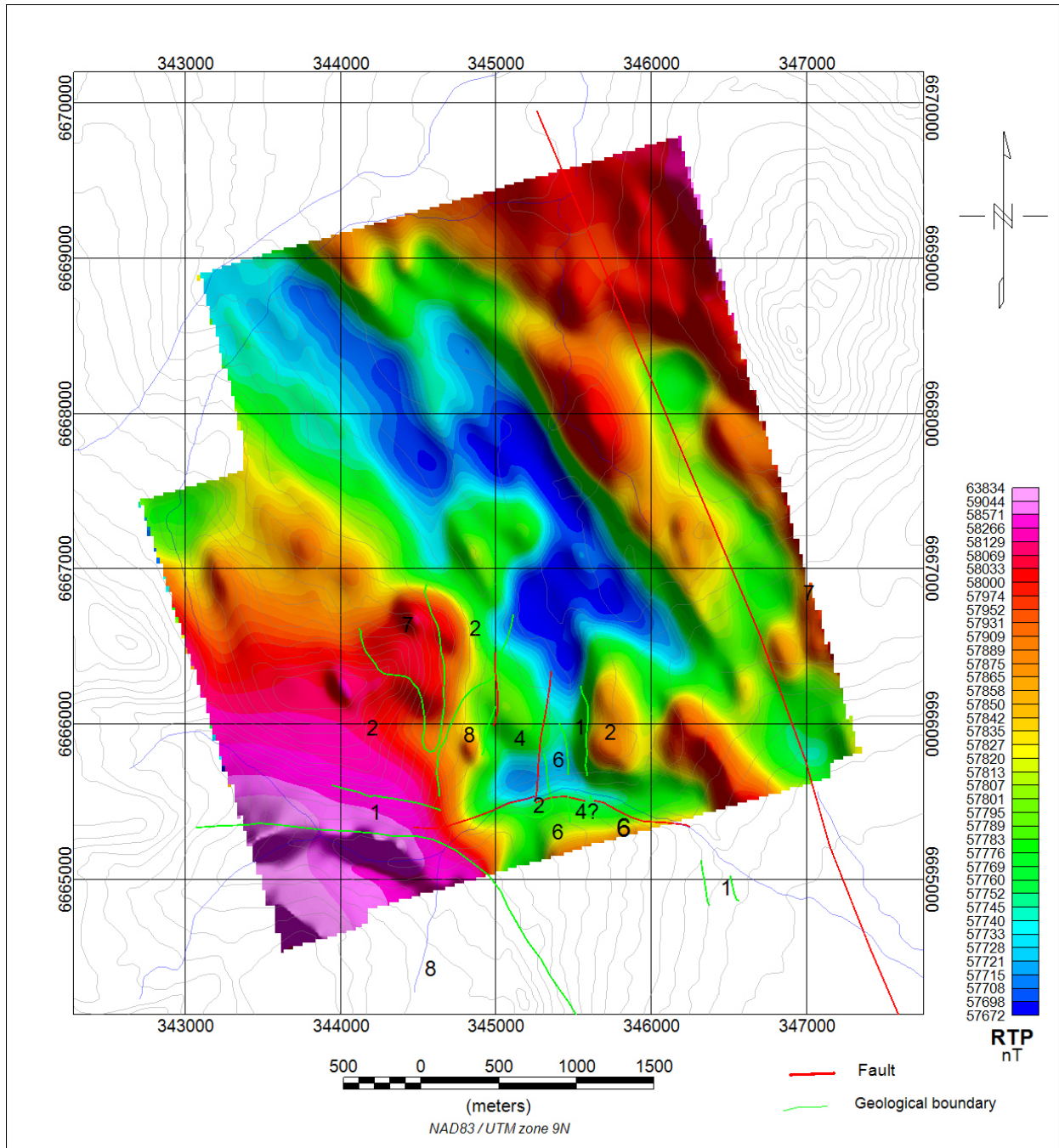


Fig.6 Color shaded relief of the reduced to the pole TMI with upward continuation to 100m.

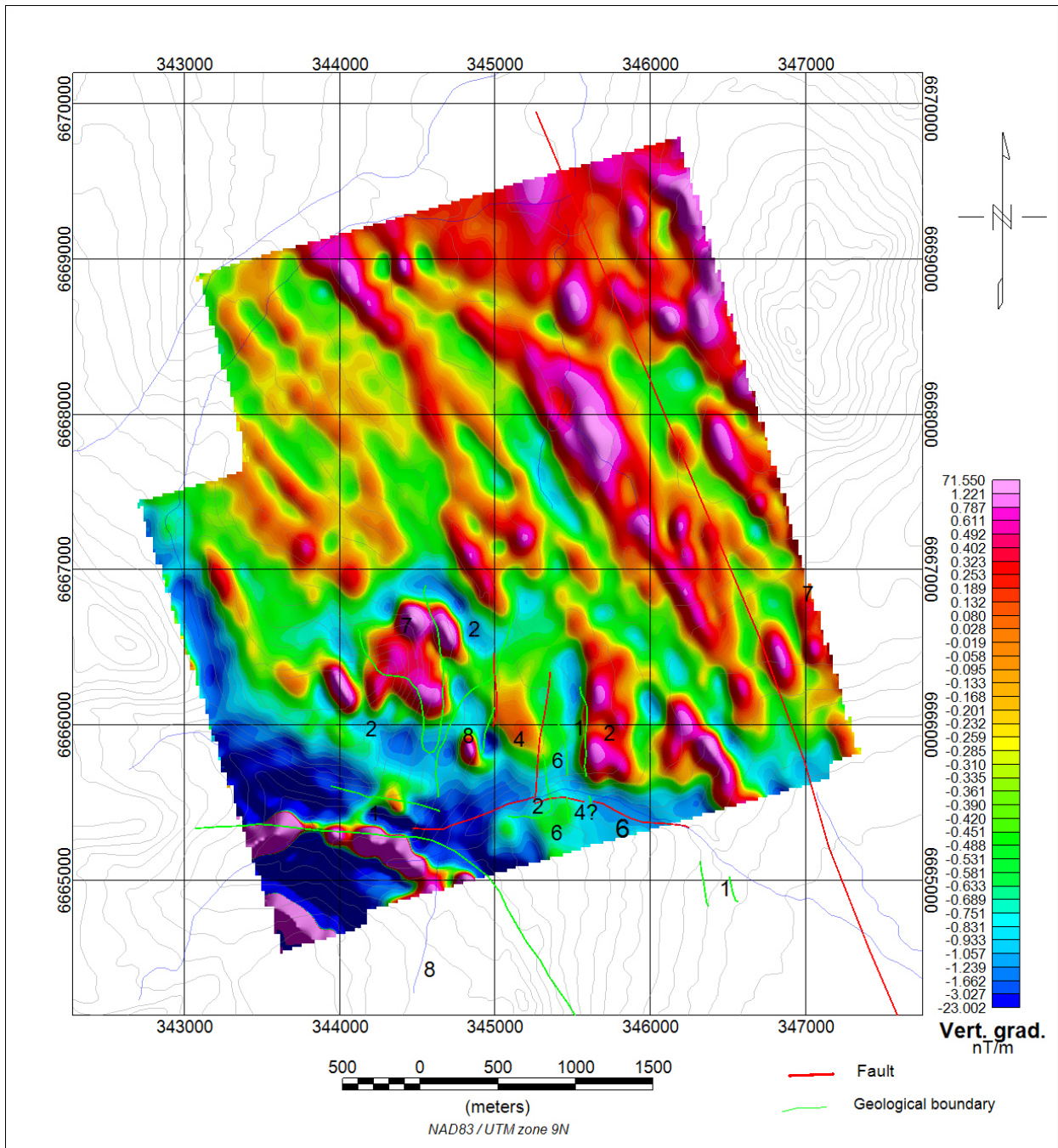


Fig.7 Color shaded relief of the vertical gradient of the magnetic field.

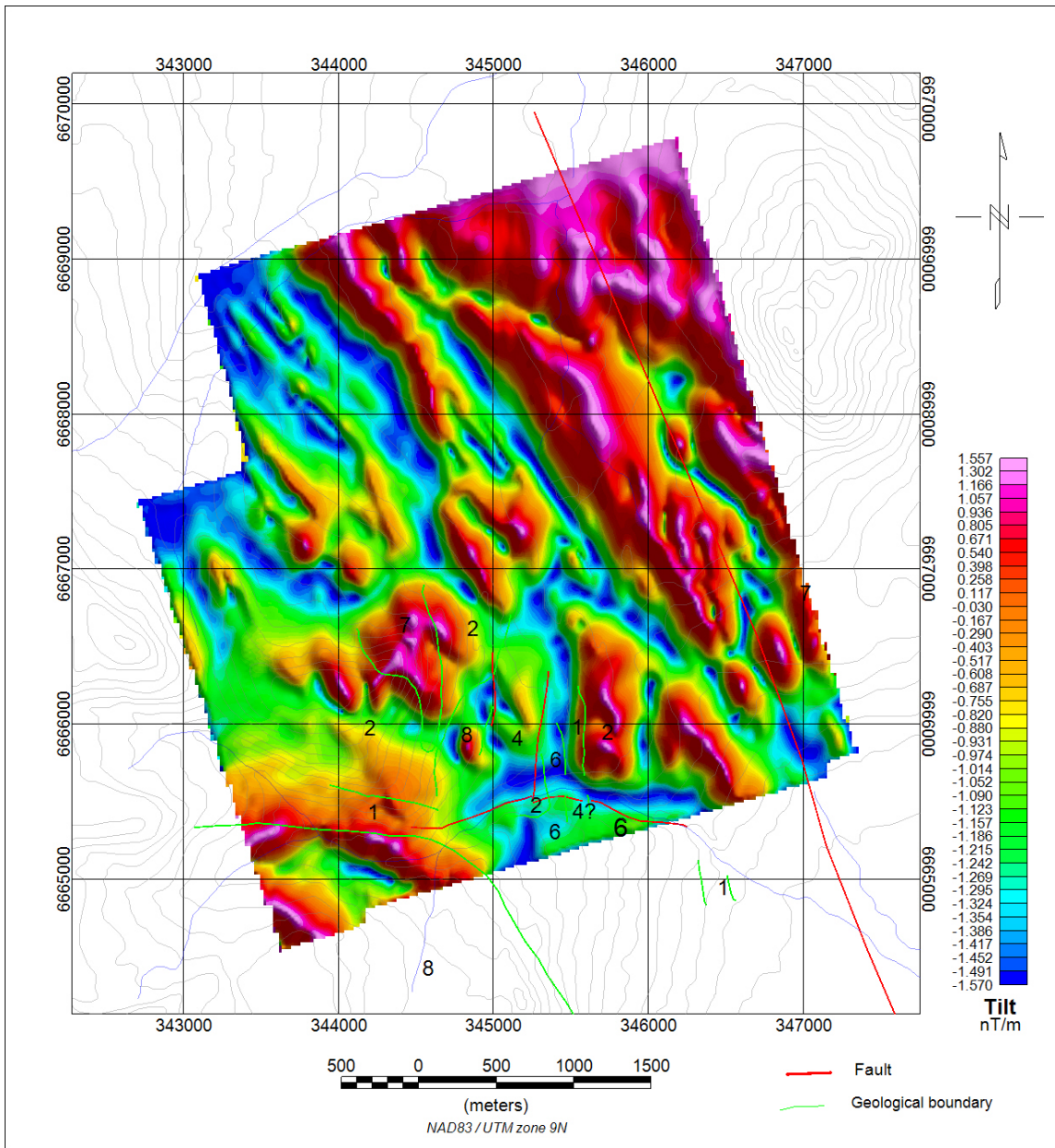


Fig. 8 Color shaded relief of the Tilt derivative.

4.3 Inversion of the magnetic data

Several computer-based techniques can be used to automatically detect magnetic sources and yield estimations of their geometrical and physical parameters. These techniques can be either used to gridded data (3D methods) or to profiles (2D methods). Euler deconvolution is a well established technique, allowing a rapid interpretation of a large amount of magnetic data. This method is mainly aimed to delineate magnetic sources boundaries and to estimate their depths.

Fig. 9 shows the results obtained with the Euler deconvolution inversion using a structural index of 1, a depth tolerance of 10% and a square deconvolution window having a size of 200×200 metres. Euler solutions have been plotted on the total gradient (analytic signal) map for better illustration. The picks of total gradient are used to located and delineate the magnetic sources boundaries. Euler solution are mostly related to shallow sources (<100 m). Most of them are related to the magnetic lineaments trending in the NW confirming the qualitative analysis of the reduced maps. The magnetic inversion indicates that the estimated depths of the magnetic structure located in the southwestern corner of the area are less than 50m.

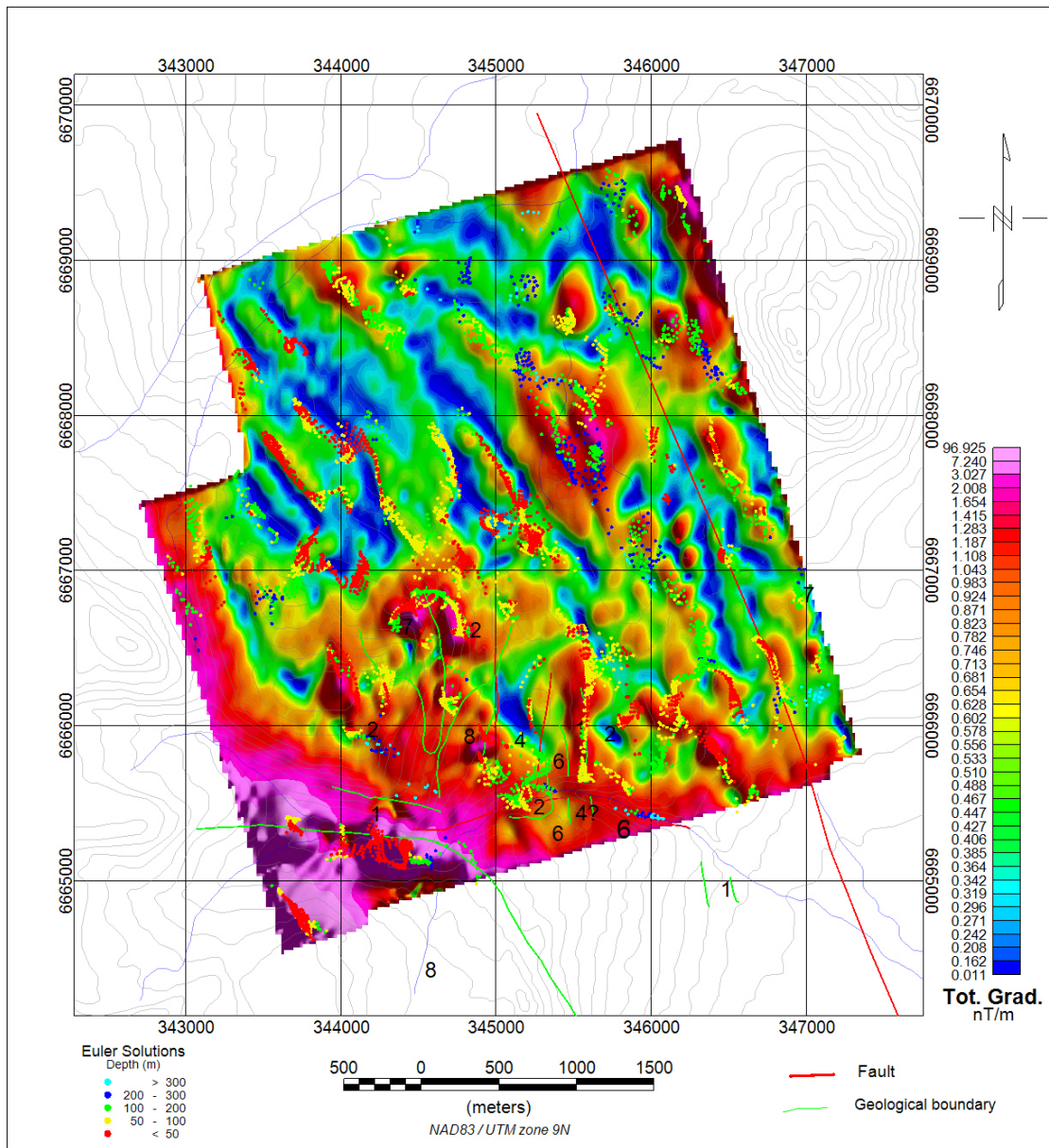


Fig. 9 Euler deconvolution solutions plotted on the total gradient image.

5. INTERPRETATION of VTEM DATA

5.1 Introduction

Transient electromagnetic surveys have proven to be a very efficient tool in mineral exploration by detecting hidden deposits characterized by higher conductivities than the medium in which they are embedded. Because Time domain systems have a much greater depth penetration compared to the Frequency domain systems, these systems are considered as a tool of choice in the mining exploration. The Geotech Helicopter VTEM system, operating in the Time domain, uses concentric-loop geometry with the receiver mounted in the centre of a larger transmitter loop. Both loops are oriented in the vertical plane. This configuration has a number of advantages, as a maximum coupling, sharper anomalies by comparison to airborne fixed wing systems, and the shape of the anomalies is independent of the flight path orientation. Furthermore, the high moment transmitter combined with the lower terrain clearance yields stronger secondary field signals in most conductors when compared to other systems. The actual VTEM systems measure both the electromagnetic induction field B and its time derivative dB/dt . This system specificity has a lot of advantages, as the dB/dt better resolves the shallow conductive sources while the B -field exhibits a better resolution for deep conductors.

5.2 VTEM anomalies shape

For concentric-loop geometry systems when both loops are oriented in the Z -axis (VTEM system) thick dipping or horizontal conductors exhibit a characteristic single peak, while steeply dipping and thin conductors manifest a double peak. The minimum indicates the location of the top of the thin conductor, and the major peak indicates the side towards which the conductor is dipping. Synthetic models anomalies were generated for the plate type conductors are provided in the Appendix A to better understand the shape of the VTEM anomalies

5.3 Analysis of the EM results

Figures 12 and 13 show the stacked profiles in pseudo-logarithmic scale of the dB/dt and B-field channels, respectively. Both maps show the existence of 2 linear anomalous zones (A and B) trending south- north roughly. Both anomalous zones are composed of anti-symmetric anomalies indicating the response of northeasterly shallow dipping conductive bedrock (Figs. 10, and 11).

The interpretation of the EM profiles was performed using in-house built software converting the EM decays into picked anomalies along the profiles and providing estimates of the conductance and the decay constant (τ) of isolated anomalies. The picked EM anomalies were posted on the late time EM channel. Figures 14 and 15 illustrate the results of the picked anomalies superimposed on the dB/dt, and B-field late time channel (3.911 ms after the current shut off), respectively.

The estimated conductance values for the Zone A anomalies are around 10 S. The calculated τ constants for this zone are ranging from 4 ms to 6 ms roughly. The anomalies of the second zone (B) are characterized by higher conductance values, ranging between 10 and 20 S, however the estimated τ values are lower (less than 4 ms) compared with those of the zone A. The picked anomaly maps show the existence of a linear NW trending conductor and bordering the southeastern side of the map.

It is worth mentioning that the observed EM anomalies are in very good spatial correlation with the observed magnetic signal as indicated in Fig. 16.

The interpretation map (Fig. 16) shows the results of the magnetic and electromagnetic analysis superimposed on the magnetic total gradient image. The magnetic interpretation suggests the existence of two cross cutting faulting systems trending in the NW and NE directions, respectively. It also shows that the detected EM anomalies are in very good correlation with the magnetic signal. As indicated in the interpretation map, anomalies of the zone A are correlated with a deep magnetic structure located at a depth between 200 m and 300 m.. However, anomalies of the zone B are correlated with a shallower linear magnetic structure (<200m). The existence of a good correlation of the detected conductive bedrocks with the magnetic signal is a good indication for the possible occurrence of massive sulfide mineralization containing magnetic minerals such as magnetite and pyrrhotite.

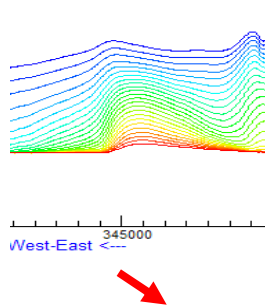


Fig. 10 EM profiles of the anomalous zone A, (line 8050). The red arrow indicates the dip direction of the conductor.

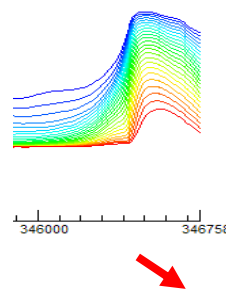


Fig. 11 EM profiles of the anomalous zone B, (line 8220) showing strong response of the late time decays. The red arrow indicates the dip direction of the conductor

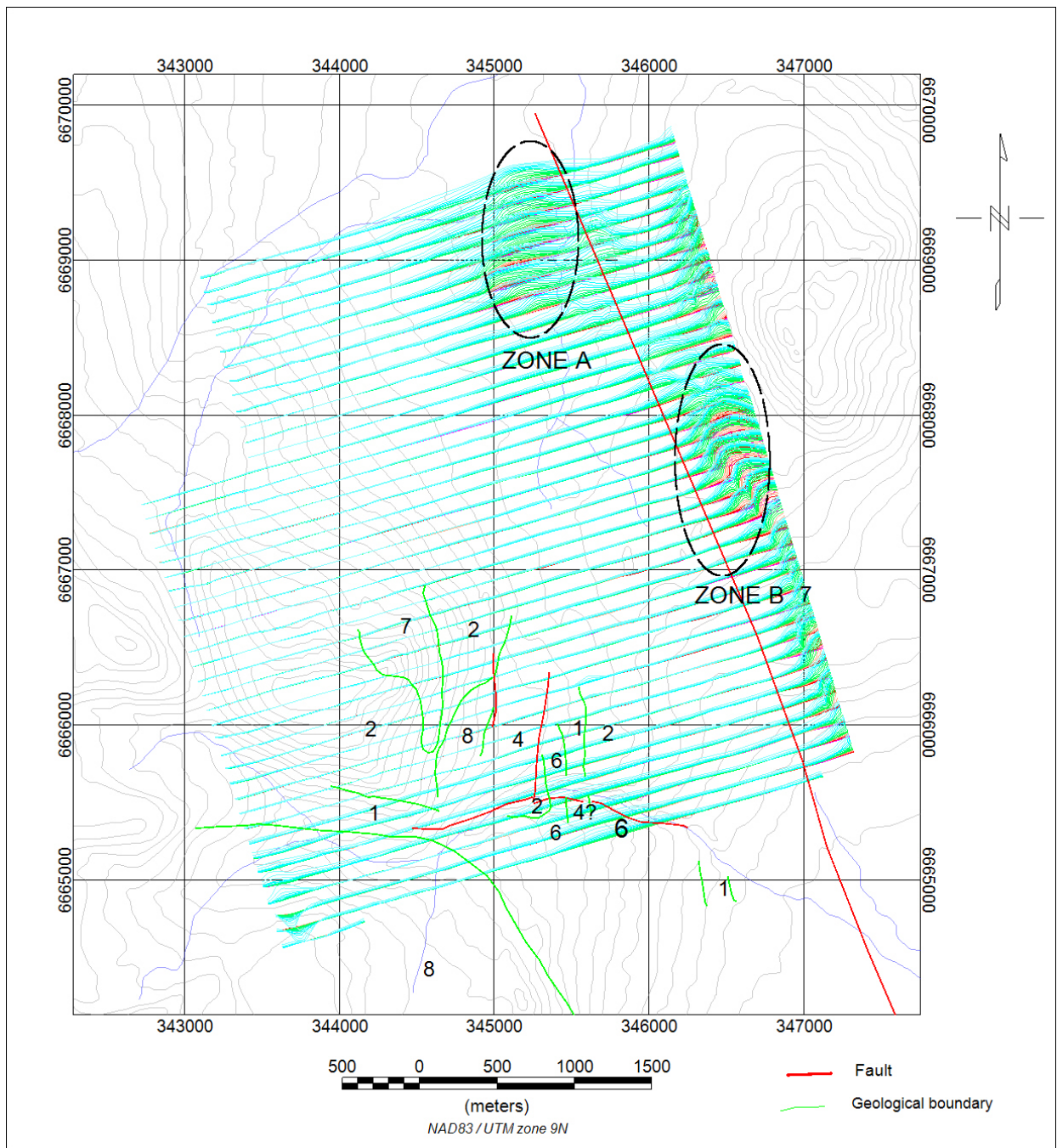


Fig. 12 Stacked EM dB/dt profiles at log-linear scale. Early time decays are in green and late time in red.

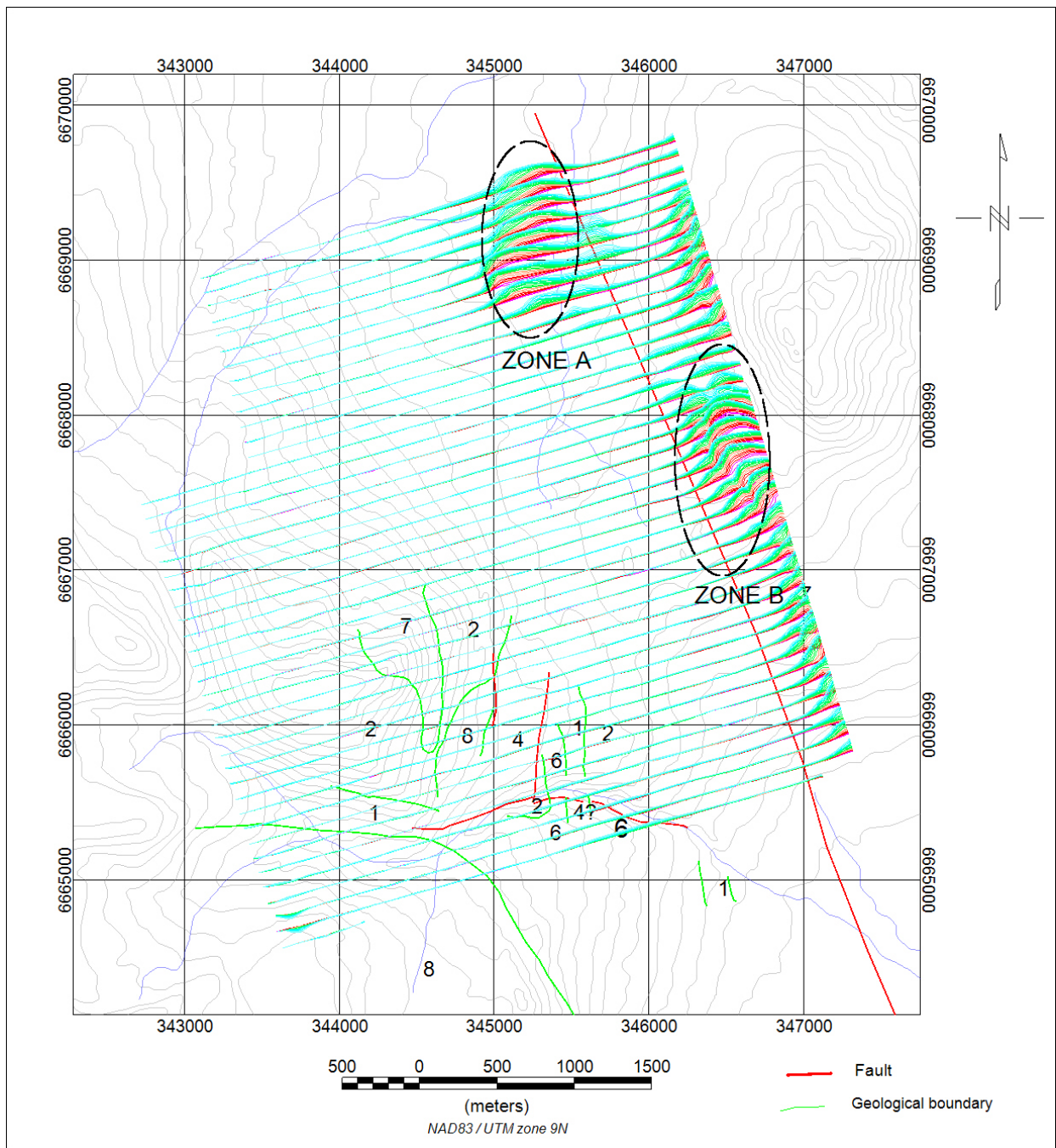


Fig. 13 Stacked EM B-Field profiles at log-linear scale. Early time decays are in green and late time in red.

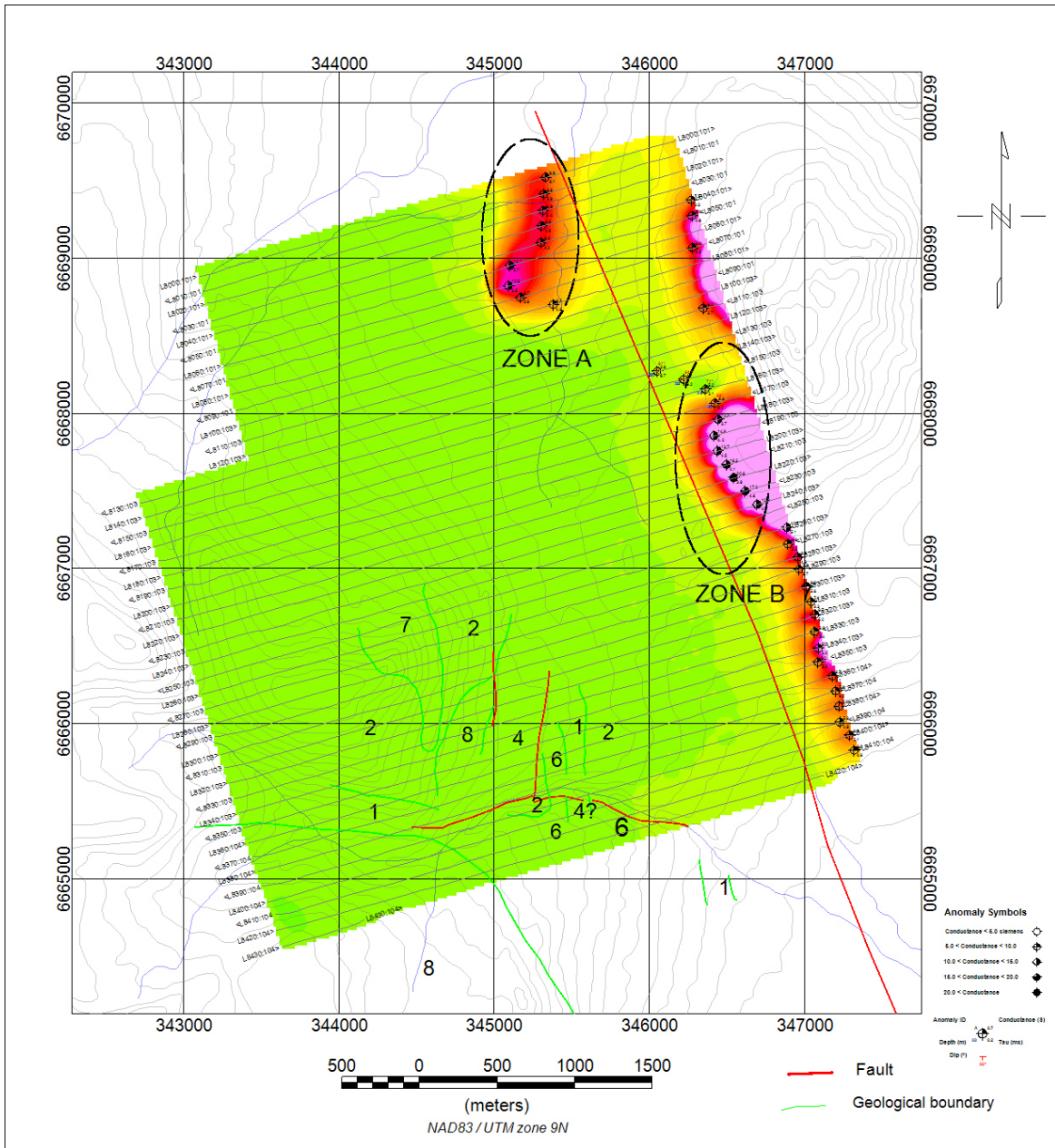


Fig. 14 EM picked anomalies plotted on the late time dB/dt channel image.

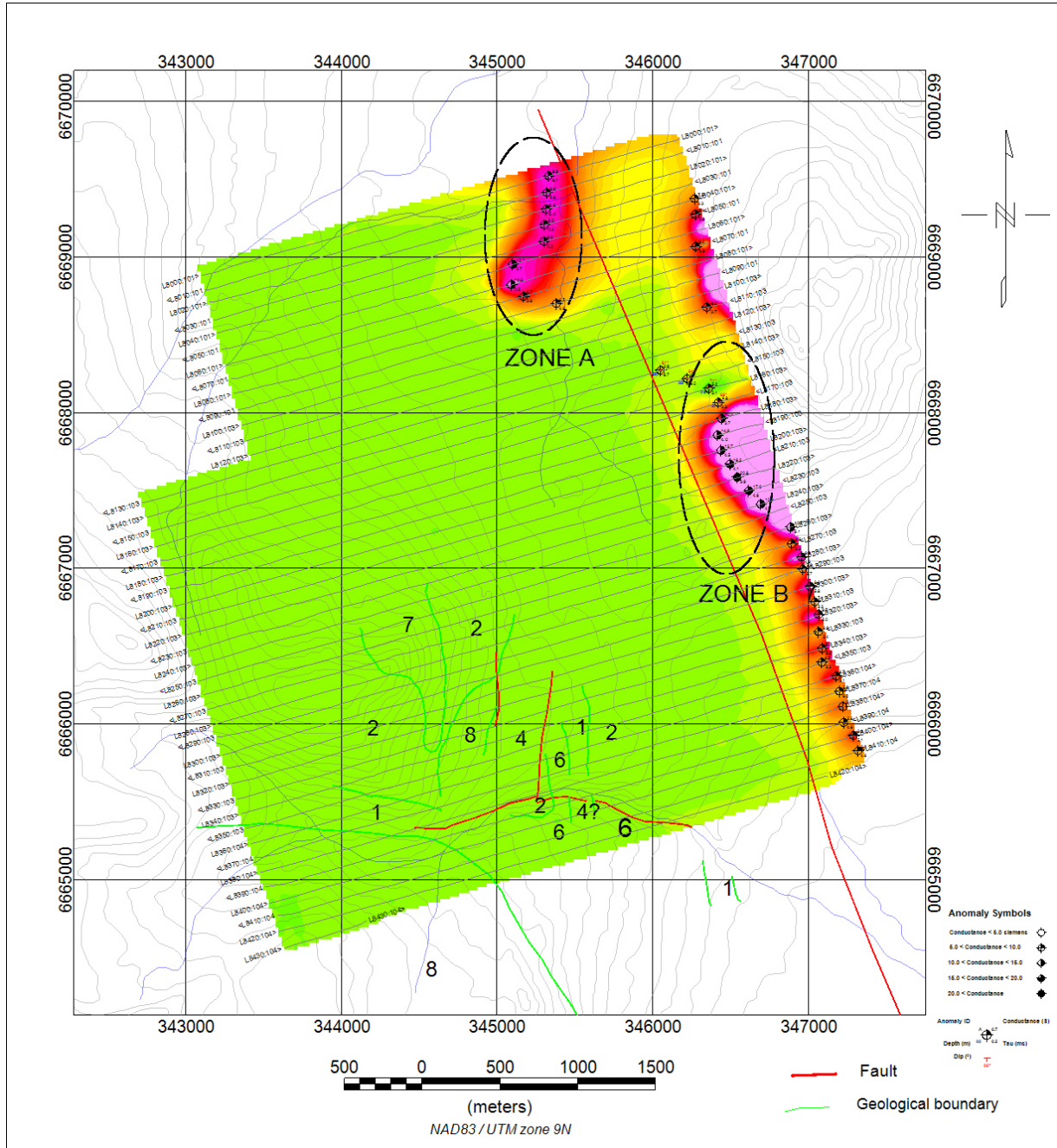


Fig. 15 EM picked anomalies plotted on the late time B-Field channel image.

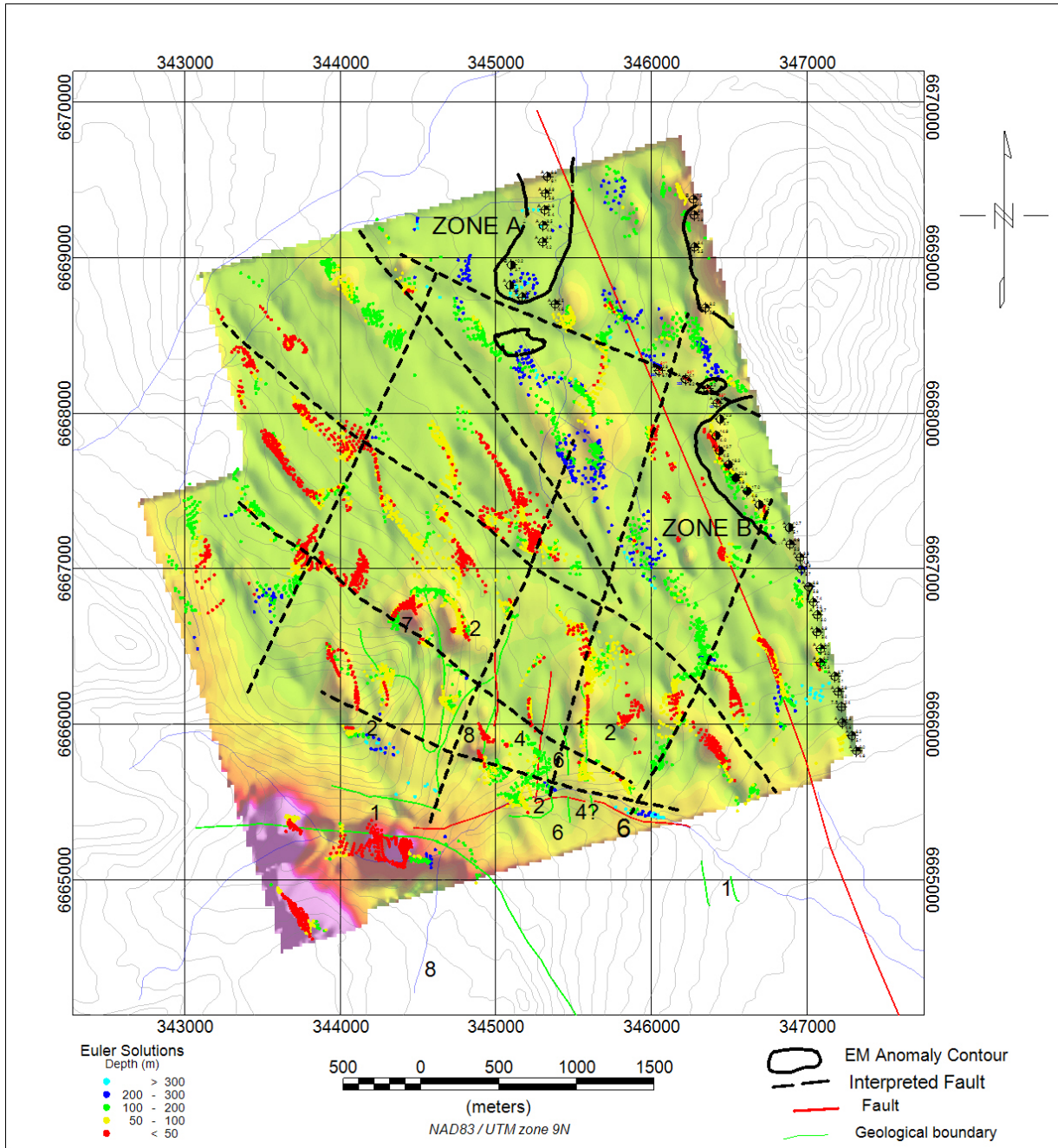


Fig. 16 Interpretation map showing the results of the magnetic and electromagnetic data analysis.

5.4 Selected Anomalies

Four individual anomalies extracted from the described above anomalous zones have been selected for modeling by converting the EM decays into CDIs . The anomalies are located on the following lines: L8020, L8050, L8210, and L8220. The summarized characteristics of the selected anomalies are given in the following table:

Line	Anomaly ID	Anomaly Type description	Conductor geometry	X-location m	Y-location m	Conductance S	Dip	Dip Azimuth	Tau ms
L8020	A	One broad anti-symmetric peak	Thick shallow dipping plate	345314	6669307	8.9	Shallow	SE	5.4
L8050	B	One broad anti-symmetric peak	Thick shallow dipping plate	345099	6668953	10.2	Shallow	SE	3.7
L8210	A	One broad anti-symmetric peak	Thick shallow dipping plate	346495	6667669	18.3	Shallow	NE	4.1
L8220	A	One broad anti-symmetric peak	Thick shallow dipping plate	346542	6667585	20.8	Shallow	NE	3.9

Table 1. Summarized results of the selected anomalies.

5.5 Conductivity Depth Sections

Conductivity depth imaging (CDI) is considered as one of the important steps in the analysis and interpretation of electromagnetic data. CDI allows providing useful information of the conductivity distribution of the considered cross section. CDI were performed for the selected lines using the EMflow software. The obtained results are shown in Figures17-20.

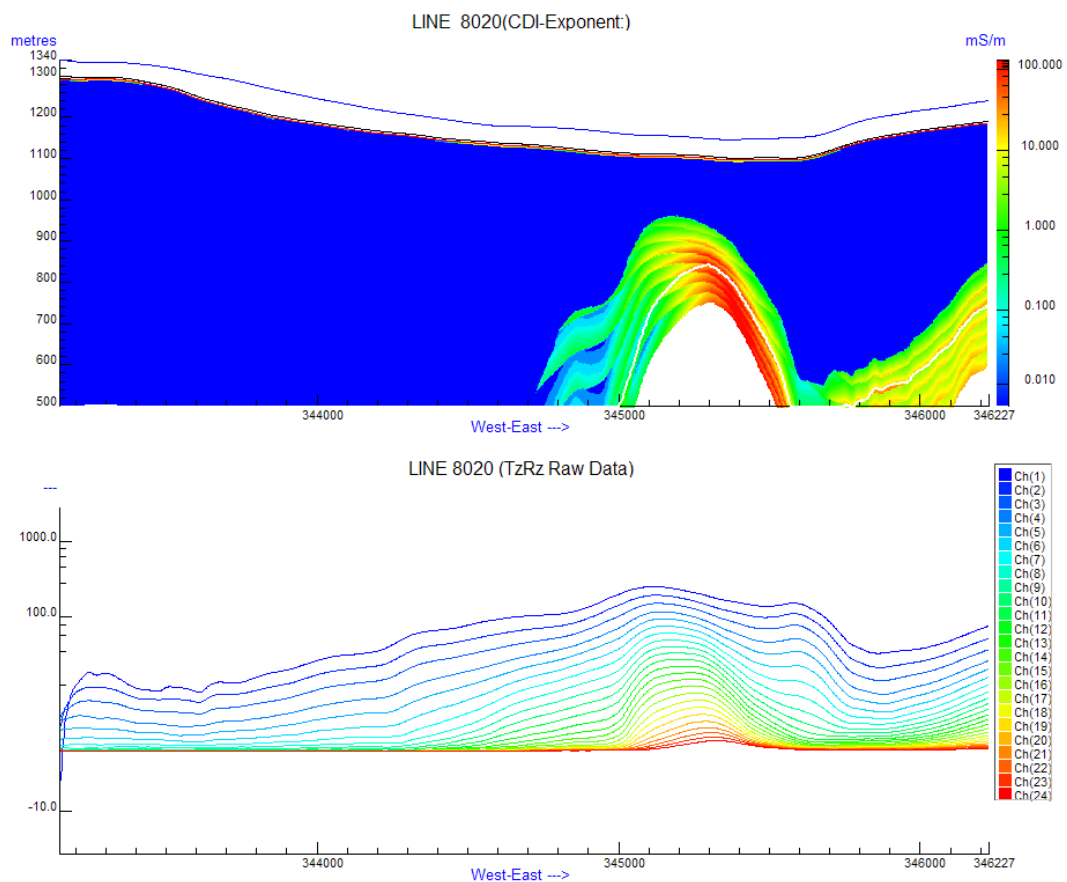


Figure17 shows the CDI section for the line L8010 (Zone A). The section indicates the presence of a good conductive bedrock at a depth less than 200 m. The bedrock is dipping in the east-southern direction. Drilling tests are recommended on this anomaly to detect a possible massive sulfide mineralization VMS type.

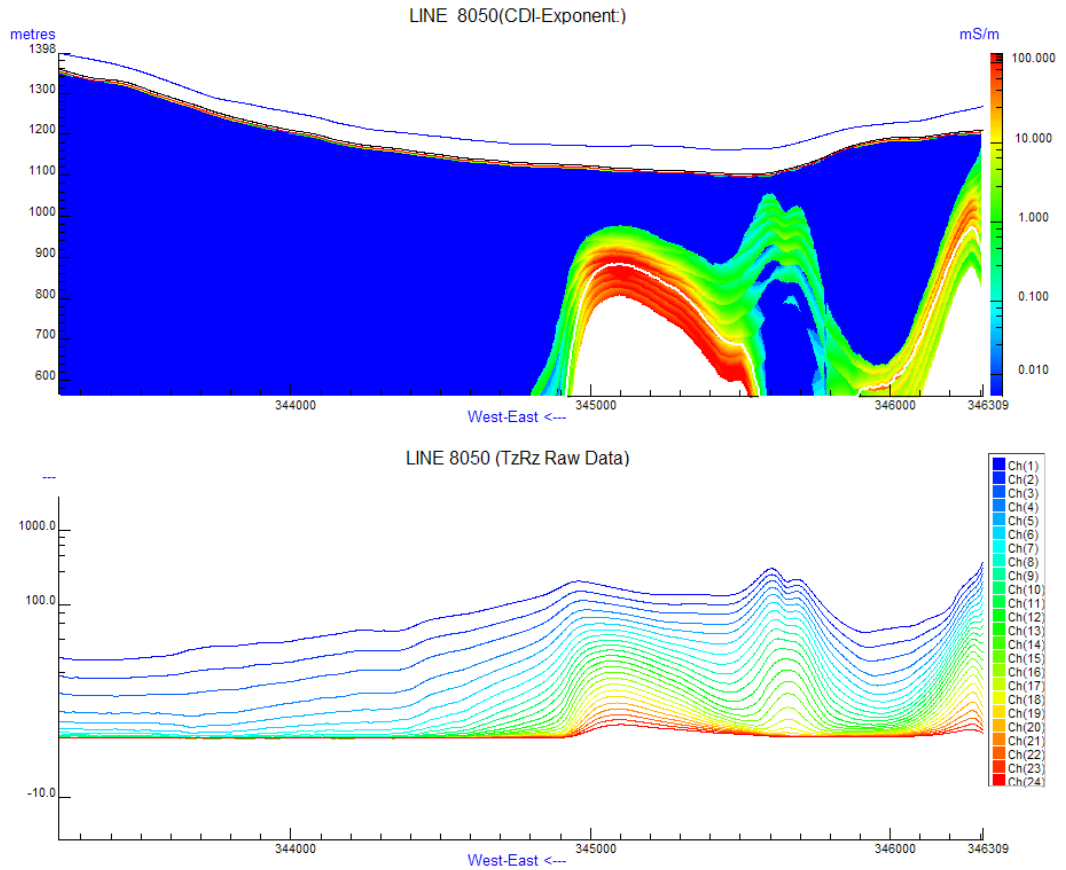


Figure 18 shows the CDI section for the line L8050 (Zone A). The section indicates the presence of a good conductive bedrock at a depth less than 200 m. The bedrock is dipping in the east-southern direction. Drilling tests are recommended on this anomaly to detect a possible massive sulfide mineralization VMS type.

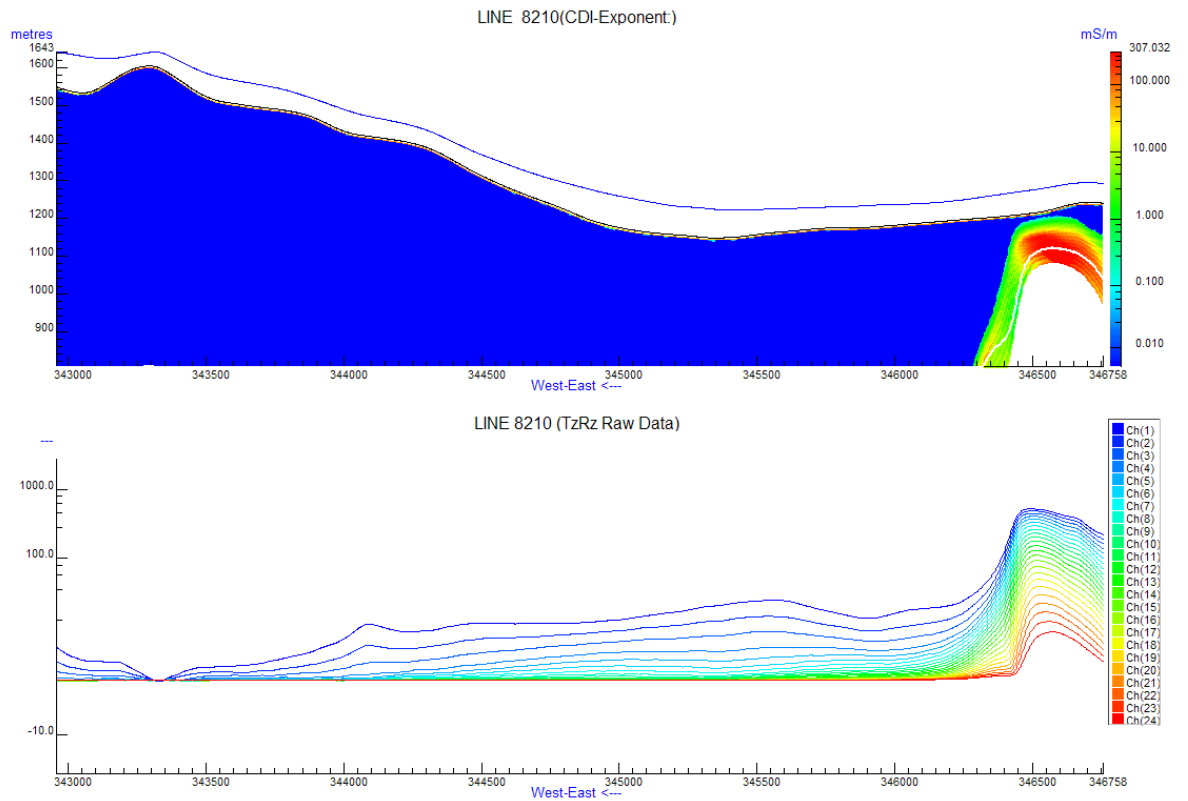


Figure 19 shows the CDI section for the line L8210 (Zone B). The section highlights the existence at the end of the profile of a shallow dipping good conductor (depth <100m). Drilling tests are recommended on this anomaly to detect a possible massive sulfide mineralization VMS type.

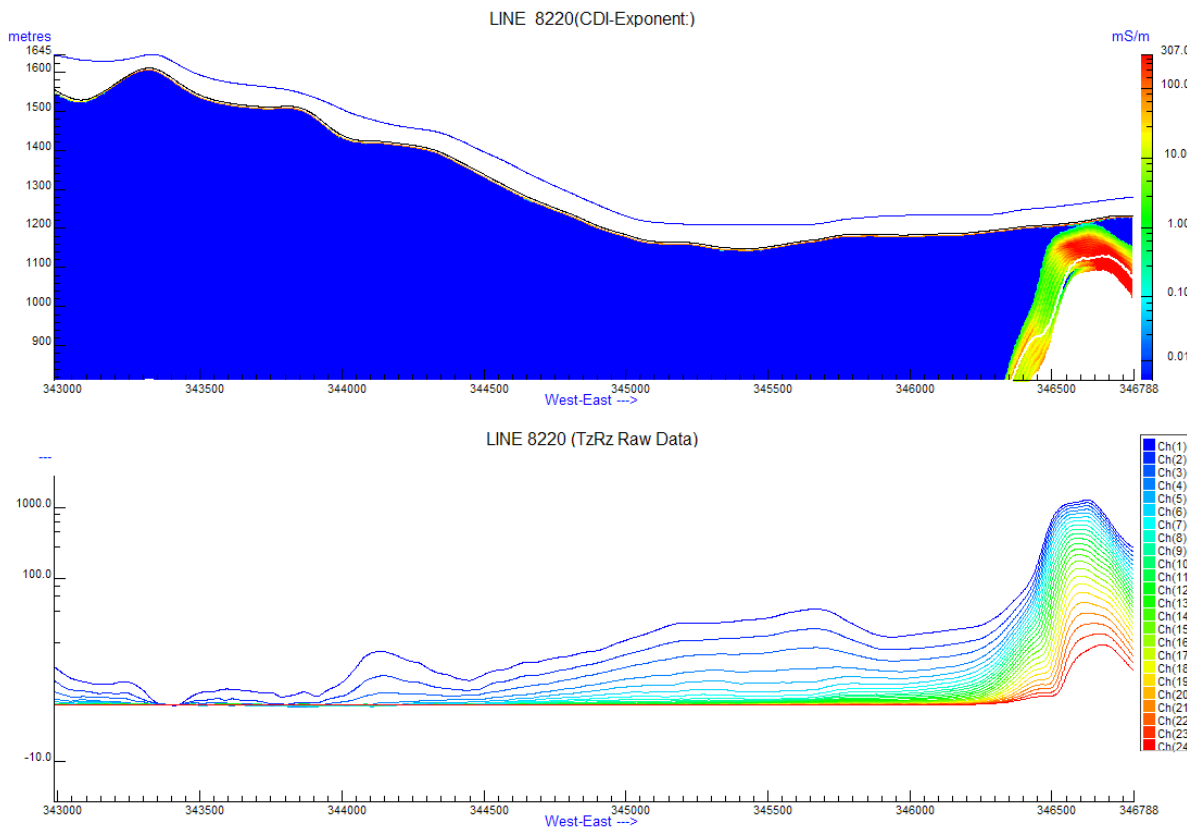


Figure 20 shows the CDI section for the line 8220 (Zone B). The section highlights the existence at the end of the profile of a shallow dipping good conductor (depth <100m). Drilling tests are recommended on this anomaly to detect a possible massive sulfide mineralization VMS type.

6. CONCLUSIONS AND RECOMMENDATIONS

The analysis of the magnetic map of the CABIN LAKE property revealed that this area is characterized by a high magnetic activity. A strong anomaly with amplitude exceeding 7000 nT with a possible mafic/ultramafic nature was observed in the SW corner of the area. Several magnetic lineaments trending in the NW direction were identified. Their origin is probably associated with a dike/faulting system. The Euler deconvolution inversion method has shown that most of the detected magnetic sources are situated at depth less than 100m. Deeper sources (>200m) are located in the eastern part of the area. The magnetic interpretation using different reduced maps suggests the presence of two cross cutting faulting systems trending in the NW and NE directions.

The VTEM survey reveals the existence of 2 anomalous zones of interest. Both zones are in very good correlation with the magnetic field, indicating the metallic nature of the detected conductive bedrocks. The picked anomaly maps and the CDI sections performed for 4 lines clearly show the existence of good conductors dipping shallowly in the eastern direction and located at relatively shallow depths (<200 m) for the first conductor and (<100m) for the second one). The analyzed anomalies can represent a good target associated with VMS mineralization.

The recommendation is to conduct some drilling tests on both anomalous zones (A, B) to determine a possible massive sulfide mineralization.

Respectfully submitted,

Dr. Nasreddine Bournas
Geotech Ltd.
December, 2007

7. REFERENCES

1. J. CHEN, A. RAICHE, AND J. MACNAE, 2000, Inversion of airborne EM data using thin-plate models, SEG 2000 expanded abstracts.
2. STOLZ, E.M.G. AND MACNAE, J.C., 1991 Evaluating EM waveforms by singular-value decomposition of exponential functions. *Geophysics*, 63, 64-74
3. A.B. REID, J.M. ALLSOP, H. GRANSE, A.J. MILLETT AND I.W. SOMERTON, 1990, Magnetic interpretation in three dimensions using Euler deconvolution, , *Geophysics*, 55, 80-91.
4. Yukon Geological Survey, www.geology.gov.yk.ca

APPENDIX A



VTEM ANOMALY MODELING

I. THIN PLATE

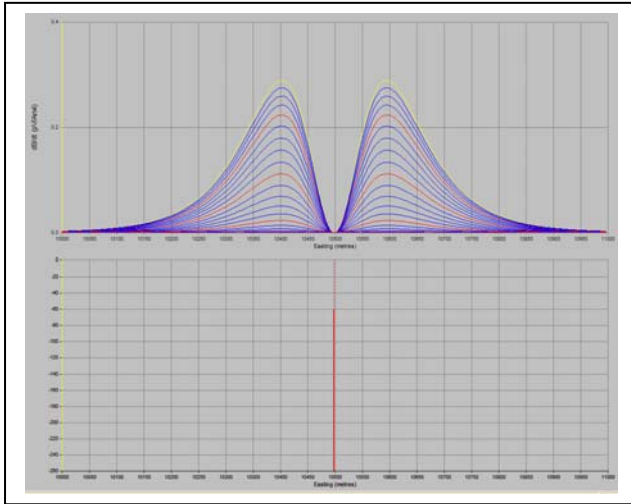


Figure A-1: dB/dt response of a shallow vertical thin plate. Depth=100 m, CT=20 S. The EM response is normalized by the dipole moment and the Rx area.

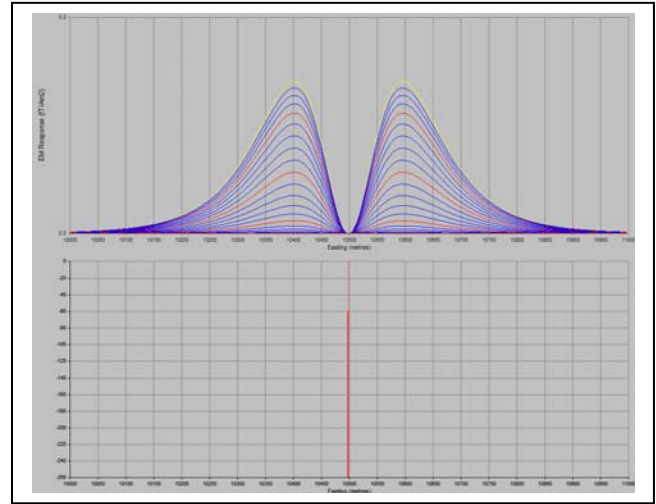


Figure A-2: B-field response of a shallow vertical thin plate. Depth=100 m, CT=20 S. The EM response is normalized by the dipole moment.

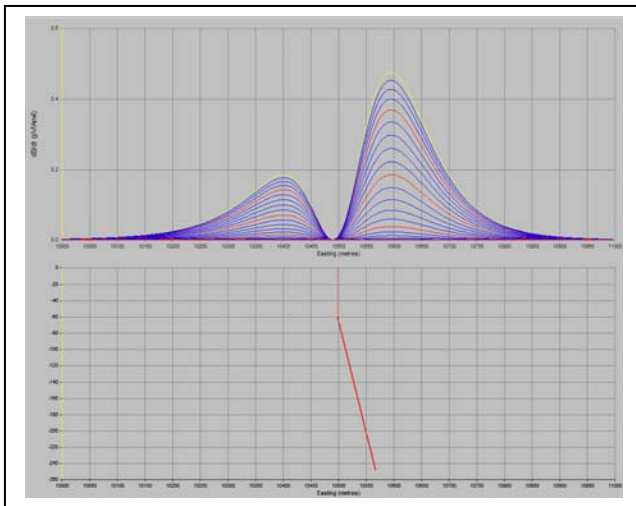


Figure A-3: dB/dt response of a shallow skewed thin plate. Depth=200 m, CT=20 S. The EM response is normalized by the dipole moment and the Rx area.

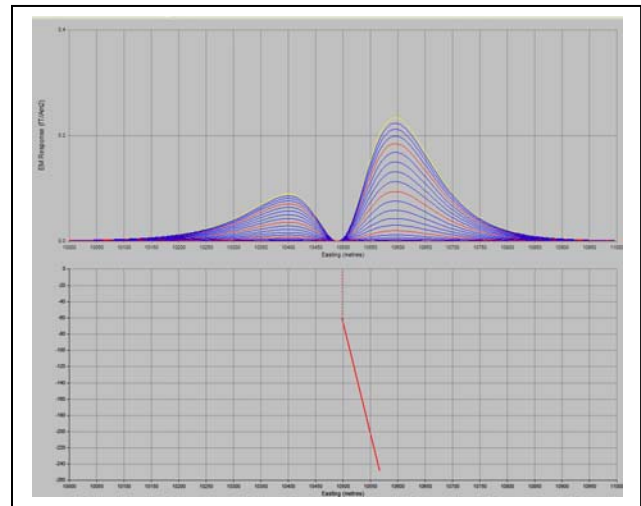


Figure A-4: B-field response of a shallow skewed thin plate. Depth=100 m, CT=20 S. The EM response is normalized by the dipole moment.

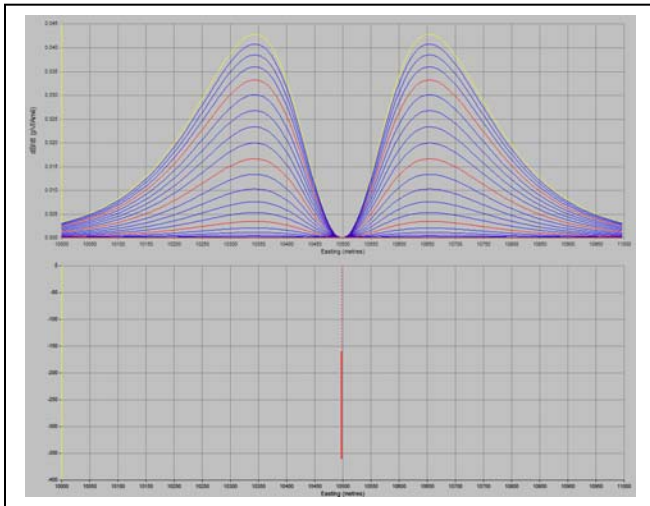


Figure A-5: dB/dt response of a deep vertical thin plate. Depth=200 m, CT=20 S. The EM response is normalized by the dipole moment and the Rx area.

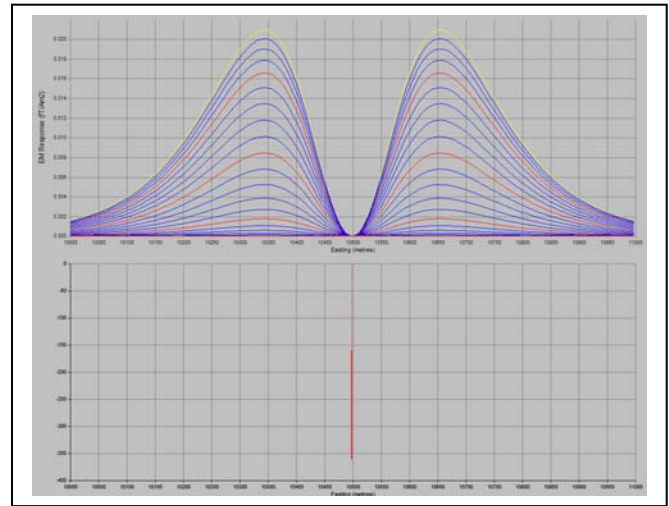


Figure A-6: B-Field response of a deep vertical thin plate. Depth=200 m, CT=20 S. The EM response is normalized by the dipole moment.

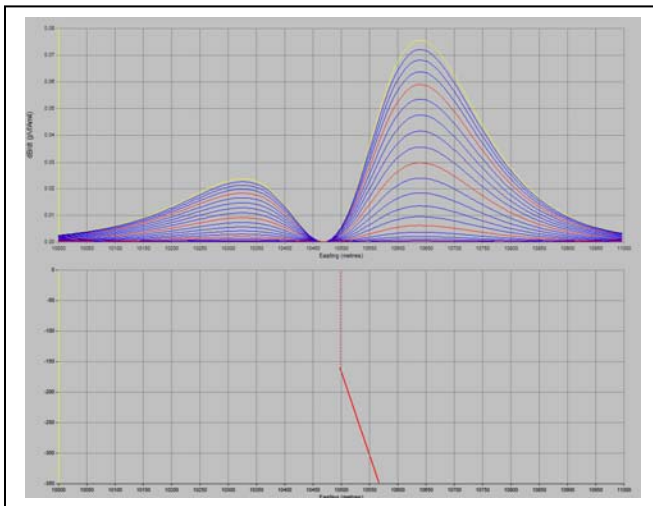


Figure A-7: dB/dt response of a deep skewed thin plate. Depth=200 m, CT=20 S. The EM response is normalized by the dipole moment and the Rx area.

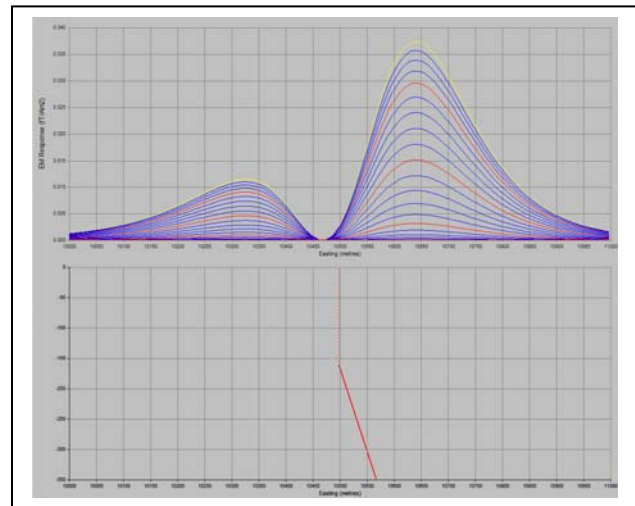


Figure A-8: B-field response of a deep skewed thin plate. Depth=200 m, CT=20 S. The EM response is normalized by the dipole moment.

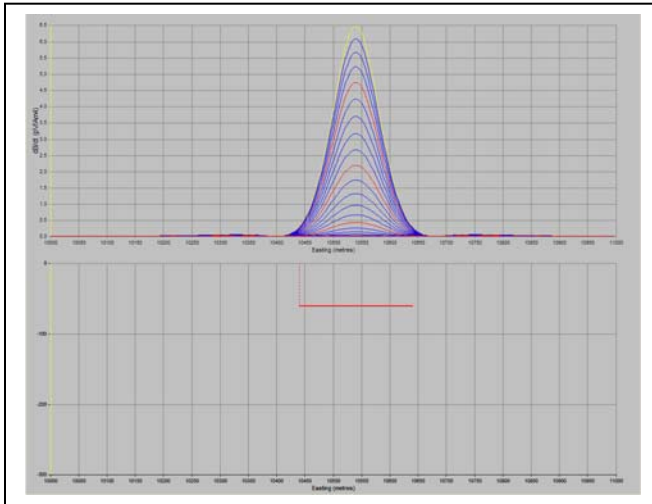


Figure A-9: dB/dt response of a shallow horizontal thin plate. Depth=100 m, CT=20 S. The EM response is normalized by the dipole moment and the Rx area.

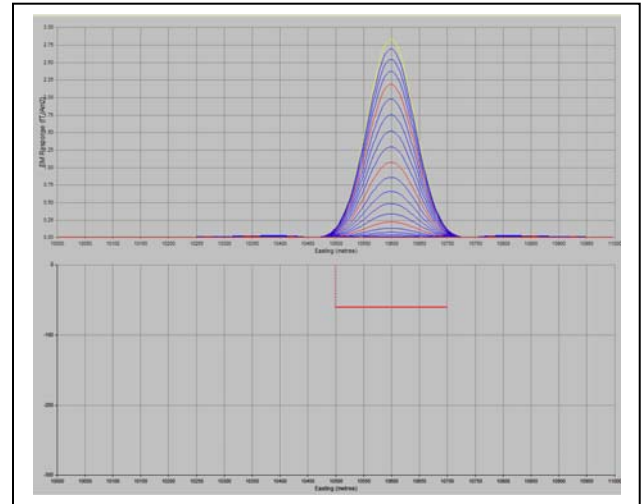


Figure A-10: B-Field response of a shallow horizontal thin plate. Depth=100 m, CT=20 S. The EM response is normalized by the dipole moment.

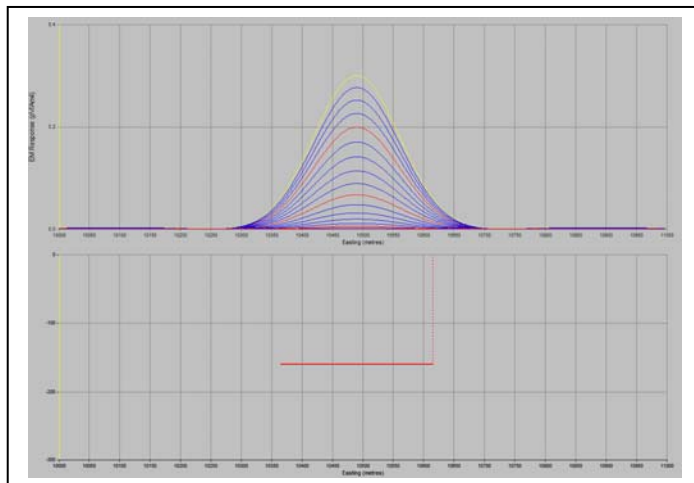


Figure A-11: dB/dt response of a deep horizontal thin plate. Depth=200 m, CT=20 S. The EM response is normalized by the dipole moment and the Rx area.

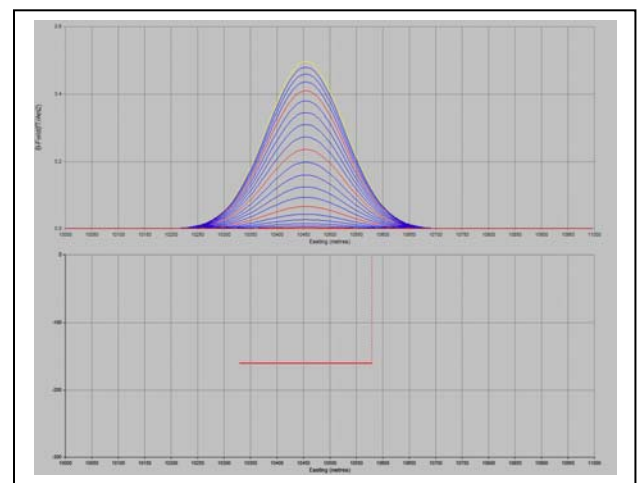


Figure A-12: B-Field response of a deep horizontal thin plate. Depth=200 m, CT=20 S. The EM response is normalized by the dipole moment.

II. THICK PLATE

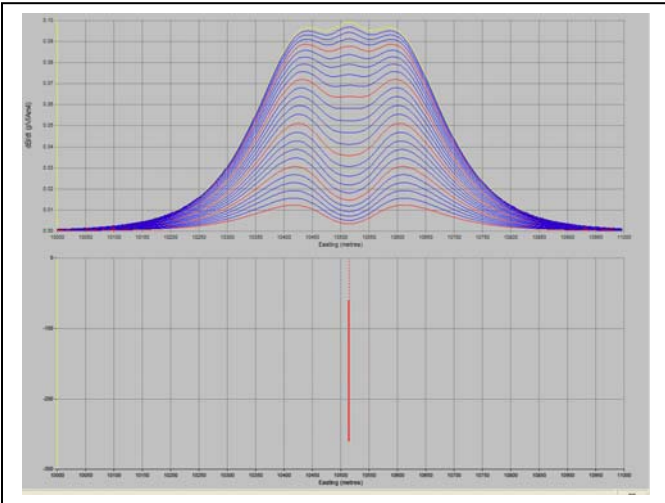


Figure A-13: dB/dt response of a shallow vertical thick plate. Depth=100 m, C=12 S/m, thickness=20 m. The EM response is normalized by the dipole moment and the Rx area.

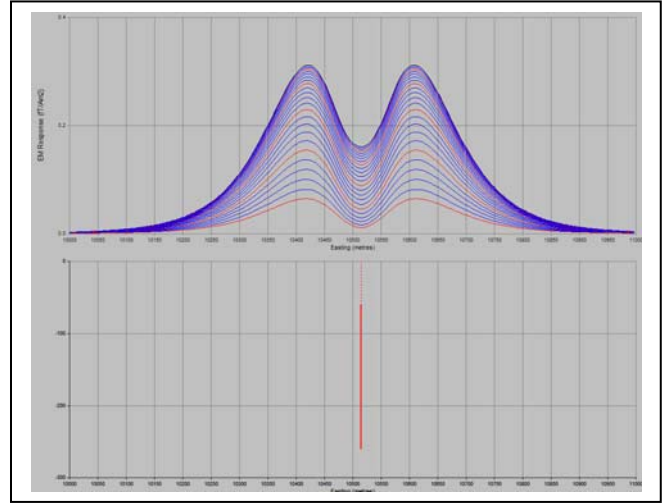


Figure A-14: B-Field response of a shallow vertical thick plate. Depth=100 m, C=12 S/m, thickness= 20 m. The EM response is normalized by the dipole moment.

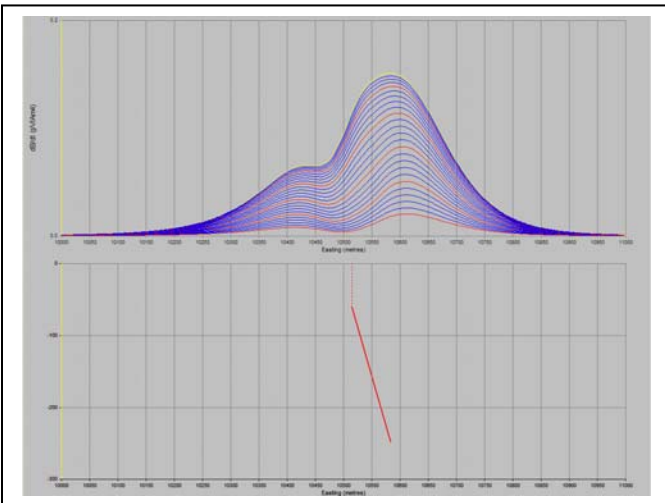


Figure A-15: dB/dt response of a shallow skewed thick plate. Depth=100 m, C=12 S/m, thickness=20 m. The EM response is normalized by the dipole moment and the Rx area.

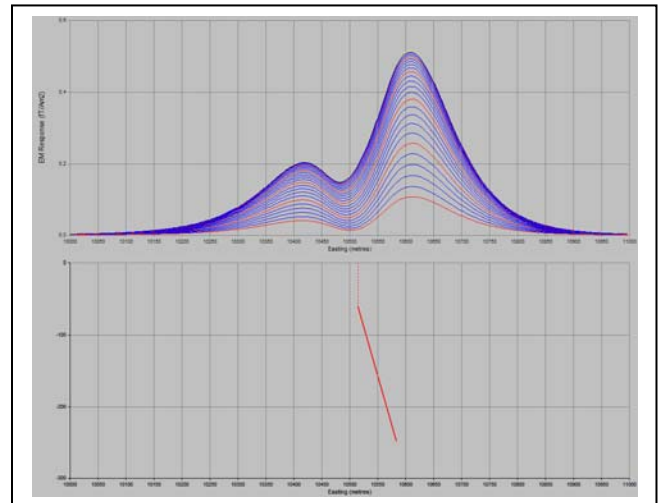


Figure A-16: B-Field response of a shallow skewed thick plate. Depth=100 m, C=12 S/m, thickness=20 m. The EM response is normalized by the dipole moment.

III. MULTIPLE THIN PLATES

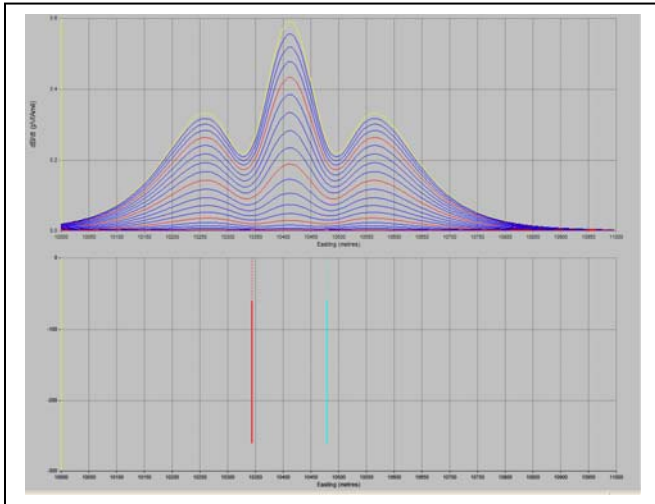


Figure A-17: dB/dt response of two vertical thin plates. Depth=100 m, CT=20 S. The EM response is normalized by the dipole moment and the Rx area.

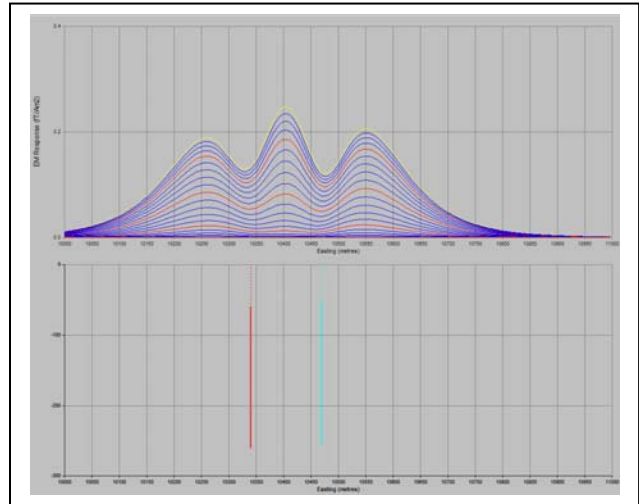
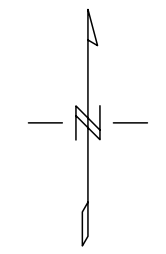


Figure A-18: B-Field response of two vertical thin plates. Depth=100 m, CT=20 S. The EM response is normalized by the dipole moment.



Survey Specifications:
Dates Flown: September 18-September 29, 2007
Survey Base: Teslin, YT
Aircraft: Astar B3 helicopter, Registration C-GTFX
Nominal Flight Line Spacing: 100 metres
Nominal Flight Line Directions: N74°E/N254°W
Nominal Tie Line Spacing: 1000 metres
Nominal Tie Line Directions: N162°E/N342°W
Nominal helicopter terrain clearance: 85 metres
EM Loop is 40 metres under helicopter
Magnetic sensor is 15 metres under helicopter

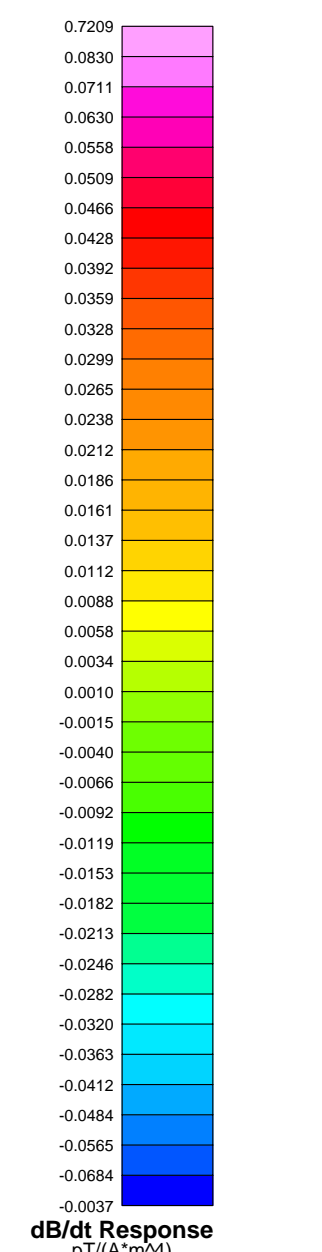
Instruments:
Geotech Time Domain Electromagnetic System (VTEM)
with concentric Rx/Tx geometry
Transmitter Loop Diameter 26 m, Base Frequency 30 Hz
Dipole Moment: 424,400 N/A
Transmitter Wave Form: Trapezoid, Pulse Width 7.22 ms
Geometrics Optically-pumped,
High Sensitivity Cesium Magnetometer
Magnetometer Resolution 0.02 nT at 10 samples/sec



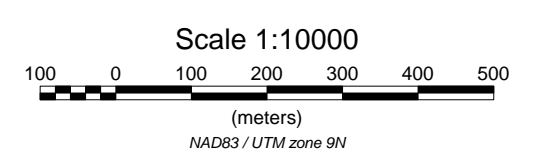
Anomaly Symbols

- Conductance < 5.0 siemens
- 5.0 < Conductance < 10.0
- 10.0 < Conductance < 15.0
- 15.0 < Conductance < 20.0
- 20.0 < Conductance

Anomaly ID Conductance (S)
Depth (m) Tau (ms)
Dip (°)



- Legend:**
- Roads
 - Lakes, Rivers
 - Swamps
 - Topographic contours

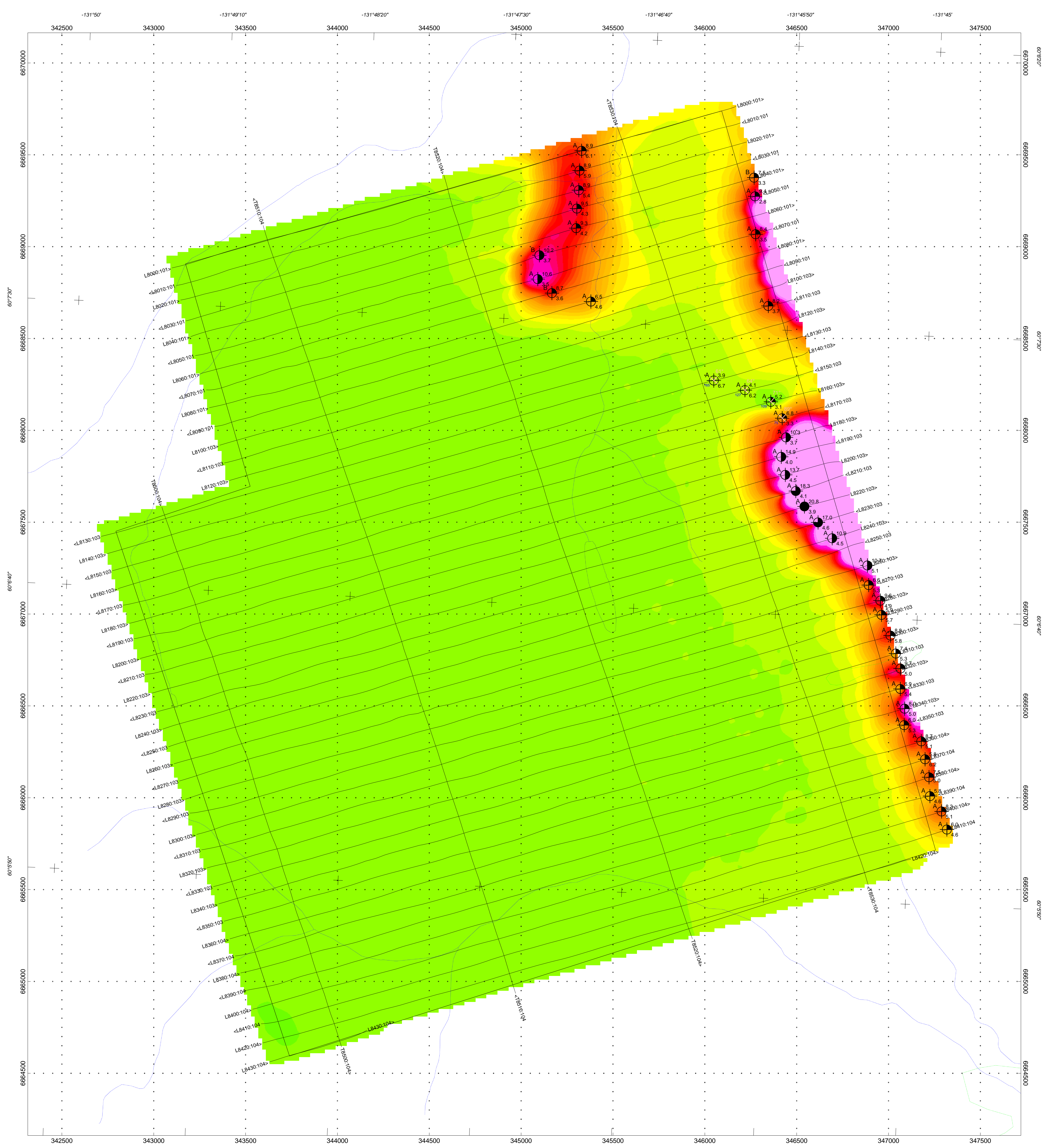


Tarsis Capital Corp.
Block CABIN LAKE
Yukon, Canada

Geotech VTEM System
**EM picked anomalies & late
Time dB/dt Channel (3.911 ms)**

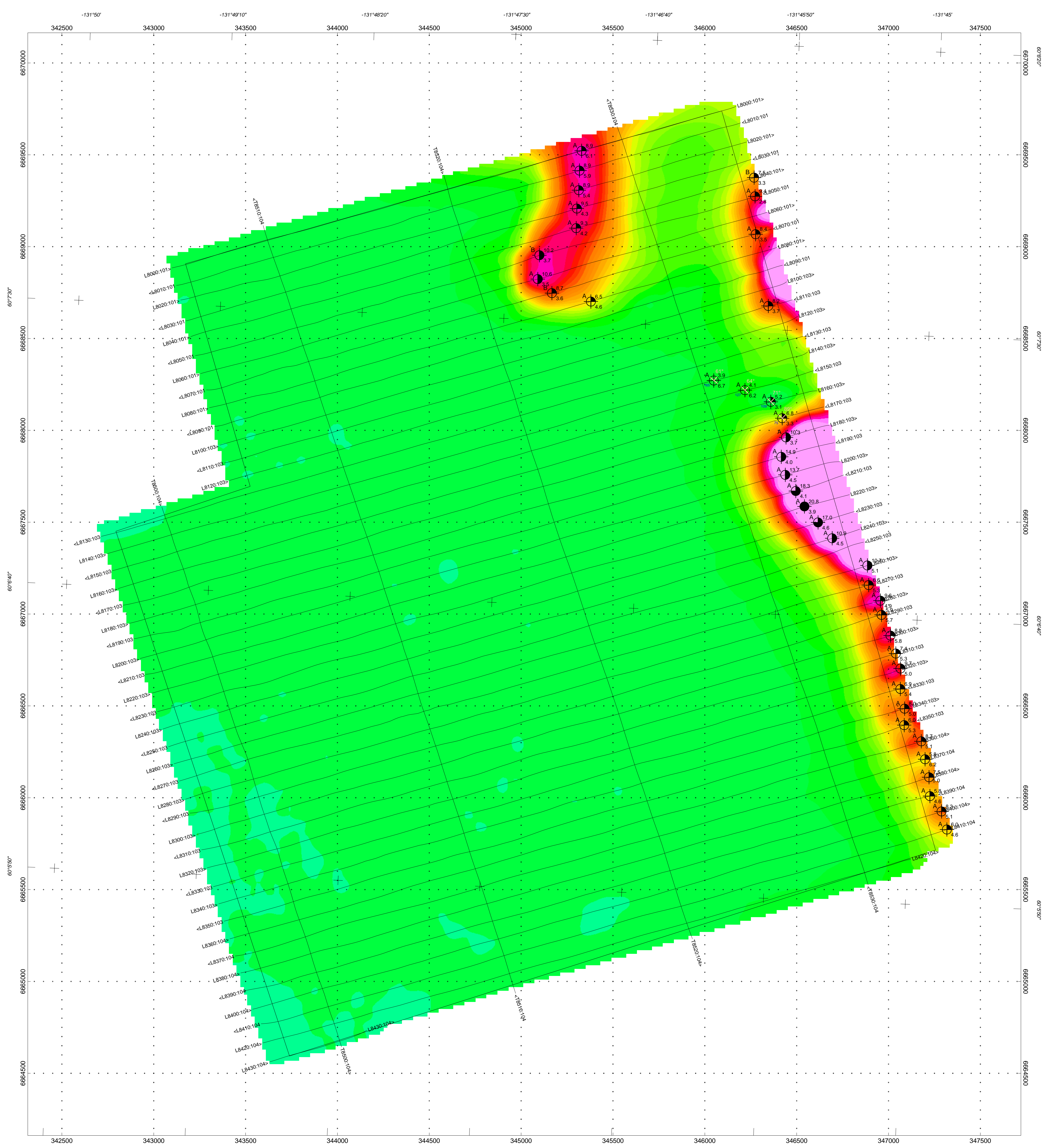
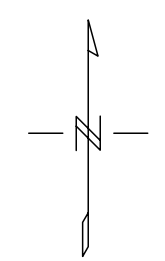
Flown and processed by Geotech Ltd.
30 Industrial Parkway South
Aurora, Ontario, Canada
www.geotechairborne.com

November 2007



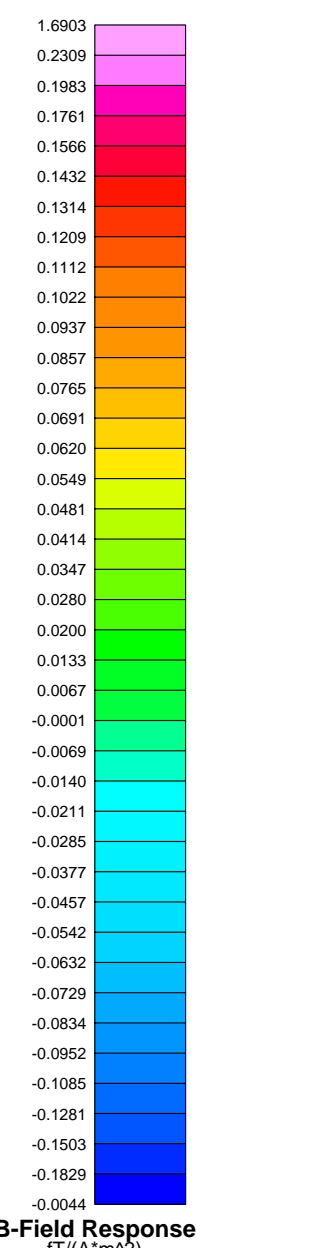
Survey Specifications:
 Dates Flown: September 18-September 29, 2007
 Survey Base: Teslin, YT
 Aircraft: Astar B3 helicopter, Registration C-GTFX
 Nominal Flight Line Spacing: 100 metres
 Nominal Flight Line Directions: N74°E/N254°W
 Nominal Tie Line Spacing: 1000 metres
 Nominal Tie Line Directions: N162°E/S342°W
 Nominal helicopter terrain clearance: 85 metres
 EM Loop is 40 metres under helicopter
 Magnetic sensor is 15 metres under helicopter

Instruments:
 Geotech Time Domain Electromagnetic System (VTEM) with concentric Rx/Tx geometry
 Transmitter Loop Diameter: 26 m, Base Frequency: 30 Hz
 Dipole Moment: 424,400 N/A
 Transmitter Wave Form: Trapezoid, Pulse Width: 7.22 ms
 Geometrics: Optically-pumped
 High Sensitivity Cesium Magnetometer
 Magnetometer Resolution: 0.02 nT at 10 samples/sec

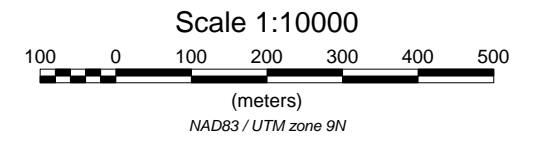


- Anomaly Symbols**
- Conductance < 5.0 siemens ○
 - 5.0 < Conductance < 10.0 ⊕
 - 10.0 < Conductance < 15.0 ⊕
 - 15.0 < Conductance < 20.0 ⊕
 - 20.0 < Conductance ⊕

Anomaly ID Conductance (S)
 Depth (m) Tau (ms)
 Dip (°) Tau (ms)



- Legend:**
- Roads
 - Lakes, Rivers
 - Swamps
 - Topographic contours



Tarsis Capital Corp.
 Block CABIN LAKE
 Yukon, Canada

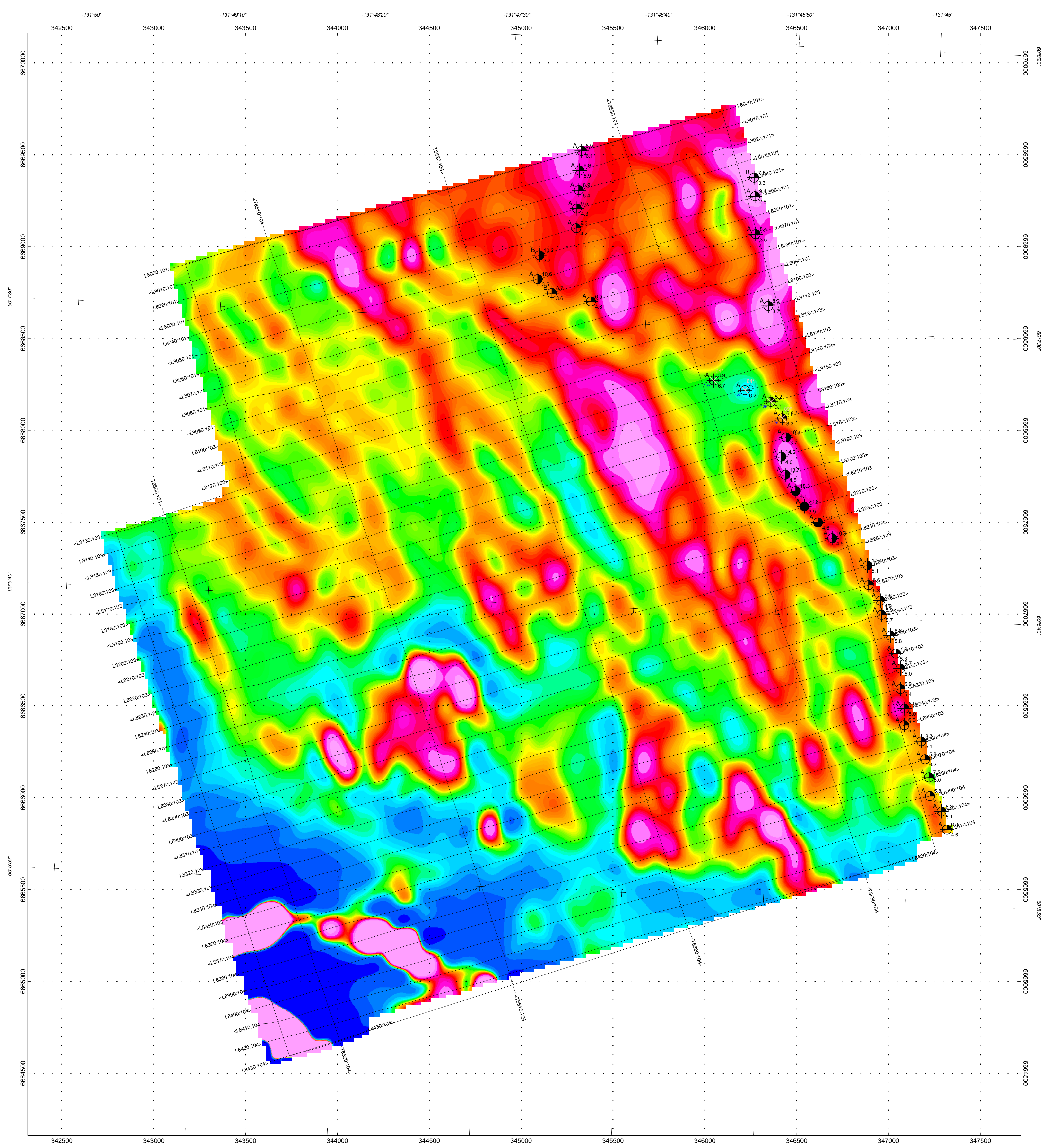
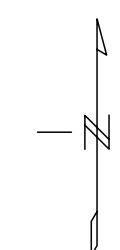
Geotech VTEM System
EM picked anomalies & late Time B-Field Channel (3.911 ms)

Flown and processed by Geotech Ltd.
 30 Industrial Parkway South
 Aurora, Ontario, Canada
 www.geotechairborne.com

November 2007

Survey Specifications:
 Dates Flown: September 18-September 29, 2007
 Survey Base: Teslin, YT
 Aircraft: Astar B3 helicopter, Registration C-GTFX
 Nominal Flight Line Spacing: 100 metres
 Nominal Flight Line Directions: N74°E/N254°W
 Nominal Tie Line Spacing: 1000 metres
 Nominal Tie Line Directions: N162°E/N342°W
 Nominal helicopter terrain clearance 85 metres
 EM Loop is 40 metres under helicopter
 Magnetic sensor is 15 metres under helicopter

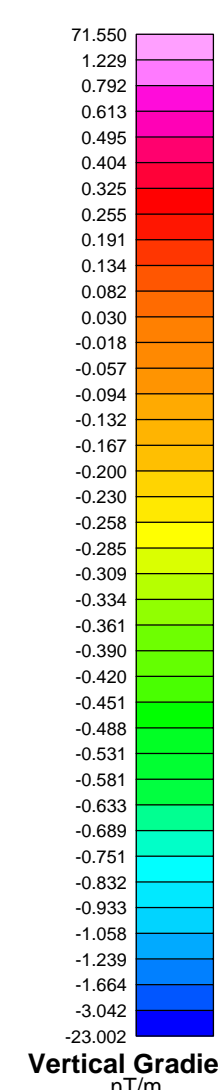
Instruments:
 Geotech Time Domain Electromagnetic System (VTEM)
 with concentric Rx/Tx geometry
 Transmitter Loop Diameter 26 m, Base Frequency 30 Hz
 Dipole Moment 424,400 N/A
 Transmitter Wave Form: Trapezoid, Pulse Width 7.22 ms
 Geometries Optically-pumped,
 High Sensitivity Cesium Magnetometer
 Magnetometer Resolution 0.02 nT at 10 samples/sec



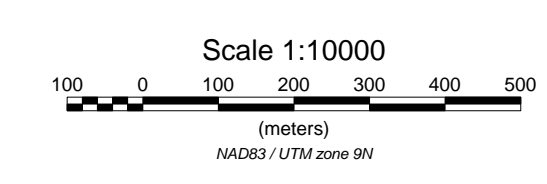
Anomaly Symbols

- Conductance < 5.0 siemens
- 5.0 < Conductance < 10.0
- 10.0 < Conductance < 15.0
- 15.0 < Conductance < 20.0
- 20.0 < Conductance

Anomaly ID Conductance (S)
 Depth (m) Tau (ms)
 Dip (°)



- Legend:**
- Roads
 - Lakes, Rivers
 - Swamps
 - Topographic contours



Tarsis Capital Corp.
 Block CABIN LAKE
 Yukon, Canada

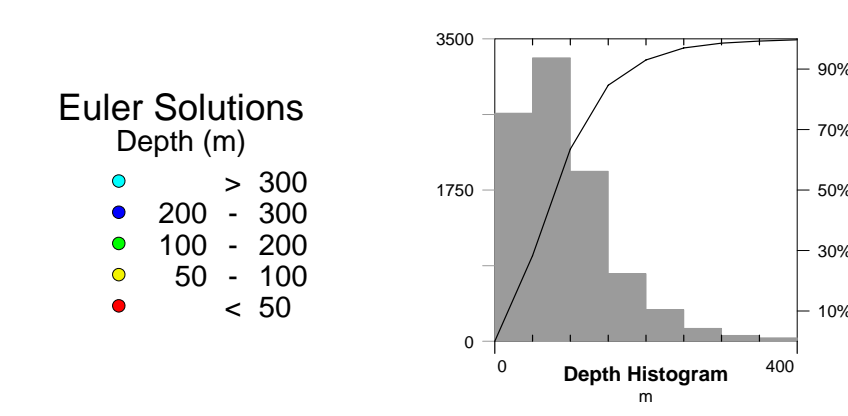
Geotech VTEM System
 Vertical gradient of TMI

Flown and processed by Geotech Ltd.
 30 Industrial Parkway South
 Aurora, Ontario, Canada
 www.geotechairborne.com

November 2007

Survey Specifications:
 Dates Flown: September 18-September 29, 2007
 Survey Base: Teslin, YT
 Aircraft: Astar B3 helicopter, Registration C-GTFX
 Nominal Flight Line Spacing: 100 metres
 Nominal Flight Line Directions: N74°E/N254°W
 Nominal Tie Line Spacing: 1000 metres
 Nominal Tie Line Directions: N162°E/N342°W
 Nominal helicopter terrain clearance 85 metres
 EM Loop is 40 metres under helicopter
 Magnetic sensor is 15 metres under helicopter

Instruments:
 Geotech Time Domain Electromagnetic System (VTEM) with concentric Rx/Tx geometry
 Transmitter Loop Diameter 25 m, Base Frequency 30 Hz
 Dipole Moment 424,400 N/A
 Transmitter Wave Form: Trapezoid, Pulse Width 7.22 ms
 Geometrics: Optically-pumped,
 High Sensitivity Cesium Magnetometer
 Magnetometer Resolution 0.02 nT at 10 samples/sec



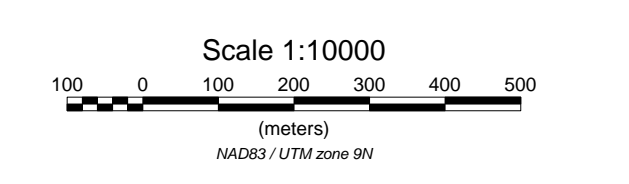
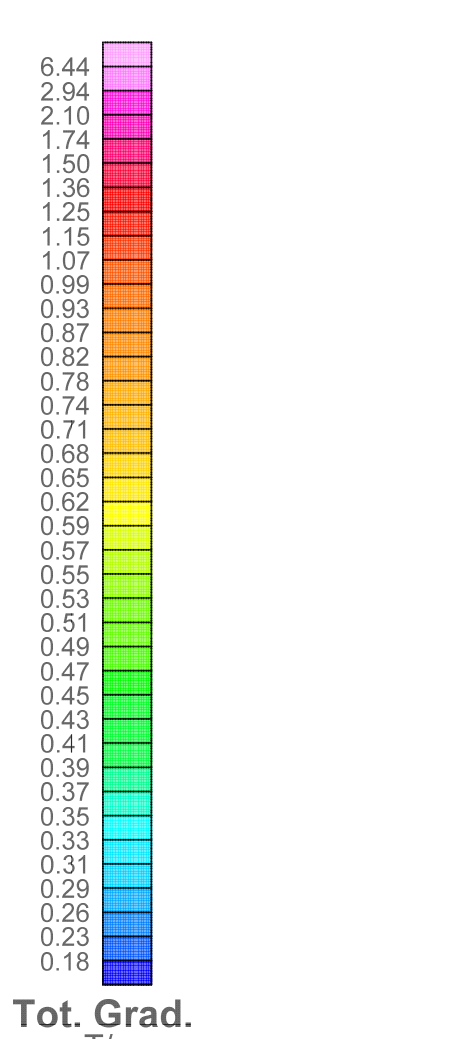
Anomaly Symbols

- Conductance < 5.0 siemens
- 5.0 < Conductance < 10.0
- 10.0 < Conductance < 15.0
- 15.0 < Conductance < 20.0
- 20.0 < Conductance

Anomaly ID, Conductance (S), Depth (m), Dip (°), Tau (ms)

— Geological boundary
 — Fault
 - - - Interpreted Fault
 ○ EM Anomaly Contour

- 8 Granodiorite: medium-grained with lesser quartz monzonite
- 7 Diorite: fine-grained undeformed
- 6 Diorite: coarse-grained sheared and chloritized
- 4 Quartz-sericite schist felsic metavolcanics
- 3 Siliceous schist, sulphide-bearing probable metasediment
- 2 Greenstone: metavolcanics and metasediments
- 1 Quartz-muscovite schist 'Quartzite' and psammite

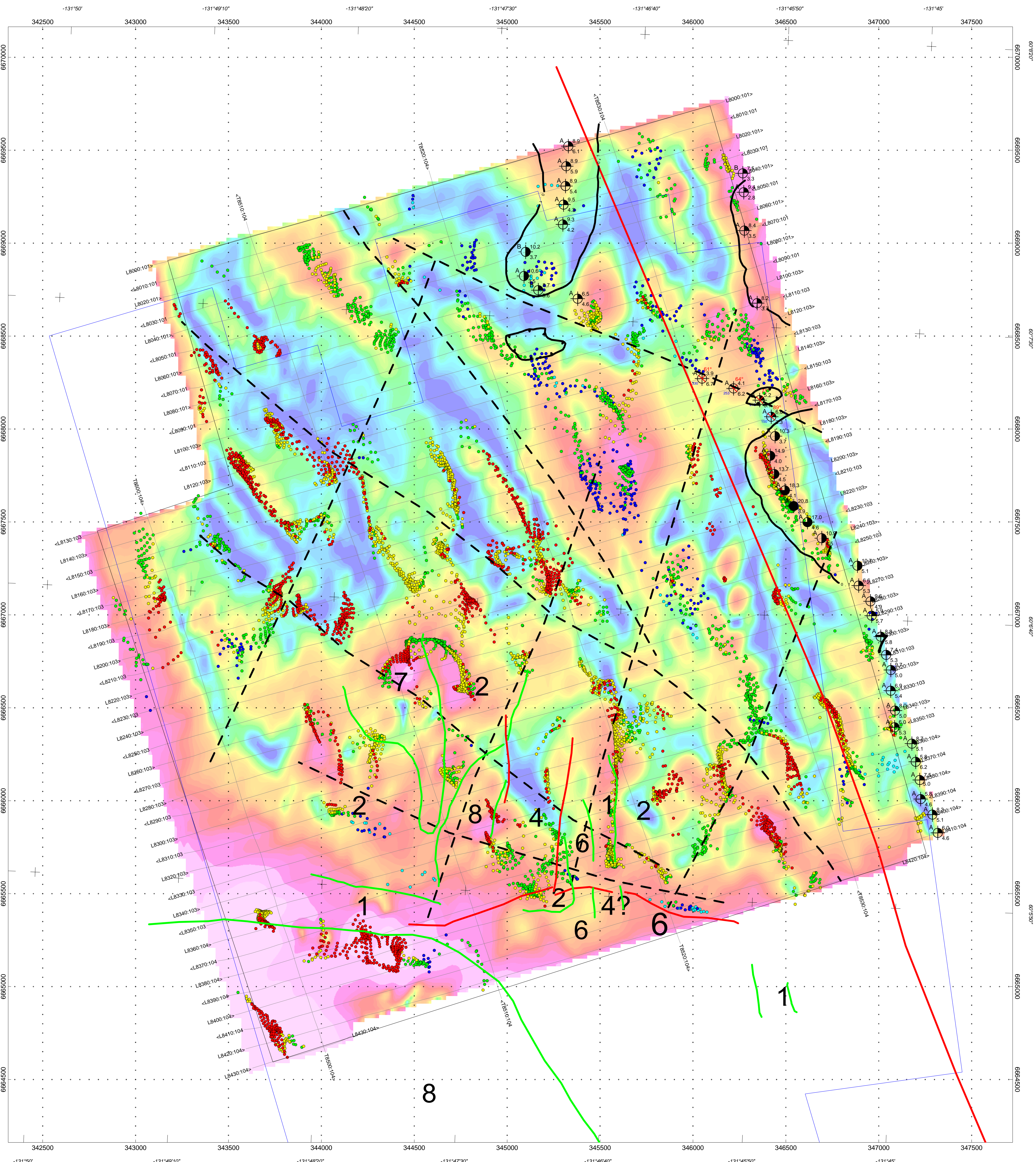


Tarsis Capital Corp.
 Block CABIN LAKE
 Yukon, Canada

Geotech VTEM System
INTERPRETATION MAP

Flown and processed by Geotech Ltd.
 30 Industrial Parkway South
 Aurora, Ontario, Canada
 www.geotechairborne.com

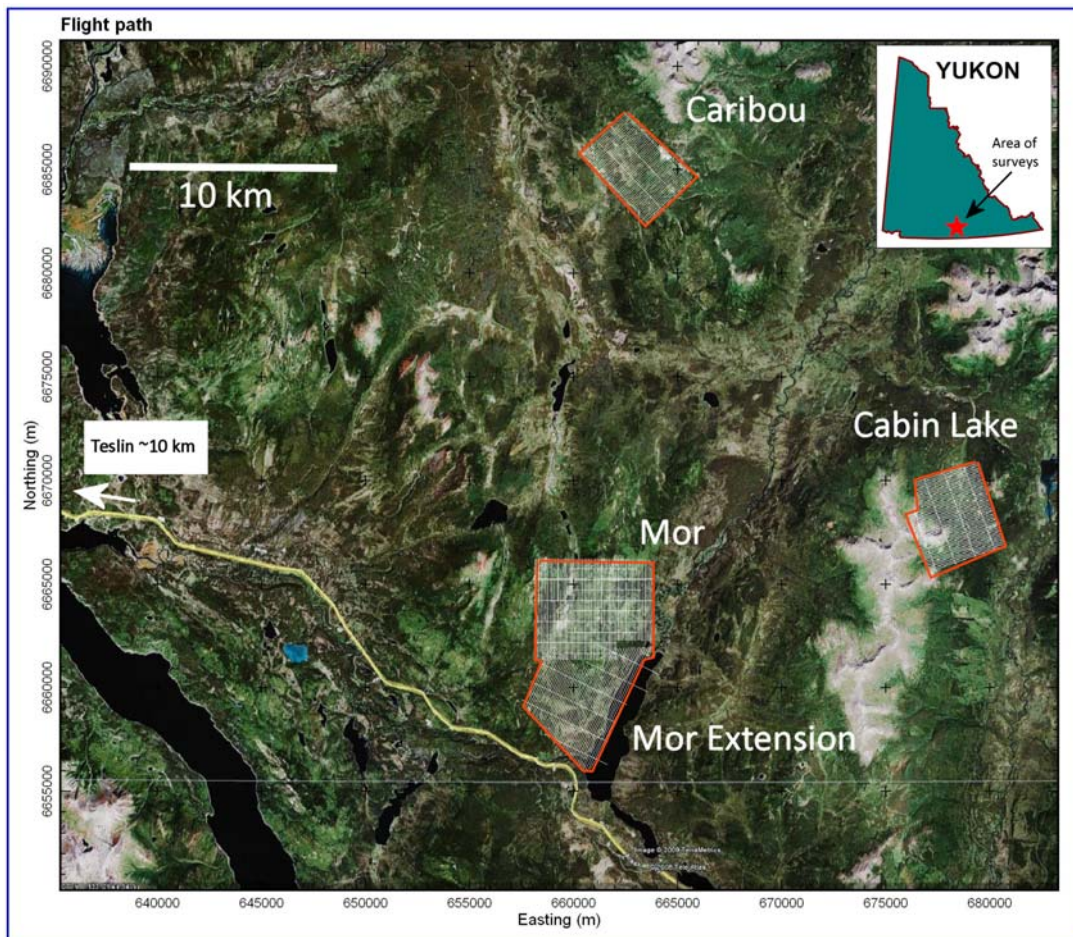
November 2007



APPENDIX IV

GEOPHYSICAL REPORT BY CONDOR CONSULTING INC.

**REPORT ON PROCESSING & ANALYSIS OF
VTEM 30 HZ EM AND MAGNETICS DATA
MOR, MOR EXTENSION, CABIN LAKE AND CARIBOU
PROPERTIES
TESLIN AREA, YUKON TERRITORY
FOR
TARSIS CAPITAL CORP.
FEBRUARY 2009**





**REPORT ON PROCESSING & ANALYSIS OF
VTEM 30 HZ EM AND MAGNETICS DATA
MOR, MOR EXTENSION, CABIN LAKE AND CARIBOU
PROPERTIES
TESLIN AREA, YUKON TERRITORY
FOR
TARSIS CAPITAL CORP.
FEBRUARY 2009**

CONTENTS

1.	SUMMARY	1
2.	INTRODUCTION.....	2
	VTEM Survey	2
	Target Model	3
	Local Geology	5
3.	PROCESSING, ANALYSIS TECHNIQUES AND PRODUCTS	9
	PROCESSING	9
	EM Data Processing.....	9
	Conductivity 3D Model	10
	Magnetic Data Processing	10
	Magnetic Data Modeling.....	10
	EM ANALYSIS TECHNIQUES.....	10
	Profile Analysis.....	10
	Picking.....	10
	Wide Zones	11
	Target Zones	11
	PRODUCTS	11
	Table 3-1 Survey Products.....	12
4.	SURVEY RESULTS.....	14
	Data Quality	14
	Magnetic Results.....	14
	Mor.....	14
	Cabin Lake	15
	Caribou.....	16
	EM Survey Results.....	16
	Mor.....	16
	Cabin Lake	24
	Caribou.....	27
	Discussion.....	29
	Mor.....	29
	Cabin Lake	29
	Caribou.....	29
5.	CONCLUSIONS & RECOMMENDATIONS	30
6.	REFERENCES.....	31
7.	APPENDICES	33
	APPENDIX A: BACKGROUND ON EM PROCESSING	34

APPENDIX B: ANOMALY LISTING	35
MOR.....	36
CABIN LAKE	37
CARIBOU	38
APPENDIX C: NOTES ON MAGNETIC PROCESSING & EM3D MODELS	39
APPENDIX D: ARCHIVE DVD	40

1. SUMMARY

This report covers the processing and analysis performed by Condor Consulting, Inc. of VTEM EM and magnetic surveys on three properties held by Tarsis Capital Corp. and being operated by Archer Cathro & Associates. The properties are the Mor, Cabin Lake and Caribou and are located east and north of community of Teslin, Yukon Territory. The primary deposit model for all three properties is VMS.

Mineralization located on the Mor property shows a strong response in the VTEM survey. Follow-up of the 2007 VTEM survey (prior to Condor Consulting, Inc.'s involvement) revealed another zone of mineralization on Mor. The present assessment suggests both areas of known mineralization have likely extensions at depth which are deemed to warrant follow-up. As well several other zones of interest were recognized and are also recommended for follow-up.

On the Cabin Lake property, one zone of interest was identified and is recommended for further work. This zone is believed to be at least several 100 meters deep and therefore a staged follow up is recommended to upgrade the target prior to drilling.

On the Caribou property, only one bedrock conductor was recognized. As this feature lies on the edge of the survey block, follow-up work to upgrade and better define the overall strike of this zone is recommended prior to drill testing.

2. INTRODUCTION

VTEM Survey

At the request of Tarsis Capital Corp. (Tarsis), Condor Consulting Inc. (Condor) has undertaken to process and analyze VTEM 30 Hz EM and magnetics data over Tarsis's Mor, Mor Extension, Cabin Lake and Caribou properties located east of Teslin, Yukon Territory. The surveys were flown in 2007 and 2008 by Geotech Ltd.; full details of the survey and equipment specifications are provided in Lev, 2007, Lev, 2008, Orlowski et al 2008 and Orlowski et al 2009. These reports are provided in digital form in Appendix D, the archive DVD.

The location of the surveys is shown in Figure 1 and the path plot in Figure 2. A total of 867 line km of data were processed and analyzed.

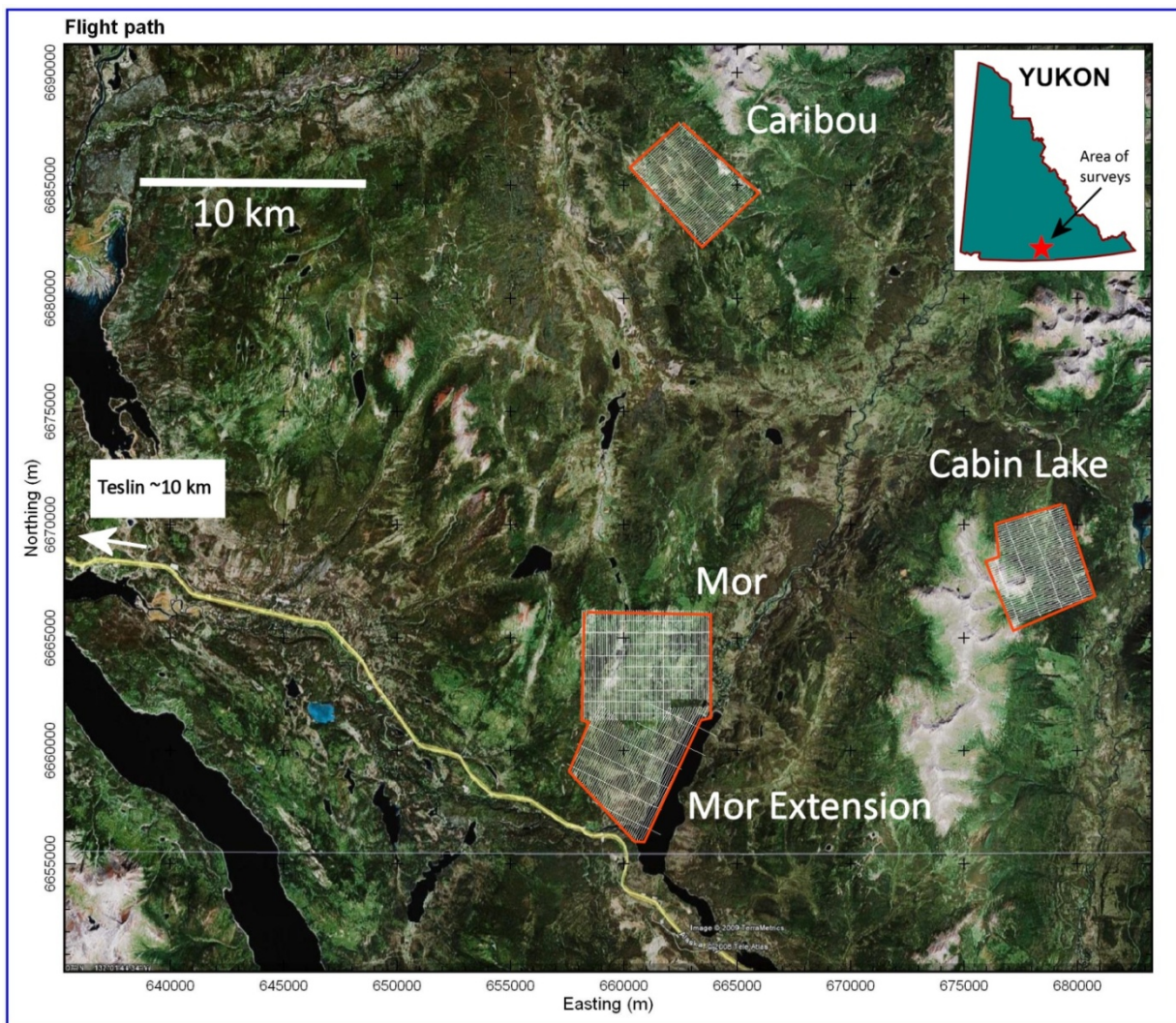


Figure 1: Location of VTEM surveys.

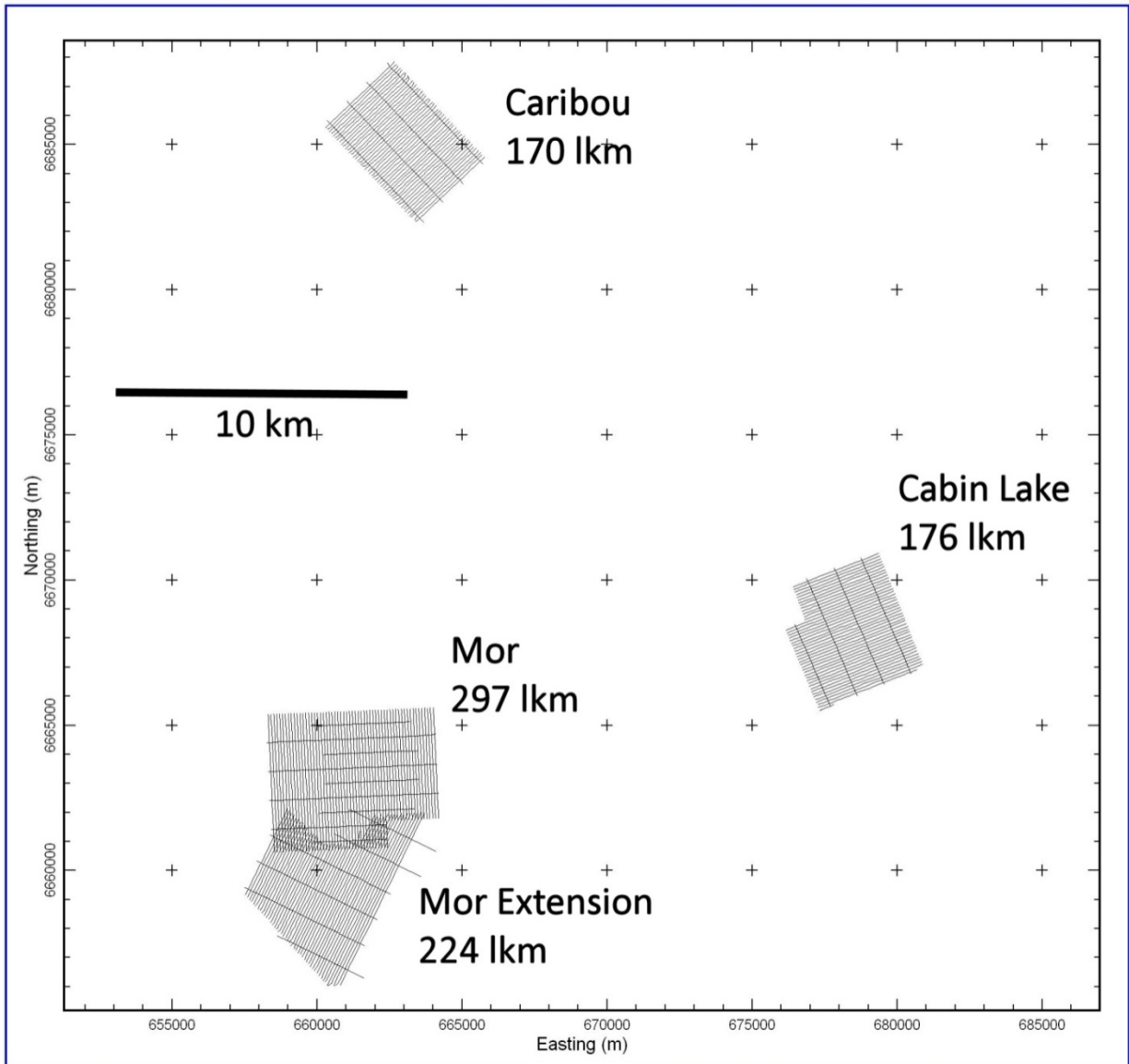


Figure 2: Flight path plots for VTEM surveys.

Target Model

The regional geology for the area is shown in Figure 3 (Downie 2007). The primary target model is VHMS (volcanic hosted massive sulfide) but Cabin Lake has the potential for intrusive related mineralization as well. The VMS-style deposits would contain significant sulfides and would be expected to be at least moderately conductive. An example of such a deposit in the area is the Kudzu Ze Kayah (Holroyd et al 1997). They report the deposit had a high conductance (40 S) and strong magnetic response (700-1 000 nT). Figure 4 shows the HLEM (horizontal loop EM or MaxMin) response over the deposit, superimposed on the magnetic response. A copy of their paper is provided in Appendix D.

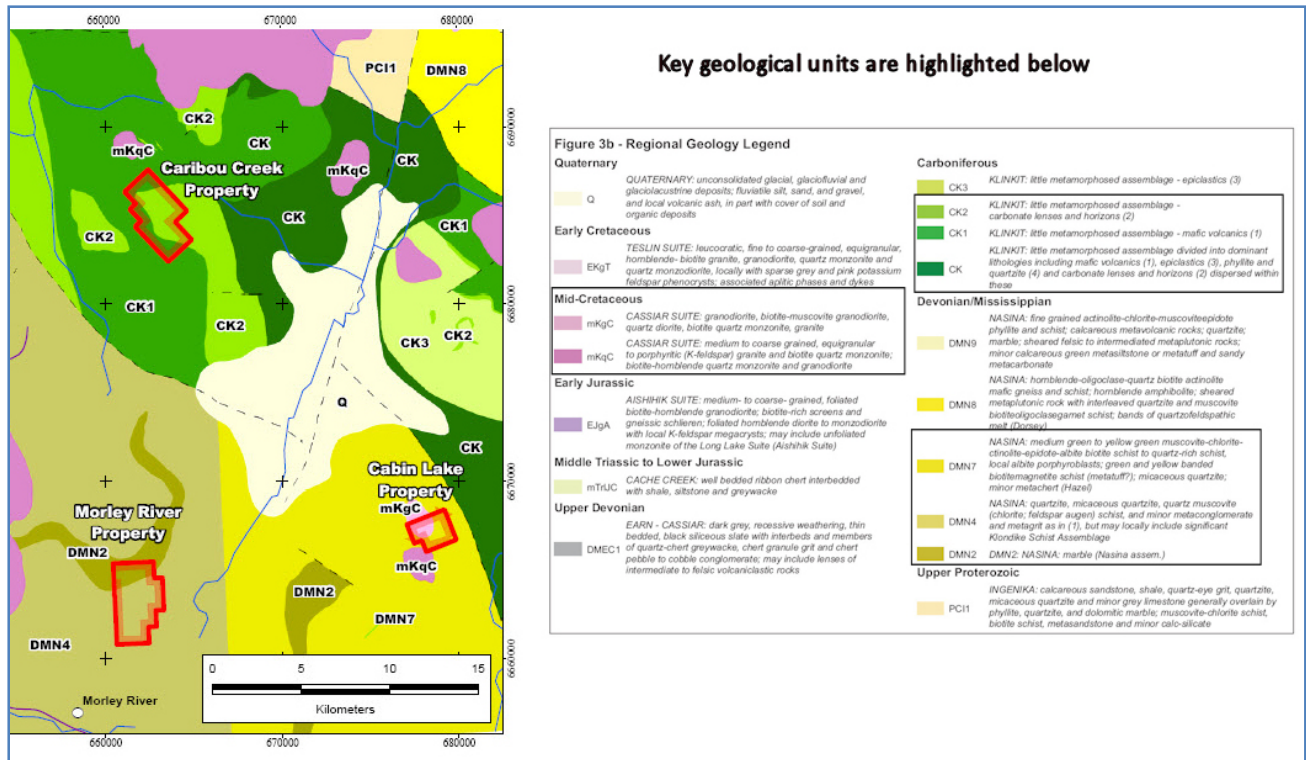


Figure 3: Regional geology for Mor, Cabin Lake and Caribou properties (from Downie 2007).

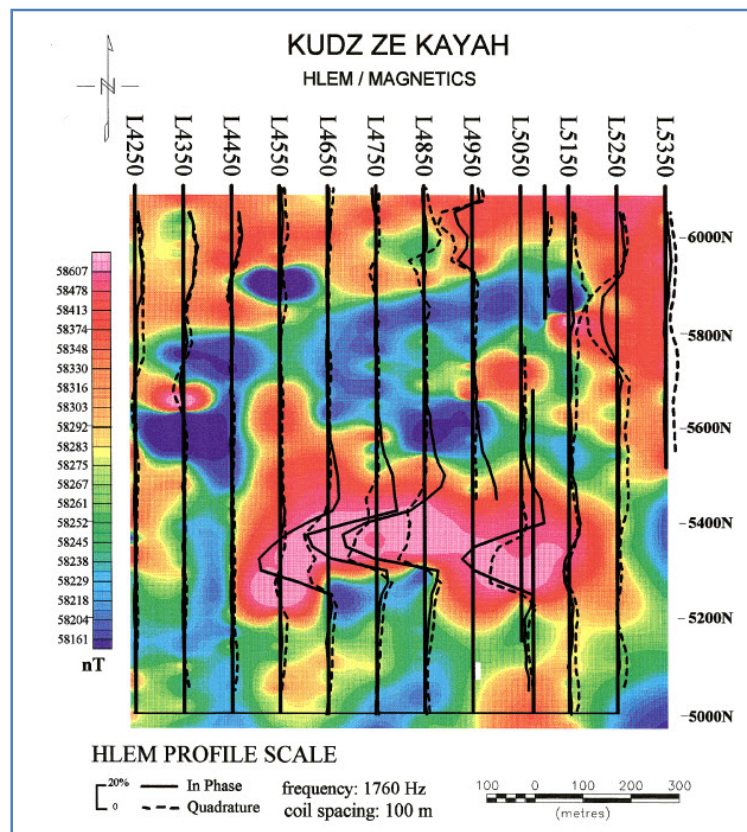


Figure 4: HLEM and magnetic results (from Holroyd et al 1997).

They note the presence of "mudstones and shales which typically have pyrrhotite disseminations, and are variably carbonaceous, making these metasediments locally both magnetic and conductive". While not an issue in the present study, these responsive sediments are a frequent part of the mineralogically favorable geology elsewhere in the Yukon.

Local Geology

MOR

Of the three projects, the Mor area is best known. The local geology is provided in Downie (2007):

The Morley River Property is mainly underlain by a thick sequence of green quartz-chlorite schist and chlorite schist of which protoliths are interpreted as mafic to intermediate volcanic tuffs and minor flows. This assemblage is mainly composed of fine grained, bright to dark green, well foliated chlorite schists/mafic tuff to lapilli tuff. The mafic rocks are interbedded with quartz chlorite schist/intermediate tuff on a centimeter to meter scale. These rocks contain varying amounts of layer parallel quartz and feldspar. Quartzite/chert was also observed locally as interbeds within the mafic dominated succession but never sufficiently thick to form a mappable unit. The rocks are strongly deformed and have a strong, nearly parallel to layering, schistosity which generally strikes east and dips moderately to the south. The sequence has been significantly thickened by tight high amplitude folds which were observed at an outcrop scale. Metamorphic grade is middle greenschist facies. This assemblage of dominantly mafic volcanics may correlate with the "greenstone sequence" of the Big Salmon Complex mapped by Mihalynuk et al (1998).

The northeast portion of the property is underlain by a grey-white, thickly bedded, medium to coarsegrained marble. This unit was observed in flat lying, conformable contact with and overlying the greenstone sequence described above. Bedding in the recrystallized limestone strikes east and dips south at 30 degrees.

One historic zone of mineralization called the Discovery Zone has been recognized and a second zone has been defined in recent work as a follow-up to the 2007 VTEM survey (source Tarsis web site: www.tarsis.ca). Downie (2007) provides the following description of the Discovery Zone:

On the Morley River Property, the main mineralized zone consists of at least four separate quartz-sericite schist/ rhyolitic tuff horizons within a dominantly mafic volcanic sequence. These horizons, where exposed, range from 20 centimeters to 1.75 meters thick, are strongly gossanous and contain pyrite with locally significant amounts of chalcopyrite, gold and silver. Mafic schists in contact with the mineralized quartz-sericite schist units are strongly pyritic and commonly anomalous in copper. The quartz-sericite schist units have been traced over a strike length of 900 meters.

These two areas are outlined in Figure 5. Both zones have a VMS affinity and could be expected to be quite conductive and likely magnetic. A detailed image over the Discovery Zone is shown in Figure 6. Prior to the first VTEM survey being performed over Mor in 2007, an IP survey was conducted over the Discovery area (Power 2004). The results of this survey are shown in Figure 7. Also shown on this figure is the basic geological mapping for the area.

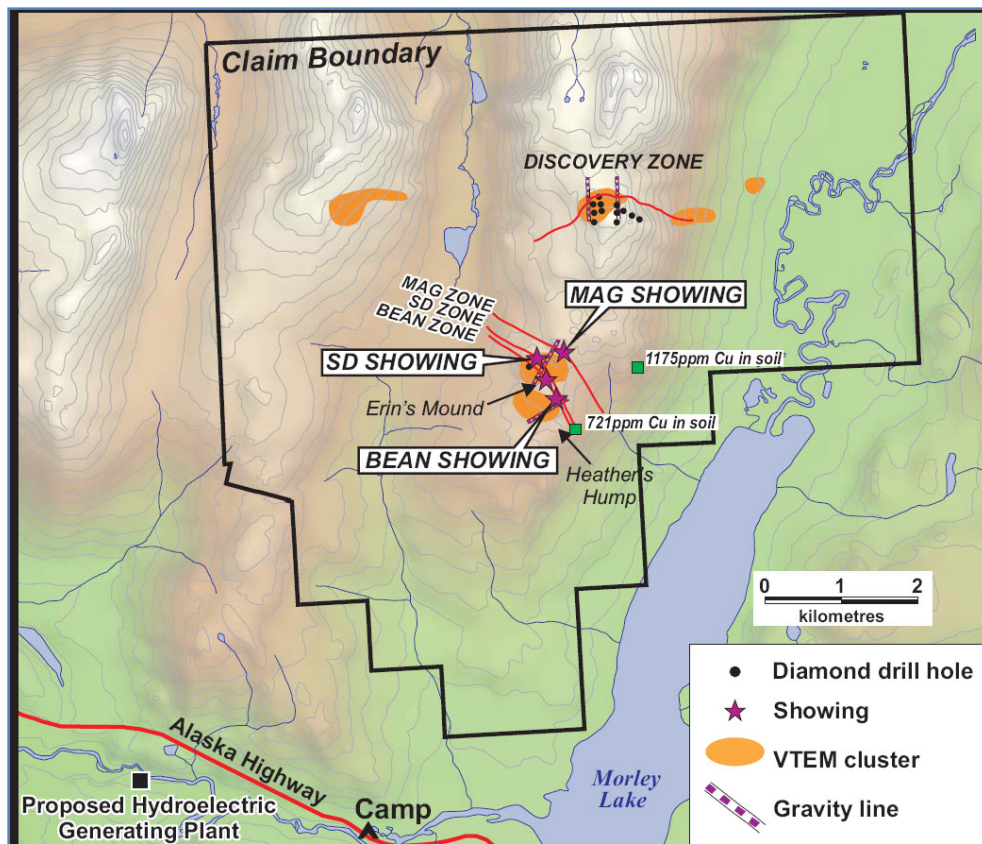


Figure 5: Location of major showings on the Mor property (source-Tarsis web site).

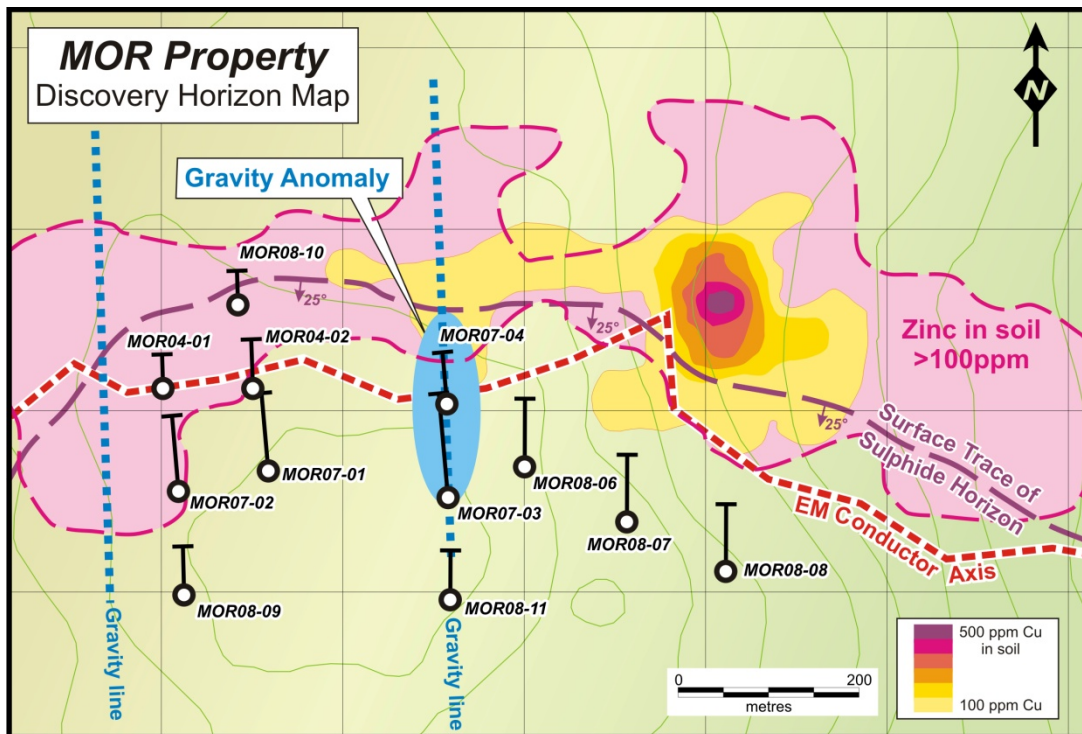


Figure 6: Mor-Discovery Zone showing drilling and geochemical results.

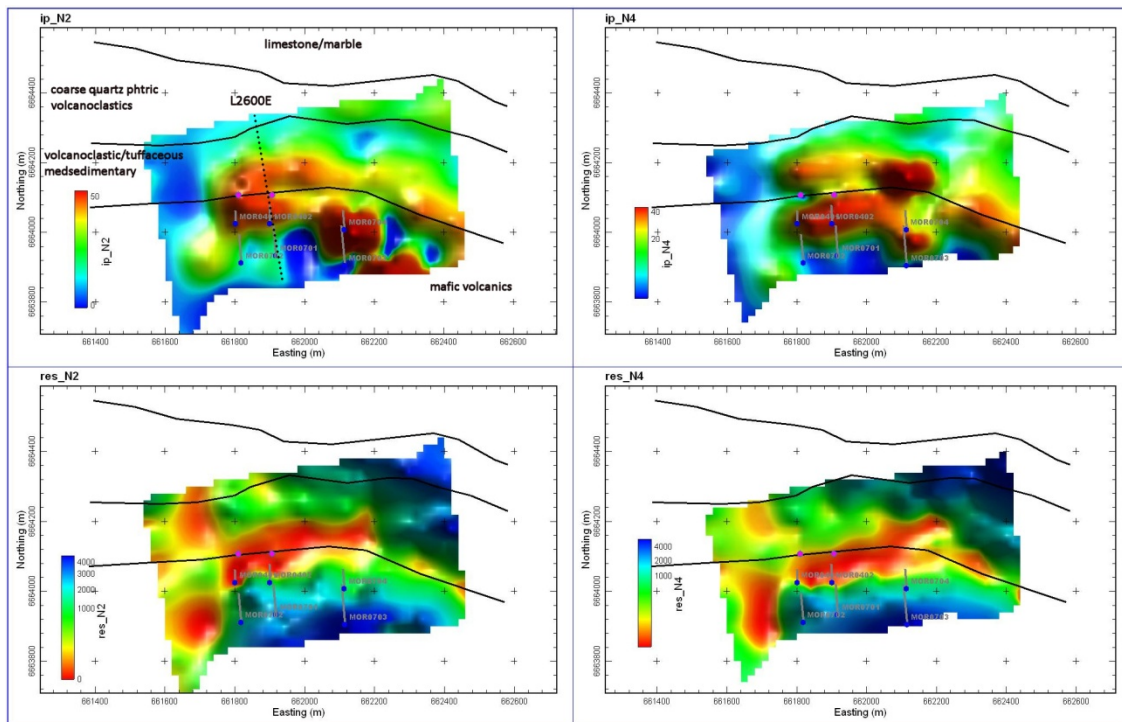


Figure 7: Mor-Discovery Zone: IP chargeability and resistivity; geology annotated in upper left image.

The IP results show the Discovery Zone is a distinct chargeability high and resistivity low. An attempt was made to correlate between the drilling results and IP outcomes and Figure 8 shows the representation of this assessment. Given the narrowness of the mineralized zones and averaging that

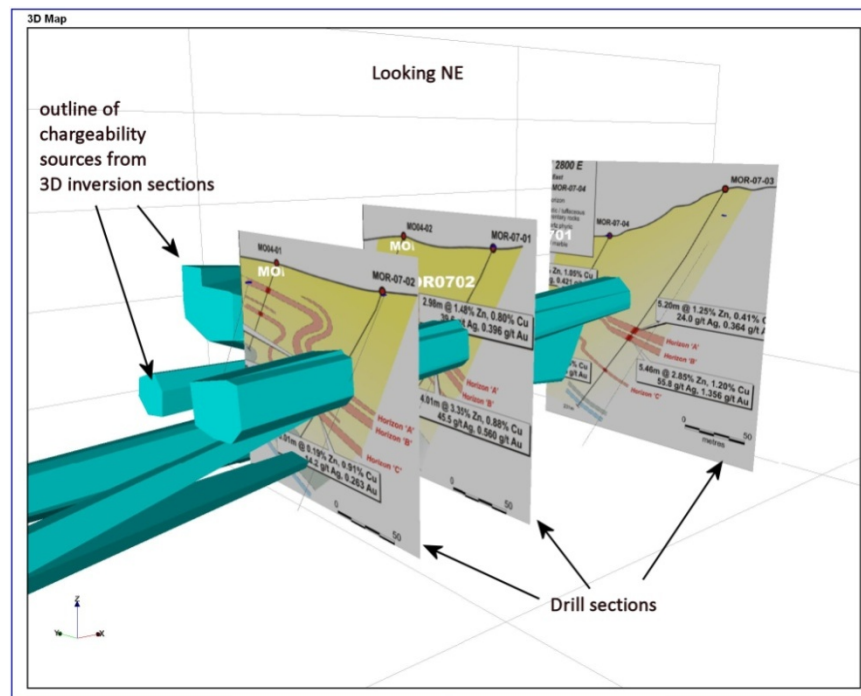


Figure 8: Mor-Discovery Zone: 3D chargeability model and drill sections.

takes place in with the IP measurement and subsequent inversion, the correlation is deemed to be satisfactory. A section of the resistivity inversion through roughly the center of the Zone (L2600E) is shown in Figure 9 (located in Figure 7 upper left image). From the inversion processing, the mineralized zone appears to have a resistivity the order of 10-50 ohm-m. This level of response would be sufficient to be detected with an airborne EM survey assuming there was a sufficient volume of material.

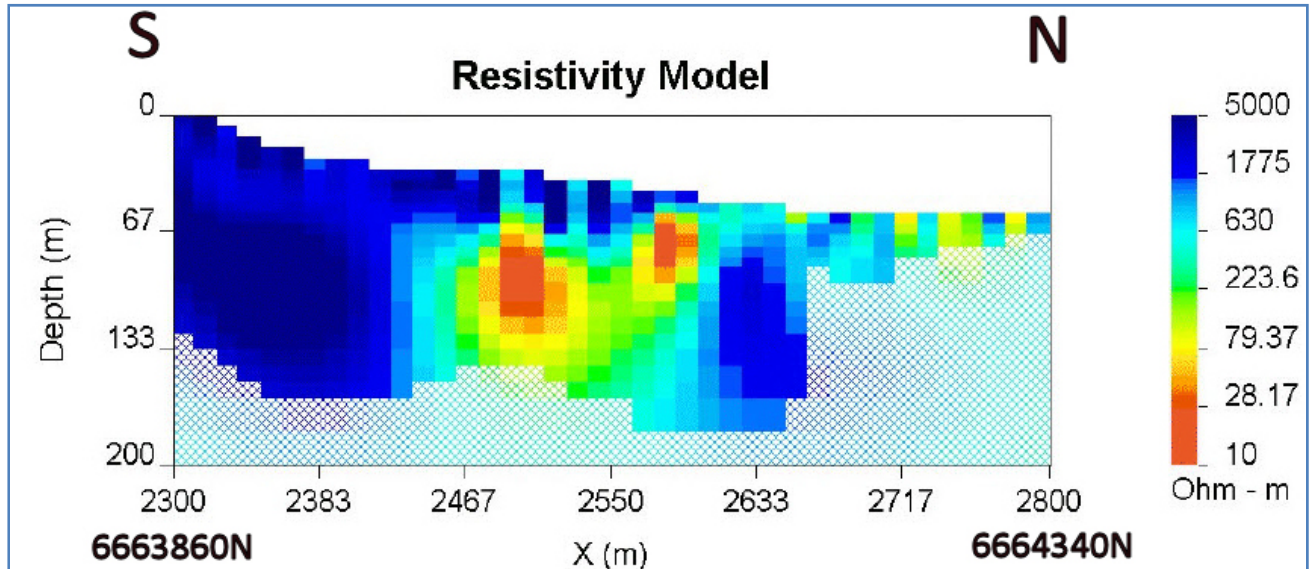


Figure 9: Mor-Discovery Zone: Inverted resistivity data for L2600E-located in Figure 7; Source-Power 2004.

Cabin Lake

No geology (apart from regional shown in Figure 3) is available.

Caribou

No geology (apart from regional shown in Figure 3) is available.

3. PROCESSING, ANALYSIS TECHNIQUES AND PRODUCTS

PROCESSING

To enhance the data and to assist interpretation, the following processing steps were carried out on the VTEM EM and magnetic data. The survey contractor provided the client with both Z off-time (dB/dT) and Z on-time (B-f) data (no X or Y data is recorded with VTEM). Condor processed both data types and selected what was deemed the best outcome for the various products provided.

EM Data Processing

Layered-Earth Inversion

The layered-earth inversion (LEI) algorithm models the EM data with a 28-layered earth model (Farquharson and Oldenburg, 1993, Ellis 1998), increasing in thickness from the surface to depth in an approximately logarithmic fashion. The first layer was 5 m thick and the deepest was 232 m thick. A starting model of 1 000 ohm-m (0.001 S/m) was used, with a reference model of 10 000 ohm-m (0.0001 S/m). The reference model is what the program defaults to at depth when there is no longer enough information to further refine the inversion outcome. The results of the inversion are presented in the form of a conductivity depth section (CDS).

Time Constant: AdTau

The AdTau program calculates the time constant (τ) from time domain decay data. The program is termed AdTau since rather than using a fixed suite of channels as commonly done, the user sets a noise level and depending on the local characteristics of the data, the program will then select the set of five channels above this noise level. In resistive areas, the earlier channels will tend to be used, whereas in conductive terrains the latest channels available can generally be used. Figure 10 shows a typical decay fit; in this case, the last five channels are used.

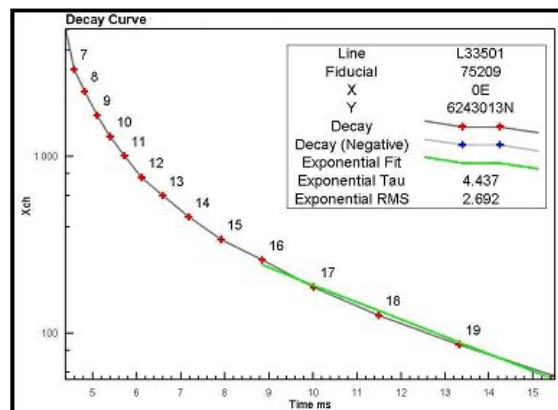


Figure 10: Typical decay showing the derivation of AdTau.

Conductivity 3D Model

Using the 1D inversions created from the EM data, a 3D voxel model of the conductivity has been created using the **encom⁺pa** application.

Additional information on the EM processing is provided in Appendix A.

Magnetic Data Processing

In addition to the normal filters available in the Geosoft application, additional processing was done using **encom⁺pa** software and algorithms described by Shi and Butt (2004) – this paper is included in Appendix C. Where one of these products is used, the prefix ZS is attached to the file name.

Magnetic Data Modeling

The magnetic data for the Mor survey block was modeled using the code Mag3D; this is a voxel-style inversion program developed at the University of British Columbia (Li and Oldenburg 1996). Details on the modeling are provided in Appendix C.

EM ANALYSIS TECHNIQUES

Profile Analysis

For discrete plate-like targets, the VTEM system produces two main types of responses; those termed inductively thin or double-peaked responses (DPR) and those termed inductively thick or single-peak responses (SPR). These basic shapes are shown in profile form in Figure 11. While these two classes of response have been picked separately, for the purposes of this review they are treated as having the same geological significance.

Picking

The MultiPlot™¹ display was the primary means to identify and rank the anomalies. This overall process is termed anomaly picking and was done on a line-by-line basis, with several passes being required to finalize the process. An EM picking scheme was used that made use of the following data:

- EM profiles
- AdTau, power line monitor and magnetic profiles and grids
- Conductivity Depth Sections (CDS)

¹ The MultiPlot is produced using the **encom⁺pa** software from Encom Technology Pty. Ltd.

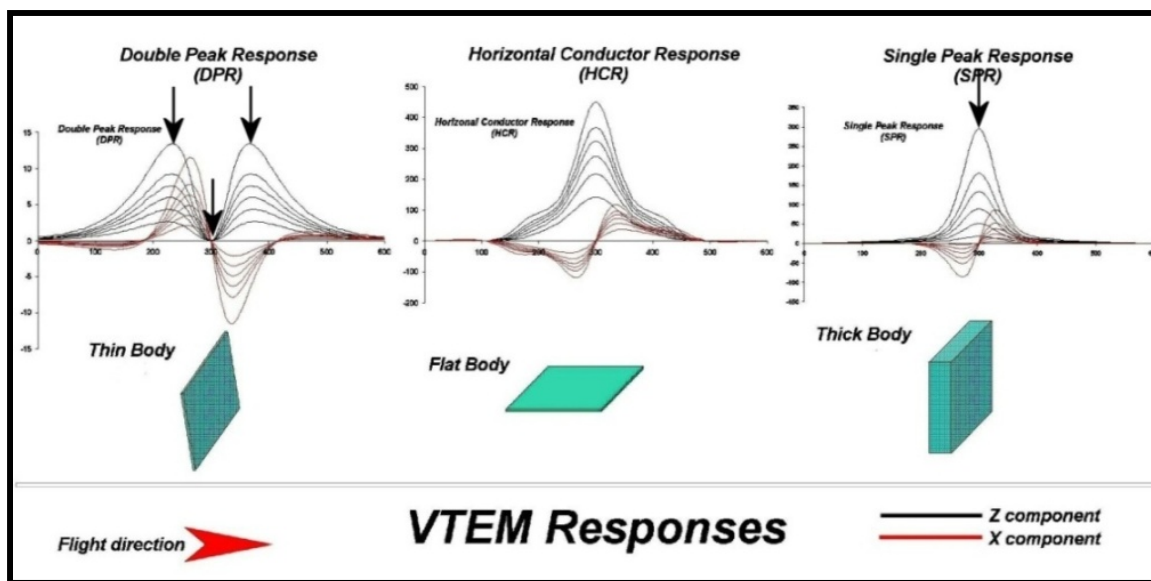


Figure 11: Examples of VTEM responses.

Wide Zones

Wide zones (WZ) are a category of picking where there a broader zone of conductivity recognized in the data. Near-surface WZ are typically related to surficial geology whereas deeper WZ are related to bedrock sources. Frequently discrete conductors and WZ are picked in the same location and represent different aspects of the same mineralized system.

Target Zones

Groupings of conductors are termed Target Zones or TZ. A TZ is deemed as a logical grouping of conductors within the data set and is based on an assessment of the distribution of individual conductor picks, plus any other available geoscience data. The TZs are then prioritized for follow up work based on their overall geophysical character and how this relates to the defined target models for the project.

PRODUCTS

Table 3-1 lists the maps and products that are provided. Other products can be prepared from the existing dataset, if required.

Base Maps: All maps are created using the following parameters:

Projection Description:

Datum: WGS84

Ellipsoid: WGS84

Projection: UTM (Zone: 8N)

Central Meridian: 135°W

False Northing: 0

False Easting: 500 000

Scale Factor: 0.9996

Table 3-1 Survey Products

TargetMaps @ 1:30 000 (1 hard copy + digital)

All maps show the indicated themes as well as the Condor discrete picks and Target Zones

- Total magnetic Intensity (TMI)
- ZS TMI-Tilt
- EM (dB/dT) Ch 1
- AdTau (dB/dT 0.002 pV/Am⁴) + Wide Zones
- DTM (from VTEM survey)

MultiPlotsTM @ 1:20 000 (digital only)

Mini-PlatesTM: TMI, TMI-ZS_Tilt and as noted below for each area:

Cabin Lake: Miniplate 3: EM B-f Ch 1, Miniplate 4: AdTau B-f 0.01 pVms/Am⁴

Caribou: Miniplate 3: EM dB/dT Ch 1, Miniplate 4: AdTau dB/dT 0.002 pV/Am⁴

MOR: Miniplate 3: EM B-f Ch 1, Miniplate 4: AdTau B-f 0.01 pVms/Am⁴

MOR-Ext: Miniplate 3: EM dB/dT Ch 1, Miniplate 4: AdTau dB/dT 0.002 pV/Am⁴

On each MultiPlotTM the picked anomalies and Target Zones are indicated along with the following:

- Profiles-EM dB/dT Ch 1-25
- Profiles-EM B-f Ch 1-25
- Profiles-Magnetics: TMI, 1st Vertical derivative and Analytic Signal
- Profiles-AdTau dB/dT (0.005 pV/ Am⁴); B-f (0.005 pVms/Am⁴) + power line monitor
- LEI-CDS dB/dT;

Cabin: (0.1-100 mS/m) + bird height

Caribou: (0.1-10 mS/m) + bird height

Mor: (0.1-50 mS/m) + bird height + drill holes² (± 50 m from section)

Mor Ext: (0.1-50 mS/m) + bird height)

² The drill holes displayed are from the data base provided by the client.

- Susceptibility Depth Section + drill holes (± 50 m from section)
- TrackMap 1: TMI-ZS Tilt filter

Mag3D Modeling

The following products are provided as part of the Mag3D modeling. Some are stand-alone and some are imbedded with other products; the letters S and I are used to flag which; S= stand-alone and I = imbedded.

- UBC mesh and sus files (S)
- Magnetic model X, Y and Z format (S)
- 3D DXFs (S)
- Susceptibility Depth Section (I- in MultiPlots)
- AVI of model (S)
- Notes on processing (S)-Appendix C

Conductivity 3D Model

Using the 1D inversions created from the EM data, a 3D voxel model of the conductivity has been created using the **encom^{pd}** application. The suite of products (primary and derived) is listed below.

- UBC mesh and con files (S)
- Conductivity model X, Y and Z format (S)
- 3D DXFs (S)
- AVI of model (S)

Processing and Analysis Report (1 copy)

On the Archive DVD (Appendix D) the following files are provided:

- Digital archive in Geosoft format
- Profile Analyst session file (to create MultiPlots™)
- Anomaly data bases in Excel and Geosoft formats
- PDFs of TargetMaps and MultiPlots™
- Processing and Analysis Report (PDF)
- Set of images from report (higher resolution than is possible to reproduce in the report).
- **encom^{pd}** Viewer (provided at no cost)

4. SURVEY RESULTS

Data Quality

The quality of the EM and magnetic data was deemed to be acceptable and shows noise levels similar to other VTEM data sets acquired in the same time frame as the present survey.

Magnetic Results

Mor

The magnetic results (TMI and TMI-Tilt) are shown in Figure 12. A number of the major linears have been marked on the images. There appears to be at least three magnetic domains or blocks in the survey area; these have been indicated in Figure 12-left image. Block A shows an alternating series of N75W trending bands with several intrusive areas or tightly folded centers (circled in orange). The Discovery Zone lies on the northern edge of one of these more discrete zones. These discrete zones could represent the locations of volcanic centers that have breached the paleostratigraphy. Massive sulfide deposits are associated with these volcanic centers.

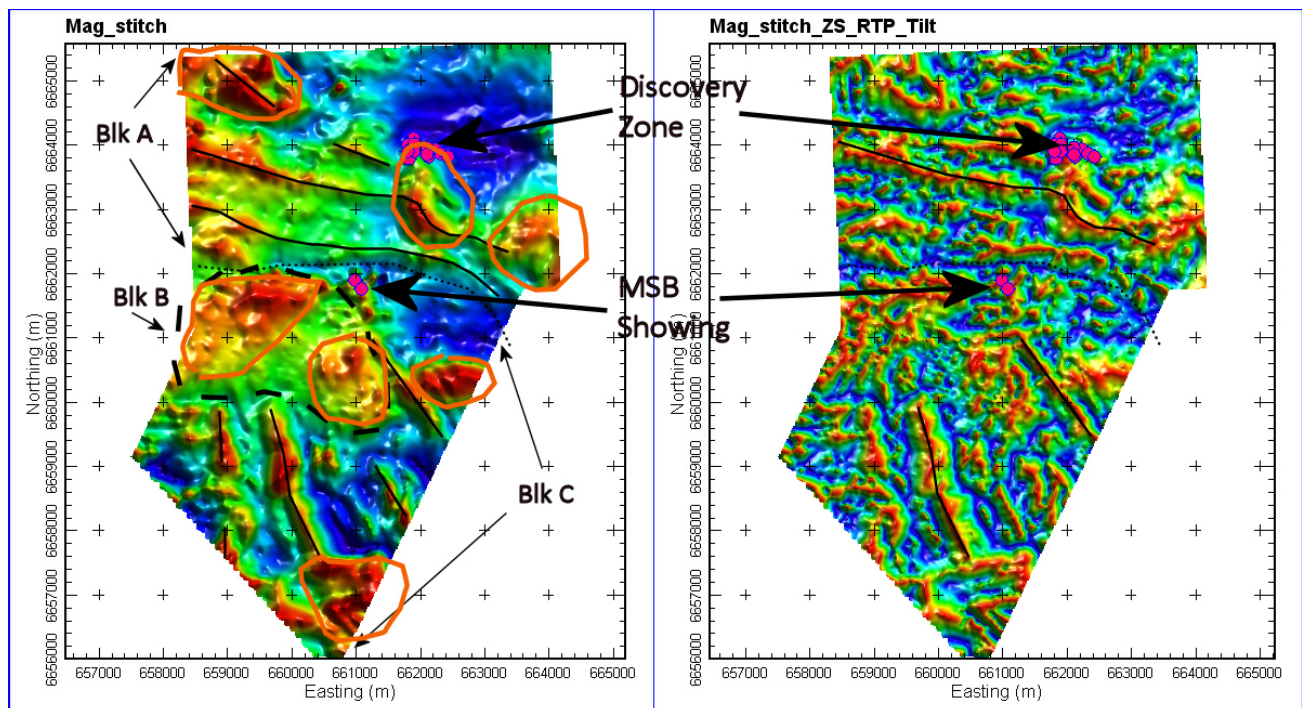


Figure 12: Mor/Mor Extension: TMI and TMI-Tilt with interpretive layer and 2007-2008 drilling (red dots).

Mag3D

A Mag3D model (UBC voxel-style model) was run for the Mor 2007 survey and the provided products are listed in Table 3-1. A snap-shot of the Mag3D model with the Tarsis drilling is shown in Figure 13. The 3D model appears to reinforce the association of mineralization at the edges of discrete magnetic zones. This could be useful in targeting other prospective areas on the property.

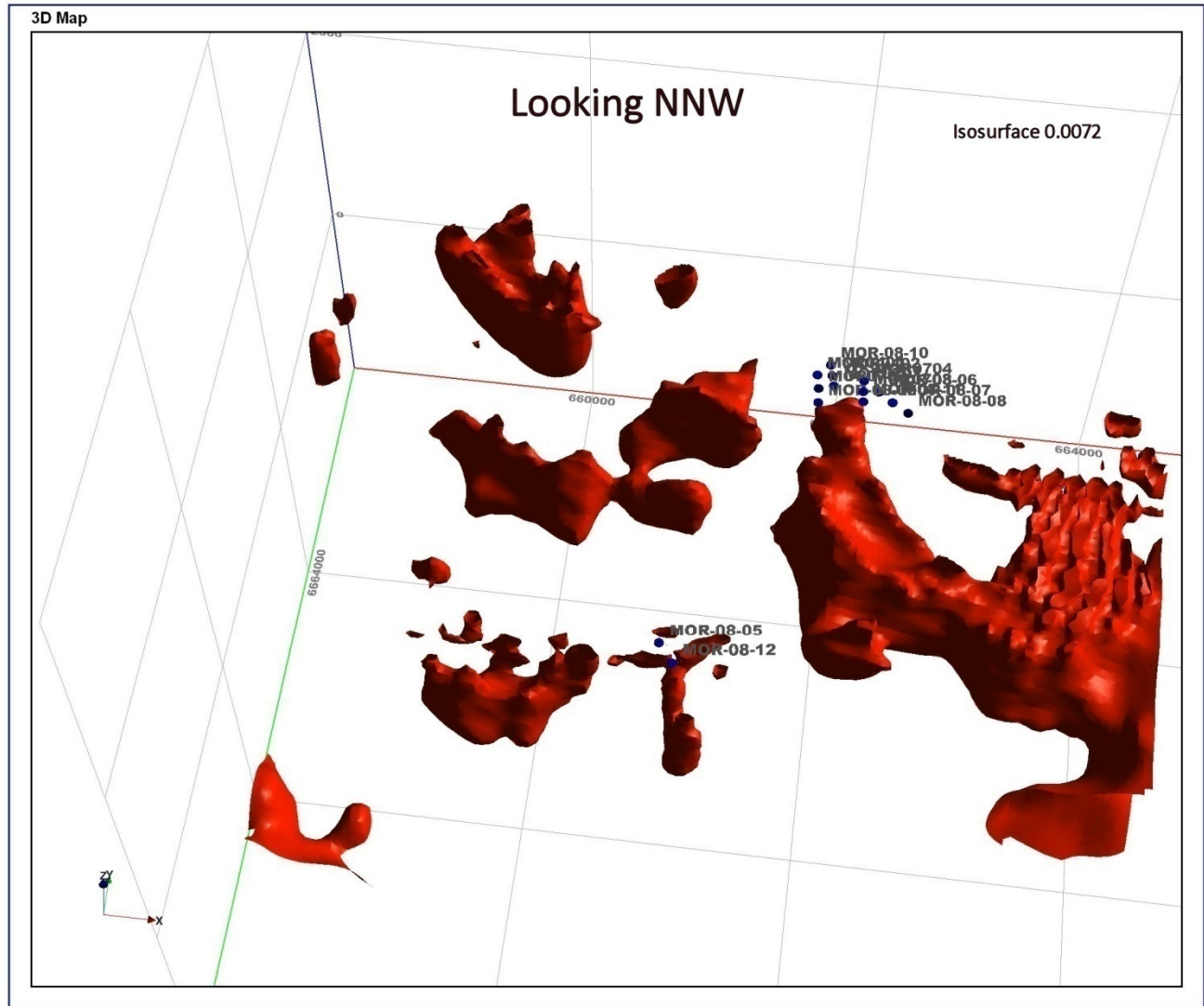


Figure 13: Mor: Mag3D model; 0.0072 SI isosurface + 2007-2008 drilling.

Cabin Lake

The TMI and TMI-Tilt images are shown in Figure 14. A number of the major linears and closures have been annotated on these images. The regional geology map suggests there are intrusives located in the northern end of the block and the SW corner (granodiorite and quartz monzonite). There are

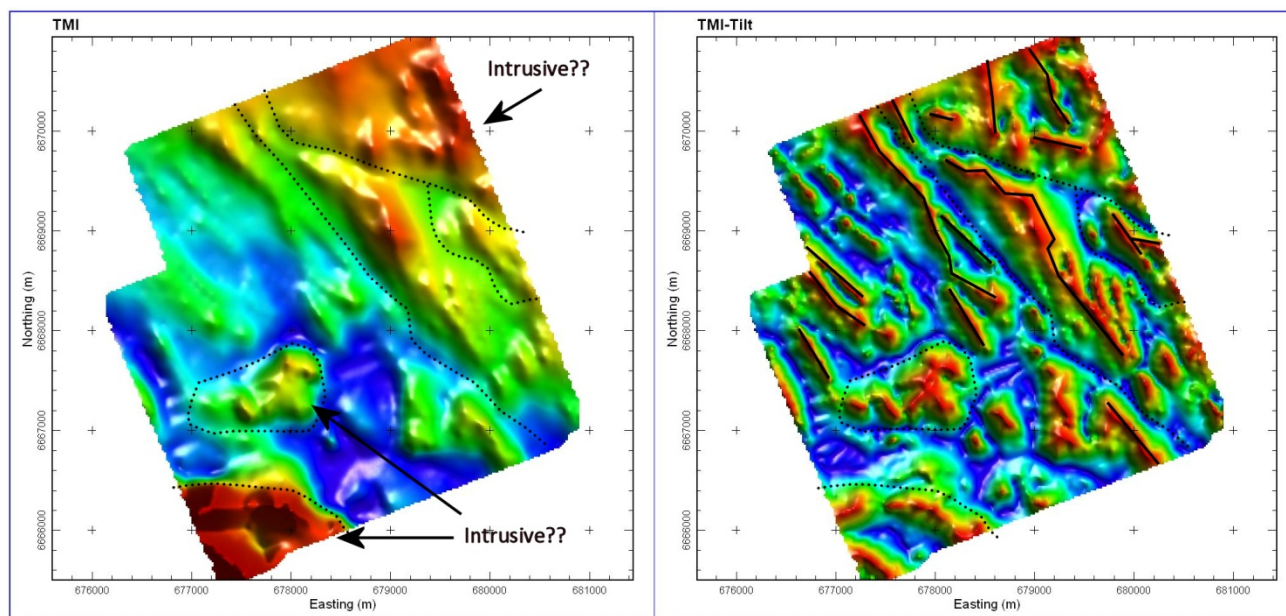


Figure 14: Cabin Lake: TMI and TMI-Tilt with interpretation.

two discrete or semi-discrete sources in the SW part of the block that are suggestive of being intrusives. A zone of elevated magnetic response in the northern end of the block could be intrusive rocks as well. The grain of the magnetic response otherwise is close to N40W. There are no 'knots' of discrete response along the linears as noted on the Mor property.

Caribou

The TMI and TMI-Tilt images are shown in Figure 15. The regional geology indicates there is a mixture of mafic volcanics and carbonate lenses. The images are dominated by a number of semi-discrete highs, showing locally what appears to be tight folding. This terrain does not look like either Cabin Lake or Mor.

EM Survey Results

Mor

The EM Channel 1 and AdTau (B-field) is shown in Figure 16. The two zones of known mineralization are highlighted with the drill hole collars (white dots). The central zone (designated as Mag Showing, SD Showing and Bean Showing in Figure 5 or shortened to MSB Area for this report) appears as a strong, very discrete feature, especially in the AdTau image. The Discovery Zone appears reasonably discrete in the EM Channel 1 image but less so in the AdTau where the zone merges into a larger more formational type feature to the east. The Mor Extension block appears to host only several large formational conductors and no discrete bedrock features were recognized.

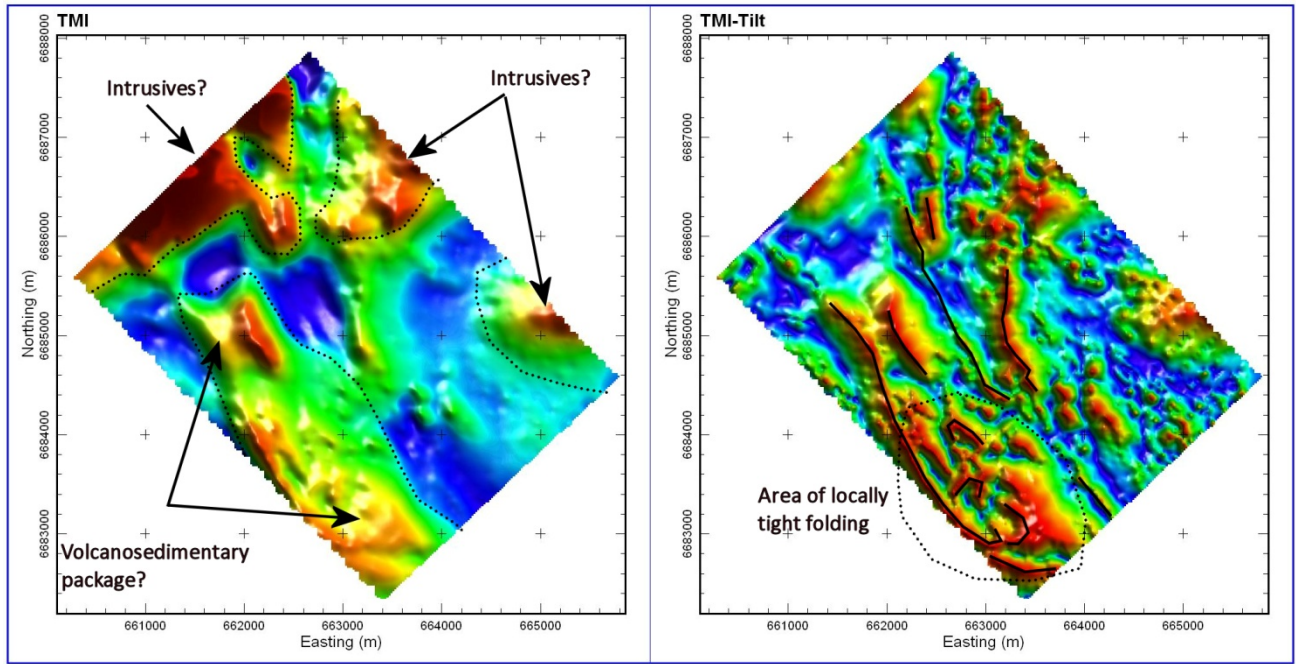


Figure 15: Caribou: TMI and TMI-Tilt with interpretation.

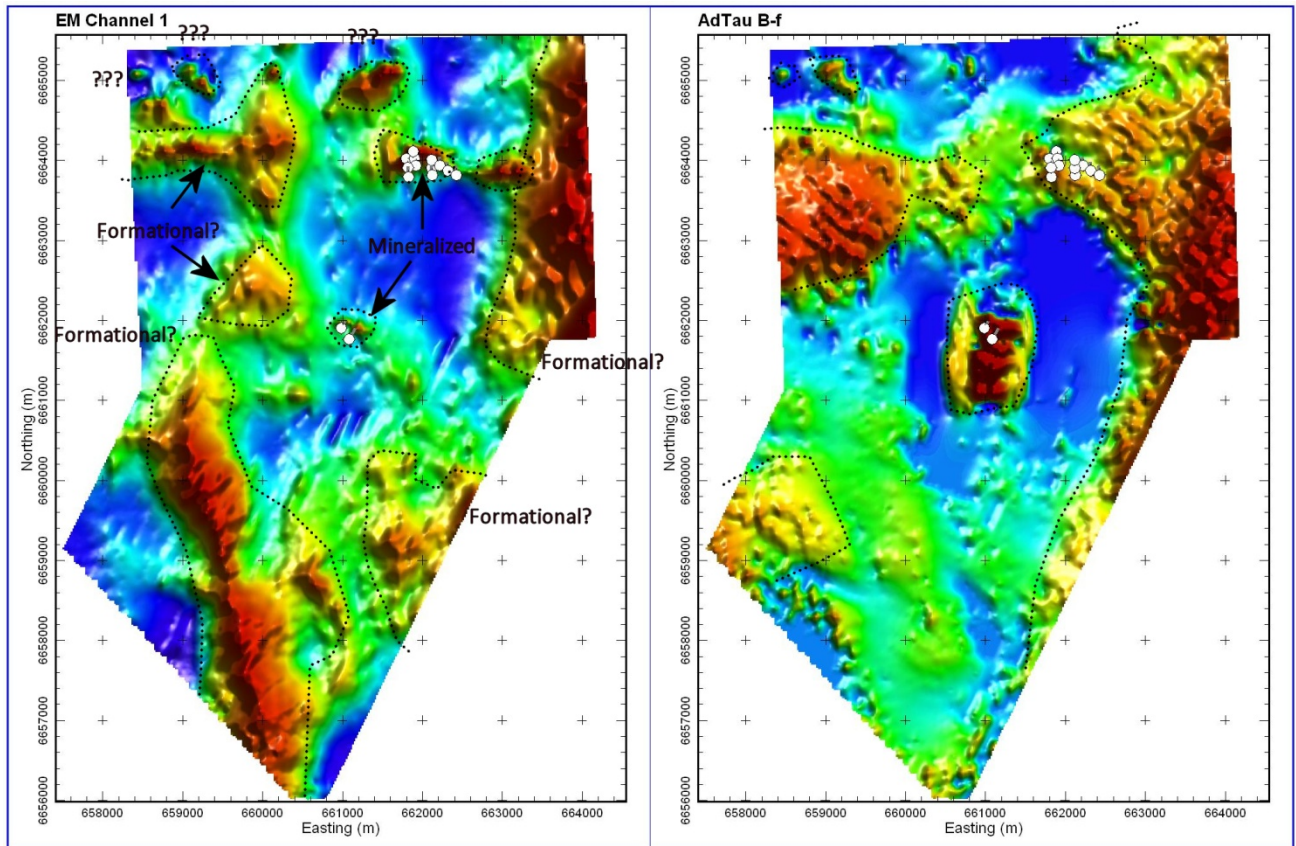


Figure 16: Mor/Mor Extension: EM Channel 1 and AdTau (B-f) with interpretation and drilling (white dots).

Figure 17 shows the same images as in Figure 16 but with the EM picks and Target Zones defined. Tarsis had an earlier assessment performed on the survey by Geotech Ltd. (Bournas 2007) and the labels applied to the zones defined by Bournas were used by Condor where they overlapped. No formal reconciliation between Geotech's and Condor's assessment of the responses has been undertaken.

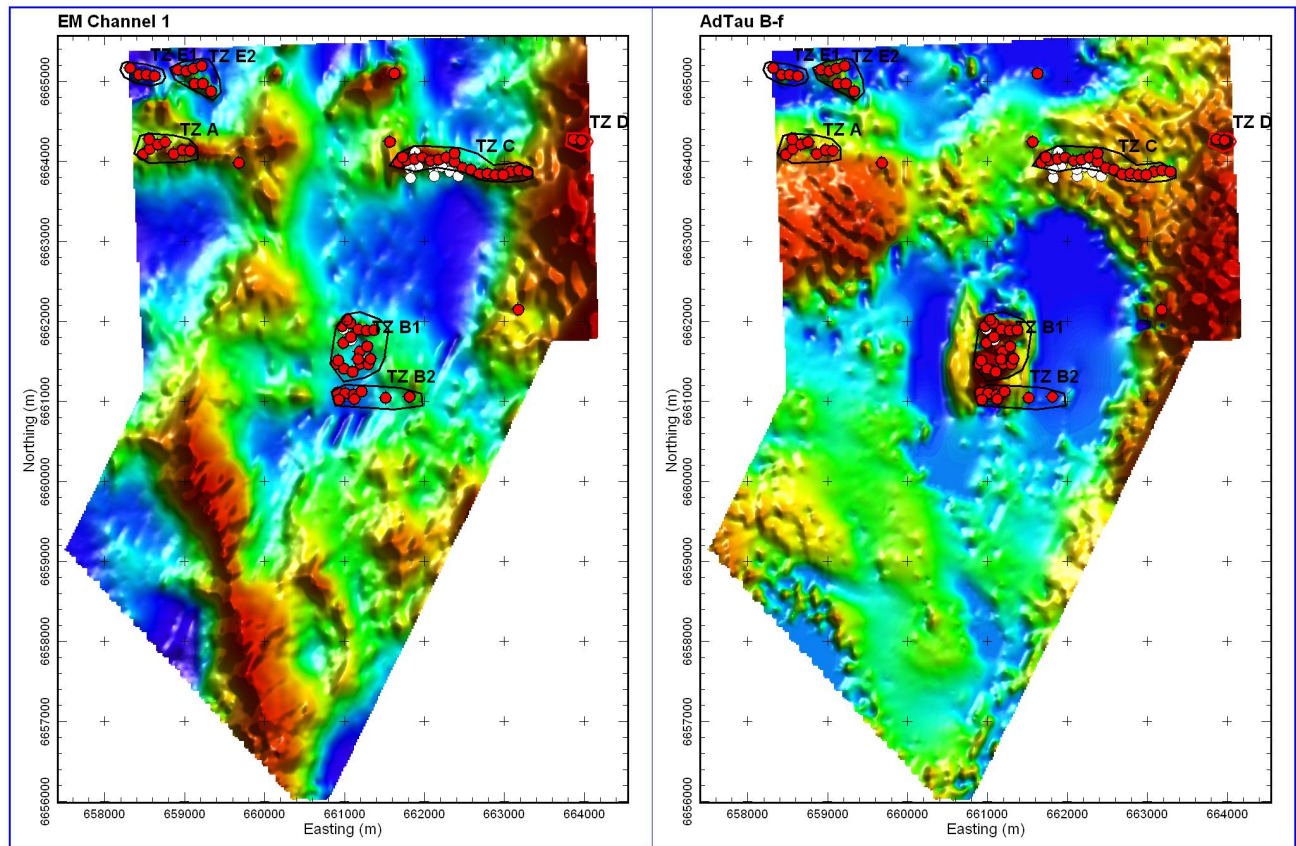


Figure 17: Mor/Mor Extension: EM Channel 1 and AdTau with EM picks (red dots), Target Zones and drilling (white dots).

EM3D

A 3D model of the EM response was created from the 1D inversions along the flight lines; an image of this is shown in Figure 18 and several AVIs and DXFs are provided as well (see Table 3-1). This image suggests there are several different styles of conductivity structure on the property. On the western side of the block, TZ A appears to be at the upper edge of a conductive sheet dipping to the south. TZ B1 and B2 are associated with a discrete “island” of high conductivity that appears disconnected from the other conductivity distributions on the property. TZ C appears as the western extension of a formational type response that extends along the eastern side of the property. TZ D lies over this formational zone. TZ E1 and E2 are isolated features in the far NW corner of the survey block.

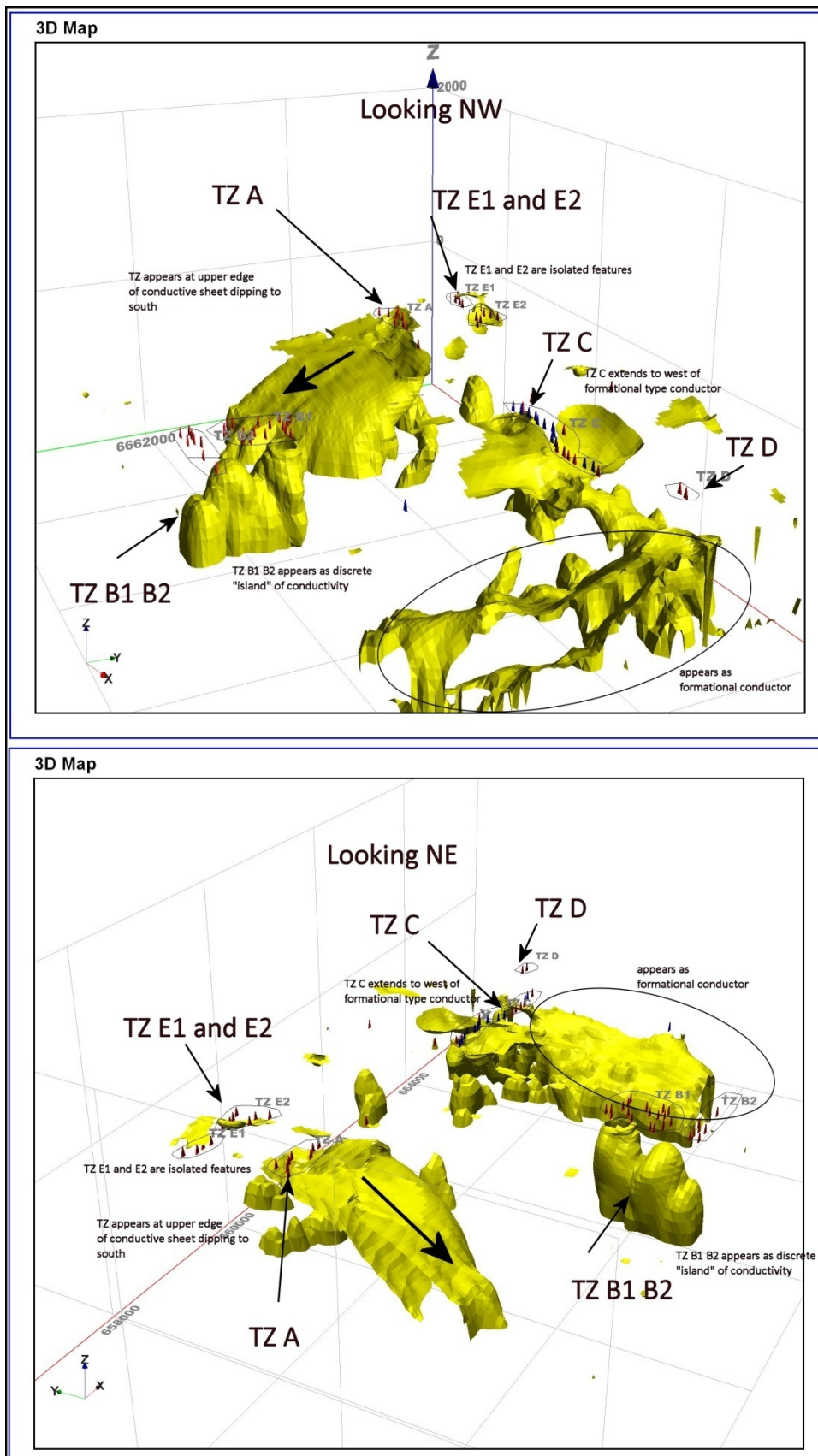


Figure 18: Mor: Views of 3D EM voxel model for Mor showing EM picks and TZs.

TZ

The various TZ are discussed in more detail. For the figures provided, both the Mag3D and EM3D voxel models are displayed.

TZ A: Figure 19: Located in the NW corner of the survey, this is a limited strike length string of discrete EM picks; appears to trend off the survey block to the west. The EM conductivity model shows the TZ to be lying at the upper edge of a southward dipping conductive sheet. The EM Channel 1 response (Figure 17) appears to highlight this upper edge whereas the AdTau appears to be responding more to the depth extent of the horizon. The voxel model and AdTau both suggest this unit is limited spatially to the western side of the survey block. The magnetic results show there are several steeply dipping magnetic highs associated with the overall EM feature. The stronger magnetic response does not appear to correlate directly with the discrete EM picks.

TZ B1 & TZ B2: Figure 20: The EM response appears as a discrete feature that has three distinct sections and these get progressively deeper moving from north to south. There seems to be a shallow magnetic body at the north end of feature with a rod-like protrusion that plunges to the south. A large magnetic source lies just to the west but does not shown any EM response.

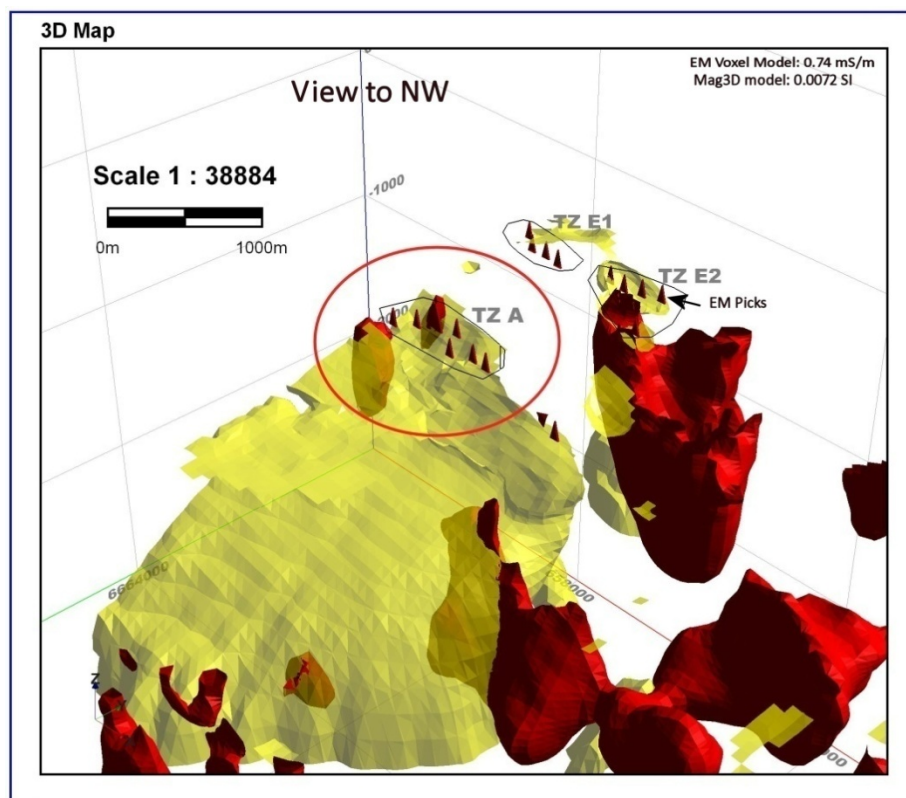


Figure 19: Mor/Mor Extension: TZ A: EM (yellow) and susceptibility (red) models.

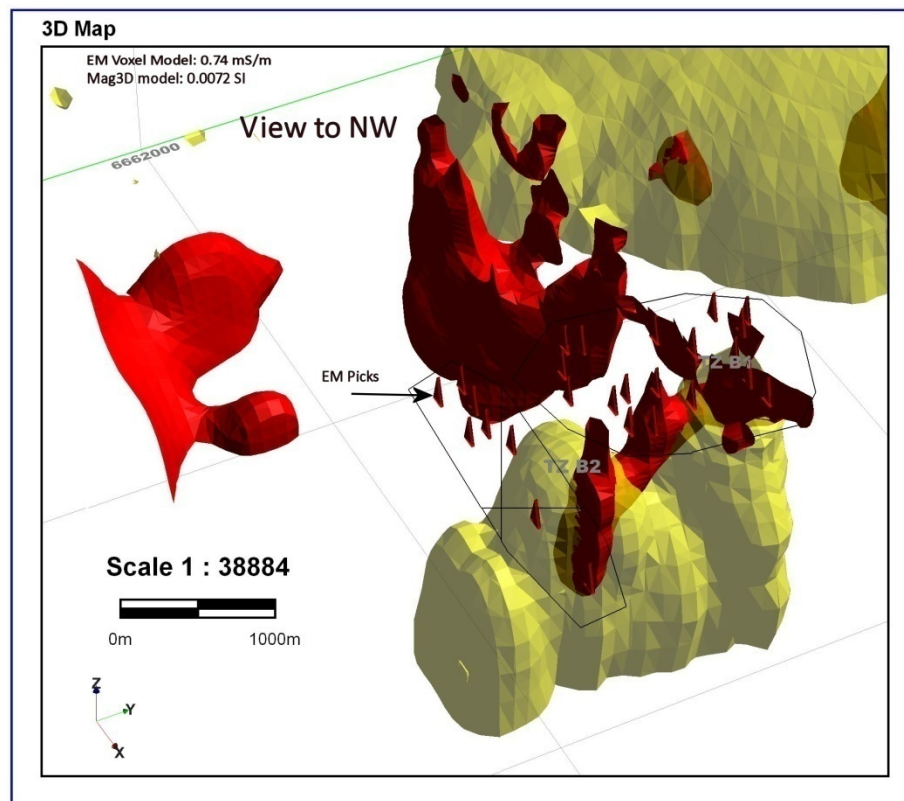


Figure 20: Mor/Mor Extension: TZs B1 and B2; EM (yellow) and susceptibility (red) models.

TZ C: Figures 21 and 22: The EM and magnetic responses in this area are quite complex. The area of known mineralization appears as discrete EM picks but does not image very well in the 3D model. There seems to be a flat-lying EM basement that is dipping off to the east towards the noted formational conductor along the eastern side of the survey block. The magnetic model shows an N-S body that stops at the western end of the TZ and extends to the south. There is another magnetic source at the eastern end of the TZ but at depth; this feature and the other appear to join up to the south and form a larger body. Conductivity appears to infill an embayment made by the magnetic model. Figure 22 provides a view of the models from the north and shows there is a zone of deeper conductivity to the NE of the Discovery Zone.

TZ D: Figure 22: This is a strike limited target with what appears to be coincident EM and magnetic responses.

TZ E1 and E2: Figure 23: There appears to be a modest conductivity zone connecting the two TZ. There also appears to be a significant magnetic body associated with TZ E1.

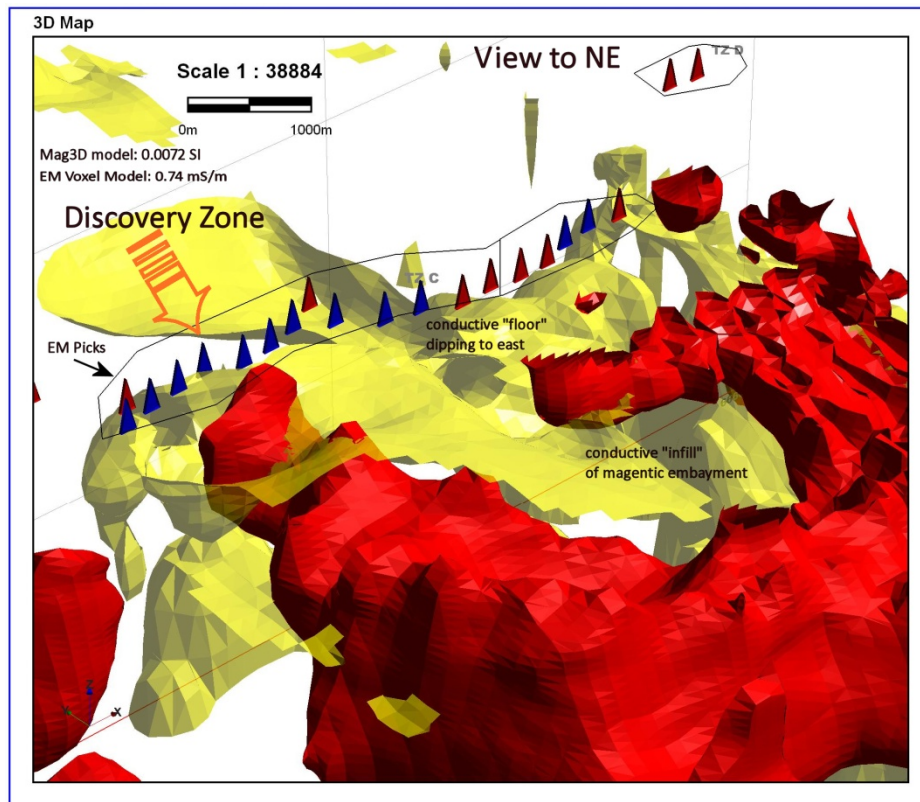


Figure 21: Mor/Mor Extension: TZs C and D; EM (yellow) and susceptibility (red) models.

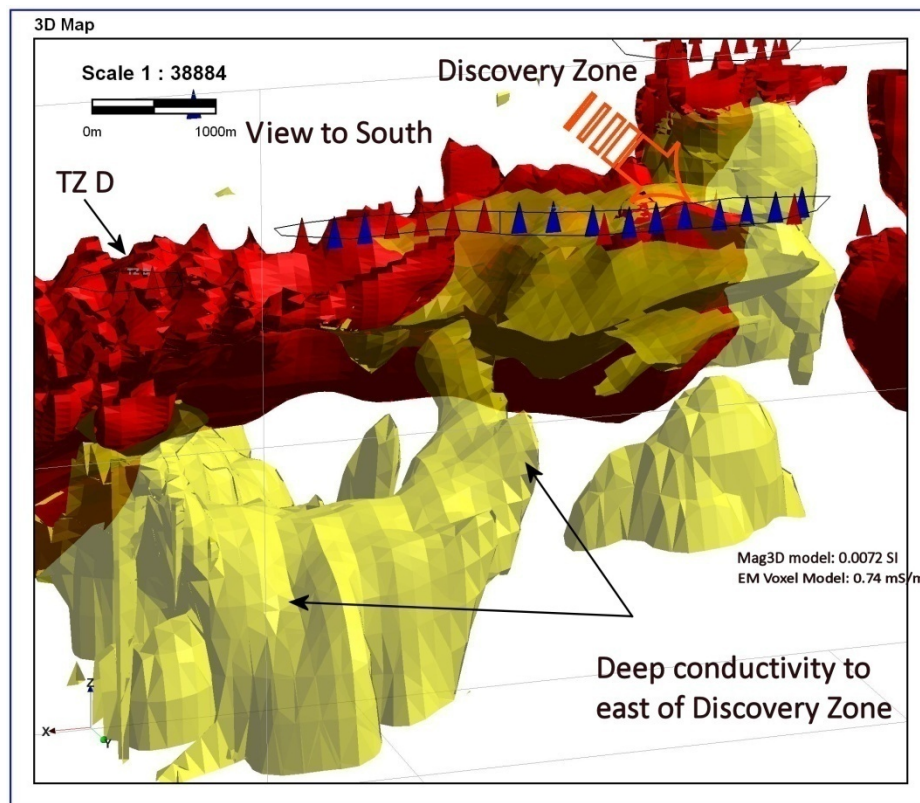


Figure 22: Mor/Mor Extension: TZs C and D; EM (yellow) and susceptibility (red) models.

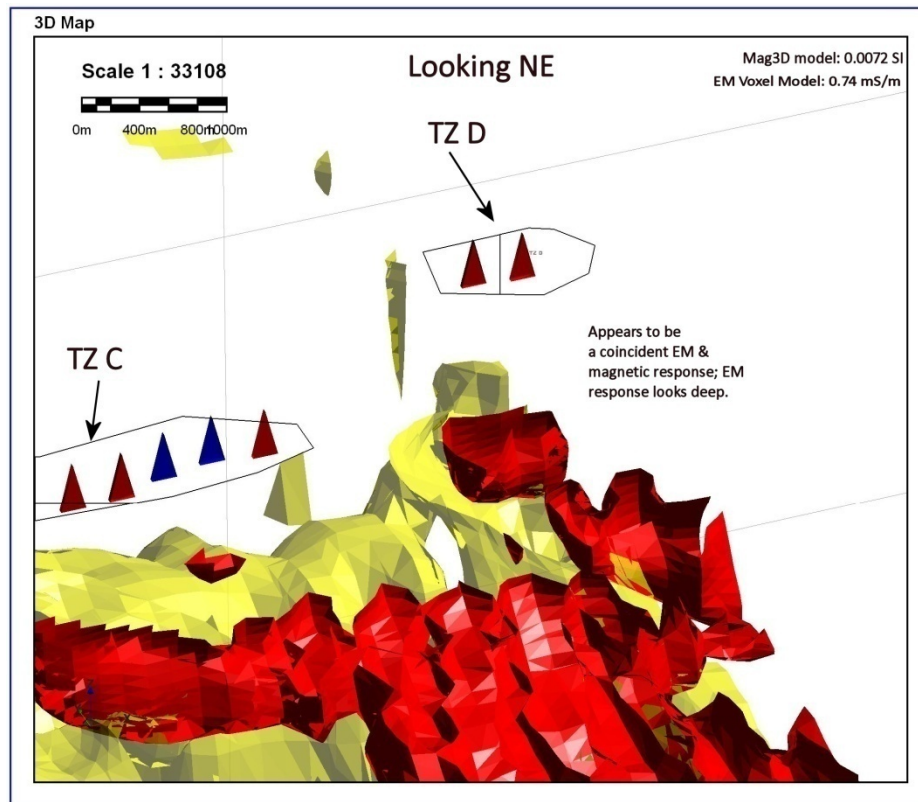


Figure 23: Mor/Mor Extension: TZ D: EM (yellow) and susceptibility (red) models.

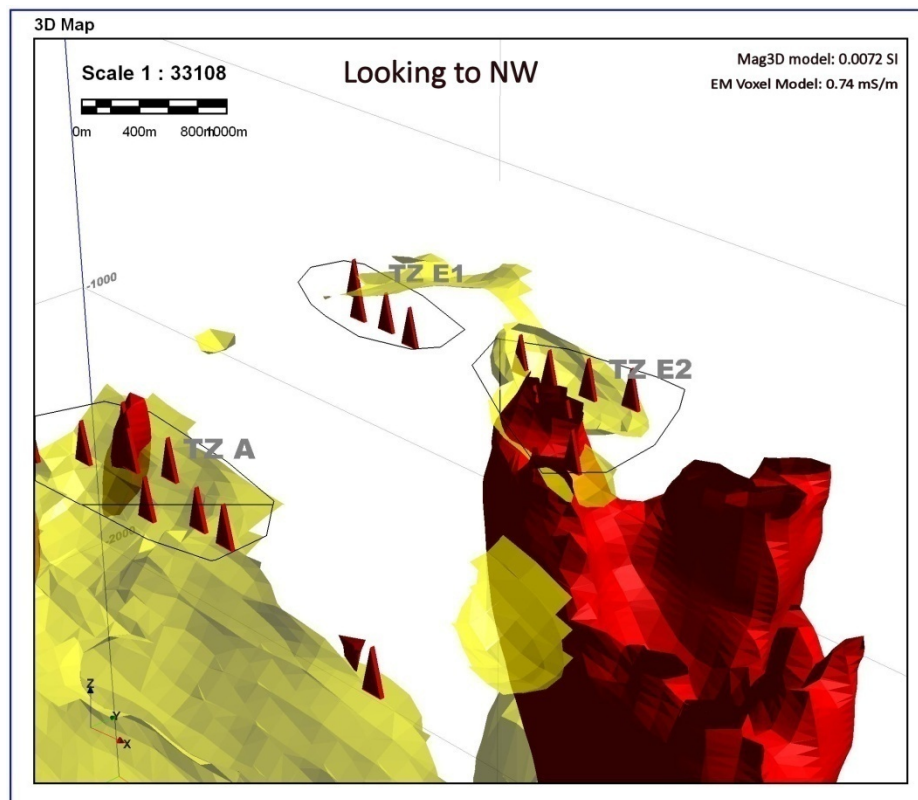


Figure 24: Mor/Mor Extension: TZs E1 and E2; EM (yellow) and susceptibility (red) models.

Cabin Lake

Figure 25 shows the EM Channel 1 and AdTau B-f response with the picking for survey block. Wide Zones were the dormant style of EM response in the survey. A number of discrete picks were selected as well, but these all appeared to represent the edges of Wide Zones rather than discrete bedrock features.

An EM voxel model was created for the survey and Figure 26 shows perspective views of three thresholds with the TZs. There appears to be a complex zone of conductivity at the northern end of the survey block that extends along the eastern margin of the block to the south. The southward extension appears to be mapping out a conductive unit that is steeply dipping along the eastern edge of the block but then dips westward and flattens out at depth. Four TZs have been selected and are discussed below.

TZ 1: Figures 26, 27 and 28: This is a limited strike length feature that lies on the western side of the formational style conductor that extends the full length of the survey in an N-S direction. In Figure 26,

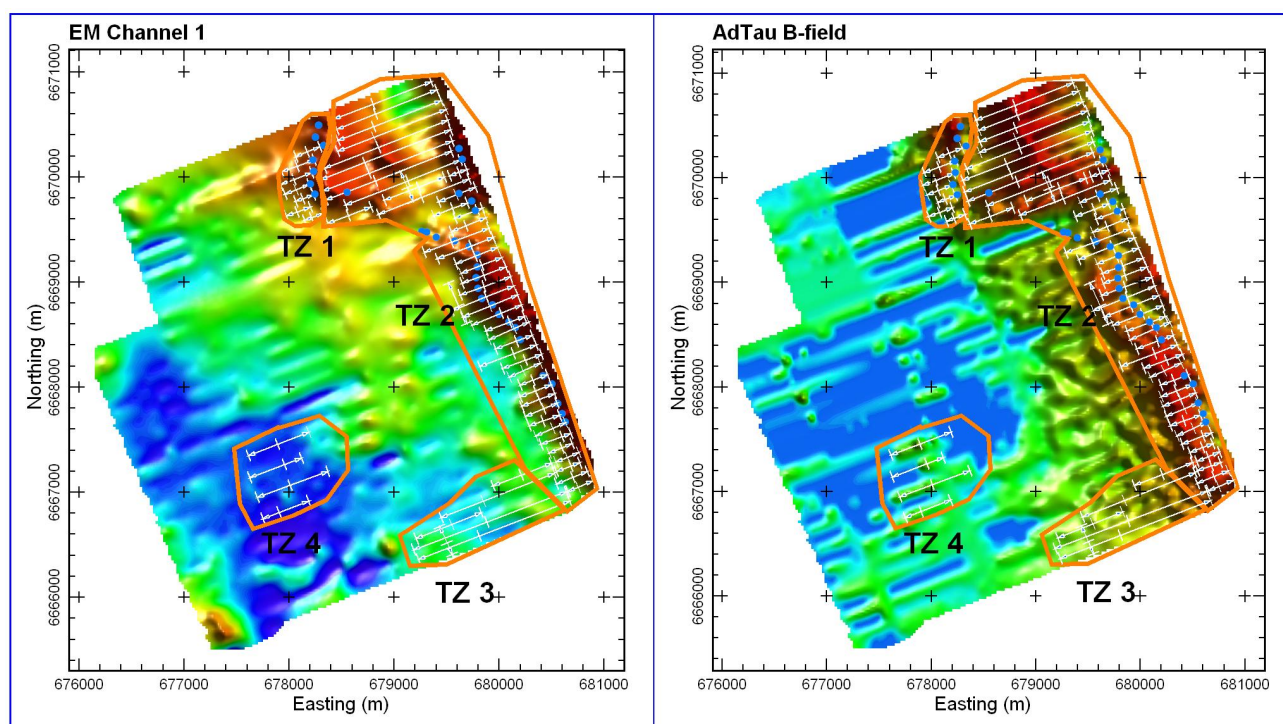


Figure 25: Cabin Lake: EM Channel 1 and AdTau (B-f) with TZs and EM picks.

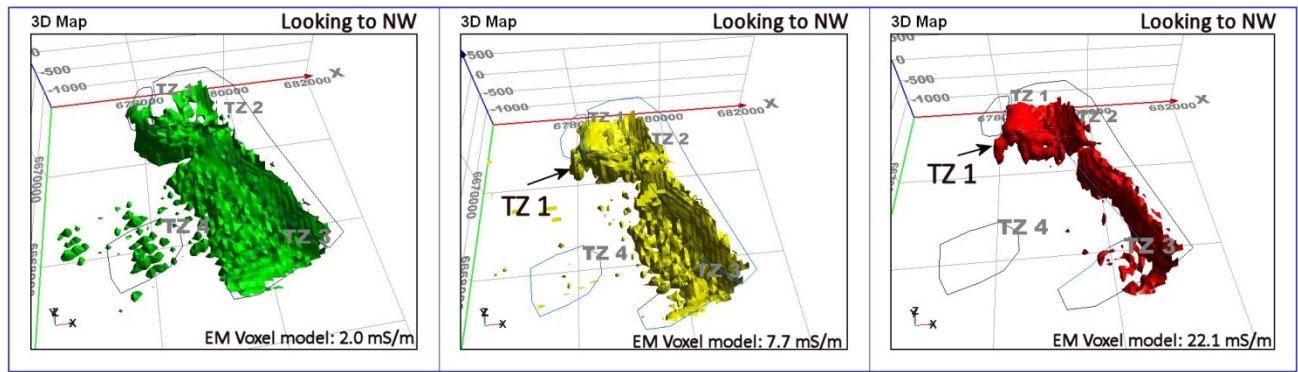


Figure 26: Cabin Lake EM voxel model with three thresholds; 2, 7.7 and 22.1 mS/m with TZ.

its location is highlighted in the central and right hand panels. Figure 27 shows the feature in more detail in the EM voxel model. L8040 passes over the top of this TZ and the geophysical outcomes along this line are shown in Figure 28. Target modeling of this feature is warranted prior to drilling but the depth appears to be the order of several hundred meters.

TZ 2: Figure 29: This zone of conductivity is deemed to be most likely formational and hence not a economic target. However, understanding how it relates to the overall geology of the survey block is deemed important. In Figure 29, two of the conductivity isosurfaces are highlighted in order to better define the Zone's overall character.

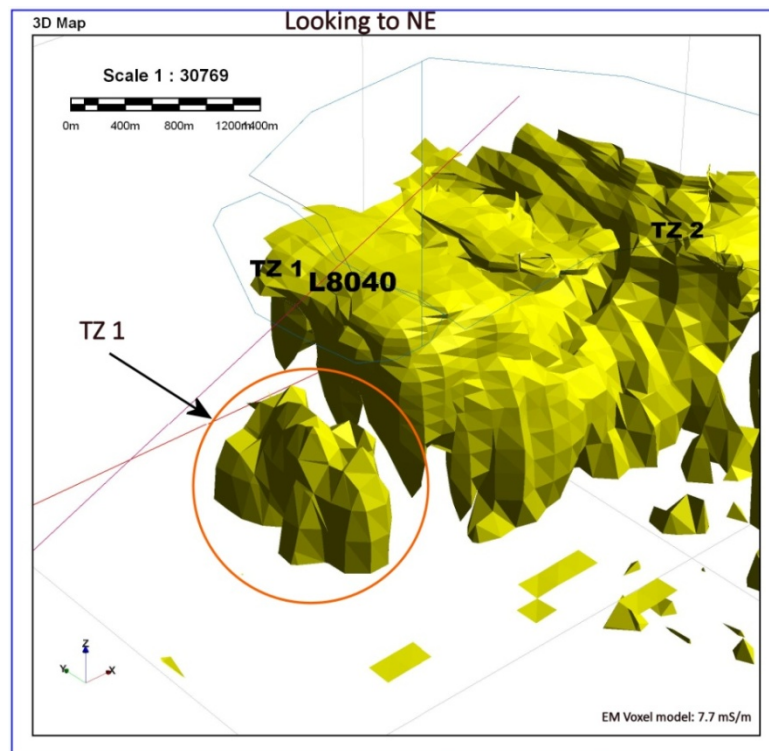


Figure 27: Cabin Lake: EM voxel model showing TZ 1.

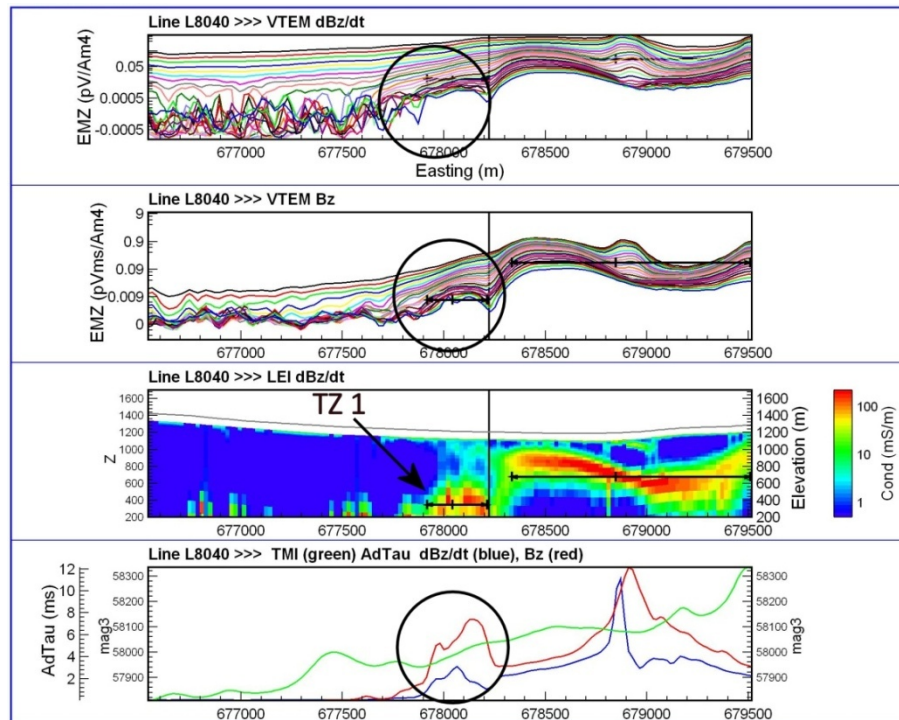


Figure 28: Cabin Lake: MultiPlot for L8040 over TZ 1.

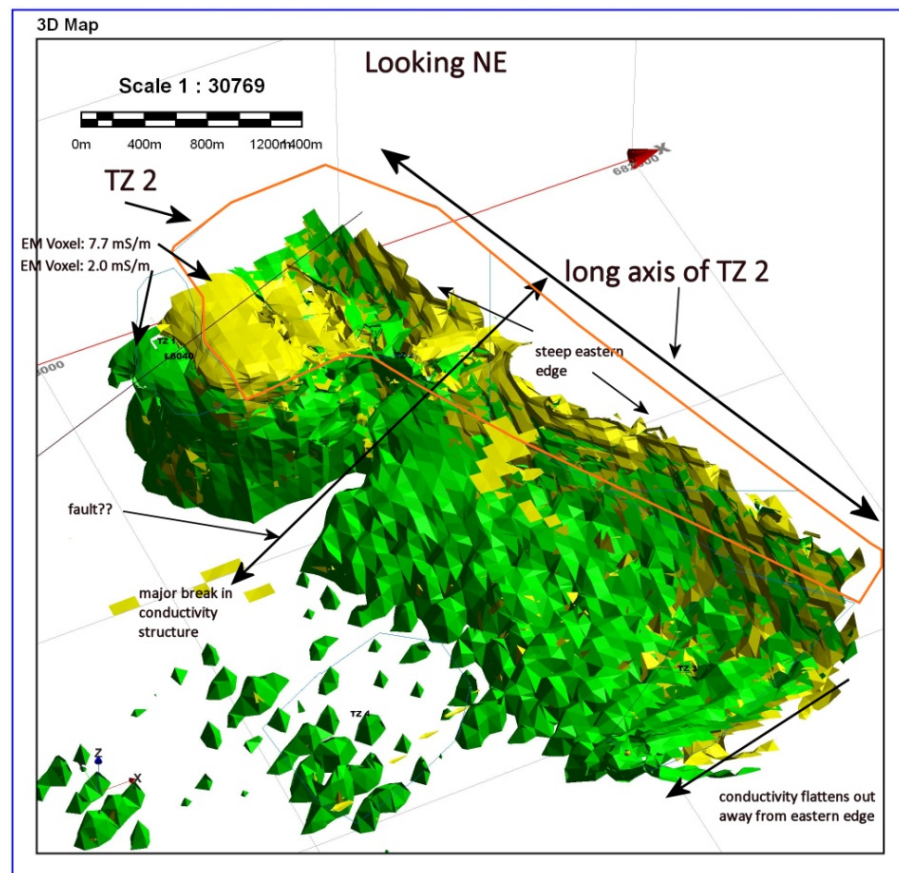


Figure 29: Cabin Lake EM voxel model for TZ 2.

TZ 3: Figure 30: Like TZ 2, this TZ appears to be a formational but represents a major change in the character of the sub-surface conductivity and hence is deemed worthy of taking note of. This TZ is not deemed to be of economic interest based on current information.

TZ 4: Figures 12, 25 and 26: This TZ is a weak change in the EM character that could represent some effect of an intrusive event located in the SW corner of the property as best expressed in Figure 12. The EM character is deemed marginal at best and follow-up using the IP technique is recommended if this TZ were to be further investigated.

Caribou

The EM Channel 1 and AdTau response is shown in Figure 31. Indicated as well is the one EM pick identified on this block. Figure 32 shows the MultiPlot over this feature. An EM voxel model was created for this block but showed no character of either a discrete target or geological mapping interest. The single pick (contained within TZ 1) is deemed to be a reliable target and given its location on the northern edge of the survey block, could extend off the grid.

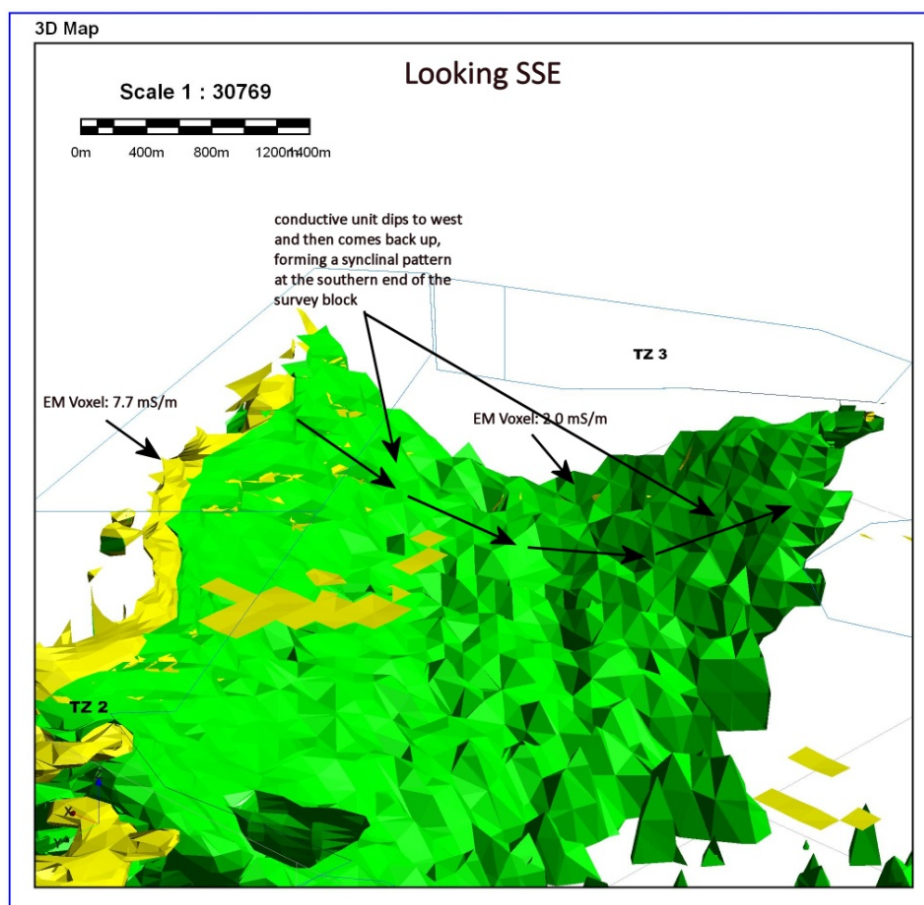


Figure 30: Cabin Lake EM voxel model for TZ 3.

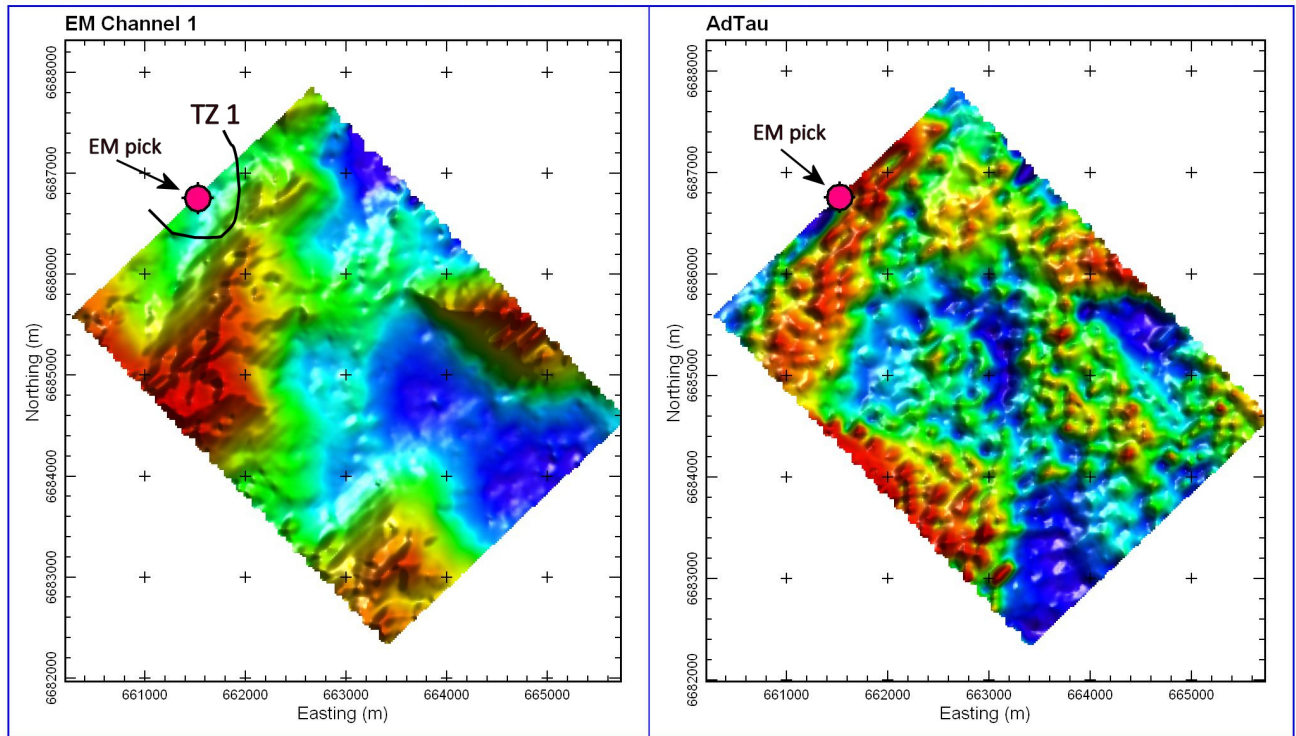


Figure 31: Caribou EM Channel 1 and AdTau showing EM pick.

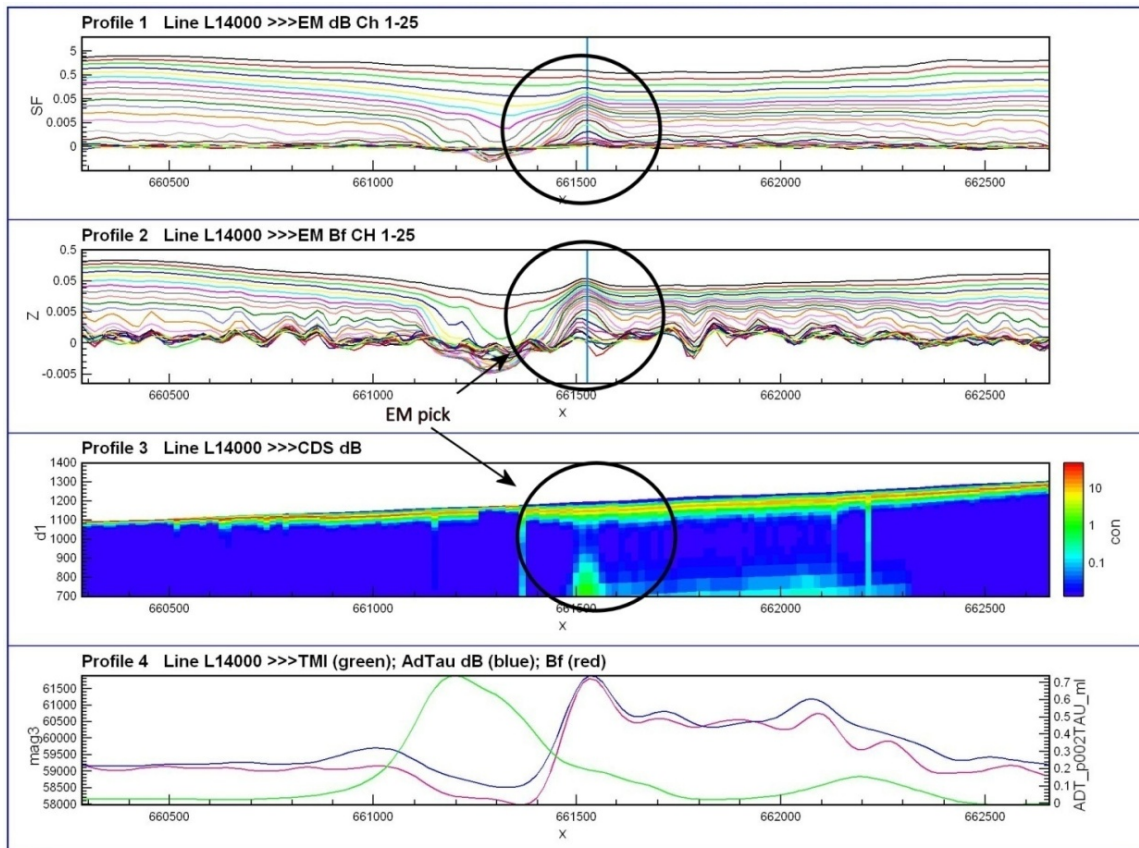


Figure 32: Caribou; MultiPlot L14000 showing EM pick

Discussion

Mor

The Mor assessment shows several untested targets of interest as well as potential extensions to the two known zones of mineralization. These outcomes are summarized below.

TZ A: Appears to be the upper edge of a formation conductor dipping to the south. Minor magnetic response. Low priority

TZ B1 and B2: Corresponds to what is termed the MSB Zone of mineralization. Geophysical modeling suggests extensions of this zone to depth to the south of the known mineralization. High priority

TZ C: Corresponds to the Discovery Zone. Geophysical modeling suggests there could be extensions to this zone both to the east and NE at depth. High priority

TZ D: Strike limited zone in interesting area. Medium priority

TZ E1 and E2: Shows interesting EM and magnetic character especially on the eastern side of the TZ. Medium-high priority.

Cabin Lake

TZ 1: This feature is deemed worthy of further assessment. High priority

TZ 2: Formational conductor. Low priority

TZ 3: Formational conductor. Low priority

TZ 4: Possible alteration halo to intrusive. Low-medium priority

Caribou

One conductor identified. Medium priority (additional geophysical or geochemical work recommended to investigate area. Staking to extend claim coverage is also recommended).

5. CONCLUSIONS & RECOMMENDATIONS

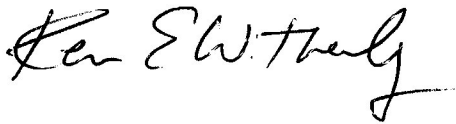
This report provides an assessment of a VTEM EM and magnetics survey over three properties in the southern Yukon held by Tarsis Capital Corp. The primary economic focus was on VMS style targets.

The Mor property appears to hold the greatest potential for further discovery given the presence of significant mineralization in several locations on the property, both of which show strong geophysical responses and appear to offer potential for extensions to known mineralization. Several other zones of interest were recognized as well.

The Cabin Lake property has one target of interest; however, this target is apparently several hundred meters depth below surface and this could preclude early stage testing unless the target can be upgraded with mapping or possibly geochemical surveying.

The Caribou property survey produced one reasonable bedrock EM response on the edge of the flight block. Follow-up mapping and geochemical work is recommended, with consideration to extend the claim block to the north to cover possible extensions to the conductive zone.

Respectfully submitted



Condor Consulting, Inc.

February 4, 2009

6. REFERENCES

Bournas, N. 2007 Report on a Helicopter-Borne Time Domain Electromagnetic Geophysical Interpretation Mor Property Yukon Territory, Canada for Tarsis Capital Corp., Geotech Ltd., December 2007

Downie, C., 2007, Technical Report for the Morley River Property MOR 1 – 52 CLAIMS, for Almaden Minerals Ltd. and Tarsis Capital Corp. January 2007.

Ellis, R. G., 1998a Inversion of airborne electromagnetic data: *Explor Geoph* Vol 29, pp 121-127.

Farquharson, C.G. and Oldenburg, D. W., 1993, Inversion of time domain EM data for a horizontally layered earth, *Geophysical Journal International*, Vol. 114, pp 433-441.

Holroyd, B. and Lajoie, J. and Klein, J. 1997 Geophysical Aspects of the Kudz Ze Kayah Massive Sulphide Discovery Southeast Yukon, Canada in “Proceedings of Exploration 97: Fourth Decennial International Conference on Mineral Exploration” *edited by* A.G. Gubins, 1997, p. 1053–1056

Lev, G., 2007, Report on a Helicopter-Borne Versatile Time Domain Electromagnetic (VTEM) Geophysical Survey, Cabin Lake property Yukon, Canada for Tarsis Capital Corp.; Geotech Ltd. November 2007

Lev, G., 2008, Report on a Helicopter-Borne Versatile Time Domain Electromagnetic (VTEM) Geophysical Survey, MOR property Yukon, Canada for Tarsis Capital Corp.; Geotech Ltd. January 2008

Li, Y., and D. W. Oldenburg, 1996, 3-D inversion of magnetic data: *Geophysics*, **61**, no.2, 394-408.

Orlowski, K., Fiset, N. and Legault, J., 2008, Report on a Helicopter-Borne Versatile Time Domain Electromagnetic (VTEM) Geophysical Survey, Caribou Property, Yukon Canada for Archer Cathro & Associates; Geotech Ltd., November 2008

Orlowski, K., Fiset, N. and Legault, J., 2009, Report on a Helicopter-Borne Versatile Time Domain Electromagnetic (VTEM) Geophysical Survey, Mor Property, Yukon Canada for Archer Cathro & Associates; Geotech Ltd., January 2009

Power, M., 2004, Induced Polarization Survey at the Mor Property, Teslin Area Yukon Territory by Aurora Geoscience Ltd. October 2004

Shi, Z and Butt, G. 2004 New enhancement filters for geological mapping, Preview, 111, 87-88, (2004)

Tarsis Web site: www.tarsis.ca

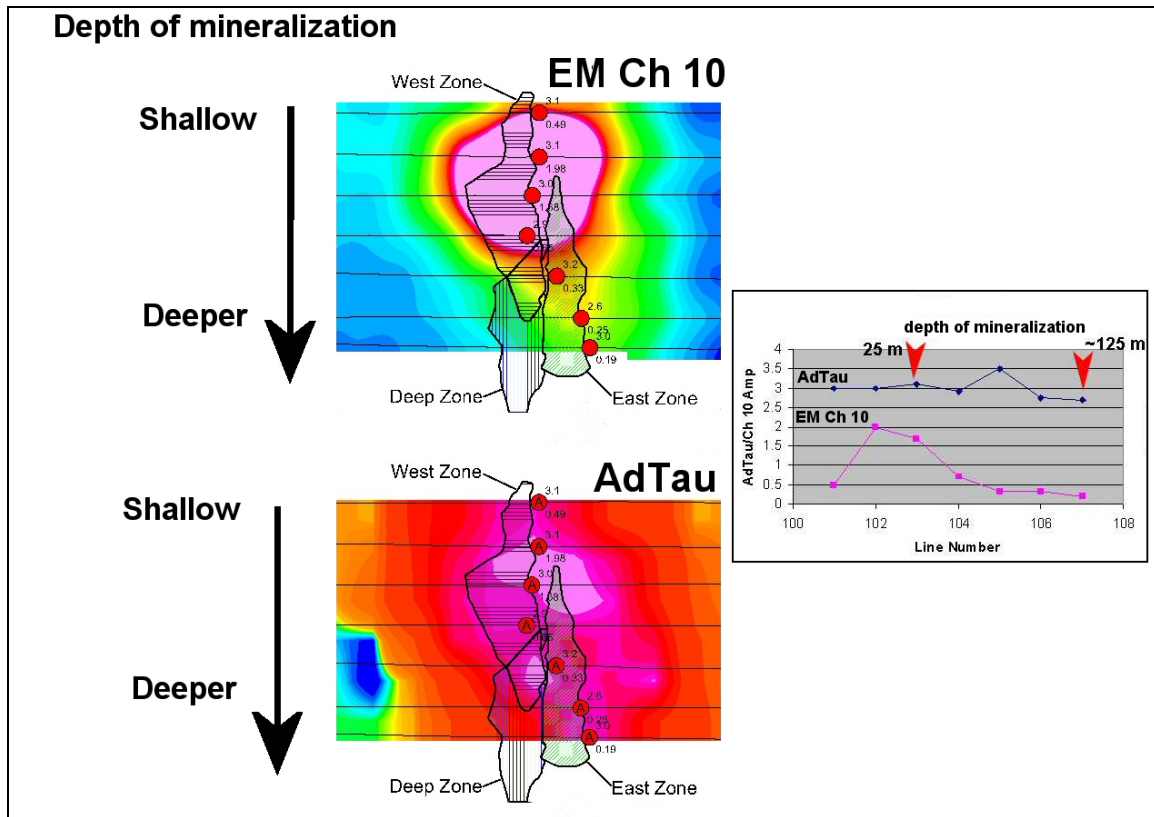
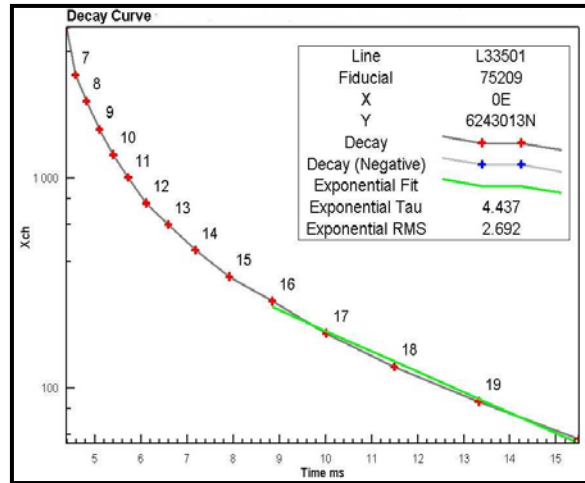
7. APPENDICES

APPENDIX A: BACKGROUND ON EM PROCESSING

Time Constant Analysis AdTau

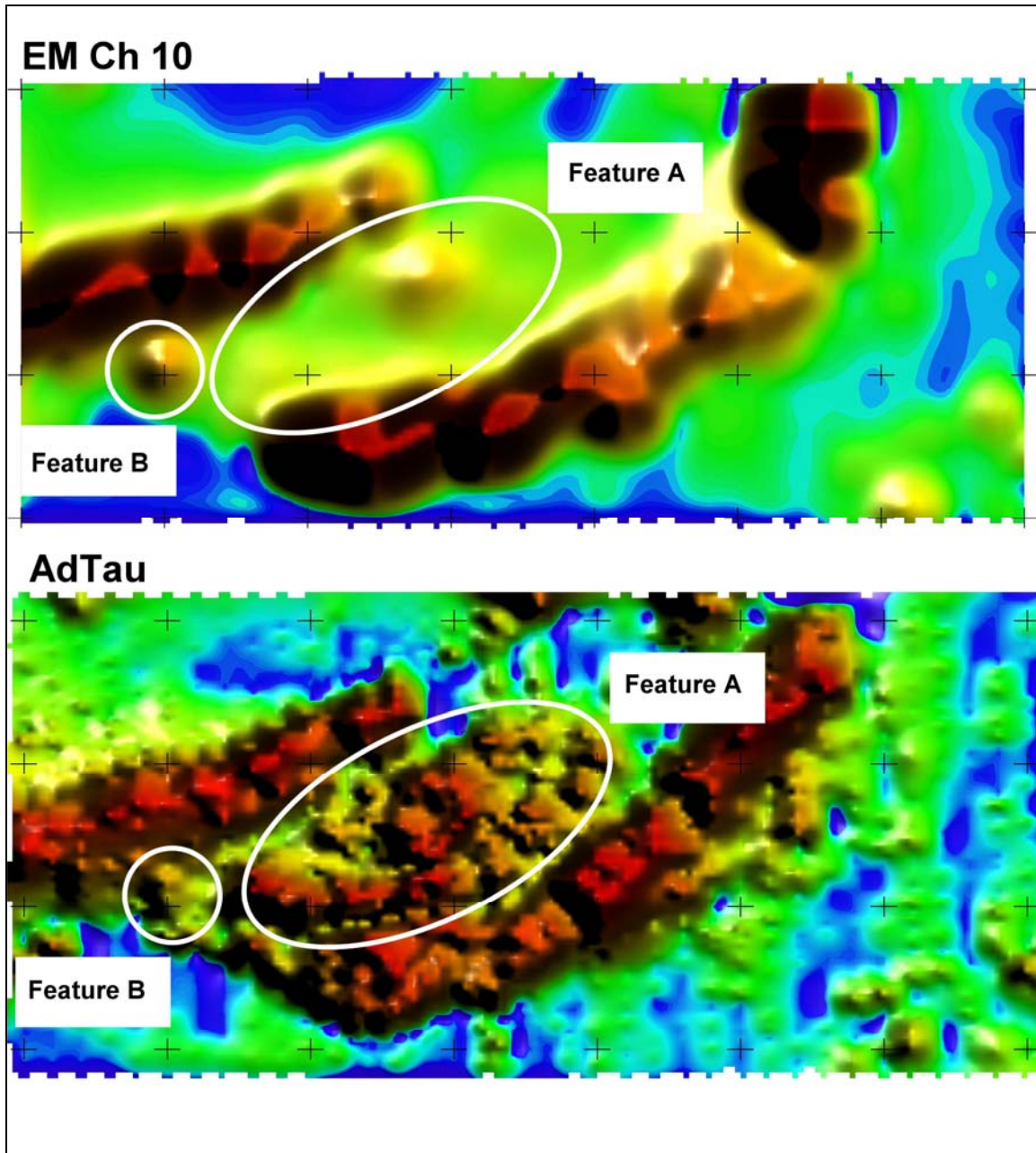


The AdTau program calculates the time constant (τ) from time domain decay data. The program is termed **AdTau** since rather than using a fixed suite of channels as commonly done, the user sets a noise level and depending on the local characteristics of the data, the program will then select the set of last five channels that are above this noise level. In resistive areas, the earlier channels will tend to be used (i.e. little late time response), whereas in conductive terrains the latest channels available can generally be used. A typical decay fit is shown on the right; the fitted late-time response is shown as the green line.



In the figure above, the upper image shows the EM amplitude plot over the Montcalm Cu-Ni Deposit and the corresponding AdTau image is underneath. From extensive drilling it is known that the deposit is shallow at the northern end (top of image) and deeper at the south. The profiles in the insert box on the right show the responses along the axis of the deposit, highlighting that the EM amplitude response is strongly affected by the depth of mineralization whereas the AdTau response is much less sensitive to depth.

The image below from the Ferguson Lake deposit (East Zone) shows another example of the benefits of examining time constant over simple EM amplitudes. The upper image is that of early time EM data; two zones are highlighted. Feature A is a large area of response with a few modest isolated highs that are bracketed by two strong linear trends. Feature B is a discrete source with what appears to be a moderately high response. The AdTau image shows Feature A to be strongly conductive and made up of a number of discrete sources. Feature B on the other hand is not particularly conductive compared to other sources in the area.



The assessment of airborne EM data requires both the proper tools and prerequisite understanding of how the tools respond in a variety of situations. For additional information the EM character of a range of deposit styles, contact Condor Consulting at www.condorconsult.com.

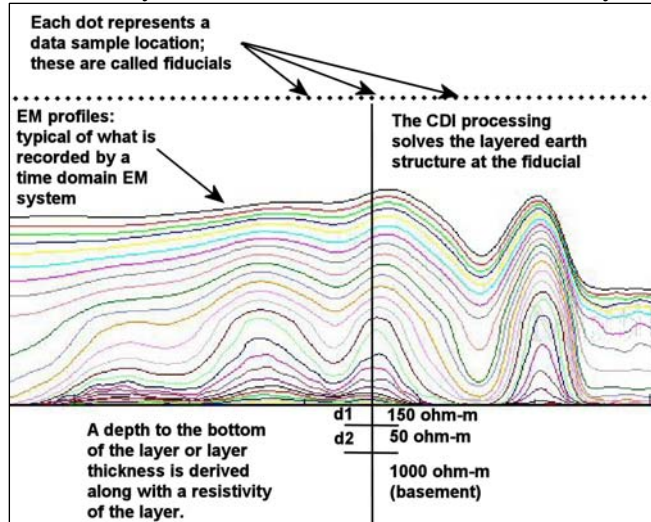
Conductivity Depth Imaging

Introduction



Condor Consulting, Inc.

Conductivity Depth Imaging or CDI of airborne EM (AEM) data is the term applied to the mathematical transformation of the EM response recorded in the measuring instrument of the survey aircraft that is transformed into a conductivity distribution of the earth. The accuracy or resolution of the outcomes of CDI is dependent on a number

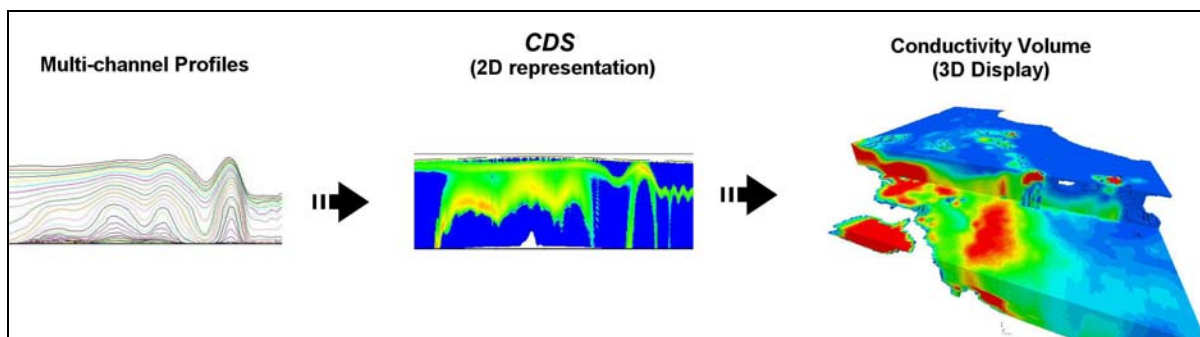


of factors including the type of EM system employed, the quality of the data the system produces, the terrain covered by the system and methodology of the CDI approach. Basically all CDI approaches in commercial use involve what is termed a 1D approximation of the earth. This means that the mathematical model being fit to the data can only capture changes in conductivity vertically in the earth. Displays of CDI outcomes in 2D (sections along lines) and 3D (gridding between lines) all rely on outcomes that are derived from initial 1D processing.

Imaging vs. Inversion: CDI processing can in turn be broken down into two major approaches in the mathematical process involved in solving the sub-surface conductivity structure; this being what is termed either imaging or inversion methodology. Both approaches are in use by survey contractor and consultants and each technique has advantages and draw backs depending on two primary factors; the EM system which acquired the data and the geological problem. Condor uses both approaches but prefers the inversion approach in most applications.

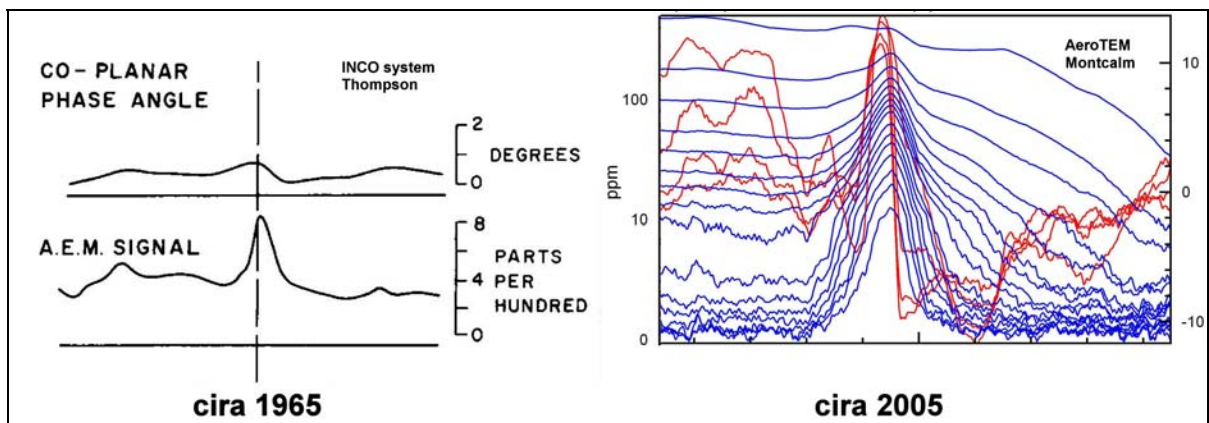
Off-time vs. Bfield: A derived Bfield outcome is now commonly delivered by the major contractors along with the traditional pure off-time data. Condor will routinely process both data streams and then assess which provides the superior outcome for subsequent use specific project assessment. Condor has found this dual processing approach is required as it is very difficult before hand to assess what data stream will provide the best outcome.

In the next several pages, examples of CDI processing will be presented which illustrate the role it can play in modern AEM interpretation. The color section showing a CDI is termed a Conductivity Depth Section or CDS.

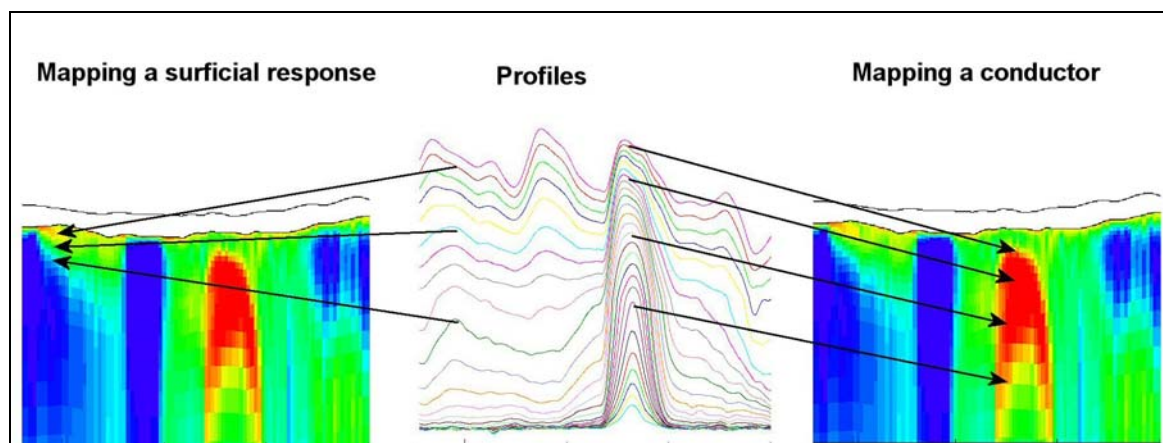


Historically, AEM was used primarily for fairly simple detect of discrete high conductance features which could represent deposits of massive sulfides such as VMS or Ni-Cu. There was little interest in extracting more information other than the X, Y location of the feature and some basic idea of the quality of the conductor. Ground follow-up for location validation and drill hole spotting was always done.

In modern exploration however, there is a far greater range of targets being sought after and in a much wider variety of settings. Even in traditional areas where AEM has been used are now deemed ‘mature’ explorers are expecting that more sophisticated acquisition and processing techniques will be required to make new discoveries.

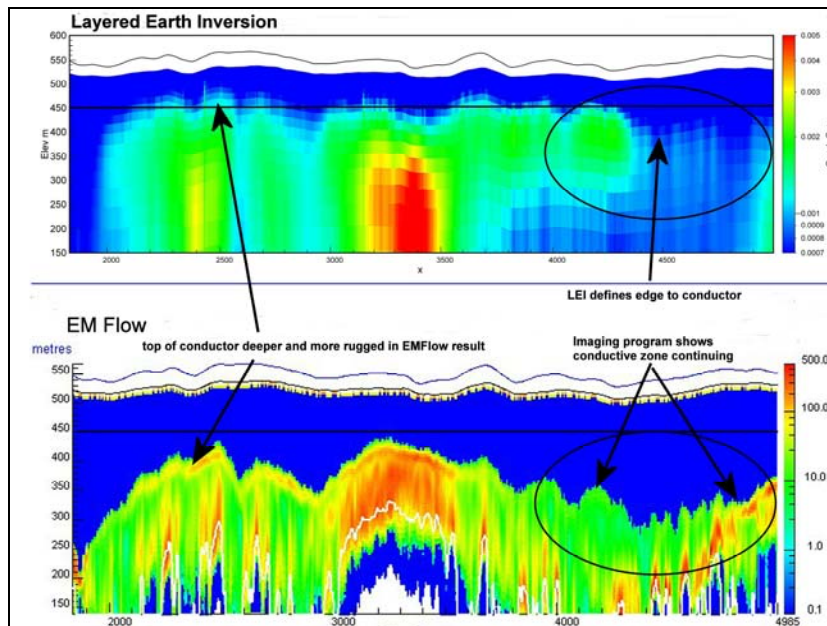


In the CDI process (this applies to either imaging or inversion approaches), those elements of the geology that are dominantly horizontal in nature can be modeled quite well whereas narrow steeply dipping features most often appear with a ‘comet-like’ shape the depth of which does not necessarily correspond all that well to the actual depth within earth. While this may seem like a major draw back to using these outcomes, a combination of experience, local calibration and access to alternate means to model the data allow the seasoned interpreter to define the subsurface geology quite well. The CDI processing at its best is a very useful means to provide a 3D conductivity “context” of the subsurface which can be extremely valuable in helping to recognize and define zones of interest.



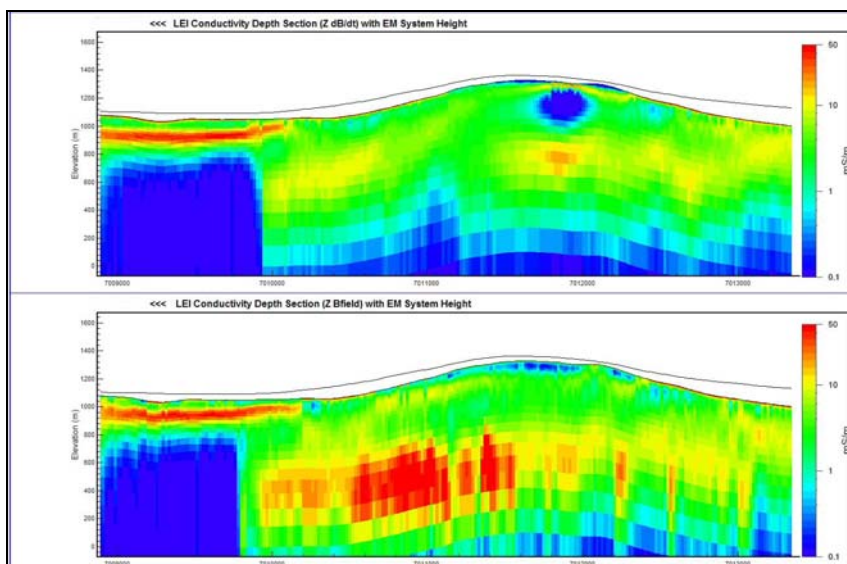
Differences between Imaging and Inversion

The image below shows the outcomes of an inversion program (termed Layered Earth Inversion or LEI) and a imaging program, in this case EMFlow. Three major differences are noted in this example (VTEM survey in the Athabasca Basin); first the depth to the major conductive zone appears deeper in the EMFlow outcome, second the topology of the basement conductor appears to be more rugged in the EMFlow outcome and third, the conductive horizon appears to end in the LEI outcome on the right hand side whereas the EMFlow result shows the zone continuing off the right and side of the image.



Differences between dB/dT and Bfield

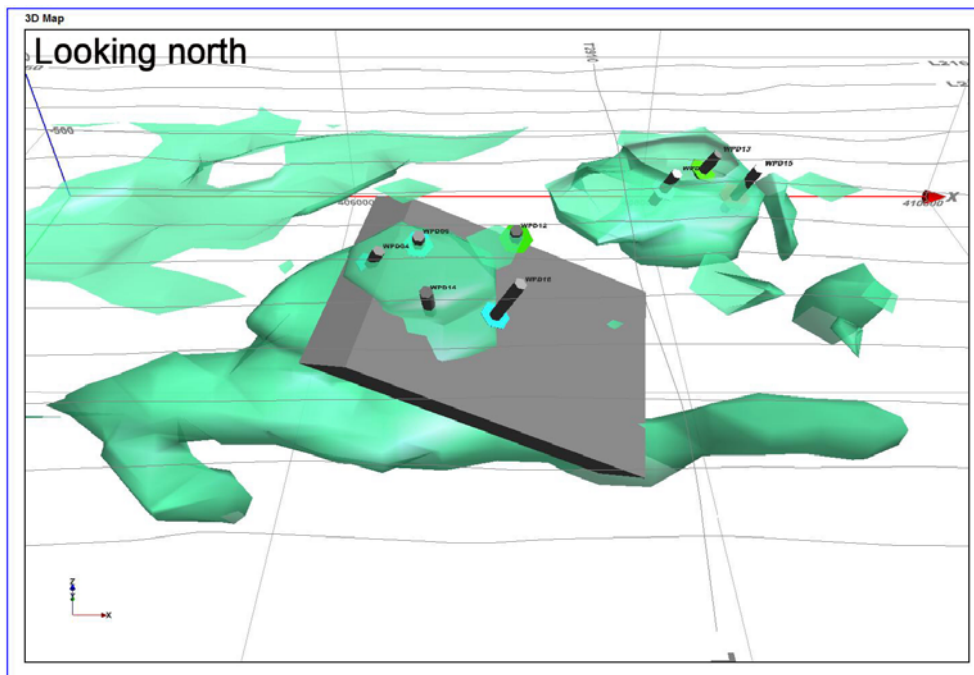
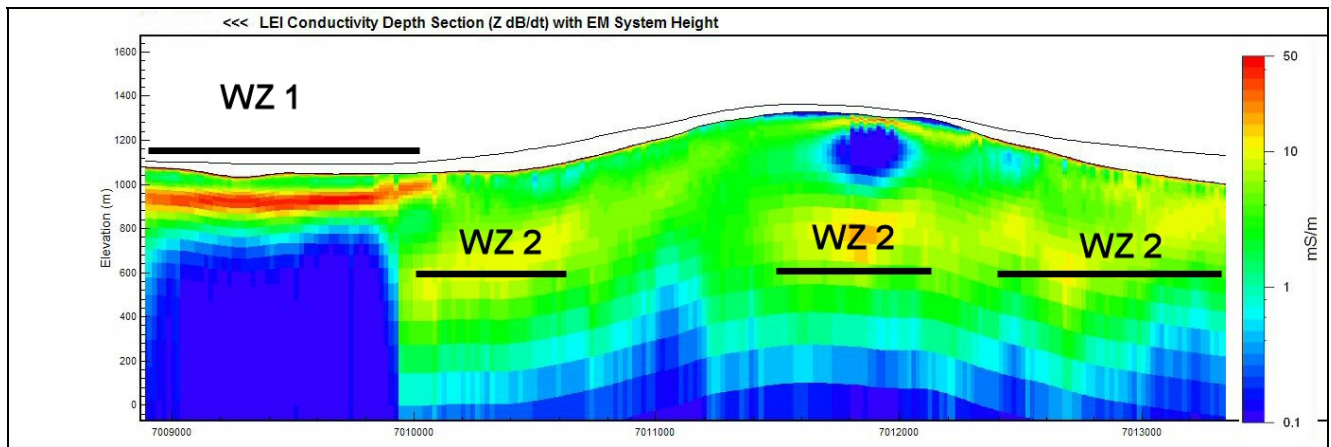
The figure below shows the outcomes of LEI processing to the dB/dT and Bfield outcomes from a VTEM survey undertaken as part of a Ni-Cu search. These results are considered typical in that while the Bfield result shows a nominal greater sensitivity to higher conductance, the results are also somewhat noisier and appear to have slightly less high frequency content than the dB/dT results.



How CDI Helps Interpretation?

A major benefit of having a CDI outcome to interpret is that it conveys a far more geological “feel” to the EM data than profiles along. This is sometimes termed “mapping” with target detection and discrimination a sub-set of this larger interpretive activity.

Using the previous image as an example, the dB/dT CDS has been annotated with what Condor terms Wide Zones. These are zones of broad conductivity in the CDS which are felt to characterize different parts of the geological section. In this case WZ-1 is a thin shallow near surface that could represent lake sediments or a in a weathered terrain, part of a distinctive weather profile over a mafic rock. The WZ-2 features are “in the earth” sources that represent zones of increased conductivity which could represent different rock units or alteration of a specific unit.



Another benefit of the CDI processing is that it in turn allows for the creation of 3D voxel models of the EM outcomes. This is often an excellent means to capture in a holistic sense the sub-surface conductivity distribution either as a stand-alone model or as part of the integrated geoscience model (referred to as a Common Earth Model). An example of such a conductivity model combined with parametric

models of specific anomalies (produced using Maxwell) and drill holes is shown in the figure to the left.

	A	B
1	Depth (M)	Layer
2	5	1
3	11	2
4	17	3
5	25	4
6	34	5
7	44	6
8	55	7
9	68	8
10	83	9
11	101	10
12	120	11
13	143	12
14	169	13
15	199	14
16	234	15
17	273	16
18	319	17
19	371	18
20	431	19
21	500	20
22	580	21
23	673	22
24	783	23
25	909	24
26	1056	25
27	1228	26
28	1426	27
29	1658	28

APPENDIX B: ANOMALY LISTING

MOR

X	Y	Line Number	FID	Line	Type	CID	ADT_BFp0 1TAU_lp	ADT_SFp0 1TAU_lp
661327	6661533	T5945	36827	5945	SPR	C	0.0	0.1
658624	6665066	L4830	9275	4830	SPR	A	0.0	0.0
658319	6665166	L4800	53102	4800	SPR	A	0.0	0.1
661515	6661043	L5100	9751	5100	SPR	A	0.0	0.1
661812	6661058	T5950	21378	5950	SPR	C	0.0	0.0
658915	6665144	L4860	18004	4860	SPR	B	0.0	0.1
661626	6665100	L5130	59780	5130	SPR	B	0.0	0.1
661976	6664049	L5160	50792	5160	DPR	A	0.1	0.1
663286	6663873	L5290	6489	5290	SPR	A	0.1	0.1
662076	6664010	L5170	48489	5170	DPR	A	0.1	0.1
662479	6663916	L5210	34762	5210	DPR	A	0.1	0.1
663186	6663889	L5280	66843	5280	DPR	A	0.1	0.1
662176	6664021	L5180	45066	5180	DPR	A	0.1	0.1
661122	6661028	T5950	21084	5950	SPR	B	0.1	0.1
661878	6664032	L5150	54096	5150	DPR	A	0.1	0.2
662274	6664050	L5190	42833	5190	DPR	A	0.1	0.1
663082	6663870	L5270	65016	5270	DPR	A	0.1	0.1
660929	6661023	T5950	21014	5950	SPR	A	0.1	0.1
662375	6664102	L5200	36953	5200	SPR	A	0.1	0.1
662377	6663998	L5200	36995	5200	DPR	B	0.1	0.1
658522	6665085	L4820	8358	4820	SPR	C	0.1	0.2
662584	6663894	L5220	32256	5220	DPR	A	0.1	0.2
658425	6665082	L4810	53816	4810	SPR	A	0.2	0.2
661566	6664245	L5120	61383	5120	SPR	A	0.2	0.2
662985	6663834	L5260	63021	5260	SPR	A	0.2	0.3
658973	6664143	L4860	17514	4860	SPR	A	0.2	0.3
658554	6664279	L4820	8001	4820	SPR	B	0.2	0.3
661776	6664015	L5140	56182	5140	DPR	A	0.2	0.4
658863	6664096	L4850	14322	4850	SPR	A	0.2	0.3
661676	6663985	L5130	59423	5130	DPR	A	0.2	0.3
658664	6664210	L4830	9548	4830	SPR	B	0.2	0.3
662887	6663832	L5250	61047	5250	SPR	A	0.2	0.3
659066	6664136	L4870	22610	4870	SPR	B	0.3	0.3
661299	6661468	L5080	14490	5080	SPR	C	0.3	0.2
659678	6663979	L4930	36687	4930	SPR	A	0.3	0.3
661728	6664055	T5920	27510	5920	SPR	A	0.4	0.4
659020	6665131	L4870	22274	4870	SPR	A	0.4	0.4
658563	6664159	L4820	7945	4820	SPR	A	0.4	0.5
658473	6664087	L4810	54152	4810	SPR	B	0.4	0.5
662791	6663848	L5240	58856	5240	SPR	A	0.5	0.5
662685	6663841	L5230	16023	5230	SPR	A	0.5	0.5
663867	6664276	L5350	21553	5350	SPR	A	0.6	0.8
661282	6661688	L5080	14406	5080	SPR	B	0.7	0.3
663964	6664263	L5360	23177	5360	SPR	A	0.8	0.9

661211	6661123	L5070	18361	5070	SPR	A	0.8	0.4
658757	6664241	L4840	12719	4840	SPR	A	0.8	0.3
661372	6661895	L5090	11018	5090	SPR	A	1.0	0.6
661009	6661101	L5050	23625	5050	SPR	A	1.6	0.2
660972	6661938	L5050	23926	5050	SPR	D	1.6	0.9
661197	6661470	L5070	18480	5070	SPR	B	1.6	0.9
661169	6661527	T5945	36778	5945	SPR	B	2.0	0.7
661071	6661981	L5060	22211	5060	SPR	A	2.0	0.8
661032	6662020	T5940	23632	5940	SPR	A	2.1	1.3
660983	6661731	L5050	23849	5050	SPR	C	2.2	0.9
661186	6661621	L5070	18543	5070	SPR	C	2.2	0.5
661115	6661087	L5060	22568	5060	SPR	D	2.7	0.3
661278	6661884	L5080	14336	5080	SPR	A	2.8	1.3
661081	6661805	L5060	22281	5060	SPR	B	3.2	1.5
660913	6661109	L5040	27944	5040	SPR	B	4.0	0.4
660993	6661409	L5050	23737	5050	SPR	B	4.0	1.2
661175	6661898	L5070	18648	5070	SPR	D	4.8	3.2
660921	6661513	T5945	36687	5945	SPR	A	5.2	1.4
660899	6661468	L5040	27783	5040	SPR	A	5.3	1.4
661102	6661371	L5060	22456	5060	SPR	C	5.4	2.6

CABIN LAKE

X	Y	Line Number	FID	Type	Line
679715.9	6669339	L8160	1442	SPR	8160
679793.7	6669259	L8170	77	SPR	8170
679791.8	6669144	L8180	1442	SPR	8180
679784.4	6669040	L8190	112	SPR	8190
679800.2	6668939	L8200	1400	SPR	8200
679836.4	6668845	L8210	105	SPR	8210
679939.6	6668784	L8220	1512	SPR	8220
679997.9	6668693	L8230	77	SPR	8230
680091.9	6668619	L8240	1575	SPR	8240
680155.8	6668565	L8250	49	SPR	8250
680202.8	6668452	L8260	1645	SPR	8260
680420.3	6668107	L8300	1575	SPR	8300
680505.1	6668031	L8310	7	SPR	8310
680555.3	6667845	L8330	14	SPR	8330
680601	6667745	L8340	1610	SPR	8340
680629.1	6667667	L8350	14	SPR	8350
679309.1	6669474	T8530	1029	SPR	8530
679574.9	6669391	L8150	189	DPR	8150
679401.2	6669428	L8140	1344	DPR	8140
679263.6	6669480	L8130	287	DPR	8130
679778.3	6669682	L8130	42	DPR	8130
679740.3	6669770	L8120	1225	DPR	8120
679616.9	6669842	L8110	84	DPR	8110
679647.5	6670168	L8080	1050	DPR	8080
679616.5	6670269	L8070	14	DPR	8070
678554.6	6669853	L8070	462	DPR	8070
678248	6669838	L8060	532	DPR	8060
678207.6	6669935	L8050	623	DPR	8050
678233.6	6670051	L8040	560	DPR	8040
678227.9	6670161	L8030	518	DPR	8030
678332.1	6670302	L8020	637	DPR	8020
678250.1	6670379	L8010	539	DPR	8010
678281.1	6670493	L8000	721	DPR	8000

CARIBOU

X	Y	Fid	Type	Line Number
661525.8	6686755	553	SPR	L14000

APPENDIX C: NOTES ON MAGNETIC PROCESSING & EM3D MODELS

3-D inversion of magnetic data

Yaoguo Li* and Douglas W. Oldenburg*

ABSTRACT

We present a method for inverting surface magnetic data to recover 3-D susceptibility models. To allow the maximum flexibility for the model to represent geologically realistic structures, we discretize the 3-D model region into a set of rectangular cells, each having a constant susceptibility. The number of cells is generally far greater than the number of the data available, and thus we solve an underdetermined problem. Solutions are obtained by minimizing a global objective function composed of the model objective function and data misfit. The algorithm can incorporate a priori information into the model objective function by using one or more appropriate weighting functions. The model for inversion can be either susceptibility or its logarithm. If susceptibility is chosen, a positivity constraint is imposed to reduce the nonuniqueness and to maintain physical realizability. Our algorithm assumes that there is no remanent magnetization and that the magnetic data are produced by induced magnetization only. All minimizations are carried out with a subspace approach where only a small number of search vectors is used at each iteration. This obviates the need to solve a large system of equations directly, and hence earth models with many cells can be solved on a deskside workstation. The algorithm is tested on synthetic examples and on a field data set.

INTRODUCTION

Magnetic surveying has been used widely over the years, resulting in a great amount of data with enormous areal coverage. Magnetic data have been used for mapping geological structures, especially in the reconnaissance stage of exploration, but when used in detailed prospecting, robust and efficient inversion algorithms must be used. However, a principal difficulty with the inversion of the potential data is the

inherent nonuniqueness. By Gauss' theorem, if the field distribution is known only on a bounding surface, there are infinitely many equivalent source distributions inside the boundary that can produce the known field. Any magnetic field measured on the surface of the earth can be reproduced by an infinitesimally thin zone of magnetic dipoles beneath the surface. From a mathematical perspective, this means there is no depth resolution inherent in magnetic field data. A second source for nonuniqueness is the fact that magnetic observations are finite in number and are inaccurate. If there exists one model that reproduces the data, there are other models that will reproduce the data to the same degree of accuracy. The severity of the nonuniqueness problem for magnetic data is illustrated in Figures 1-3. (The gray scale in all figures indicates susceptibility in SI units for model sections and magnetic data in nT for data plots.) A 3-D dipping prism of uniform susceptibility in Figure 1 produces the surface magnetic field shown in Figure 2, which consists of 441 data. Slices of a 3-D susceptibility model that adequately reproduces the 441 data are shown in Figure 3. That result, however, bears little resemblance to the true model. Susceptibility is concentrated near the surface and displays zones of negative values. This mathematical model solution provides little information about the true structure that is useful.

Faced with this extreme nonuniqueness, previous authors have mainly taken two approaches in the inversion of magnetic data. The first is parametric inversion, where the parameters of a few geometrically simple bodies are sought in a nonlinear inversion and values are found by solving an overdetermined problem. This methodology is suited for anomalies known to be generated by simple causative bodies, but it requires a great deal of a priori knowledge about the source expressed in the form of an initial parameterization, an initial guess for parameter values, and limits on the susceptibility allowed (e.g., Bhattacharyya, 1980; Zeyen and Pous, 1991). Nonuniqueness is not generally an issue because only a small subset of possible models is considered due to the restrictive nature of the inversion algorithm. A related, but unique, approach in Wang and Hansen (1990) assumes polyhedral causative bodies and

Presented at the 63rd Annual International Meeting, Society of Exploration Geophysicists. Manuscript received by the Editor May 2, 1994; revised manuscript received June 29, 1995.

*UBC-Geophysical Inversion Facility, Dept. of Geophysics and Astronomy, University of British Columbia, 129-2219 Main Mall, Vancouver, BC V6T 1Z4, Canada.

© 1996 Society of Exploration Geophysicists. All rights reserved.

inverts for the position of the vertices of these bodies using the spectrum of the magnetic data. The method is general in principle but has difficulties both in constructing the causative bodies from the recovered vertices and in obtaining the susceptibility distribution.

In the second approach to inverting magnetic data, the earth is divided into a large number of cells of fixed size but of unknown susceptibility. Nonuniqueness of solution is recognized and the algorithm produces a single model by minimizing an objective function of the model subject to fitting the data. Green (1975) minimizes a weighted model norm with respect to a reference model, and this allows the interpreter to guide the inversion by varying the weighting according to the avail-

able information. Last and Kubik (1983) choose to minimize the total volume of the causative body so that the final model is compact and structurally simple. Guillen and Menichetti (1984) minimize the moment of inertia of the causative body with respect to the center of gravity or an axis passing through it. Their inversion result is guided by the estimate of the central depth and dip of the causative body. These approaches have merit but they are not flexible enough to handle problems we are concerned with. This is especially true of methods that attempt to collapse the anomalous susceptibility into a single body; such a solution is rarely an adequate representation of geologic structure.

In our inversion approach, we first make a decision about the variable in which the interpretation is to be made, that is, whether susceptibility, log susceptibility, or some function of susceptibility is sought. Next, we form a multicomponent objective function that has the flexibility to generate different types of models. The form of this objective function is such that it can correct for the undesirable aspects of the mathematically acceptable model in Figure 3, namely-the concentration of susceptibility near the surface, the excessive structure, and the existence of negative susceptibilities. Our objective function incorporates an optional reference model so that the constructed model is close to that. It penalizes roughness in three spatial directions, and it has a depth weighting designed to distribute the susceptibility with depth. Additional 3-D weighting functions in the objective function can be used to incorporate further information about the model. Such information might be available from other geophysical surveys, geological data, or the interpreter's qualitative or quantitative understanding of the geologic structure and its relation to the magnetic susceptibility. These 3-D weighting functions can also be used to answer questions about the existence of susceptibility features found from previous inversions. Negative susceptibilities are prevented by making a transformation of

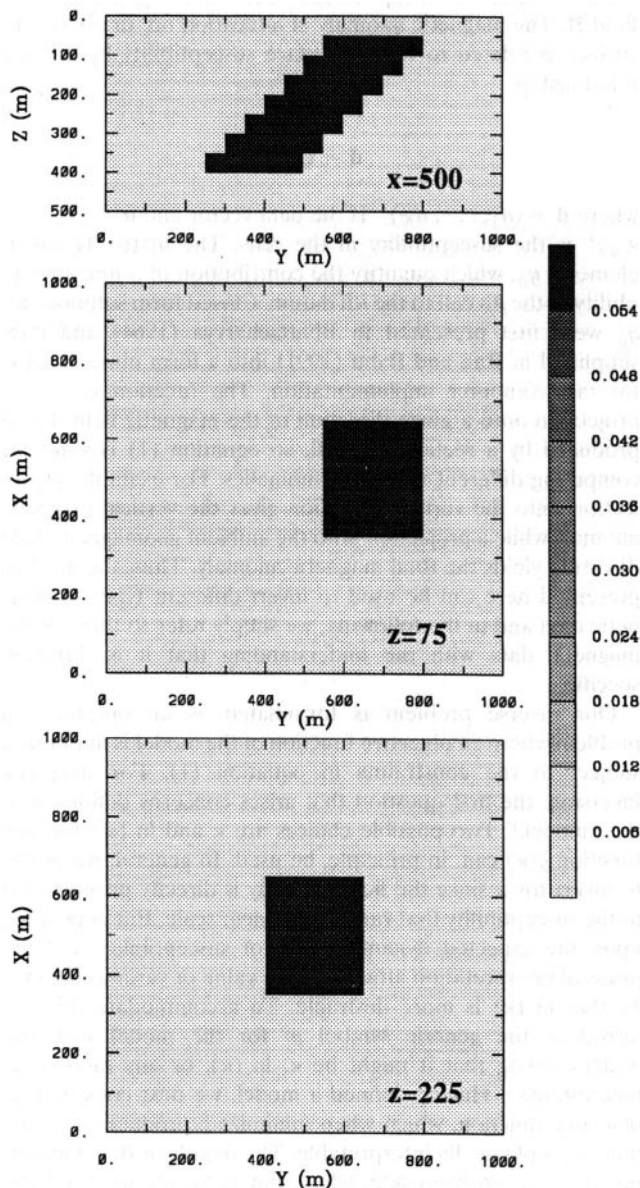


FIG. 1. Slices through a 3-D magnetic susceptibility model composed of a dipping slab in a nonsusceptible half-space. The slab is buried at a depth of 50 m and extends to 400-m depth at a dip angle of 45° . The gray scale indicates the value of magnetic susceptibility in SI units.

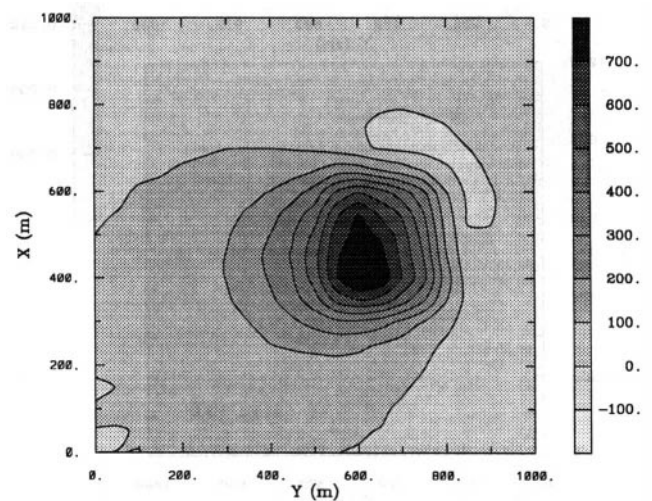


FIG. 2. The total field anomaly produced by the slab model in Figure 1. The inducing field has direction $I = 75^\circ$ and $D = 25^\circ$ and a strength of 50 000 nT. Uncorrelated Gaussian noise, with a standard deviation of 2% of the datum magnitude plus 1 nT, is added to the data. The gray scale indicates the magnetic anomaly in nT.

variables and solving a nonlinear inverse problem. The numerical solution for the inversion is accomplished by dividing the earth into a large number of cells so that relatively complex geologic bodies can be constructed. The computational difficulties often encountered in solving large matrix systems are avoided by working explicitly with a generalized subspace algorithm.

The paper begins by outlining our inversion methodology and empirically estimating parameters for the depth weighting based upon synthetic inversion of single 3-D prisms. Data from two synthetic models are then inverted. The paper concludes

by inverting a field data set over a copper-gold porphyry deposit and a subsequent discussion.

INVERSION METHODOLOGY

Each magnetic anomaly datum observed above the surface can be evaluated by calculating the projection of the anomalous magnetic field onto a given direction. Let the source region be divided into a set of rectangular cells by an orthogonal 3-D mesh and assume a constant magnetic susceptibility value κ within each cell. Further we assume that there is no remanent magnetization and that the demagnetization effect is negligible. Thus only the induced magnetization is considered. This magnetization is uniform within each cell and is given by the product of the susceptibility and the inducing geomagnetic field \mathbf{H} . The magnetic anomaly at a location on, or above, the surface is related to the subsurface susceptibility by a linear relationship

$$\mathbf{d} = \mathbf{G}\boldsymbol{\kappa}, \quad (1)$$

where $\mathbf{d} = (d_1, \dots, d_N)^T$ is the data vector and $\boldsymbol{\kappa} = (\kappa_1, \dots, \kappa_M)^T$ is the susceptibility in the cells. The matrix \mathbf{G} has as elements g_{ij} , which quantify the contribution of a unit susceptibility in the j th cell to the i th datum. Closed form solutions for g_{ij} were first presented in Bhattacharyya (1964) and later simplified in Rao and Babu (1991) into a form more suitable for fast computer implementation. The function g_{ij} is the projection onto a given direction of the magnetic field that is produced by a rectangular cell, so equation (1) is valid for computing different magnetic anomalies. For example, a projection onto the vertical direction gives the vertical magnetic anomaly while a projection onto the ambient geomagnetic field direction yields the total magnetic anomaly. Thus, the method presented here can be used to invert different types of magnetic data and in the following, we simply refer to them as the magnetic data with the understanding that it is direction specific.

Our inverse problem is formulated as an optimization problem where an objective function of the model is minimized subject to the constraints in equation (1). For magnetic inversion, the first question that arises concerns definition of the "model." Two possible choices are κ and $\ln(\kappa)$, but any function $g(\kappa)$ can, in principle, be used. In general, we prefer to invert for κ since the field anomaly is directly proportional to the susceptibility that varies on a linear scale. But depending upon the expected dynamic range of susceptibility and the physical interpretation attached to its value or variation, it may be that $\ln(\kappa)$ is more desirable. To accommodate this, we introduce the generic symbol m for the model with the understanding that it might be κ , $\ln(\kappa)$, or any monotonic function $g(\kappa)$. Having defined a model, we next construct an objective function, which when minimized, produces a model that is geophysically interpretable. The details of the objective function are problem dependent, but generally we need the flexibility to be close to a reference model m_0 and also require that the model be relatively smooth in three spatial directions. Here we adopt a right-handed Cartesian coordinate system with x positive north and z positive down. Let the model objective function be

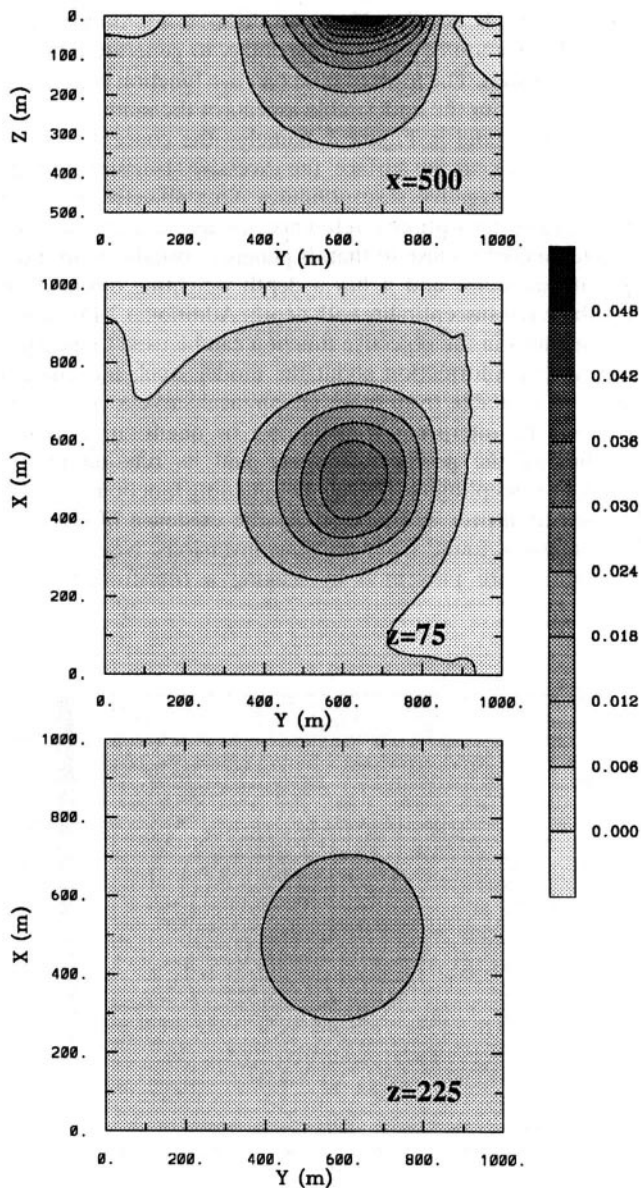


FIG. 3. The susceptibility model constructed by minimizing $\|\boldsymbol{\kappa}\|^2$ subject to fitting the data in Figure 2. As a mathematical solution, this model provides little, if any, information about the subsurface susceptibility distribution. It effectively illustrates the nonuniqueness inherent to the inversion of static magnetic field data.

$$\begin{aligned}
\phi_m(m) = & \alpha_s \int_V w_s \{w(z)[m(\mathbf{r}) - m_0]\}^2 dv \\
& + \alpha_x \int_V w_x \left\{ \frac{\partial w(z)[m(\mathbf{r}) - m_0]}{\partial x} \right\}^2 dv \\
& + \alpha_y \int_V w_y \left\{ \frac{\partial w(z)[m(\mathbf{r}) - m_0]}{\partial y} \right\}^2 dv \\
& + \alpha_z \int_V w_z \left\{ \frac{\partial w(z)[m(\mathbf{r}) - m_0]}{\partial z} \right\}^2 dv, \quad (2)
\end{aligned}$$

where functions w_s , w_x , w_y , and w_z are spatially dependent weighting functions while α_s , α_x , α_y , and α_z are coefficients that affect the relative importance of different components in the objective function. Here, $w(z)$ is a depth weighting function. It is convenient to write equation (2) as $\phi_m(m) = \phi_{ms} + \phi_{mv}$, where ϕ_{ms} refers to the first term in equation (2) and ϕ_{mv} refers collectively to the remaining three terms that involve variation of the model in three spatial directions.

The objective function in equation (2) has the flexibility of constructing many different models. The reference model m_0 may be a general background model that is estimated from previous investigations, or it could be the zero model. The reference model would generally be included in ϕ_{ms} but can be removed if desired from any of the remaining terms. Often we are more confident in specifying the value of the model at a particular point than in supplying an estimate of the gradient. The relative closeness of the final model to the reference model at any location is controlled by the function w . For example, if the interpreter has high confidence in the reference model at a particular region, he or she can specify w_s to have increased amplitude there compared to other regions of the

extra information is incorporated, the inversion derives a model that not only fits the data, but more importantly, also has a likelihood of representing the earth. From the viewpoint of magnetic inversion, such an approach allows one to construct a most-likely earth model that uses all available information, and it can also be used to explore the nonuniqueness. These two aspects form the foundation of a responsible interpretation.

The kernels (values of g_{ij}) for the surface magnetic data decay with depth. It is for this reason that an inversion that minimizes $\|m - m_0\|^2 = \int (m - m_0)^2 dv$ subject to fitting the data will generate a susceptibility that is concentrated near the surface. To counteract the geometric decay of the kernels and to distribute susceptibility with depth, we introduce a weighting of the form $w(z) = (z + z_0)^{-\beta/2}$ into ϕ_{ms} , and optionally include it in ϕ_{mv} . The values of β and z_0 are investigated in the following section, but their choice essentially allows equal chance for cells at different depths to be nonzero.

The next step in setting up the inversion is to define a misfit measure. Here we use the 2-norm measure

$$\phi_d = \|\mathbf{W}_d(\mathbf{d} - \mathbf{d}^{obs})\|_2^2, \quad (3)$$

and we assume that the contaminating noise on the data is independent and Gaussian with zero mean. Specifying \mathbf{W}_d to be a diagonal matrix whose i th element is $1/\sigma_i$ where σ_i is the standard deviation of the i th datum, makes ϕ_d a chi-squared variable distributed with N degrees of freedom. Accordingly $E[\chi^2] = N$ provides a target misfit for the inversion.

The inverse problem is solved by finding a model m that minimizes ϕ_m and misfits the data by a predetermined amount. This is accomplished by minimizing $\phi(m) = \phi_m + \lambda^{-1}(\phi_d - \phi_d^*)$, where ϕ_d^* is our target misfit and λ is a Lagrangian multiplier. To perform a numerical solution, we first discretize the objective function in equation (2) using a finite-difference approximation according to the mesh defining the susceptibility model. This yields

$$\begin{aligned}
\phi_m(\mathbf{m}) = & \phi_{ms} + \phi_{mv} = (\mathbf{m} - \mathbf{m}_0)^T \mathbf{W}_s^T \mathbf{W}_s (\mathbf{m} - \mathbf{m}_0) + (\mathbf{m} - \mathbf{m}_0)^T (\mathbf{W}_x^T \mathbf{W}_x + \mathbf{W}_y^T \mathbf{W}_y + \mathbf{W}_z^T \mathbf{W}_z) (\mathbf{m} - \mathbf{m}_0) \\
\equiv & (\mathbf{m} - \mathbf{m}_0)^T \mathbf{W}_m^T \mathbf{W}_m (\mathbf{m} - \mathbf{m}_0) = \|\mathbf{W}_m (\mathbf{m} - \mathbf{m}_0)\|_2^2, \quad (4)
\end{aligned}$$

model. The weighting functions w_s , w_x , w_y , and w_z can be designed to enhance or attenuate structures in various regions in the model domain. If geology suggests a rapid transition zone in the model, then a decreased penalty for variation can be put there, and the constructed model will exhibit higher gradients provided that this feature does not contradict the data. Therefore, the reference model and four 3-D weighting functions allow for the incorporation into the inversion of additional information other than the magnetic data. The additional information can be from previous knowledge about the susceptibility, from other geophysical surveys, or from the interpreter's qualitative or quantitative understanding about the geologic structure and its relation to susceptibility. When this

where \mathbf{m} and \mathbf{m}_0 are M -length vectors. The individual matrices \mathbf{W}_s , \mathbf{W}_x , \mathbf{W}_y , \mathbf{W}_z are calculated straightforwardly once the model mesh and the weighting functions w_s , w_x , w_y , w_z , and $w(z)$ are defined (see Appendix). The cumulative matrix $\mathbf{W}_m^T \mathbf{W}_m$ is then formed. For our formulation, the matrix \mathbf{W}_m is never computed explicitly but we shall use it to derive our final equations.

The inverse problem is solved by minimizing $\phi(\mathbf{m})$ with an appropriate minimization technique. To reduce computation and to invoke positivity, we use a subspace methodology. In its general form, the subspace technique allows the model parameter to be both positive and negative, and thus to ensure positive susceptibility, we may need to invoke a transformation

of variables. Whether or not the transformation is required depends upon the relationship between m_i and κ_i . If $m_i = \ln(\kappa_i)$, so that interpretations are carried out in the logarithmic domain, then no further transformation is necessary since κ_i will be positive irrespective of the sign of m_i . However, if $m_i = \kappa_i$, or $m_i = g(\kappa_i)$, and $g(\kappa)$ is a positive function, then a transformation is required. All possibilities can be handled by introducing a new parameter p , such that $m_i = f(p_i)$, where $f(p)$ is a monotonic function whose inverse and first-order derivative exist. This mapping is then incorporated directly into the subspace minimization process.

Let $\mathbf{p}^{(n)}$ denote the parameter vector at the n th iteration and $\delta\mathbf{p}$ denote the sought perturbation. Performing a Taylor expansion of the perturbed model objective function about the point $\mathbf{p}^{(n)}$ yields

$$\phi_m(\mathbf{p}^{(n)} + \delta\mathbf{p}) = \|\mathbf{W}_m \mathbf{F} \delta\mathbf{p} + \mathbf{W}_m(\mathbf{m}^{(n)} - \mathbf{m}_0)\|^2, \quad (5)$$

where \mathbf{F} is a diagonal matrix with elements

$$F_{ii} = \left. \frac{\partial f_i}{\partial p} \right|_{p=p^{(n)}} = \left. \frac{\partial m_i}{\partial p} \right|_{p=p^{(n)}}. \quad (6)$$

A similar Taylor expansion applied to the misfit objective functional $\phi_d(\mathbf{p}^{(n)} + \delta\mathbf{p})$ yields

$$\phi_d = \|\mathbf{W}_d \mathbf{G} \mathbf{F} \delta\mathbf{p} + \mathbf{W}_d(\mathbf{d}(\mathbf{p}^{(n)}) - \mathbf{d}^{obs})\|^2. \quad (7)$$

At each iteration we desire a perturbation that minimizes equation (4) subject to generating a data misfit of $\phi_d = \phi_d^{*(n)}$, where $\phi_d^{*(n)}$ is the target misfit at the n th iteration. In the subspace technique we represent the perturbation as

$$\delta\mathbf{p} = \sum_{i=1}^q \alpha_i \mathbf{v}_i \equiv \mathbf{V} \boldsymbol{\alpha}, \quad (8)$$

where the M -length vectors \mathbf{v}_i ($i = 1, q$) are as yet arbitrary. Writing the objective function to be minimized in terms of the coefficients $\boldsymbol{\alpha}$ yields

$$\begin{aligned} \phi(\boldsymbol{\alpha}) = & \|\mathbf{W}_m \mathbf{F} \mathbf{V} \boldsymbol{\alpha} + \mathbf{W}_m(\mathbf{m}^{(n)} - \mathbf{m}_0)\|^2 \\ & + \lambda^{-1} (\|\mathbf{W}_d \mathbf{G} \mathbf{F} \mathbf{V} \boldsymbol{\alpha} + \mathbf{W}_d(\mathbf{d}(\mathbf{p}^{(n)}) - \mathbf{d}^{obs})\|^2 - \phi_d^*). \end{aligned} \quad (9)$$

Differentiating with respect to the coefficients $\boldsymbol{\alpha}$ yields the final equations

$$\mathbf{B} \boldsymbol{\alpha} = \mathbf{b},$$

$$\mathbf{B} = \mathbf{V}^T \mathbf{F}^T (\mathbf{G}^T \mathbf{W}_d^T \mathbf{W}_d \mathbf{G} + \lambda \mathbf{W}_m^T \mathbf{W}_m) \mathbf{F} \mathbf{V},$$

$$\begin{aligned} \mathbf{b} = & -\mathbf{V}^T \mathbf{F}^T \mathbf{G}^T \mathbf{W}_d^T \mathbf{W}_d (\mathbf{d}^{(n)} - \mathbf{d}^{obs}) \\ & - \lambda \mathbf{V}^T \mathbf{F}^T \mathbf{W}_m^T \mathbf{W}_m (\mathbf{m}^{(n)} - \mathbf{m}_0). \end{aligned} \quad (10)$$

We note that the matrix \mathbf{B} is $q \times q$ and therefore the system of equations is easily solved if q is small. At each iteration, we search for a value of λ that yields the target misfit for that iteration. If the target misfit cannot be reached, then the value

of λ that achieves the smallest misfit is taken. The search is usually accomplished by solving equation (10) a number of times using different λ values. Once the optimum value of λ is found, the system is solved again to obtain the coefficients $\boldsymbol{\alpha}$ and the model perturbation. This iterative process is continued until the final expected data misfit is achieved and the model objective function undergoes no significant decrease with successive iterations. Subspace vectors \mathbf{v}_i are generated mainly from the gradients of the data and model objective functions. The data are grouped to form subobjective functions of misfit, and a steepest descent vector corresponding to each subobjective function is used as a subspace vector. Partitioning of the data can be formed by grouping data that are spatially close, or by grouping data such that each group has approximately the same contribution to the total data misfit. Both approaches have worked well. The model objective function is partitioned and the gradient vector associated with each of the four components in the model objective function provides additional subspace vectors. In addition, a constant vector is always included, and the selected subspace vectors are orthonormalized before being used in the search. More details on the implementation of the subspace method for the linear inverse problem can be found in Oldenburg and Li (1994).

The final item of practical importance is the specification of the mapping needed to ensure positivity of susceptibility. The positivity is required since we are dealing only with induced magnetization, and the presence of negative susceptibility is negligible in practical geophysical applications. Although our formalism permits the minimization of $m = g(\kappa)$, the two most common situations are $m = \ln(\kappa)$ and $m = \kappa$. When $m = \ln(\kappa)$, we set $p = m$ and hence the matrix \mathbf{F} in equation (10) is the identity matrix. If $m = \kappa$, we use the two-stage mapping proposed in Oldenburg and Li (1994). It is composed of an exponential segment and a straight line. The two segments are joined together such that the mapping and its first derivative are both continuous. The mapping is given by

$$\kappa = \begin{cases} 0 & p < p_b \\ e^p - \kappa_b & p_b \leq p \leq p_1 \\ (p - p_1 + 1)e^{p_1} - \kappa_b & p > p_1 \end{cases}, \quad (11)$$

where $p = p_1$ is the transition point between exponential and linear segments, and κ_b is selected to be small enough such that susceptibilities smaller than κ_b are not significantly different from zero when the final interpretation is carried out. Here, κ_1 and hence p_1 are chosen so that the ratio $(\kappa_1 + \kappa_b)/\kappa_b$ does not exceed about two orders of magnitude. This prevents the elements F_{ii} from becoming too disparate. We note that the i th row of \mathbf{V} is multiplied by F_{ii} , and if this value is too small, the i th row of \mathbf{V} is essentially annihilated and there will be no possibility of adjusting the value of the i th cell. However, if the ratio is too small, the flexibility in the mapping will be restricted and this affects the convergence rate of the algorithm. In the limit that $\kappa_b \rightarrow \kappa_1$, the nonlinear mapping degenerates into a linear truncation and the inversion will not converge. However, between the above two extremes, there is a wide range of values for the ratio that can yield a good mapping. Based upon numerical experiments (Oldenburg and Li, 1994), we have chosen a value of 50.0 for this ratio for the examples throughout this paper.

DEPTH WEIGHTING

It is well known that static magnetic data have no inherent depth resolution. For instance, when minimizing $\|m\|_2^2 = \int m^2 dv$, structures tend to concentrate near the surface regardless of the true depth of the causative bodies. In terms of model construction, this is a direct manifestation of the nature of the kernels whose amplitudes rapidly diminish with depth. The tendency to put structure at the surface can be overcome by introducing a depth weighting to counteract this natural decay. Intuitively, a weighting that approximately compensates for the decay gives cells at different depths equal probability to enter into the solution with a nonzero susceptibility. Before proceeding with the details of the weighting function for magnetic inversion, we illustrate the necessity, and effectiveness, of such a weighting function using a simple 1-D problem.

Consider a set of data $\mathbf{d} = (d_1, \dots, d_N)^T$ generated from the equation

$$d_i = \int_0^1 g_i(z)m(z) dz, \quad i = 0, \dots, N, \quad (12)$$

where the kernels are

$$g_i(z) = e^{-az} \cos(2\pi iz).$$

The decay factor e^{-az} causes the constructed model $m_c(z)$ to have structure concentrating toward the region of small z in the classic model construction that minimizes $\|m\|_2^2$, since the model will be a linear combination of the kernels, i.e.,

$$m_c(z) = \sum_{i=0}^N \alpha_i e^{-az} \cos(2\pi iz). \quad (13)$$

This is shown in Figure 4a and 4b for two different models. These models are constructed from five data ($i = 0, 4$) to which noise has been added. It is apparent that the constructed model is shifted toward small z where the amplitude of kernels is relatively large. One way to counteract the bias is to seek a solution in model space that is spanned by the nondecaying portion of the kernels, in this case just the cosine functions. The desired model would have the form

$$m_c(z) = \sum_{i=0}^N \tilde{\alpha}_i \cos(2\pi iz), \quad (14)$$

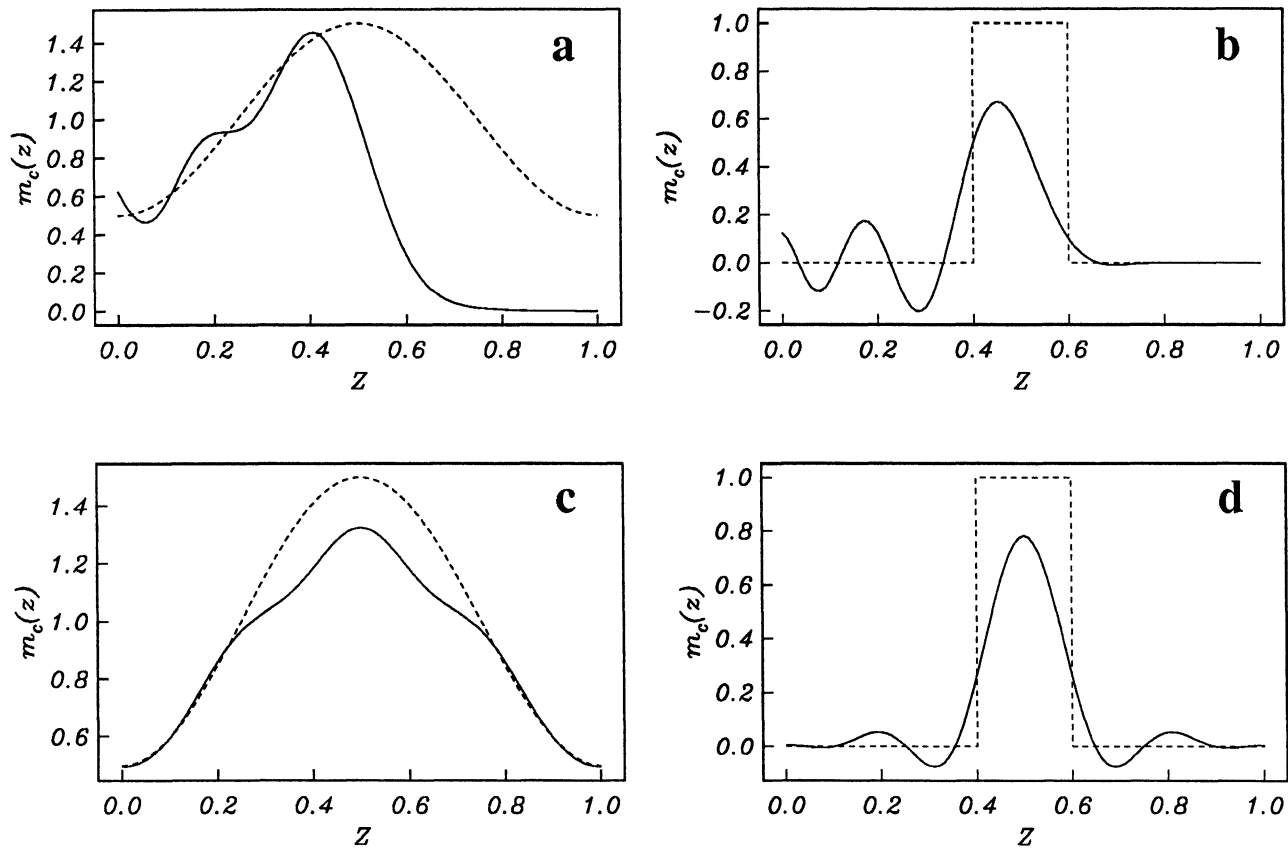


FIG. 4. A 1-D example showing the use of a weighting function in the inversion procedures to counteract the natural decay in the kernel function. In all panels the dashed line shows the true model. Panels (a) and (b) show, for the two different true models, respectively, the model constructed using the original kernel functions with the decaying factor e^{-az} . Notice the shift of the recovered model towards the small z region. Panels (c) and (d) show the weighted models recovered by applying a weighting function $w(z) = e^{-az/2}$. They are better representations of the true model.

where $\tilde{\alpha}_i$ are coefficients. Free from the influence from the decay factor, a model constructed from this set of basic functions should have a better chance of having significantly high values at depth.

We accomplish this by finding an appropriate weighting function $w(z)$. We first rewrite the data equation as

$$d_i = \int_0^1 \frac{g_i(z)}{w(z)} w(z) m(z) dv \equiv \int_0^1 g_i^w(z) m^w(z) dv, \quad (15)$$

where $g_i^w(z)$ are the weighted kernels and $m^w(z)$ is the weighted model. Then the inverse problem is solved by minimizing $\|m^w(z)\|^2$ and the solution is given by

$$m_c^w(z) = \sum_{i=0}^N \tilde{\alpha}_i g_i^w(z). \quad (16)$$

Dividing $m_c^w(z)$ by the weighting function and substituting in $g_i^w(z)$ yields

$$m_c(z) = \sum_{i=0}^N \tilde{\alpha}_i \frac{g_i(z)}{w^2(z)} = \sum_{i=0}^N \tilde{\alpha}_i \frac{e^{-az} \cos(2\pi iz)}{w^2(z)}. \quad (17)$$

This equation can be made identical to equation (14) by choosing $w(z) = e^{-az/2}$. Carrying out the weighted inversion for the above two data sets produces models shown in Figures 4c and 4d. They are much better representations of true models.

This methodology is then applied to the inversion of surface magnetic data by finding the appropriate weighting function that counteracts the depth decay of the data kernels. There is no distinct separable factor defining the decay in the kernel, therefore we resort to an empirical estimate. Since the decay rate depends upon the observation height as well as the size and aspect ratios of the cells making up the 3-D model, such estimates are expected to be problem dependent. Numerical experiments indicate that the function of the form $(z + z_0)^{-3}$ closely approximates the kernel's decay directly under the observation point, given a correctly chosen value of z_0 . This is consistent with the fact that, to first order, a cubic-shaped cell acts like a dipole source whose magnetic field decays by inverse distance cubed. The value of z_0 can be obtained by matching the function $(z + z_0)^{-3}$ with the kernel function beneath the observation point. Thus, a reasonable candidate for the depth weighting function is given by

$$w(z) = \frac{1}{(z + z_0)^{3/2}}. \quad (18)$$

The susceptibility model constructed by minimizing a model objective function consisting of only ϕ_{ms} , i.e.,

$$\phi_m(m) = \int_V (w(z)m(x, y, z))^2 dv, \quad (19)$$

subject to fitting the data should place the recovered anomaly at approximately the depth of the causative body. This hypothesis is tested by inverting surface data produced by a susceptible cubic body at three different depths. The cube is 200 m on a side. Data are calculated over a 21 X 21 grid of 50-m spacing

in both directions, and 2% Gaussian noise is then added. The observation is assumed to be 1 m above the surface and the inducing field has $I = 75^\circ$, $D = 25^\circ$. The region directly beneath the data grid is taken as the model domain and discretized into 4000 cells (20 cells in each horizontal direction and 10 along depth) of 50 m on a side.

Given the stated data parameters and model discretization, the estimated value of z_0 in the depth weighting function is 25 m. Figure 5 shows the comparison of the kernel beneath a datum point and the function $w^2(z)$. This weighting function is used to invert surface data caused by the susceptible prism, and the results of minimizing ϕ_{ms} are shown in Figure 6. Each panel in the figure is the cross-section through the center of the model obtained by inverting the data set produced by a cube at a different depth. They are rather good recoveries in terms of source depth, which is indicated by the superimposed outline of the true body in each section.

In the above analysis we have established a practical way for estimating an appropriate depth weighting function that distributes the susceptibility more uniformly with depth. The weighting is valid when the model objective function consists only of ϕ_{ms} . In general, we like to include a penalty against roughness and thereby produce a model that is smooth. To incorporate the above weighting scheme in the spatial variations, we make the following argument. Since minimizing ϕ_{ms} tends to provide a reasonable depth distribution, we wish only to improve the model's smoothness while maintaining the depth characteristic. A conceptually consistent approach would be to apply the roughness measures to the weighted model. We form a generic model objective function

$$\begin{aligned} \phi_m(m) = & \alpha_s \int_V w_s \{w(z)[m(\mathbf{r}) - m_0]\}^2 dv \\ & + \alpha_x \int_V w_x \left\{ \frac{\partial w(z)[m(\mathbf{r}) - m_0]}{\partial x} \right\}^2 dv \\ & + \alpha_y \int_V w_y \left\{ \frac{\partial w(z)[m(\mathbf{r}) - m_0]}{\partial y} \right\}^2 dv \end{aligned}$$

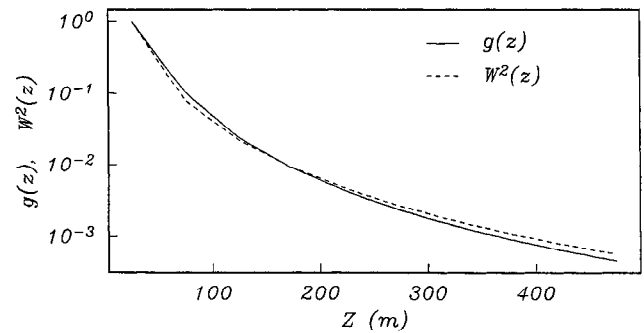


FIG. 5. Comparison of the kernel function (solid) directly beneath the observation point with the estimated curve (dashed) given by $w^2(z) = (z + z_0)^{-3}$ with $z_0 = 25$ m. The source cell is a cube of 50 m on a side. Here, z denotes the depth to the center of the cell. Both curves are normalized for comparison.

$$+ \alpha_z \int_V w_z \left\{ \frac{\partial w(z)[m(\mathbf{r}) - m_0]}{\partial z} \right\}^2 dv, \quad (20)$$

where the depth weighting is applied inside the derivatives of the roughness components and the reference model m_0 can be removed from any term if desired. This type of depth weighting has proven to work satisfactorily on a number of synthetic examples and is the default choice in our algorithm. The examples to be presented in the following sections all use this depth weighting function.

Before proceeding further, we remark that the above weighting represents only one possibility. One could potentially design a different weighting by incorporating the depth weighting in the usual 3-D weighting functions w_x, w_y, w_z . Such an approach applies the depth weighting outside the derivative operators directly. However, the decay rate of the depth weighting for each component will be different, and it is difficult to establish a consistent rule for the choice of the different weightings. In addition, the extra set of parameters required by such a weighting scheme introduces more subjectivity into the inversion process. We have not explored this approach in detail; however,

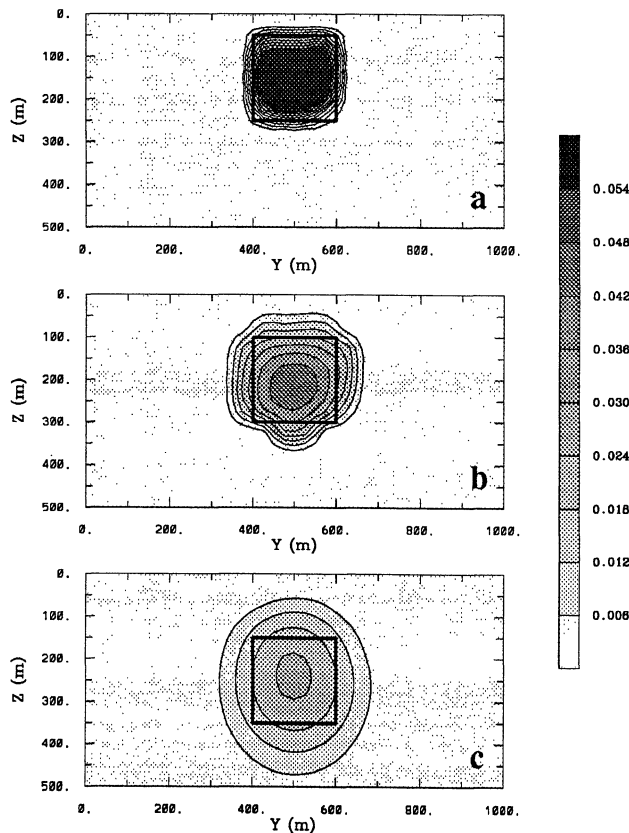


FIG. 6. Cross-sections through the center of the recovered model for a cube at a central depth of 150, 200, and 250 m. The cube is 200 m on a side. The inversion uses the weighting function derived from the kernel decay estimated in Figure 5. The true position of the cube is outlined in each cross-section. As the true source depth increases and, as a result, the high-frequency content in the data decreases, the recovered model becomes increasingly smooth and attains a smaller amplitude. However, the depth of the recovered model is close to the true value.

it is observed that straightforward inclusion of the depth weighting derived above into the 3-D weighting function in the form of $\int_V w_z w^2(z) \{ \partial[m(\mathbf{r}) - m_0] / \partial z \}^2 dv$ can yield reasonable results.

PRACTICAL ASPECTS OF DATA PREPARATION

The data used in the inversion are the residual data obtained by subtracting a regional field from the initial observation. The inversion algorithm has been developed under the assumptions that the surface magnetic anomaly is produced by the induced magnetization only and that there are no remanent magnetization or demagnetization effects present. Incorrect removal of regional field, or any deviation from the above assumptions, is expected to cause a deterioration in the inversion results. Furthermore, the susceptibility distribution is mathematically represented by a piece-wise constant function defined on a user-specified grid of cells. Magnetic sources, however, have a wide range of physical sizes. In some cases, source dimensions will be significantly smaller than the size of cells in the mathematical model. If measurements are taken close to such a source, the resulting anomaly will have a width that is significantly smaller than that produced by a single cell in the mathematical model and this may produce artifacts. We ameliorate this problem by inverting data that have been upward continued to a height approximately equal to the width of the surface cells in the model. We arrive at this conclusion from a numerical experiment. We first generate the magnetic field H_ℓ from a small localized surface source that is assumed to be a cube of width ℓ . At each height h above the surface, a one-parameter inverse problem is carried out to find a uniform susceptibility of a large surface cube that has a width of L and shares a common horizontal center with the small cube. If H_L is the field of the large cell that best reproduces H_ℓ then the misfit functional,

$$r(h) = \frac{\int_{\Delta S} (H_\ell - H_L)^2 ds}{\int_{\Delta S} H_\ell^2 ds}, \quad (21)$$

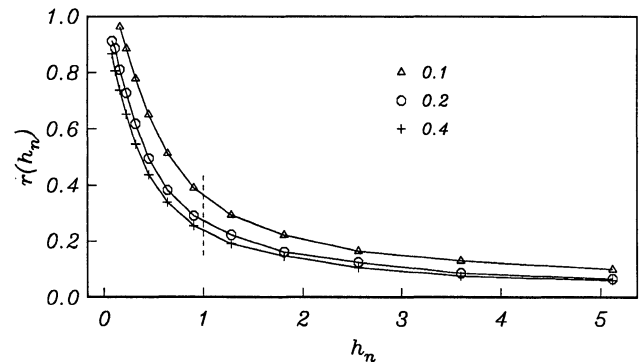


FIG. 7. The misfit between magnetic field as a result of a small cubic source and the field as a result of a larger cubic model cell having a best fitting susceptibility. The numbers indicate the ratio of the cell width. The misfit is plotted as a function of the observation height normalized by the width of the model cell. Note that the misfit decreases rapidly until the height is approximately equal to the width of the model cell, and that it changes slowly thereafter.

can be computed, where ΔS is the surface area of the data map. Figure 7 shows the misfit function $r(h)$ for trial values of $\ell/L = 0.1, 0.2, 0.4$. We note that $r(h)$ decreases rapidly until $h \approx L$, and that it changes slowly thereafter. Since the above misfit analysis is a worst case scenario because the contaminating body is located at the surface, the suggestion of upward continuing the data to a height approximately equal to the width of surface cells may be somewhat conservative, and inversionists may want to vary this. However, in many field surveys, magnetically susceptible small bodies exist close to the surface and hence upward continuing the data prior to inversion is prudent.

SYNTHETIC EXAMPLES

As the first example, we invert the total field anomaly data given in the Introduction. The model consists of a 3-D dipping slab buried in a nonsusceptible half-space (slab model). Figure 1 shows three slices through the slab model. The susceptibility of the slab is 0.06 (SI unit). Under an inducing field with a strength of 50 000 nT and a direction at $I = 75^\circ$ and $D = 25^\circ$, the slab model produces the surface total magnetic anomaly shown in Figure 2, which consists of 441 data over a 21×21 grid of 50-m spacing. The data have independent Gaussian noise added whose standard deviation is equal to 2% of the accurate datum magnitude plus 1 nT. We invert these 441 noise-contaminated data to recover the susceptibility of an earth model parametrized by 4000 cells of 50 m on a side (20 cells in each horizontal direction and 10 in depth).

The data are partitioned into 49 groups to provide 49 search vectors for the subspace algorithm. In addition, each component in the model objective function provides one basis vector, and a constant vector is included. For the depth weighting, the value of z_0 is estimated as 25 m. The additional 3-D weightings in the objective function are all set to unity. The reference susceptibility model is set to zero. For the nonlinear mapping, we choose $\kappa_b = 0.0002$ and $\kappa_1 = 0.01$.

First, we invert the data by minimizing an objective function composed only of the ϕ_{ms} and using $m = \kappa$ as the model parameter. A total of 51 subspace vectors are used at each iteration. The inversion reaches the expected misfit in 13 iterations but a few extra iterations are performed in an attempt to further reduce the value of the model objective function while keeping the misfit at the target value. By iteration 18, the objective function is decreasing by less than 1% per iteration, and the process is terminated. The constructed susceptibility model is shown in Figure 8 and can be compared with the true model in Figure 1. The tabular shape of the anomaly and its dipping structure are clear, and the depth extent is reasonably recovered. The amplitude of the recovered model is slightly higher than the true value, but the dip angle inferred from the recovered model is close to the true value. We point out that the model sections should be plotted using gray shading for each cell to reflect the piece-wise constant nature of the model. However, when the model has only a small number of cells in each spatial direction, the structural trends are more readily shown when contours are used. For this reason, we have contoured the model sections.

Next, the same data are inverted using a model objective function that includes penalty terms on spatial roughness, ϕ_{mv} . The depth weighting is applied to all terms, as in equation (20).

The inversion uses 54 subspace vectors and achieves the expected misfit in 13 iterations. The recovered model is shown in Figure 9. It is smoother, has a slightly lower amplitude than the model in Figure 8, and it recovers the essential features of the true model such as the depth and dip angle.

It is observed, in this example and in other synthetic and field test examples, that minimizing either the first term in the model objective function in equation (20), ϕ_{ms} , or using all four terms, generates models that are reasonable representations of the true structure. In the absence of prior information, both models can provide useful information about the subsurface susceptibility distribution. However, the model minimizing ϕ_{ms} can be obtained at less computational cost. Further-

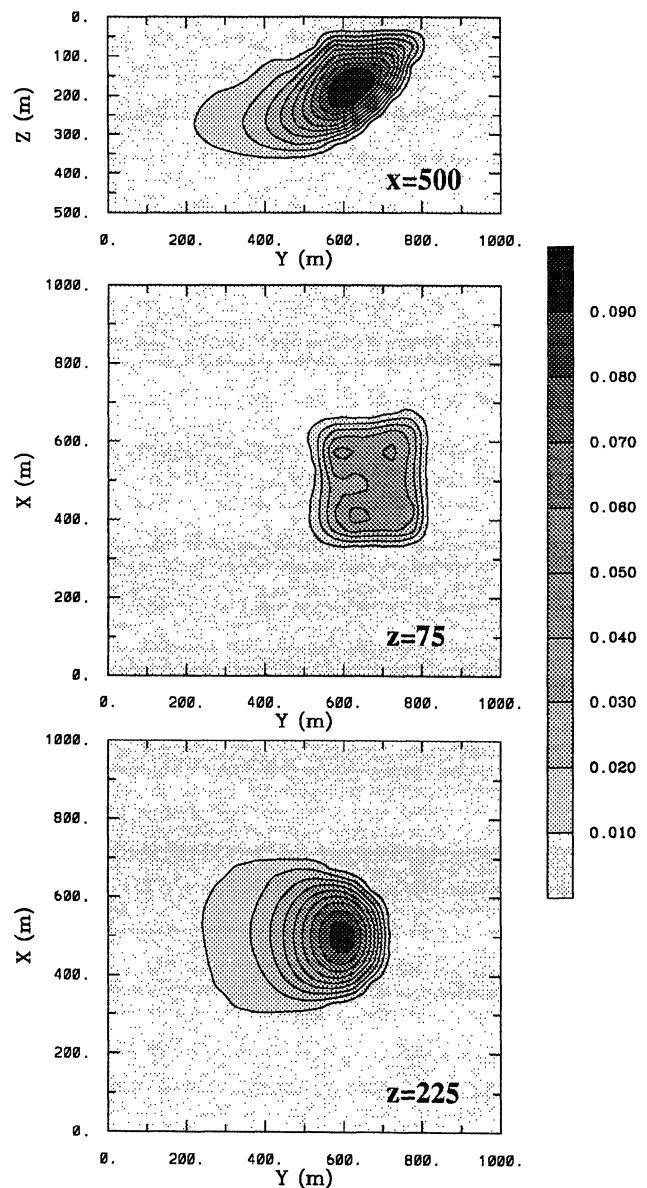


FIG. 8. Model obtained from inverting the data shown in Figure 2 by minimizing only ϕ_{ms} , which has the depth weighting applied. This is to be compared with the true model in Figure 1. The major features in the true model, such as dip angle and depth extent, are evident in the recovered model.

more, the depth weighting in this case is rather well supported by mathematical analysis whereas it is an argued extension for the three roughness components. Therefore, a reasonable approach to inverting field data might be a two-step process. The data can be inverted first by minimizing ϕ_{ms} , and the resultant model may be used in the interpretation as a preliminary result. If there are interesting features present and if one desires to refine the model by incorporating prior information to enhance or attenuate the structural complexity in different regions, a second inversion can be carried out using an objective function consisting of both ϕ_{ms} and ϕ_{mv} . The model obtained by minimizing ϕ_{ms} can then be used in this inversion

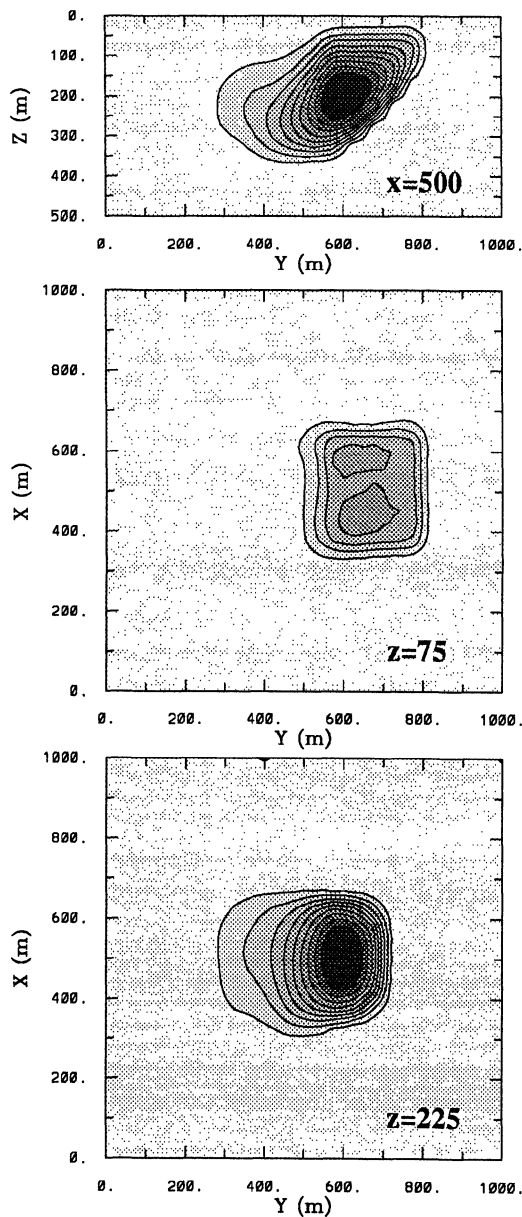


FIG. 9. The model derived from inverting the slab model data in Figure 2 by minimizing the model objective function having both ϕ_{ms} and ϕ_{mv} . The same depth weighting is used. This model appears to be smoother and has a smaller amplitude than that in Figure 8.

as an initial model. The available prior information can be incorporated into the second inversion by forming a reference model and 3-D weighting functions, w_x, w_y, w_z .

We now invert the same data by using $m = \ln(\kappa)$ as the model. It is not possible to incorporate a zero susceptibility as the reference model, so we minimize an objective function consisting of ϕ_{mv} with the reference model removed. The same depth weighting is applied to all terms of ϕ_{mv} . Since $\kappa = e^m$, the positivity of the susceptibility is ensured without invoking the transformation of variables. The result is shown in Figure 10a. This is a cross-section at $x = 500$ m and plotted on a logarithmic scale in accordance with the model used in the inversion. The inverted susceptibility shows the presence of the dipping anomaly as a broad region of high susceptibility. However, the interpretation based upon such a model can be complicated by the variations of susceptibility that are small and have little effect on the surface data. We have replotted the cross-section on a linear scale in Figure 10b and the anomalous region is now delineated more clearly. Its top portion indicates the tabular body and defines the depth to the

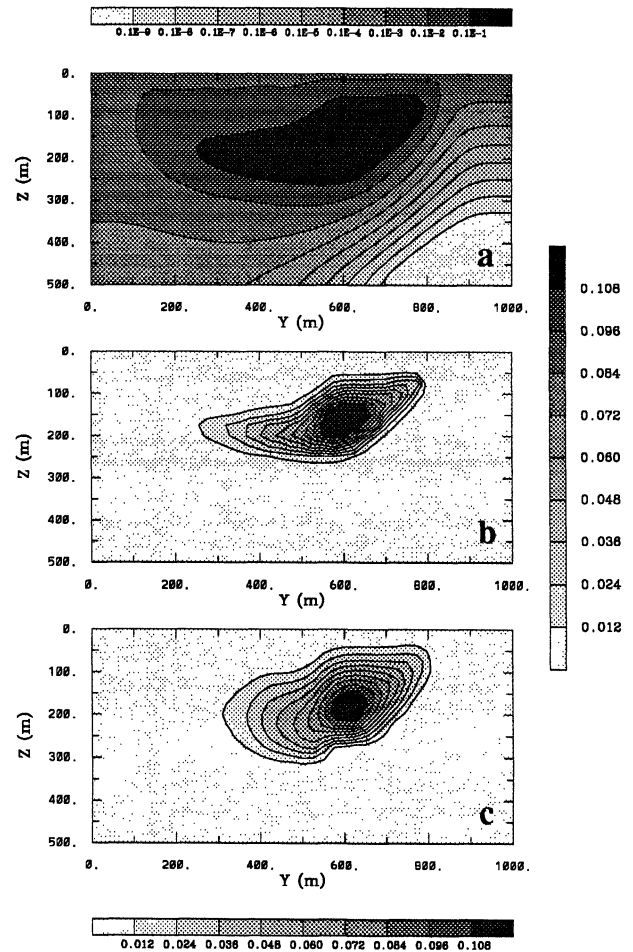


FIG. 10. The model obtained from inverting the data shown in Figure 2 by using $m = \ln(\kappa)$ as the model and minimizing ϕ_{mv} with the reference model removed. The inverted logarithmic susceptibility in cross-section at $x = 500$ m is shown in (a) and it is replotted on a linear scale in (b). As a comparison, the result obtained by using $m = \kappa$, and the same objective function is shown in (c).

top and dipping angle. The anomaly terminates at a shallower depth than the true model and has a nearly horizontal extension to the left. As an exact comparison, Figure 10c is the susceptibility model obtained by minimizing ϕ_{mv} but using $m = \kappa$ as model and invoking the positivity. This is a smoother model and exhibits more gradual changes in the susceptibility. It has a slightly deeper extent than the model in Figure 10b. With the exception of details toward the bottom, however, both models provide almost the same information about the anomalous susceptibility region. It might be concluded that inversion using either linear or logarithmic susceptibility is viable for practical applications. However, we note that the presentation in Figure 10b is inconsistent with the model used in the inversion. Since the inverted susceptibility is easier to interpret on a linear

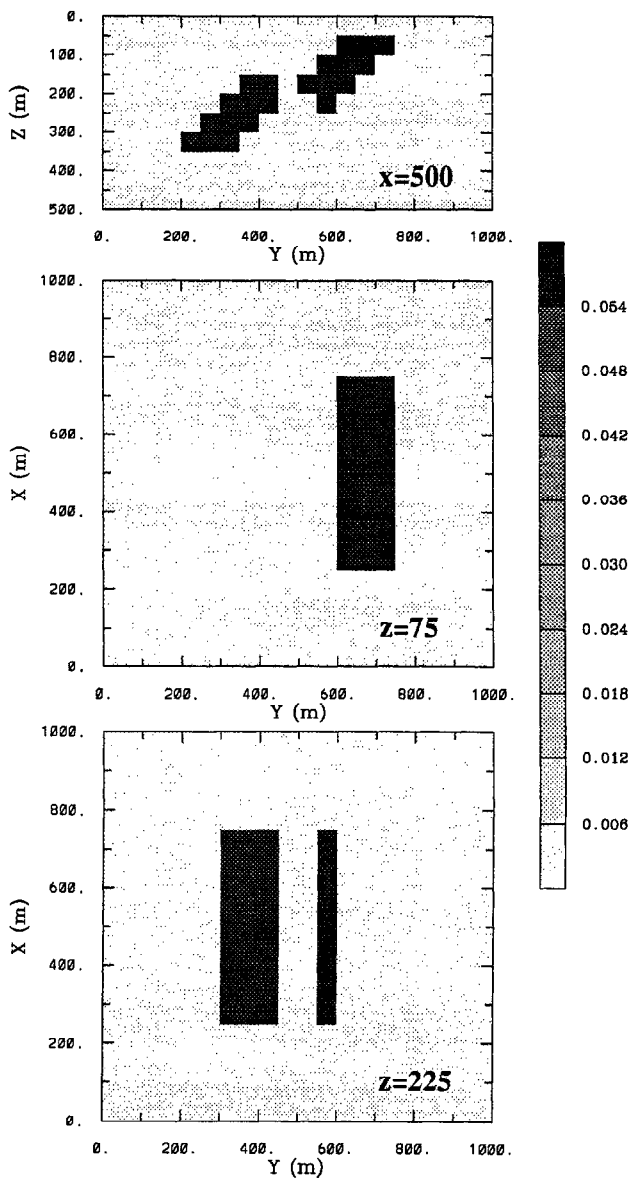


FIG. 11. The second synthetic test example. The top and bottom portions of the anomalous susceptibility are offset to simulate a normal fault structure. It also has a large strike length in the north direction.

scale as demonstrated here, and since the magnetic data are linearly related to the susceptibility, we generally prefer to work with the susceptibility κ as the model in the inversion.

As the second example we invert the total field anomaly data produced by a slightly more complicated model and with two different inducing field directions. The true model is shown in Figure 11 in the same format as before. It is a dipping slab having its top and bottom portions offset to simulate the result of a normal faulting. The faulted slab strikes north. The data from this model, when the inducing field has a direction of $I = 45^\circ$ and $D = 45^\circ$, are shown in Figure 12. Again Gaussian noise has been added to the data. The inversion minimizes an objective function consisting of ϕ_{ms} and ϕ_{mv} that have the same depth weighting and nonlinear mapping as used to produce the results in Figure 9. Figure 13 displays the recovered model in three slices. It shows two distinct anomalous regions of susceptibility that correspond to those in the true model. The dipping structure is evident from the top block. On plan view, the strike direction and the strike length of the anomaly are also well recovered.

When the inducing field direction is $I = 0^\circ$ and $D = 45^\circ$, the surface anomaly with added Gaussian noise is that shown in Figure 14. Carrying out the inversion using an identical model objective function generates the model shown in Figure 15. It is similar to the model shown in Figure 13, which is recovered under an inducing field at 45° inclination. Again, the two separate blocks, the dipping direction, and the length and direction of the strike, are all reasonably recovered. This is a positive result in that, although the surface anomalies have very different expressions under different inducing field directions, the inversion algorithm is able to consistently recover the source structure. Moreover, the algorithm had no difficulty in inverting data generated from an inducing field having zero inclination; such data often pose problems in interpretations that include a reduction to pole.

We emphasize that positivity has played a pivotal role in all the inversions. Magnetic data generally have regions of nega-

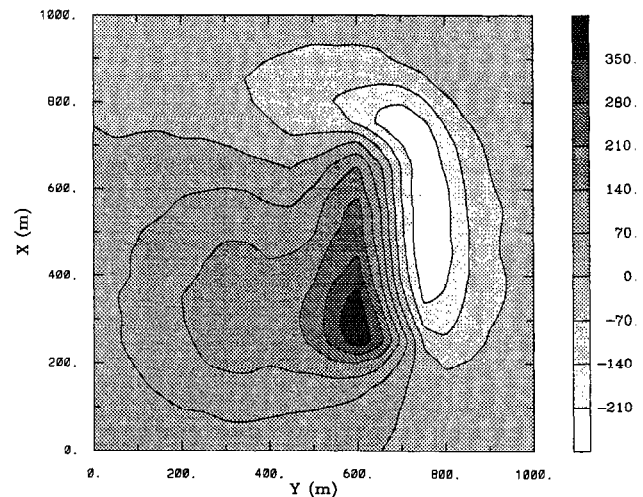


FIG. 12. The surface total field anomaly produced by the faulted slab in Figure 11, under an inducing field at $I = 45^\circ$ and $D = 45^\circ$. Uncorrelated Gaussian noise is again added to the data.

tive values that result from dipping bodies or inclined inducing field, or both. Without positivity, the constructed susceptibility is often negative and the dipping bodies appear more vertical. Recovery of correct dip and, to some extent, depth to the top of the anomalous body, are often the result of invoking positivity. Once the positivity is imposed, it is no longer true that an equivalent stratum that reproduces the data exists at any depth. Therefore, cells of anomalous susceptibility cannot be placed arbitrarily close to the surface, and no equivalent source can be constructed with negative susceptibilities. This restricts the class of admissible models and, consequently, reduces the nonuniqueness.

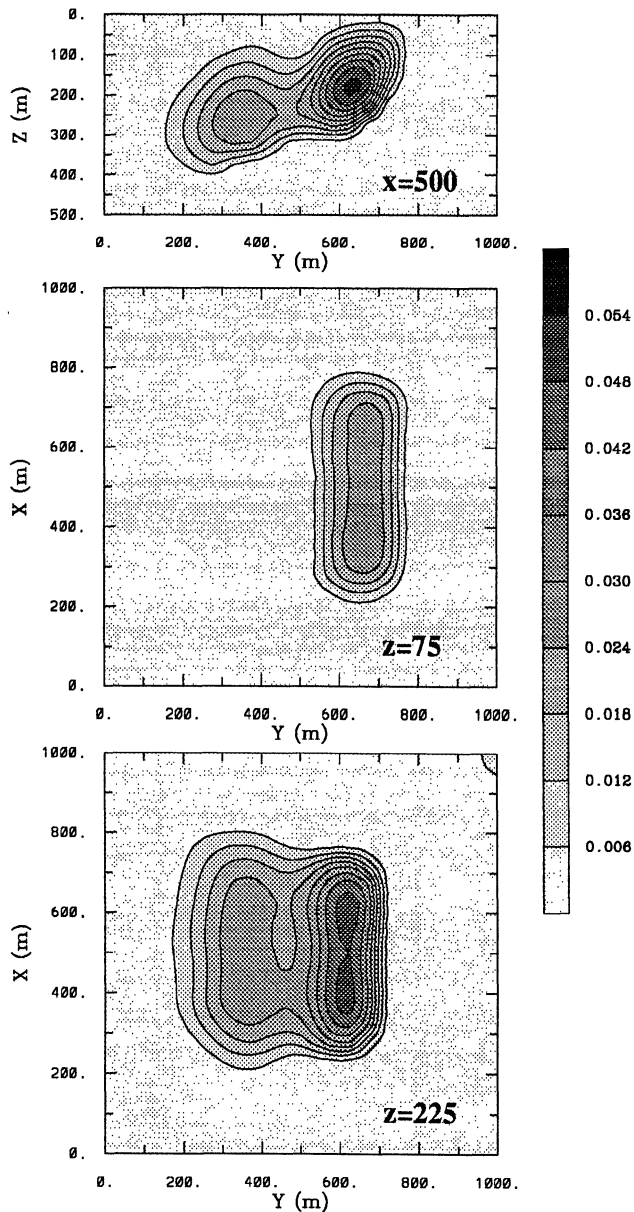


FIG. 13. The susceptibility model recovered from the data shown in Figure 12. It is seen that both the top and bottom block of the true model are recovered and the strike direction and length are well defined.

FIELD EXAMPLE

As the final example, we invert field data taken over a copper-gold porphyry deposit at Mt. Milligan in central British Columbia. The host rocks for the deposit are early Mesozoic volcanic and sedimentary rocks and contain intrusive monzonitic rocks that have accessory magnetite. Porphyry-style alteration and copper-gold mineralization are contemporaneous with the intrusive events. The copper and gold are known to be concentrated in the potassic alteration assemblage, which is mainly around the contact of the monzonite intrusions and may extend outward and into fractured volcanic rocks. Among other minerals, magnetite is one of the strong indicators of the potassic alteration. Ground magnetic data are acquired in the region at 12.5-m spacing along lines in the east direction and spaced 50 m apart. Our study of the data set has focused on a 1.2 km x 1 km area, which covers a large monzonite body known as the MBX stock and contains a reasonably isolated set of magnetic anomalies. Fairly detailed information about the geology is available through a major drilling program, but no susceptibility logs were available.

Magnetic data from a larger area were first upward continued to 20 m. A regional field was then defined and removed from the upward continued data. The continuation operation suppresses the noise in the data and also facilitates the discretization of the topographic surface for the model so that all observation points remain above the discretized surface. Although the original data were collected at 12.5-m spacing, we use the data at 25-m spacing. This yields 1029 data points at varying elevations. Figure 16 shows the data contoured according to their horizontal locations. The direction of the inducing field is $I = 75^\circ$ and $D = 25.73^\circ$. Several major magnetic highs are observed in the map. However, the influence of anomalies adjacent to the map is also visible along the edges. We choose a model domain that is horizontally larger than the data area, coincides at the top with the highest point on the topographic surface, and extends to 450-m depth. The model is discretized horizontally at a 25-m interval beneath the area of data. In the

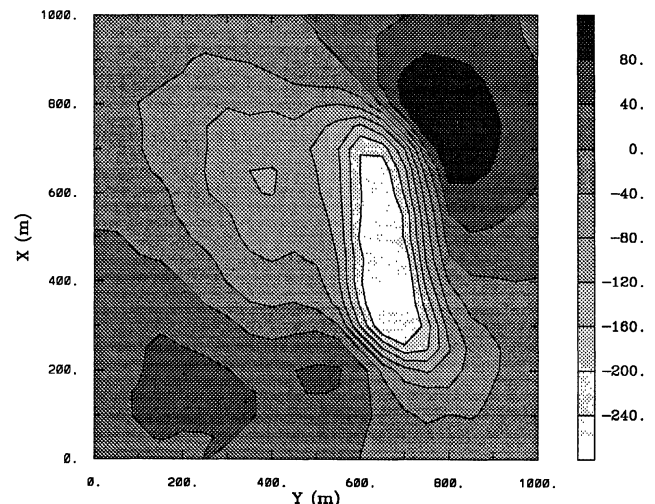


FIG. 14. The surface total field anomaly produced by the faulted slab in Figure 11 under an inducing field at $I = 0^\circ$ and $D = 45^\circ$. Uncorrelated Gaussian noise is added to the data.

vertical direction, the first 100 m is divided at a 12.5-m interval so that the surface can be adequately discretized onto the model mesh. Below the depth of 100 m, an interval of 25 m is used. This results in a mesh with 52 x 44 x 22 cells. Once the mesh is defined, the topography is discretized onto it. The 43 428 cells below this surface define the susceptibility model, and the inverse problem is therefore formalized by inverting 1029 data to recover the susceptibilities in those cells. The depth weighting is referenced to the top of the model domain. Each datum is assumed to have an error whose standard deviation is equal to 5% of its magnitude plus 10 nT. The error estimate includes not only the repeatability of the instrument reading but also the geological noise and errors introduced by the inaccurate recording position and by separating the anomalous field from the initial total field measurements. One

hundred subspace vectors generated by dividing the data map into small subareas are used in the inversion. We use a nonlinear mapping with $\kappa_b = 0.0002$ and $\kappa_1 = 0.02$. The recovered model is shown in Figure 17 as one plan-section and three cross-sections. From the plan-section, two concentrated susceptibility highs are observed in the central region. Surrounding them are three linear anomalies trending northeast. In the cross-sections, the major anomalies are seen at moderate depths but there is considerable variation in the depth to the top. There are also smaller anomalies extending to the surface. In general, there are more detailed structures near the surface and the model becomes increasingly smooth at greater depths. As required by the objective function, there is no excessive structure associated with each unit of high susceptibility region. Comparison with drill logs indicates that the recovered magnetic susceptibility highs are mostly associated with the monzonite intrusions and with faults or fracture zones. Figure 18 compares the recovered susceptibility model with the geology (Cam DeLong, personal communication) in the cross-section at $x = 600$ m. The large susceptibility high is spatially well-correlated with the MBX stock and reflects the initial magnetite content in the intrusion. Two smaller susceptibility highs are present east of the stock. The high at $y = 650$ m coincides with the boundary of stock and porous trachytic units while the high at $y = 900$ m coincides with the upper portion of the Rainbow dyke. These are locations of the most intensive potassic alterations and the susceptibility highs are indicative of the magnetite produced by the alteration process. Over all, this is a rather encouraging result.

CONCLUSION

We have developed an algorithm to invert surface magnetic data for general 3-D susceptibility distributions. Although we have illustrated the algorithm using examples on the scale pertinent to mining applications, the method is general and applicable to problems on different scales ranging from environmental to regional investigations. To overcome the inherent nonuniqueness, we obtain the solution by minimizing a

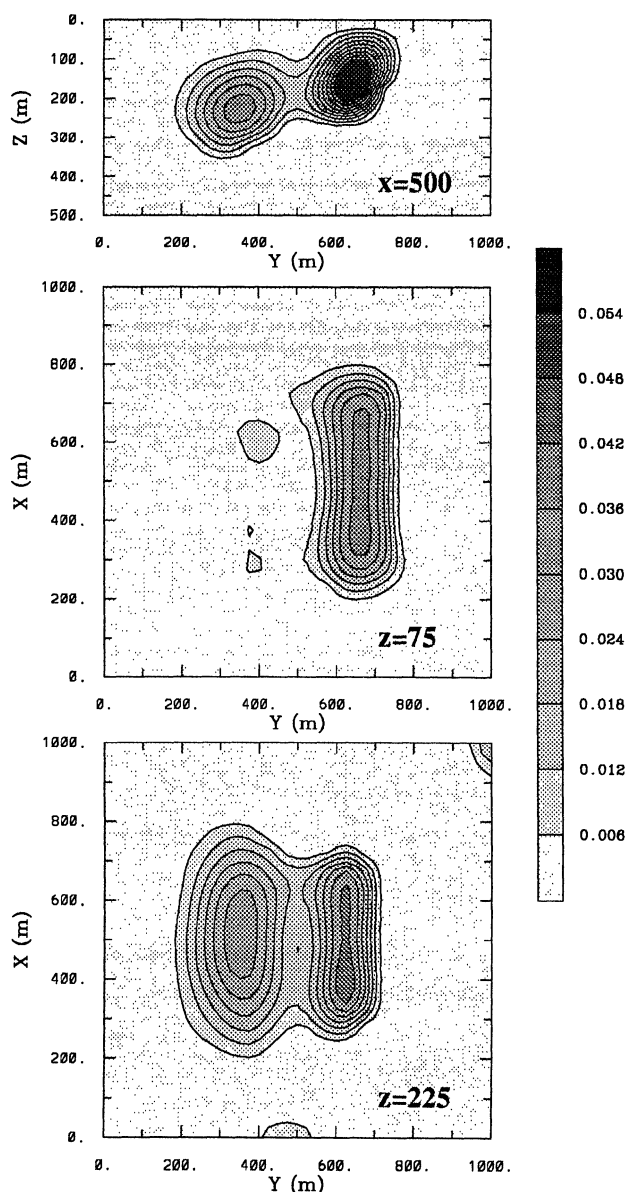


FIG. 15. The susceptibility model recovered from the data shown in Figure 14. This model is similar to that shown in Figure 13.

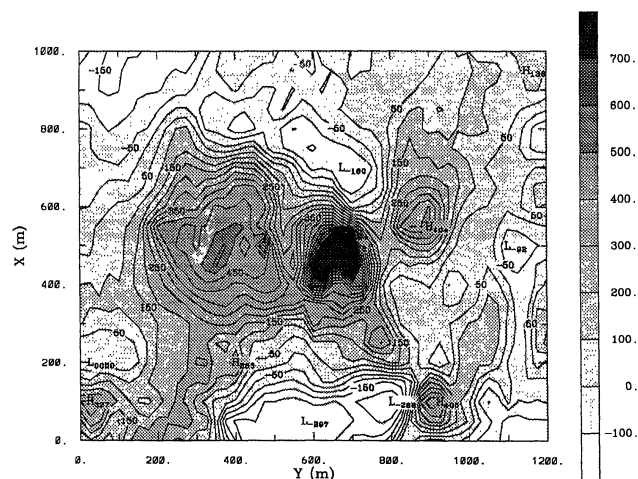


FIG. 16. The extracted total field anomaly from ground magnetic data at Mt. Milligan Copper-gold porphyry deposit. The data are contoured according to their horizontal locations in this map, although they are at different elevations.

specific objective function of the model. Our model objective function has the ability to incorporate prior information into the inversion via a reference model and 3-D weighting functions. A crucial feature of the objective function is a depth weighting function that counteracts the natural decay of the kernel functions. The parameters of the depth weighting depend upon the discretization of the model but are easily calculated. The minimization is carried out using a subspace technique that reduces the computational effort and allows the positivity constraint of susceptibility to be incorporated. Both susceptibility and logarithmic susceptibility can potentially be used as the model in the inversion. Since the data are linearly related to susceptibility, and since usually absolute values of susceptibility are required for interpretation rather than relative values, especially in regions of very low susceptibility, we have generally chosen to work with susceptibility. To suppress the noise from small magnetic bodies near the surface, we recommend in general that the data be upward continued to a height comparable with the width of the surface cell before inversion.

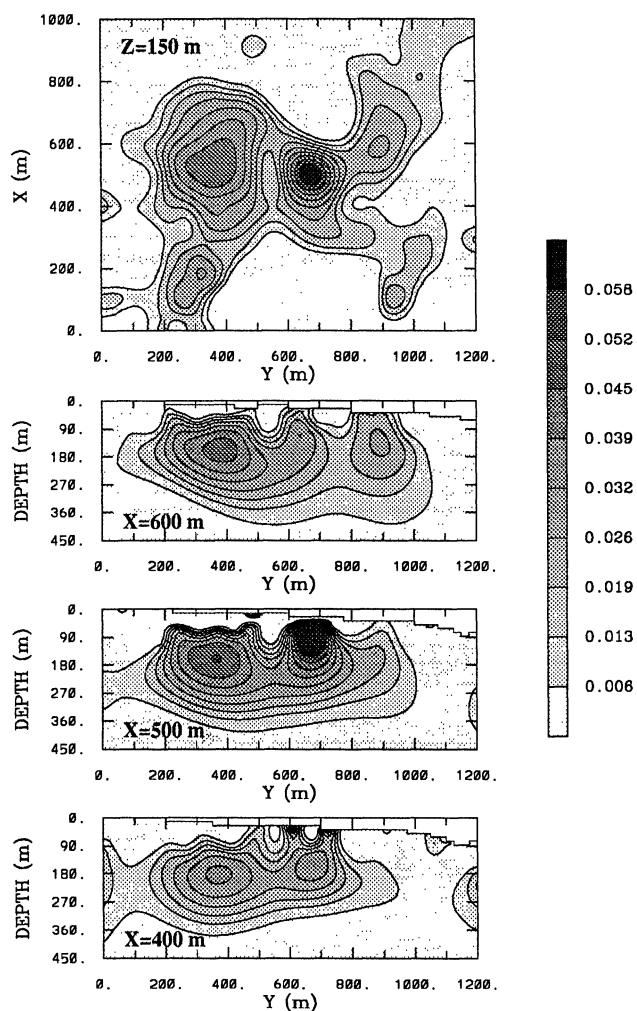


FIG. 17. The recovered susceptibility model shown in one plan-section and three cross-sections. The plan-section is at the depth of 150 m and the three cross-sections are at $x = 600, 500,$ and 400 m, respectively.

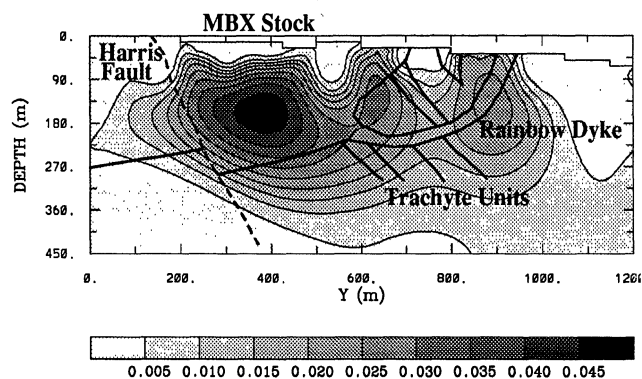


FIG. 18. Comparison of the recovered susceptibility model in a cross-section ($x = 600$) with the geology for the Mt. Milligan deposit. The susceptibility high within the MBX stock reflects the initial magnetite in the intrusive while the susceptibility highs near the Rainbow dyke are related to the magnetite produced by potassic alteration.

Applications of our inversion to synthetic data sets have produced models representative of the true structures and demonstrated the ability of the algorithm to construct consistent models at different magnetic latitudes. Inversion of field data has produced a susceptibility model that is consistent with the known geology and mineralization information. These results represent an encouraging conclusion: although the inversion of magnetic data seems impossibly nonunique when one has a large number of cells, inversions using a properly designed model objective function can produce susceptibility distributions that yield meaningful geologic information.

ACKNOWLEDGMENTS

This work was supported by an NSERC IOR grant and an industry consortium "Joint and Cooperative Inversion of Geophysical and Geological Data." Participating companies are Placer Dome, BHP Minerals, Noranda Exploration, Cominco Exploration, Falconbridge, INCO Exploration & Technical Services, Hudson Bay Exploration and Development, Kennecott Exploration Company, Newmont Gold Company, Western Mining Corporation, and CRA Exploration Pty.

REFERENCES

- Bhattacharyya, B. K., 1964, Magnetic anomalies due to prism-shaped bodies with arbitrary magnetization: *Geophysics*, **29**, 5 17-53 1.
- 1980, A generalized multibody model for inversion of magnetic anomalies: *Geophysics*, **45**, 255-270.
- Green, W. R., 1975, Inversion of gravity profiles by use of a Backus-Gilbert approach: *Geophysics*, **40**, 763-772.
- Guillen, A., and Menichetti, V., 1984, Gravity and magnetic inversion with minimization of a specific functional: *Geophysics*, **49**, 1354-1360.
- Last, B. J., and Kubik, K., 1983, Compact gravity inversion: *Geophysics*, **48**, 713-721.
- Oldenburg, D. W., and Li, Y., 1994, Subspace linear inversion methods, *Inverse Problems*, **10**, 915-935.
- Rao, D. B., and Babu, N. R., 1991, A rapid methods for three-dimensional modeling of magnetic anomalies: *Geophysics*, **56**, 1729-1737.
- Wang, X., and Hansen, R. O., 1990, Inversion for magnetic anomalies of arbitrary three-dimensional bodies: *Geophysics*, **55**, 1321-1326.
- Zeyen, H., and Pous, J., 1991, A new 3-D inversion algorithm for magnetic total field anomalies: *Geophys. J. Int.*, **104**, 583-591.

APPENDIX
MODEL OBJECTIVE FUNCTION

Our inversion method uses a model objective function of the form

$$\begin{aligned} \phi_m(m) = & \alpha_s \int_V w_s \{w(z)[m(\mathbf{r}) - m_0]\}^2 dv \\ & + \alpha_x \int_V w_x \left\{ \frac{\partial w(z)[m(\mathbf{r}) - m_0]}{\partial x} \right\}^2 dv \\ & + \alpha_y \int_V w_y \left\{ \frac{\partial w(z)[m(\mathbf{r}) - m_0]}{\partial y} \right\}^2 dv \\ & + \alpha_z \int_V w_z \left\{ \frac{\partial w(z)[m(\mathbf{r}) - m_0]}{\partial z} \right\}^2 dv. \end{aligned} \quad (\text{A-1})$$

The numerical evaluation of this functional is carried out by introducing the model mesh and evaluating all terms using a finite-difference approximation. The discretized model objective function has the form

$$\begin{aligned} \phi_m(\mathbf{m}) = & (\mathbf{m} - \mathbf{m}_0)^T (\underline{\mathbf{W}}_s^T \underline{\mathbf{W}}_s + \underline{\mathbf{W}}_x^T \underline{\mathbf{W}}_x + \underline{\mathbf{W}}_y^T \underline{\mathbf{W}}_y \\ & + \underline{\mathbf{W}}_z^T \underline{\mathbf{W}}_z) (\mathbf{m} - \mathbf{m}_0) \\ \equiv & (\mathbf{m} - \mathbf{m}_0)^T \underline{\mathbf{W}}_m^T \underline{\mathbf{W}}_m (\mathbf{m} - \mathbf{m}_0) \end{aligned} \quad (\text{A-2})$$

Each component matrix can be written as the product of three individual matrices and one coefficient. That is,

$$\underline{\mathbf{W}}_i = \alpha_i \underline{\mathbf{S}}_i \underline{\mathbf{D}}_i \underline{\mathbf{Z}}, \quad i = s, x, y, z, \quad (\text{A-3})$$

where $\underline{\mathbf{S}}_i$ are diagonal matrices representing the spatially dependent 3-D weighting functions, $\underline{\mathbf{D}}_i$ are the finite-difference operators for each component, and $\underline{\mathbf{Z}}$ is a diagonal matrix representing the discretized form of depth weighting function $w(z)$.

The elements of $\underline{\mathbf{S}}_i$ are given by $\sqrt{w_i}$. They are defined over each cell for $\underline{\mathbf{S}}_s$, and over each interface between adjacent cells in the respective directions for $\underline{\mathbf{S}}_x$, $\underline{\mathbf{S}}_y$, and $\underline{\mathbf{S}}_z$. $\underline{\mathbf{D}}_s$ has elements $\sqrt{\Delta x \Delta y \Delta z}$ on its diagonal, where Δx , Δy , and Δz are the cell width. The matrix $\underline{\mathbf{D}}_x$ has two elements $\pm \sqrt{\Delta y \Delta z / \delta x}$ in each row, where δx is the distance between the centers of cells adjacent in the x - direction. Similarly, $\underline{\mathbf{D}}_y$ and $\underline{\mathbf{D}}_z$ have elements $\pm \sqrt{\Delta x \Delta z / \delta y}$ and $\pm \sqrt{\Delta x \Delta y / \delta z}$, respectively, where δy and δz are the distances between centers of adjacent cells in the y - and z - directions. Once the mesh is defined and all weighting functions, w_s , w_x , w_y , w_z , and $w(z)$ are chosen, equation (A-3) is evaluated straightforwardly and $\underline{\mathbf{W}}_m^T \underline{\mathbf{W}}_m$ is formed.

New enhancement filters for geological mapping

Zhiqun Shi*
Encom Technology Australia
zhiqun.shi@encom.com.au

Graham Butt
Encom Technology Australia
graham.butt@encom.com.au

SUMMARY

Two types of filters have been developed for the purpose of enhancing weak magnetic anomalies from near-surface sources while simultaneously enhancing low-amplitude, long-wavelength magnetic anomalies from deep-seated or regional sources. The Edge filter group highlights edges surrounding both shallow and deeper magnetic sources. The results are used to infer the location of the boundaries of magnetised lithologies. The Block filter group has the effect of transforming the data into “zones” which, similar to image classification systems, segregate anomalous zones into apparent lithological categories. Both filter groups change the textural character of a dataset and thereby facilitate interpretation of geological structures.

The effect of each filter is demonstrated using theoretical model studies. The models include both shallow and deep sources with a range of magnetisations. Comparative studies are made with traditional filters using the same theoretical models. In order to simulate real conditions, Gaussian noise has been added to the model response. Techniques for noise reduction and geological signature enhancement are discussed in the paper.

The new approaches are applied to actual magnetic survey data covering part of the Goulburn 1:100 000 scale map sheet area, New South Wales. Some new geological inferences revealed by this process are discussed

Key words: Enhancement filters, magnetic sources, geological mapping.

INTRODUCTION

High-resolution aeromagnetic survey data represent a rich source of detailed information for mapping surface geology as well as for mapping deep tectonic structure. Traditional enhancement techniques, such as first vertical and horizontal derivatives (1VD, 1HD), analytic signal (AS), and high-pass in-line or grid filters are used in enhancing magnetic anomalies from near-surface geology.

In recent years the potential field tilt filter has been introduced (Miller and Singh, 1994) and it has achieved recognition for its value in the analysis of potential field data for structural mapping and enhancement of both weak and strong magnetic anomalies (Verduzco *et al.*, 2004). The total horizontal derivative of the TMI reduced to the pole is also widely used for detecting edges or boundaries of magnetic sources (Cordell and Grauch, 1985; Blakely and Simpson, 1986; Phillips, 1998).

Several disadvantages pertain to the use of these traditional filters. They often only diffusely identify source location and

boundaries, particularly in colour image presentations. They usually emphasise short wavelength anomalies at the expense of signal from deeper magnetic sources and the range of amplitudes remaining in the filtered output may dominate the source boundary information being sought. In addition, some traditional filters emphasise noise with resultant impact on the interpretation of source boundaries.

This paper identifies new processes which have been developed to address these disadvantages and provide output which can improve map-based interpretations.

Unless otherwise stated, all filters have been operated on TMI data reduced to the pole (RTP).

METHOD AND RESULTS

Theoretical Model Testing

A theoretical 2D grid of total magnetic intensity (TMI) computed at the surface was created by forward 3D modelling of the TMI response from a set of theoretical magnetic sources having variable width, strike extent, depth, depth extent (DE), dip, magnetic susceptibility and strike azimuth. A list of these parameters is presented in Table 1. In two of the sources, remanence was simulated using negative magnetic susceptibility. The TMI of the theoretical models was computed at a geomagnetic inclination of -60 degrees using a notional east-west line spacing of 200 m and a grid cell size of 40 m. The TMI grid was then reduced to the pole (RTP) (Figure 1).

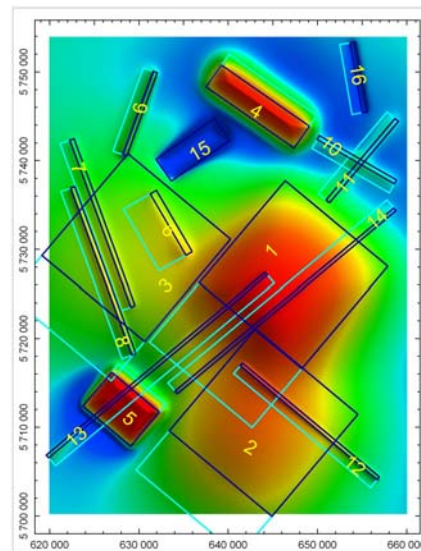


Figure 1. RTP image derived from multiple theoretical 3D magnetic sources, shown as wire frame outlines

A set of traditional filters was operated on the theoretical RTP grid. They include AS, 1VD, modulus of horizontal derivatives (MS) and Tilt and the results are presented in

Figure 2. The output grids variously show discontinuous trending (crossed sources in upper right of AS image), diffuse, weak edges (deep source in centre right of the MS image) and lack of precise source edge definition (IVD and Tilt).

Model Label	Depth (m)	Width (m)	DE (m)	Dip (deg)	Magnetic Susceptibility (SI)	Strike Length (m)	Azimuth (deg)
1	4000	15000	15000	120	0.010	15000	-050
2	6000	15000	10000	120	0.010	15000	-050
3	10000	15000	10000	120	0.010	15000	-050
4	1000	3000	4000	70	0.010	12000	-055
5	500	5000	2000	60	0.010	7000	-050
6	1000	800	2000	150	0.005	8000	-030
7	600	500	2000	120	0.001	20000	-020
8	200	500	2000	120	0.001	20000	-020
9	500	500	2000	120	0.003	10000	020
10	1000	500	2000	120	0.003	10000	-060
11	1000	500	2000	120	0.003	12000	040
12	200	400	2000	120	0.001	20000	-050
13	500	400	1000	40	0.002	32000	050
14	500	400	1000	140	0.001	32000	050
15	600	3000	4000	90	-0.002	8000	055
16	400	600	2000	120	-0.010	8000	-010

Table 1. List of parameters of theoretical magnetic sources

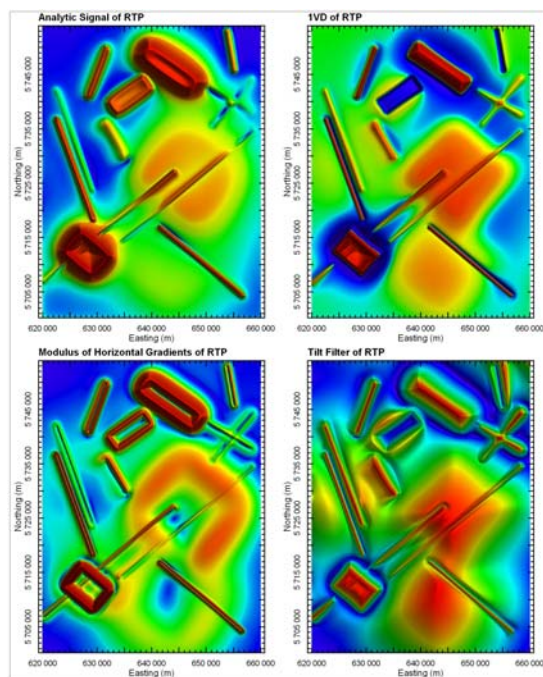


Figure 2. Comparison of enhancement filters of RTP: AS, IVD, MS and Tilt filter. The models used are those depicted in Figure 1.

Edge Filters

The first avenue of development was to increase the sharpness of the anomalies used to map the edge of the magnetic sources. The MS grid yields anomaly peaks over the source edge locations, whereas these edges coincide with gradients in the IVD, Tilt and AS filtered outputs. None of these filters produces easily interpreted edges in image form when the sources are weakly magnetised or are deep.

A new linear, derivative-based filter termed the ZS-Edgezone filter has been developed to improve edge detection in these situations. Its effect is shown in Figure 3 using the same theoretical models discussed earlier. The advantages of the filter are greatly increased anomaly sharpness over source edges and compression of the amplitude range so that differences in the original TMI amplitudes do not persist to

dominate the edge interpretation. This has the ancillary effect that the method can be modified to provide automated edge conversion to vectors for use in GIS systems.

Although this filter significantly improves the precision of edge determination, it is subject to normal potential field limitations which determine that source edges cannot be resolved where the source is narrow relative to its depth. The filter also can produce a “halo” type artefact due to superposition of the response of a limited depth extent shallow source (Figure 1, Model 6) on that of deeper sources. A similar “halo” effect can be seen around the edges of remanently magnetised Model 15, also in Figure 1.

The ZS-Edge filter (Figure 4) has also been developed to map source edges. This filter differs from the ZS-Edgezone filter in that a greater contribution of the TMI anomaly amplitude over the source is retained, thereby improving anomaly characterisation at the expense of edge sharpness.

Both these filters produce edges which migrate down-dip towards the deepest edge of the source. This effect produces anomaly asymmetry that can assist interpretation of dip, although this effect is more pronounced for the ZS-Edge filter than for the ZS-Edgezone filter. Down-dip source extensions are depicted in cyan in Figure 1.

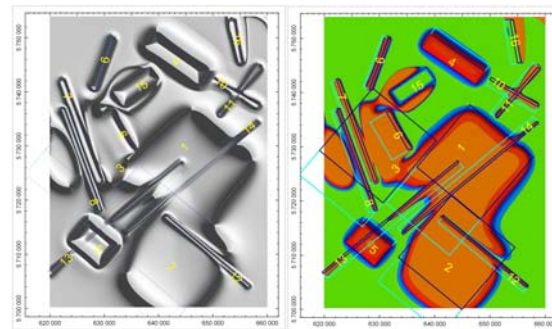


Figure 3. Anomaly edge and block enhancements using the ZS-Edgezone (left) and ZS-Block filters (right). Model positions are shown using wire frames.

Block Filters

In attempting to improve edge detection filters, an obvious progression is to highlight the magnetic regions whose edges have been mapped. To do this, a set of filters called “block” filters has been developed.

The Block filter group has the effect of transforming the potential field data into “zones” which, similar to image classification systems, segregate anomalous zones into apparent lithological categories. These filters can be imported for use in image classification systems or displayed in RGB space with other grids for empirical classification purposes.

The block filters, like the edge filters, are linear, derivative-based filters which use a combination of derivative and amplitude compression techniques to render the magnetic data into regions whose edges are sharply defined and whose amplitudes have a reduced range in comparison to the original TMI.

The ZS-Block filter (Figure 3) and the ZS-Plateau filter (Figure 4) depict the magnetic data as a 2D plan of apparent magnetic source distribution. Artefacts may occur as discussed for the edge filters.

The choice of ZS-Block, ZS-Plateau or ZS-Area filters will depend on the data characteristics of each magnetic survey and on the end-use requirement. The ZS-Plateau filter, for example, yields less variation in amplitude “texture” over a magnetic unit than either the ZS-Block or ZS-Area filters.

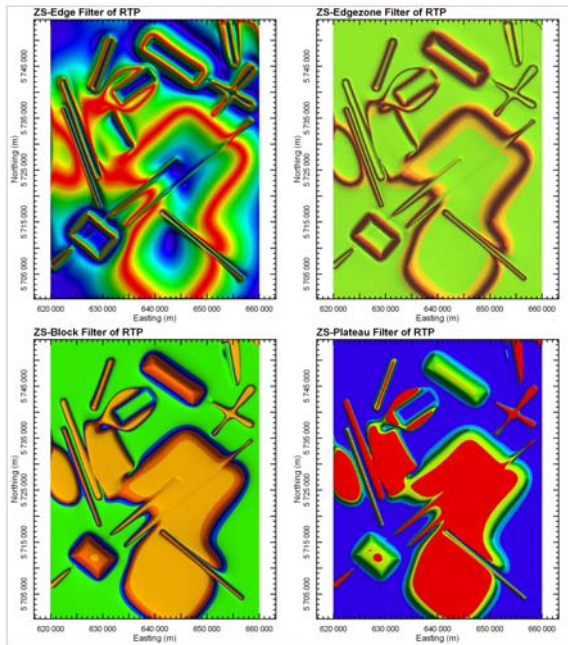


Figure 4. Comparison of ZS-Edge, ZS-Edgezone, ZS-Block and ZS-Plateau filtered outputs of RTP data

Effects of Noise

The influence of noise on the operation of these enhanced grids was tested by adding a large component of noise to the theoretical TMI profile data. This noise had a Gaussian distribution with a standard deviation equal to ten percent of the TMI standard deviation. The noise-modified TMI profile data were then de-spiked using a non-linear technique. Both the noise-affected and the de-spiked TMI data were then gridded and converted to RTP. The RTP data were then processed both with the traditional and newly developed filters.

Figure 5 shows the effect of the noise on the computations. The image of the noise-affected 1VD RTP data (top right) shows that weak and deep sources have been severely masked by the noise. Significant improvement can be achieved by using de-spiked data (lower left) or by low-pass grid filtering — for example, using an upward continuation filter (lower right).

Figure 6 shows that if real data with significant noise is encountered, a standard de-spiking or low-pass smoothing procedure may be used to achieve successful application of both the traditional and newly developed filters.

Figure 6 also depicts the use of enhanced outputs in RGB space to provide examples of how the combination of amplitude information (red colour) with edge information (green and blue colours) can be used to highlight source boundaries and remanence in a single image.

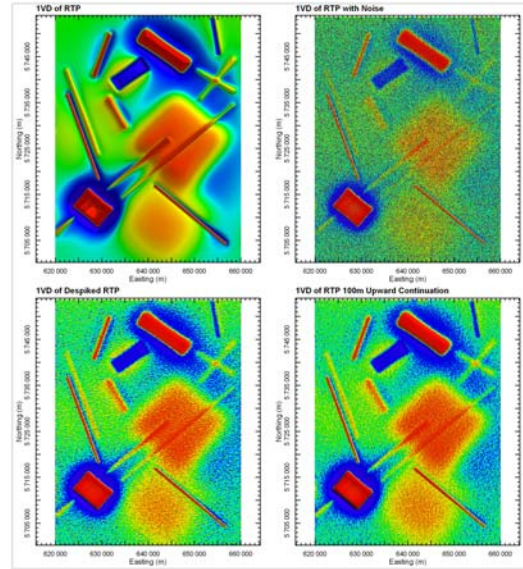


Figure 5. Comparison of 1VD of original model RTP data (top left) with noise-affected RTP data (top right) and noise-reduced RTP data (lower images)

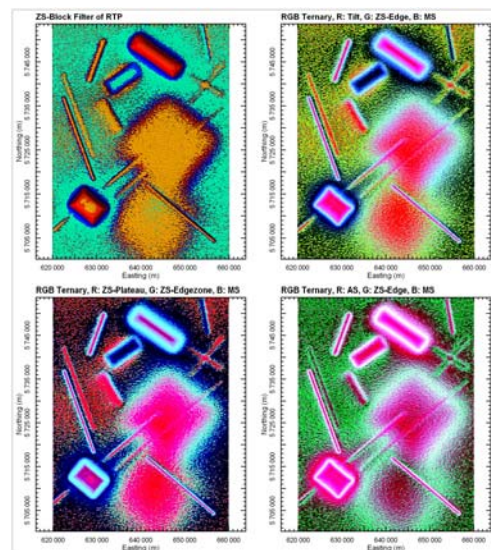


Figure 6. ZS-Block filter using noise-reduced RTP data (top left) and examples of filter combinations in RGB space using noise-reduced RTP data

Application to Field Data, Goulburn 1:100 000 Scale Map Sheet Area, New South Wales

Both the traditional and new enhancement filters were applied to test their suitability for geological definition to airborne magnetic survey data over the Goulburn 1:100 000 scale map sheet area (Johnson *et al*, 2003). These data were acquired as part of a joint program between the NSW Department of Mineral Resources and Geoscience Australia, with 250 m-spaced east-west flightlines. The magnetometer sensor occupied a nominal terrain clearance of 80 m. This dataset was selected since new detailed geological mapping had been recently completed. All the enhancements have been computed using TMI data reduced to the pole.

Figure 7 shows a comparison of part of the Goulburn 1:100 000 map sheet area surface geology with the ZS-Area

filter output. In the area surrounding location C, the ZS-Area filter transforms the magnetic data into separate magnetic units, which comprise the Devonian Bindook Volcanic Complex. The magnetic regions correlate closely with mapped andesites (Dkqa–cream coloured unit in Figure 7) whilst the intervening less-magnetic units correlate with rhyolitic ignimbrites (Dkqy–red unit in Figure 7)

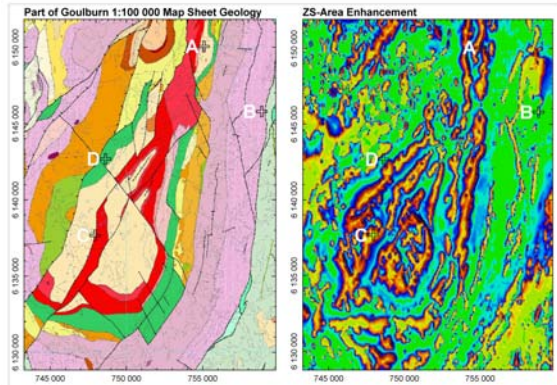


Figure 7. Comparison of geology and ZS-Area enhancement over the Bindook Volcanic Complex

Figure 8 displays some of the advantages of the edge detection filters. At location A, ambiguity concerning the continuity of Qualigo Formation units (cream and red units in Figure 7) is resolved by the ZS-Edgezone filter. At location B, a subtle lineament is confirmed, whilst at location D, the extent of the Bullamalita Conglomerate (green unit in Figure 7) is clearly mapped by the ZS-Edge filter. Structural breaks are often more easily interpreted using these transforms, for example, immediately southwest of location D.

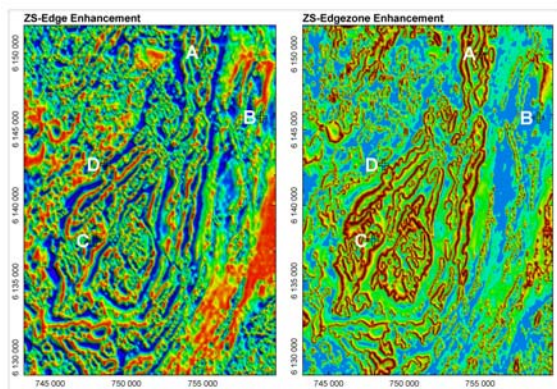


Figure 8. Comparison of ZS-Edge and ZS-Edgezone enhancements over the Bindook Volcanic Complex

Figure 9 shows standard RTP and Tilt transforms over the same area for reference.

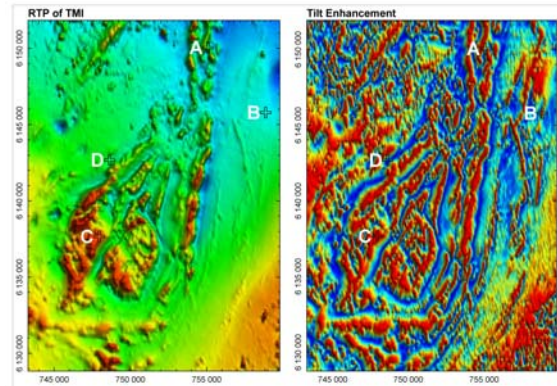


Figure 9. Comparison of RTP and Tilt filters over the Bindook Volcanic Complex

CONCLUSIONS

Traditional filters used to enhance magnetic data, including the more recently developed potential field tilt filter, are currently used to assist in determination of the location and extent of magnetic units.

Newly developed derivative-based filters may be used to improve the precision of source edge detection and, by extension, the determination of the spatial extent of magnetic units. These filters are demonstrated to perform successfully on both strongly magnetised features as well as on weakly magnetised or deep magnetic features. Artefacts may result particularly where anomaly superposition occurs.

The impact of noise in real data may be accommodated by these new methods provided noise-reduction techniques are employed.

The new filter outputs may be used as part of regional or detailed geological mapping projects, including in classification systems or in RGB space, to improve lithological discrimination and mapping.

The speed of magnetic unit mapping can be considerably increased through reliance on edge detection filters. Further improvements in mapping speed can be envisaged through automated conversion of edge anomalies to vector files.

ACKNOWLEDGMENTS

The authors would like to acknowledge the New South Wales Department of Mineral Resources for permission to use aeromagnetic and geological data from the Goulburn 1:100 000 map sheet area and helpful comments by David Robson during the project.

The authors wish to acknowledge Encom Technology for permission to publish the results of research into the proprietary filters used in this paper. The 3D modelling was carried out using Encom ModelVision Pro software, whilst processing and data visualisation were accomplished using Geosoft OASIS montaj and Encom Geoscape.

REFERENCES

Blakely, R. J. and Simpson, R. W., 1986, Locating edges of source bodies from magnetic or gravity anomalies, *Geophysics*, 51, 1494-1498.

Buckingham, A.J, Dentith, M.C., and List, R.D, 2003, Towards a system for content-based magnetic image retrieval: *Exploration Geophysics*, 34, 195-206.

Cordell, Lindrith, and Grauch, V.J.S., 1985, Mapping basement magnetization zones from aeromagnetic data in the San Juan Basin, New Mexico pp.181-197. In Hinze, W.J., ed., *The utility of regional gravity and magnetic maps: Society of Exploration Geophysicists*,

Johnson A.J. *et al.*, 2003, Goulburn 1:100 000 Sheet 8828 Geology Map, New South Wales Department of Mineral Resources.

Miller, H.G., and Singh V., 1994, Potential field tilt — a new concept for location of potential field sources: *Journal of Applied Geophysics*, 32, 213-217.

Phillips, J.D., 1998, Processing and interpretation of aeromagnetic data for the Santa Cruz Basin–Patagonia Mountains Area, South-Central Arizona: United States Geological Survey Open-File Report 02-98.

Verduzco, B., Fairhead, J. D., Green, C. M., and MacKenzie, C., 2004, New insights into magnetic derivatives for structural mapping: *The Leading Edge*, 23 (2), 116-119.

Tarsis - Mor – 3D Magnetic Inversion Specifications

The University of British Columbia 3D magnetic inversion program, version 4.0, was used for the inversions.

The area to invert was determined by the extents of the magnetic data: 658300E, 664200E, 6660600N, 6665625N.

The original TMI data came from a Geosoft grid: Mag1_lev.grd. The topography came from the grid Dem_ml.grd. The magnetic data was gridded at 50 m cells, the topography was gridded at 20 m cells. Both grids, although being leveled, were further decorrugated by Condor Consulting prior to the inversion.

Since the data was TMI, not RTP, the magnetic field information was provided to the inversion program. For both the inducing magnetic field and the induced magnetic field, an inclination of 76.6 degrees and a declination of 26.1 degrees were used. The Earth's field strength of 57765 nT was used.

A magnetic sensor height above topography of 70 m was used. The inversion results are not considered to be highly dependent on the survey height and 5m error would not be significant.

The finite element mesh for the inversion employed a cell size of 50 m by 50 m in the east and north dimensions, and the cell height varied wrt depth. There were 119 cells in the easting, 101 in the northing. In the vertical direction, there were 33 air cells, being 20 m thick and the ground cells started at 30 m thick and progressively increased in thickness through 40 vertical cells. Depth of mesh, excluding rim & air cells, was 1500m. In addition to the cells specified above, seven rim (buffer) cells required by the finite element algorithm were used on the sides of the mesh and five added to the bottom.

Over the spatial extents of the windowed data there was negligible regional trend and only a simple 0th order shift of 57421 nT was performed on the data. No further preparation of the data was required.

The error estimate provided to the inversion program was .504 nT for all data, which was 0.0001 times the standard deviation of the data plus 0.5 nT.

Two inversions were run, the first with a starting and reference model of 0.0 nT. The model from the first inversion was sharpened then used as the reference for the second inversion. The final inversion finished with the final data misfit ranging from 0.000 nT to 9.36 nT and an average of 0.303 nT. The standard deviation of the misfits was 0.399 nT.

The final finite element voxel model was trimmed by 7 cells on the east and west, 7 cells on the north, and south, and 5 cells from the bottom to removed the finite element buffer cells. The voxel model was further cleaned by nulling the voxels where there was no data.

Scott Thomas, February 4, 2009

APPENDIX D: ARCHIVE DVD